ALTERNATING CURRENT LOSS MEASUREMENT OF POWER CABLE CONDUCTORS WITH LARGE CROSS SECTIONS USING ELECTRICAL METHODS

vorgelegt von
Master of Science
René Suchantke
geboren in Berlin

von der Fakultät IV - Elektrotechnik und Informatik
der Technischen Universität Berlin
zur Erlangung des akademischen Grades

Doktor der Ingenieurwissenschaften
- Dr.-Ing. -

genehmigte Dissertation

Promotionsausschuss:
Vorsitzender: Prof. Dr.-Ing. Kai Strunz
Gutachter: Prof. Dr.-Ing. Ronald Plath
Gutachter: Prof. Dr.-Ing. Steffen Großmann
Gutachter: Prof. Dr.-Ing. Rolf Schuhmann

Tag der wissenschaftlichen Aussprache: 13. Juli 2018

Berlin 2018

Dedicated to my beloved wife and biggest critic Isabell.

You, the people, have the power,
the power to create machines,
the power to create happiness!
You, the people, have the power
to make this life free and beautiful,
to make this life a wonderful adventure. *[...]*

Let us fight for a world of reason,
a world where science and progress
will lead to all men's happiness.

Charlie Chaplin

ABSTRACT

High voltage power cables for bulk AC power transport use the *Milliken* conductor design from a certain cross section up to decrease transmission losses. It is not possible to reliably assess their AC losses by simulation or other calculation methods in advance, as the performance of this complex design strongly depends on manufacturing processes and quality. The exact knowledge of the AC resistance is important, because it is a critical design parameter for the thermal dimensioning of the cable and whole cable systems. Therefore, it is necessary to accurately determine the AC losses by measurement using the electrical or the calorimetric method. This work focuses on the electrical method solely, as it can be performed much faster with less logistical effort. The goal is to have a measurement setup, where the *measured* losses are as close as possible to the *true* losses. The *true* losses result in conductor heating, which limits the transmission power. They are also called *Joule* losses.

Theoretical calculations, FEM simulations in *Comsol Multiphysics* and measurements have been used in combination to evaluate different, possible influences in AC resistance measurements. After the problem definition and the presentation of the methodology, past advances and concepts focusing on AC resistance determination were shown. Then, after the basics were made clear to the reader, the measurement circuit was defined and different error sources in measurement setups were evaluated. These included the influence of the sheath and return conductor position upon *true* and *measured* losses, the influence of current homogenization and placement of voltage tap-offs. A recommendation for the preparation, setup and measurement procedure was given. At the end, multiple *Milliken* conductors were measured using the proposed method and compared to the IEC standard.

It was shown that the electrical measurement method is able to measure the *true* AC losses of complex conductors consisting of insulated wires. One important requirement is that the voltage pick-up loop is large enough to capture enough complex magnetic field originating from the conductor under test. On the other side, complex magnetic fields caused by *eddy currents* in adjacent conductors should not be captured by the pick-up loop as they also affect the *measured* losses. Using 2 equally spaced return conductors in the same plane as the conductor under test and the average of at least 4 evenly distributed voltage pick-up loops located at the surface of the insulation of the cable, will deliver results of sufficient accuracy.

The findings of this thesis indicate that great care must be taken for multiple aspects in the AC resistance measurement of complex conductors. Engineers performing AC resistance measurements have to be aware of error sources, specifically the interplay between conductor positions and *apparent* losses. The electrical measurement method needs to be thoroughly prepared, especially regarding the contacting of current path and voltage tap-offs. Nevertheless, the effort concerning time and logistics is still significantly smaller compared to a calorimetric measurement.

ZUSAMMENFASSUNG

Hochspannungskabel für die Übertragung großer Mengen elektrischer Energie verwenden ab einem bestimmten Querschnitt die *Millikenleiter*-Bauweise zur Senkung der Wechselstromverluste. Es ist nicht möglich, die Verluste dieser komplexen Leiter verlässlich vorab zu berechnen, da die Performance dieses Leiterdesigns unter anderem stark von Einflüssen der Fertigung abhängt. Eine genaue Kenntnis der Wechselstromverluste ist allerdings zwingend notwendig, da diese zur thermischen Dimensionierung des Kabels und ganzer Kabelsysteme genutzt werden. Es ist daher erforderlich, die Verluste durch Messungen zu bestimmen. Zur Auswahl stehen die elektrische und die kalorimetrische Messmethode, wobei sich diese Arbeit exklusiv auf erstere fokussiert. Diese ermöglicht eine schnellere Messung der Verluste mit geringerem logistischen Aufwand. Das Ziel jeder Messung sollte sein, dass die Diskrepanz zwischen *gemessenen* und den *echten* Wechselstromverlusten des Innenleiters so gering wie möglich ist. Die *echten* Verluste sind unbekannt und tragen in Betrieb maßgeblich zur Erwärmung des Innenleiters bei, was gleichzeitig die Übertragungsverluste des Kabels senkt.

Um verschiedene mögliche Einflüsse in Wechselstromwiderstandsmessungen zu evaluieren, wurden Theorie, FEM Simulationen in *Comsol Multiphysics* und Messungen in Kombination eingesetzt. Nach der Definition des Problems und des Ziels wurde die Methodik vorgestellt. Anschließend wurden relevante Konzepte zur Ermittlung von Wechselstromverlusten aufgezeigt. Darauf folgt die Definition des Messaufbaus und das Herausstellen relevanter Einflüsse auf die Messungen. Als am relevantesten stellten sich der Einfluss von Kabelschirm und Rückleiter auf die *gemessenen* und *echten* Verluste des Kabels heraus. Hinzu kommt ein signifikanter Einfluss der Stromhomogenisierung und der Positionierung der Spannungsabgriffe auf dem Leiter. Danach wurde eine Empfehlung für die Vorbereitung, den Aufbau und die Durchführung der Messung gegeben. Am Ende wurden verschiedene *Millikenleiter*-Designs mit den vorgeschlagenen Methoden vermessen und mit der aktuellen IEC Norm verglichen.

Die Untersuchungen haben gezeigt, dass die elektrische Methode unter gewissen Voraussetzungen dazu im Stande ist, die *echten* Wechselstromverluste von komplexen Leitern mit isolierten Einzeldrähten zu messen. Eine Anforderung ist beispielsweise, dass die Spannungsmessschleife groß genug ist, um komplexe Magnetfelder, die vom zu untersuchenden Leiter erzeugt werden, einzufangen. Allerdings darf die Messschleife nicht so groß sein, dass andere komplexe Magnetfelder, erzeugt von Wirbelströmen in umgebenden Leitern, in die Messschleife einkoppeln. Diese können die gemessenen Verluste sonst direkt beeinflussen. Der empfohlene Aufbau zur Messung der Wechselstromverluste von *Millikenleitern* verwendet 2 äquidistant platzierte Rückleiter, die in einer Ebene mit dem zu untersuchenden Leiter liegen. Die Messung der Spannung erfolgt aus dem Mittelwert von mindestens 4, gleichmäßig um die Oberfläche der Isolation des Kabels verteilten, Spannungsmessschleifen.

Die Analyse des Problems hat gezeigt, dass die Wechselstromverlustmessung von komplexen Leitern genauer Kenntnisse über mögliche Störeinflüsse bedarf. Die Auswirkung der Positionierung der Leiter auf die *gemessenen* Verluste sollten vom Anwender verstanden sein und in der Versuchsvorbereitung und Ausführung weitestgehend eliminiert werden. Auch für die elektrische Methode müssen daher einige Maßnahmen und Vorbereitungen — insbesondere hinsichtlich der Kontaktierung der Spannungsabgriffe und Strompfadkontaktierung — zur akkuraten Messung getroffen werden. Im Vergleich zur kalorimetrischen Methode sind diese vorbereitenden Maßnahmen allerdings wesentlich weniger zeitintensiv.

PUBLICATIONS

It takes many good deeds to build a good reputation,
and only one bad one to lose it.
Benjamin Franklin

In the following, publications related to the topic of this thesis are listed, where the author took direct part during his research activity at Technische Universität Berlin:

[CIG18] CIGRE, ed. *Basic principles and practical methods to measure the AC and DC resistance of conductors of power cables and overhead lines*. D1.54. CIGRE, 2018.

[Sch+14] Gero Schröder, René Suchantke, Hendrik Just, Rolf Schuhmann, and Ronald Plath. "Maßnahmen zur Reduzierung des Skin-Effekts bei Energiekabeln durch optimierte Leiterkonstruktionen und deren messtechnische Bewertung." In: *Diagnostik elektrischer Betriebsmittel 2014*. ETG-Fachbericht. Berlin u.a.: VDE-Verl., 2014. ISBN: 978-3-8007-3648-5.

[Sch+15] Gero Schröder, Volker Waschk, Ronald Plath, Rolf Schuhmann, and René Suchantke. "Measures to reduce skin-effect losses in power cables with optimized conductor design and their evaluation by measurement." In: *Jicable 2015 - 9th International Conference on Insulated Power Cables*. Paris, France, 2015.

[SPS16] René Suchantke, Ronald Plath, and Rolf Schuhmann. "Besonderheiten bei der Messung von Wechselstromwiderständen von kurzen Leitern und kurzen Kabelstücken mit großen Querschnitten: Difficulties with AC resistance measurements of short conductor- and cable samples with large cross-sections." In: *VDE-Hochspannungstechnik 2016*. ETG-Fachbericht. Berlin: VDE-Verlag, 2016. ISBN: 978-3-8007-4310-0.

[SPW15] René Suchantke, Ronald Plath, and Volker Waschk. "A numerical approach to optimize HVAC conductor designs based on parameter sweeps of influenceable construction steps." In: *ISH 2015 - The 19th International Symposium on High Voltage Engineering*. Pilsen, Czech Republic, 2015.

E-Mail address of the author of this thesis: suchantke.rene@gmail.com.

ACKNOWLEDGMENTS

If I have seen further
it is by standing on the shoulders of giants.
Isaac Newton

My first and biggest thank you goes to my advisor Prof. Dr.-Ing. Ronald Plath from the Technische Universität Berlin for putting the trust in me to be able to work on that topic. I thank him for the social network and freedom he offered, which gave me the possibility to look into this topic as deep as I thought it would be necessary to progress in that field. I am also thankful for the opportunity to present my work at different international conferences and workshops. Moreover, I am thankful for being introduced to the CIGRE working group D1.54 by Prof. Dr.-Ing. Plath.

I would also like to thank Prof. Dr.-Ing. Rolf Schuhmann from the Technische Universität Berlin for the support and help on theoretical and strategic considerations in this research project. Both project advisors, Prof. Plath and Prof. Schuhmann, gave me the opportunity to learn a lot during the whole process from writing project proposals up to actual research activity.

I am also deeply honored that Prof. Dr.-Ing. Steffen Großmann from Technische Universität Dresden agreed to supervise my work and took the time to proofread this thesis and provide useful hints for increased quality. Moreover, I thank him for the opportunity to discuss this work with his team at his department.

I deeply appreciate the excellent work done by my student employee Nick Wieczorek throughout this work. His outstanding understanding of the underlying physics often helped to progress at a much faster rate. I am thankful for the great work in the laboratory and on cumbersome theoretical tasks such as the derivation of complex formulas. In addition to that, I thank my co-worker on this research project Christian Lehmann for guidance and verification of some of my theoretical thoughts on this topic. A warm thank you also to my coworker Simon Spelzhausen for discussions concerning the structuring of this work. I would also like to thank the whole High Voltage Engineering department team for helping and supporting me on numeral occasions.

I am also thankful to *NKT GmbH*, *Südkabel GmbH* and *General Cable* (*NSW*) for the opportunity to measure various cable conductors during this project. This helped giving this work the necessary practical background and relation to common industry practices. A special thanks to Dominik Häring and Dr. Gero Schröder from *Südkabel GmbH* and to Mathias Behle, Dr. Volker Waschk and Dag Willén from *NKT GmbH* for enduring deep discussions on that topic. I also thank Dr. Michael Beigert from *Norddeutsche Seekabelwerke* (*NSW*) for the opportunity to measure *Milliken* conductor samples.

I thank Prof. Dr.-Ing. Arnulf Kost for strategic advices and sharing his knowledge on *skin effect* problems.

I am also grateful to the CIGRE Working Group D1.54 members for giving me the opportunity to participate at such an interesting topic and on such a deep level. Especially, I'd like to thank the convenor Dr. Boris Dardel. Thank you to Toni Israel and Dr. Ziqin Li for interesting discussions on theoretical considerations. Also a big thank you to Dr. Cory Liu for talks on measurement systems and the opportunity to measure *Southwire Company*'s specially designed bimetallic conductor.

At the end, I want to thank the DFG (*Deutsche Forschungsgemeinschaft/German Research Foundation*) for financially supporting this research project and therefore contributing to the advance in knowledge on this important topic. This work is a result of sponsored project "Investigations on AC losses of power cables by simulation and measurement" with project number 289991964[1].

1 The project can be found at http://gepris.dfg.de/gepris/projekt/289991964?language=en (visited on 08/02/2018).

CONTENTS

LIST OF FIGURES

LIST OF TABLES

LISTINGS

ACRONYMS & ABBREVIATIONS

AC	alternating current
ACPD	alternating current potential drop
ACSR	aluminum conductor steel reinforced
ADC	analog-to-digital converter
BC	boundary condition
BD	boundary distance
CIGRE	Conseil International des Grands Réseaux Électriques
CUT	conductor under test
DC	direct current
DCPD	direct current potential drop
DOF	degrees of freedom
EHV	extra high voltage
emf	electromotive force
emu cgs	electromagnetic unit centimetre-gram-second
FEM	finite element method
FFT	fast Fourier transform
HV	high voltage
HVAC	high voltage alternating current
HVDC	high voltage direct current
IEC	International Electrotechnical Commission
IEEE	Institute of Electrical and Electronic Engineers
mef	magnetic and electric field
MQS	magnetoquasistatic
OHL	overhead lines
pd	potential difference
PDE	partial differential equation
PEC	perfect electric conductor
PMC	perfect magnetic conductor
PPL	paper-polypropylene laminated
rms	root mean square

MATHEMATICAL CONVENTIONS

SYMBOL	DESCRIPTION
j	imaginary number: $\mathrm{j}^2 = -1$
$\vec{X}$	indicates that X is a vector
$\underline{X}$	indicates that X is a complex quantity
$\hat{X}$	indicates that X is the peak value
$\underline{\hat{X}}$	indicates that X is a phasor
$\underline{\vec{\hat{X}}}$	indicates that X is a vectorial phasor
$\boldsymbol{X}$	abbreviation used for $\underline{\vec{\hat{X}}}$
$\|X\|$	indicates that the norm (absolute magnitude) of X is taken
$R_X \| \| R_Y$	resistance R_X is parallel to resistance R_Y
X^*	shows the complex conjugate of X
X'	indicates the derivative of X
$\times$	cross product
$\wedge$	logical "and"
$\mathrm{X}^\top$	gives the transpose of matrix X
$\ldots$	indicates that a formula is continued on the next line
$\mathrm{d}\vec{s}$	vector boundary element
$\mathrm{d}\vec{A}$	vector area element
$\mathrm{d}V$	volume element
$\oint_C$	line integration around closed boundary curve C
$\iint_A$	surface integration over surface A
$\iiint_V$	volume integration over volume V
$\frac{\mathrm{d}}{\mathrm{d}x}$	differentiation with respect to x
$\frac{\partial}{\partial x}$	partial differentiation with respect to x

FUNCTION	DESCRIPTION
arctan	inverse trigonometric function of tan
ber_ν, bei_ν	Kelvin functions – real and imaginary part of J_ν
ber'_ν, bei'_ν	derivatives of Kelvin functions ber_ν, bei_ν
cosh	hyperbolic cosine
$G_{1,2,3}$	abbreviation for combined Bessel functions
H_ν	Bessel function of the third kind and ν^{th} order
I_ν	modified Bessel function of the first kind and ν^{th} order
Im	takes the imaginary part of an expression
J_ν	Bessel function of the first kind and ν^{th} order
K_ν	modified Bessel function of the second kind and ν^{th} order
ker_ν, kei_ν	Kelvin functions – real and imaginary part of K_ν
ker'_ν, kei'_ν	derivatives of Kelvin functions ker_ν, kei_ν
ln	natural logarithm
$\log_b(x)$	logarithm of x to base b
Re	takes the real part of an expression
tanh	hyperbolic tangent function
u_n,v_n	Kelvin functions (obsolete notation)
u'_n,v'_n	derivatives of Kelvin functions (obsolete notation)
Y_ν	Bessel function of the second kind and ν^{th} order

PHYSICAL CONSTANTS

SYMBOL	VALUE	CONSTANT NAME	UNIT
c	299 792 458	speed of light	m/s
e	2.718 281 828 ...	Euler's number	
ε_0	$8.854\,187\ldots \times 10^{-12}$	permittivity of vacuum	As/(Vm)
μ_0	$4\pi \times 10^{-7}$	permeability of vacuum	Vs/(Am)
μ_{cgs}	1	permeability of vacuum in emu cgs system	
π	3.141 592 653 ...	pi	

SYMBOLS

SYMBOL	DESCRIPTION	UNIT
a	front voltage tap-off	
A	conductor cross section	m^2
$\boldsymbol{A}, \underline{\vec{A}}$	magnetic vector potential	V s/m
A_{L}	surface area of voltage loop	m^2
b	rear voltage tap-off	
b_{b}	real part of ξ (abmhos is a unit in *emu cgs* system (Section 3.1.3))	$\sqrt{\text{abmhos cm/s}}$
$\boldsymbol{B}, \underline{\vec{B}}$	magnetic flux density	$\mathrm{V\,s/m^2}$
c	factor in bi-media conductor formula	
$\underline{C}$	factor in tubular conductor formula	
d	distance between two conductors	m
d_{CUT}	diameter of the CUT	m
d_{min}	minimum distance (influence of *proximity effect* losses < 0.1 %)	m
d_{VL}	extension of voltage leads perpendicular from CUT's surface	m
$d_{\text{VL,min}}$	minimum extension of voltage leads necessary to account for *true* losses	m
$\boldsymbol{D}, \underline{\vec{D}}$	electric displacement field	$\mathrm{A\,s/m^2}$
$\boldsymbol{E}, \underline{\vec{E}}$	electric field intensity	V/m
f	frequency	1/s
f_0	frequency value at reference temperature	1/s
f_T	frequency value at measurement temperature	1/s
F	mechanical force	N
$\underline{g}$	factor in *proximity effect* calculation	$\sqrt{\text{s/(abmhos cm)}}$
$\underline{h_n}$	factor in *proximity effect* calculation	$\sqrt{\text{s/(abmhos cm)}}$
h_{r}	height of rectangular conductor	m

SYMBOL	DESCRIPTION	UNIT
$\boldsymbol{H}, \underline{\vec{H}}$	magnetic field intensity	A/m
$\underline{i}_{\mathrm{im}}$	internal current through the voltmeter	A
$\boldsymbol{I}, \underline{I}$	total conductor current	A
$\boldsymbol{J}, \underline{\vec{J}}$	current density	$\mathrm{A/m^2}$
$\underline{J}_{\mathrm{s}}$	surface current density	$\mathrm{A/m^2}$
$\boldsymbol{J_{\mathrm{t}}}$	total current density (conduction plus displacement current)	$\mathrm{A/m^2}$
$\underline{J}_{x,\mathrm{AC}}$	x-component of AC current density	$\mathrm{A/m^2}$
$\underline{J}_{z,\mathrm{AC}}$	z-component of AC current density	$\mathrm{A/m^2}$
$J_{z,\mathrm{DC}}$	z-component of DC current density	$\mathrm{A/m^2}$
k	Kelvin function argument for solid & tubular conductors	$\mathrm{m^{-1}}$
k_{k}	geometric ratio for *proximity effect* calculations	
k_{s}	function argument for loss calculation (IEC 60287-1-1)	
l	length of the conductor	m
l_{meas}	measuring length	m
$l_{\mathrm{to,i}}$	length between voltage tap-off and insulated conductor section	m
L_{iAC}	AC internal inductance per-unit length	H/m
L_{iDC}	DC internal inductance per-unit length	H/m
$\underline{m}$	Bessel function argument for solid & tubular conductors	$\mathrm{m^{-1}}$
mef.omega	angular frequency (*Comsol Multiphysics*)	$\mathrm{s^{-1}}$
mef.Qh	volumetric loss density (electromagnetic) (*Comsol Multiphysics*)	$\mathrm{W/m^3}$
$\underline{M}_n$	factor in *proximity effect* calculation	$\mathrm{m^{-1}}$
n	running index	
$\underline{n_n}$	Bessel function argument for bi-media conductors in medium n	$\mathrm{m^{-1}}$
$\underline{N}_n$	factor in *proximity effect* calculation	
$\underline{o}_n$	factor in *proximity effect* calculation	$\sqrt{\mathrm{s/(abmhos\ cm)}}$
p	*principle of similitude parameter* (*pos parameter*)	$\sqrt{\mathrm{m/(\Omega s)}}$
p_n	geometric parameter of *proximity effect* calculation	
p_{V}	volumetric loss density	$\mathrm{W/m^3}$
P_{C}	isolated conductor losses	W/m
P_{CUT}	losses in the inner conductor due to *skin effect* and cable sheath	W/m
$P_{\mathrm{Prox,M}}$	additional losses in inner conductor caused by metal framework	W/m
$P_{\mathrm{Prox,P}}$	additional losses in inner conductor caused by other phases of the system	W/m
$P_{\mathrm{Prox,S}}$	additional losses in inner conductor caused by cable sheath	W/m
$P_{\mathrm{Skin,C}}$	*skin effect* losses of of inner conductor alone	W/m
q	factor in *proximity effect* calculation	

SYMBOL	DESCRIPTION	UNIT
$\underline{Q}_n$	factor in *proximity effect* calculation	
r	radial coordinate (distance to conductor center in cylindrical coordinates)	m
r_1	inner radius of tubular conductor	m
r_2	outer radius of tubular conductor	m
r_c	radius of conductor	m
R	resistance per-unit length	Ω/m
R_0	resistance per-unit length at reference temperature	Ω/m
R_AC	AC resistance per-unit length	Ω/m
$R_\mathrm{AC,C}$	analytical AC resistance per-unit length of an isolated solid conductor	abmhos/cm
$R_\mathrm{AC,Ref}$	AC resistance of reference CUT	Ω/m
R_DC	DC resistance per-unit length	Ω/m
$R_\mathrm{DC,0}$	DC resistance per-unit length at reference temperature	Ω/m
$R_{\mathrm{DC},n}$	DC resistance per-unit length of medium n	Ω/m
$R_\mathrm{DC,Ref}$	DC resistance of reference CUT	Ω/m
$R_{\mathrm{DC},T}$	DC resistance per-unit length at measurement temperature	Ω/m
R_im	internal resistance of the voltmeter	Ω
R_meas	*measured* AC resistance	Ω/m
R_T	resistance measured at measurement temperature	Ω/m
R_true	*true* resistance of the CUT	Ω/m
R_virt	*virtual* resistance of the CUT (obtained by simulation)	Ω/m
R_VL	resistance of voltage lead wires	Ω
R_λ	specific thermal resistance	$\mathrm{K\,m/W}$
s	geometric parameter of *proximity effect* calculation	
$\boldsymbol{S}, \underline{\vec{S}}$	*Poynting vector*	$\mathrm{W/m^2}$
t	conductor thickness	m
T	temperature	K
T_0	reference temperature	K
T_SF	temperature scaling factor	
$\underline{u}$	voltage	V
$\underline{u}_\mathrm{meas}$	*measured* voltage	V
v_diff	diffusion phase velocity	m/s
V	electric scalar potential	V
w	factor in *proximity effect* calculation	
w_r	width of rectangular conductor	m
x	Cartesian coordinate	m
x_s	*skin effect* factor argument (IEC 60287-1-1)	
X_AC	AC electrical reactance per-unit length	Ω/m
X_iAC	AC internal electrical reactance per-unit length	Ω/m
X_meas	*measured* AC inductance per-unit length	Ω/m

SYMBOL	DESCRIPTION	UNIT
X_{virt}	*virtual* reactance (obtained by simulation)	Ω/m
y	Cartesian coordinate	m
y_{s}	*skin effect* factor (IEC 60287-1-1)	
z	Cartesian coordinate	m
$\underline{z}_0$	Bessel function argument for *proximity effect* calculation	
$\underline{Z}_0$	analytical AC internal impedance per-unit length of an isolated solid conductor	abmhos/cm
$\underline{\alpha}$	function argument for *Infinitively Wide Strip* formula	$\sqrt{\mathrm{abmhos}/(\mathrm{cm\ s})}$
α_T	temperature coefficient	$1/\mathrm{K}$
$\underline{\gamma}$	Bessel function argument for coaxial cable calculation	m^{-1}
$\underline{\Gamma}$	Bessel function argument for *proximity effect* calculation	$\sqrt{\mathrm{abmhos\ cm/s}}$
δ	skin depth	m
δ_n	skin depth in medium n	m
ΔR_{virt}	increase in *virtual* resistance caused by the AC losses of the sheath only	Ω/m
ΔT	temperature drop across a material	K
ΔV; $\Delta\varphi$	potential difference	V
$\underline{\varepsilon}_{\mathrm{i}}$	induced emf	V
ε_{r}	electric permittivity	
$\underline{\zeta}$	Bessel function argument for *proximity effect* calculation	$\sqrt{\mathrm{abmhos\ cm/s}}$
$\underline{\lambda}_n$	factor in *proximity effect* calculation	
μ	product of magnetic permeability of the conductors times μ_0	$\mathrm{Vs}/(\mathrm{Am})$
μ'	product of magnetic permeability of the space between conductors times μ_0	$\mathrm{Vs}/(\mathrm{Am})$
μ_{r}	magnetic permeability	
$\mu_{\mathrm{r},n}$	magnetic permeability of medium n	
$\underline{\xi}$	Bessel function argument for *proximity effect* calculation	$\sqrt{\mathrm{abmhos\ cm/s}}$
$\Xi_{1,2,3,4}$	prefactor of Bessel functions	
ϱ	electric charge density	$\mathrm{A\,s/m^3}$
σ	electrical conductivity	$\mathrm{S/m}$
σ_0	reference electrical conductivity	$\mathrm{S/m}$
σ_n	electrical conductivity of medium n	$\mathrm{S/m}$
σ_{sd}	standard deviation	
v_l	relative maximum error of length measurement	
$v_{R_{\mathrm{AC}}}$	relative maximum error of R_{AC}	
v_T	relative maximum error of temperature measurement	
v_o	maximum relative overall error of the measurement	
Ψ_0	gauge-fixing potential	$\mathrm{A/m}$
ω	angular frequency ($\omega = 2\pi f$)	$1/\mathrm{s}$

1 INTRODUCTION AND SCOPE OF THIS WORK

> The beginning is the most important part of the work.
> *Plato*

The purpose of this chapter is to introduce the reader to high voltage (HV) power cables and the motivation of this thesis. At the beginning, a brief description of recent developments in electric power transmission networks is given. Moreover, the rising demand for HV power cables is pointed out. Next, a typical power cable setup is displayed, giving the reader a better understanding of different components of HV cables. Afterwards, the target value of this thesis—losses due to *Joule heating* in the inner conductor—is defined. Following, recent international standards for power cable ratings are reviewed as well as different available measurement methods to evaluate conductor losses caused by *Joule heating*. Some similar measurement methods are described afterwards, which also lay stress on similar aspects as the herein used electrical measurement method. As a basic understanding of the underlying problematic is then present, the chapter is concluded with the motivation and goal of this thesis.

1.1 ELECTRIC POWER TRANSMISSION NETWORKS

Expected growth in demand for electrical energy worldwide during the next decades, makes an expansion of existing power grids inevitable [Ben09; EUR13; IEA17]. Especially in Germany and other countries, where integration of renewable energy sources is favored, it is necessary and planned to extend the existing power grid [Deu10; Tag15; 50H+17]. According to the network development plan presented by the German transmission system operators—*50Hertz Transmission GmbH*, *Amprion GmbH*, *TenneT TSO GmbH* and *TransnetBW GmbH*—depending on different possible scenarios, new alternating current (AC) transmission systems with a total length of 1200 km are required for a safe network operation until 2030. Moreover, existing power line routes shall be extended by new systems—overhead lines (OHL) and cable systems with direct current (DC) and AC—of approximately 7600 km to 8500 km in length [50H+17, p. 99].

In addition to the generation and consumption, one crucial element in the supply chain is the transmission of electrical power. Depending on the extent of power to be transmitted, environmental impacts, the distance and other requirements, different transmission systems are used. In general, it can be concluded that for bulk power transmission commonly high voltage alternating current (HVAC) systems are used[1]. For longer distances—from approximately 80 km up for cable systems and from round about 600 km up for OHL—high voltage direct current (HVDC) transmission systems can be more cost-efficient [Hof12; Sie14]. The main benefit of applying high voltage is the possibility to decrease the conductor current, while keeping

1 This is valid for distances of tens of kilometers for submarine cables and underground power cables and—depending on the voltage level—distances up to hundreds of kilometers for OHL.

the transferred electric power constant. By reducing the magnitude of necessary conductor current, transmission losses are lowered. Even though dielectric losses also increase with higher voltages, losses in the inner conductor make up most of the losses in power cables.

Some reasons to give HV power cables priority over OHLs can be:

- limited space for OHLs in urban areas,
- limited social acceptance for OHLs,
- installation in submarine environment,
- possible reduction of operating costs under certain conditions [BP10],
- lower failure rates compared to OHLs [HDS10],
- reduced exposure of magnetic fields compared to OHLs [Beno9].

Nonetheless, choosing an appropriate transmission system always depends on the specific situation. Giving a generalized recommendation is not sensible.

With the advantages listed above, increasing experience and stability of HV power cable systems, HVAC cables will remain a crucial element in future energy grids worldwide. As the maximum transmission voltage is fixed by OHL networks, it is in most cases more reasonable to increase the ampacity of a cable first instead of further increasing the operating voltage [Meu12, p. 15].

1.2 HIGH VOLTAGE POWER CABLES

Figure 1.1 shows a schematic drawing of a power cable. Even though there are many different power cable designs, some basic components are almost always present.

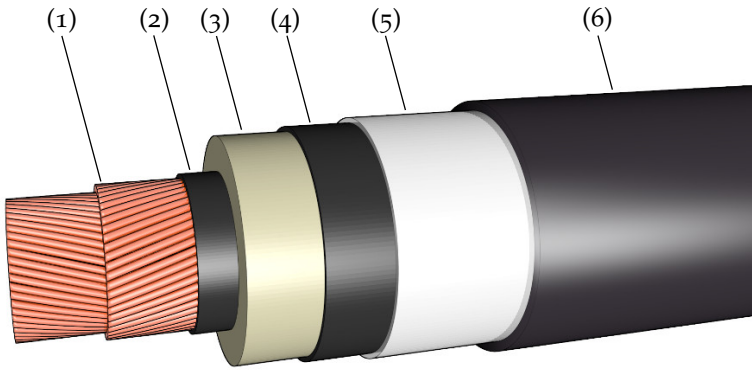

Figure 1.1: Schematic drawing of an exemplary HV power cable; (1) inner conductor; (2) conductor screen/shield; (3) insulation; (4) insulation screen/shield; (5) metallic sheath or screen wires; (6) polymeric outer sheath

The inner conductor (1) carries the current and is typically made of highly conductive metal such as copper or aluminum. It is designed to have minimum losses and enable bending of the cable. Later, in Section 3.2, a detailed description of stranded and segmented conductors, typically used for HV

power cables, is given. Conductor shield and insulation shield (2 & 4) allow a homogeneous radial electric field distribution in the insulation material (3). Moreover, they avoid gaps in regions of strong electric field distributions (in between conductive parts) [PO99, p. 31]. They typically consist of a semi-conductive material like graphite. If needed, additional radial water barriers can be applied to prevent water entering from the cable's surrounding. The insulation for HV and extra high voltage (EHV) cables is either build of impregnated paper or extruded polymer. In terms of estimating the long-term behavior of a cable, this component is the most critical one [PO99, p. 30]. The metal sheath of a cable (5) has multiple tasks and its design strongly depends on parameters like: rated short-circuit current, laying pattern of the cable system, environment and the maximum allowed weight of the cable. Typical designs include: copper or aluminum wires (with an optional copper counter helix) in combination with a thin aluminum laminated sheath, a lead sheath, a solid aluminum sheath (optional: spiral or ring corrugated) or steel pipes. The latter is used for gas pressure or high-pressure oil cable systems [PO99, p. 34]. Some of its main purposes—given by [PO99, p. 32]—are to:

- return the capacitive charging current,
- conduct fault currents,
- reduce the electrical influence on the surrounding in case of a fault.

The outer polymeric sheath (6) serves as a mechanical protection for the metallic sheath. In addition thereto, it protects the cable against corrosion by water. Usually another corrosion protection made of bitumen-based compounds is necessary to completely protect the cable sheath from moisture [PO99, p. 35].

1.2.1 *Definition of Target Value & Losses*

In this thesis, the focus lies on the evaluation of losses due to *Joule heating* in the inner conductor, also called *ohmic heating* or *resistive heating*. As stated 2016 by the International Electrotechnical Commission (IEC), *Joule losses* in transmission cables account for approximately 2.5 % of the transmitted power [IEC06a]. Reducing these losses by only a fraction, can prevent wasting tremendous amounts of electrical energy and hence tons of CO_2 emitted worldwide. Electric current $\underline{I}$—given in A—in combination with a conductor's resistive characteristic causes *Joule heating*. This undesirable heat loss P_C—given in W/m—limits the current carrying capacity of a wire or cable by heating it up [And97, p. 115]. This further increases its electrical resistance and thereby the thermal load on the conductor or cable. The heat generated by *Joule losses* is not further used and will escape the cable by heat convection, heat conduction and radiation. The efficiency of heat dissipation depends on multiple cable system parameters such as laying depth, surrounding material, relative position to other phases and so on [And05]. Losses due to thermodynamic effects such as the *Seebeck effect*, *Peltier effect* and the *Thomson and Seebeck effect* are not part of this thesis, as their contribution to the overall losses in power cables is negligible, if present at all. Nevertheless, for the measurement of small voltages these effects should be known and reviewed, when temperature gradients are present in the measurement setup. In case of HV power cables, one way to subdivide the total losses is shown in Figure 1.2.

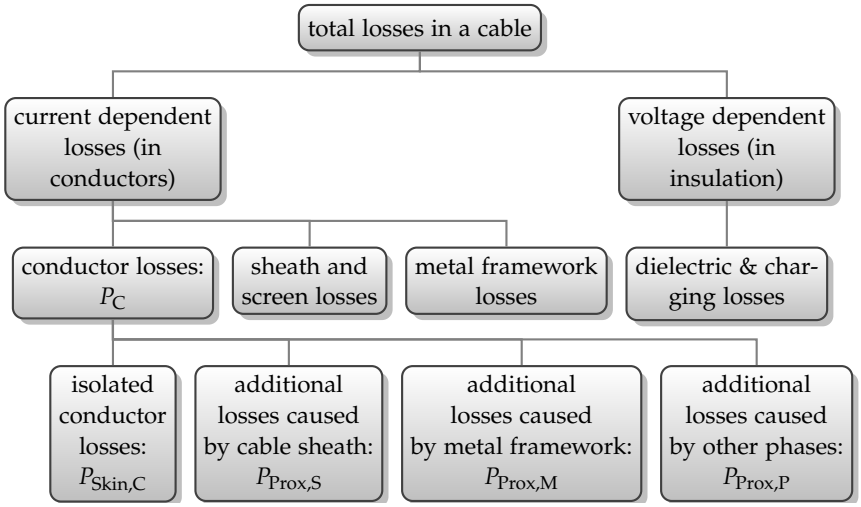

Figure 1.2: Classification of losses in HV power cables including information taken from [Meu12; Bra96]; the interaction between both (e.g.: current dependent losses heat up the insulation and increase voltage dependent losses) are neglected

The total losses in a cable consist of losses in the dielectric of the cable—voltage dependent—and losses related to the current in conductors [Meu12]. In this thesis all materials are linear and losses and resistances are always given per-unit length for better comparison. In case of non-magnetic conductors, current dependent losses are proportional to the magnitude of the total current squared times the resistance of the conductor[2]. Current dependent losses can arise in all conducting materials near the cable. Hence, they are further subdivided into losses in the actual conductor P_C, losses in the sheath/screen of the cable and losses in nearby metal framework, which is not part of the cable itself. Sheath and metal framework losses additionally depend on their grounding condition.

It will be shown later, that all of these losses can influence each other. Because the main share of losses appears in the inner conductor P_C, the following work focuses exclusively on these losses. In Figure 1.2 P_C is further subdivided[3] into:

- losses apparent when the conductor is not affected by any other conducting material or currents (isolated) $P_{Skin,C}$[4],
- losses whose origin is the proximity to the sheath or sheath currents $P_{Prox,S}$[5],
- losses whose origin is the proximity to metal frameworks of any kind $P_{Prox,M}$,
- losses whose origin is the proximity to other phases of the cable system $P_{Prox,P}$.

The geometrical configuration of inner conductor and sheath for a specific cable is known and remains constant along the cable system above a certain

2 This neglects heating effects which are typically negligible [Arn41b, p. 53]
3 Note that sheath losses and metal framework losses can be subdivided analogously.
4 "Skin" and "Prox" are abbreviations for the *skin effect* and *proximity effect*, which are extensively described in Chapter 3.
5 Later it will be shown that these additional losses can be neglected for typical power cable sheath geometries. This was also shown exemplarily in [HR15].

manufacturing tolerance. Contrary thereto, the location of additional metal framework and other phases depends on the installation location and actual laying configuration of the system. These losses—$P_{\text{Prox,M}}$ and $P_{\text{Prox,P}}$—will be disregarded as they will vary for every phase and every specific application of a given cable. As the sheath currents can also vary under operation and hence change their influence on $P_{\text{Skin,C}}$, this thesis primarily focuses on $P_{\text{Skin,C}}$ only. In general, these losses of the inner conductor—which is the conductor under test (CUT)—are given in W/m and are defined as:

$$P_{\text{CUT}} = P_{\text{Skin,C}} = \frac{1}{l} \iiint_V p_{\text{V}} \cdot \mathrm{d}V = \frac{1}{l} \operatorname{Re}\left(\iiint_V \underline{\vec{E}} \cdot \underline{\vec{J}}^{*} \cdot \mathrm{d}V \right) \quad . \tag{1.1}$$

In Equation (1.1), adapted from [Alb11, p. 104] and [LŠT66, p. 18], l is the conductor length in m, p_{V} is the volumetric loss density in W/m^3, Re takes the real part of the expression, $\underline{\vec{E}}$ is the intensity of the electric field in V/m, $\underline{\vec{J}}$ is the current density in A/m^2, V in combination with the integral symbol indicates a volume evaluation of the integral. The volume in this case is the complete CUT. Complex vector quantities are root mean square (rms) values and * indicates the complex conjugate. These field quantities depend on location and angular frequency ω. In most cases 2D problems and homogeneous conductors are considered. With the conductor axis being parallel to the z-axis and *constitutive relation*

$$\underline{\vec{J}} = \sigma \underline{\vec{E}} \tag{1.2}$$

Equation (1.1) simplifies to Equation (1.3):

$$P_{\text{CUT}} = \sigma \iint_A \|\underline{E}_z\|^2 \cdot \mathrm{d}\vec{A} = \frac{1}{\sigma} \iint_A \left\|\underline{J}_z\right\|^2 \cdot \mathrm{d}\vec{A} \quad . \tag{1.3}$$

Above, σ is the electrical conductivity in S/m and A in combination with the integral symbol indicates a surface evaluation of the integral. The surface in this case is the cross section of the CUT. Underlined symbols indicate complex quantities. The double vertical lines take the norm of the expression embraced. The resistance—DC and AC—of a conductor in Ω/m can generally be derived from its losses by

$$R = \frac{P}{\|\underline{I}\|^2} \quad , \tag{1.4}$$

where P can be a placeholder for any of the losses mentioned previously and $\underline{I}$ is the total rms current through the regarded cable part and defined by:

$$\underline{I} = \iint_A \underline{\vec{J}} \cdot \mathrm{d}\vec{A} \quad . \tag{1.5}$$

In measurements $\underline{I}$ is the test current through the CUT and used as the reference phase. Even though the general case is always given, theoretically $\underline{I}$ is purely real in these cases. All vector quantities are given in rms as only the time-harmonic case is investigated in this thesis. If no magnetic materials affect the conductor and thermal heating is neglected, the resistance of a conductor is independent of the current [Arn41b, p. 53]. Under operating conditions HV cable sheaths are typically grounded on one side, on both sides or cross-bonded. Typical cable sheath geometries do not influence P_{C}

significantly. This will be further shown in Chapter 4.

Concluding one can say that the target value of this thesis is the isolated AC resistance, respectively the AC losses of the inner conductor only. To include or measure losses originating from other conductive parts nearby is not desirable as these losses can vary in every configuration or operating condition.

1.2.2 *Standards for Power Cable Ratings*

There are different standards available for calculating the current carrying capacity of a power cable. The IEC released its most recent power cable rating standard in 2006 [IEC06b] with an amendment from 2014 called IEC 60287-1-1:2006/AMD1:2014 [IEC14]. In 2005, the *international council on large electric systems* called Conseil International des Grands Réseaux Électriques (CIGRE) released brochure B1.03, which deals with the calculation of losses, especially for large segmented power cable conductors [Cig05]. The related standard from the Institute of Electrical and Electronic Engineers (IEEE) was released in 1994 and reaffirmed in 2014 [IP94].

While all these brochures are giving advice on how to calculate these losses up to certain cross sections and the IEC giving an empirical value called k_s factor[6], there is no standard for the measurement of the AC resistance of a power cable. Nevertheless, CIGRE Working Group B1.03 points out different measurement methods and techniques to improve accuracy [Cig05, p. 45]. This shortage is currently being tackled by CIGRE Working Group D1.54, which makes an assessment of available measurement methods and recommends appropriate methods to determine AC and DC losses of power cables with large cross sections by measurements [Cig18][7].

Table 1.1—taken from the most recent IEC standard—provides k_s factor values, which should be used for loss calculation if no measurement can be performed. Function argument k_s is used for the calculation of the *skin effect* factor argument x_s.

Depending on the value of x_s Equation (1.7), Equation (1.8) or Equation (1.9) is used to calculate the *skin effect* factor y_s.

$$x_s = \sqrt{\frac{\omega \mu_0}{\pi R_{DC}} k_s} \tag{1.6}$$

$$\text{For } 0 < x_s \leq 2.8: \quad y_s = \frac{x_s^4}{192 + 0.8 x_s^4} \tag{1.7}$$

$$\text{For } 2.8 < x_s \leq 3.8: \quad y_s = -0.136 - 0.0177 x_s + 0.0563 x_s^2 \tag{1.8}$$

$$\text{For } x_s > 3.8: \quad y_s = 0.354 x_s - 0.733 \tag{1.9}$$

$$\frac{R_{AC}}{R_{DC}} = 1 + y_s \tag{1.10}$$

6 A solid round conductor has by definition a k_s factor of 1, whereby a conductor without AC losses would have a k_s factor of 0.

7 At this moment, it shall be pointed out once again that the author took direct part in creating and editing this CIGRE brochure. Any information used from the brochure is cited appropriately. If no work is cited and found in the CIGRE brochure as well, it is the author's own work.

Equation (1.10) neglects the *proximity effect*. R_{DC} is the DC resistance in Ω/m at 20 °C, R_{AC} is the AC resistance in Ω/m at 20 °C, ω is the angular frequency[8] in s^{-1} and μ_0 is the permeability of vacuum in $Vs/(Am)$.

Table 1.1: k_s values from IEC 60287-1-1:2006/AMD1:2014; *Milliken* conductors are in the focus of this work and are described in detail in Section 3.2.2

type of conductor	conductor insulation system	k_s
Copper (Cu)		
Round, solid	All	1.00
Round, stranded	Fluid/Paper/PPL	1.00
Round, stranded	Extruded/Mineral	1.00
Round, *Milliken*	Fluid/Paper/PPL	0.435
Round, *Milliken*, insulated wires	Extruded	0.35
Round, *Milliken*, bare unidirectional wires	Extruded	0.62
Round, *Milliken*, bare bidirectional wires	Extruded	0.80
Sector-shaped	Fluid/Paper/PPL	1.00
Sector-shaped	Extruded/Mineral	1.00
Aluminum (Al)		
Round, solid	All	1.00
Round, stranded	All	1.00
Round, *Milliken*	All	0.25

Figure 1.3 shows the resulting resistance ratios according to the IEC standard for different conductor types using the conductivities defined later in Table 2.3.

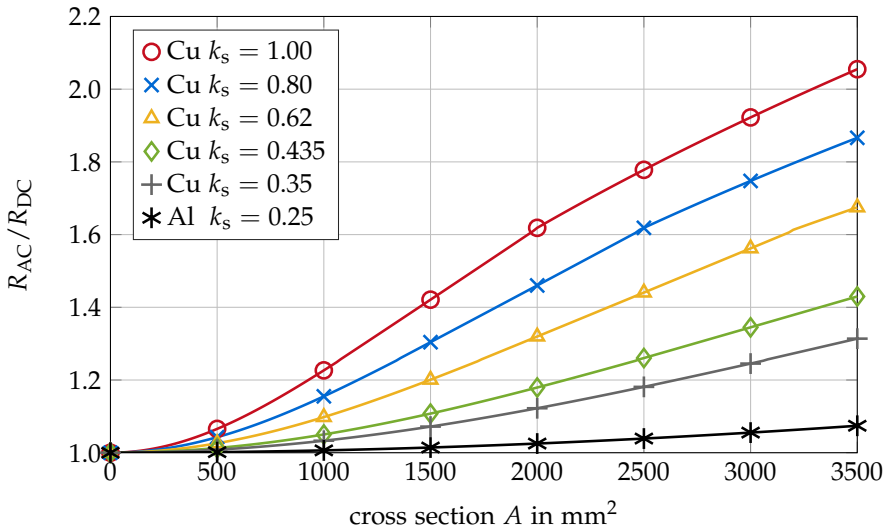

Figure 1.3: Resistance ratio at 50 Hz plotted over conductor cross section for different k_s factors at 20 °C according to IEC standard 60287-1-1:2006/AMD1:2014

The k_s factors are approximations and qualitatively show the differences in losses for different conductor types. Nevertheless, the recent standard recommends a measurement for the determination of the AC resistance [Cig05,

8 The angular frequency is defined by frequency f with $\omega = 2\pi f$. Unit Hz is defined as $1/s$.

p. 52; IEC14, p. 5]. The reason is that the manufacturing of a complex conductor—especially the condition of the strand insulation—has a great influence on the performance, which can hardly be assessed without measurement. The construction of segmented conductors is extensively discussed in Section 3.2.

1.2.3 *State of the Art AC Resistance Measurement Methods*

A variety of methods is available for AC loss determination of power cables. Electric methods derive *Joule losses* from a direct measurement of electrical parameters, whereas calorimetric methods derive *Joule losses* from a rise of conductor temperature. For both methods multiple variants are available. The most important ones are briefly sketched below. The measurement of the magnitude and phase of the current through the CUT is typically conducted with high accuracy current transformers, Rogowski coils or by determination of the voltage drop across a resistance standard with low inductance (also called shunt resistance) [Gra79, p. 102; Ols+99]. Independent of the chosen method, *Joule losses* in other metallic parts can influence the measurement. This is further discussed in Chapter 4. For both approaches, if the measurement is not performed at operating temperature, the results have to be extrapolated to the maximum operating temperature, which is typically 90 °C for cables with polymeric insulations. This is shown in Section 2.4.2. Nevertheless, measurements at operating temperature can be advantageous as some conductor properties—which affect *Joule losses*—potentially change with temperature [Gra79, p. 102].

1.2.3.1 *Electrical Methods*

In general, when using electrical methods, great care must be taken to avoid the influence of electromagnetic fields upon the *measured* voltage, due to pick-up loops formed by the voltage lead wires, the CUT and the measurement system [Gra79, p. 102]. This effect is extensively discussed in Chapter 4 and presents the main challenge of this method. Measurements with power meters are often impracticable, because the voltage drop across typical HV cable conductors often lies in the nV to µV range for short sample lengths and practical measurement currents [Däu+00]. Figure 1.4 shows different options available for current and voltage measurement. The order of the following variants of electrical measurement methods is chronological regarding their first use. More information on these principles can be found in [Cal13].

AC BRIDGE METHOD First AC resistance measurements were performed with Heaviside bridges in 1915, in 1935 with Arnold bridges and later in 1978 with precision Kelvin bridges [Arn35; Kat+78; Liu16, p. 10]. Some power cable measurements using AC bridges can be found in [FG33; MBH51; Ast55; YD63; CMR77]. The basic working principle of an AC bridge is a comparison of the unknown resistance—the CUT—to multiple known and calibrated reference resistances. The resistances are commonly arranged in different legs of a bridge circuit. When a state of balance is reached—the resistances in both legs are identical—the unknown resistance can be calculated with the help of the known resistances [Cal13, p. 100].

AC POTENTIOMETER Measurements with AC potentiometers have been presented in [Sal48; ME49; BM68; Jac70]. According to [Cig05, p. 46], AC potentiometers only have a limited applicability because of the long time it takes for them to be properly tuned. AC potentiometers basically compare a known voltage to an unknown voltage and change the resistance of the potentiometer—similar to an AC bridge—until it draws no more current from the measurement circuit. This indicates a balanced state and can provide the phase and magnitude of the unknown voltage signal [Jac70].

LOCK-IN AMPLIFIER Lock-in amplifiers use a reference signal, in this special case the conductor current, which provides the measurement frequency and then amplify the signal of interest—the voltage drop over the CUT—which has the same frequency. It provides information about magnitude and phase of the *measured* signal [Sta95]. Measurements performed with Lock-in amplifiers are shown in [Ols+99; Juu+11] and are also used for AC loss measurements of superconductors. In [Cig05, p. 48] the application of a Lock-in amplifier in combination with compensating coils is described for cable conductors with large cross sections.

ADC AC VOLTMETERS This variant is used throughout this work and is based on digitizing the *measured* voltage signal with the help of an analog-to-digital converter (ADC). Afterwards, a fast Fourier transform (FFT) makes the voltage of the base frequency analyzable. It is described in detail in Section 2.2 and was first presented 2011 in [RSS11a] and [SKP11a]. More measurement results of power cable conductors using digital sampling voltmeters were later shown in [SKP11b; Sch+12; Sjö13; Sch+14; Sch+15a; Sch+15b].

METHODS TO IMPROVE ACCURACY CIGRE brochure [Cig05, p. 48] proposes different methods to increase the accuracy of electrical measurements, as the inductive part of the *measured* voltage can be many times greater than the resistive part in some measurement setups. It is recommended that one can either superimpose a suitable signal compensating the *measured* inductive part or eliminate the inductive component by using FFT [Cig05, p. 48].

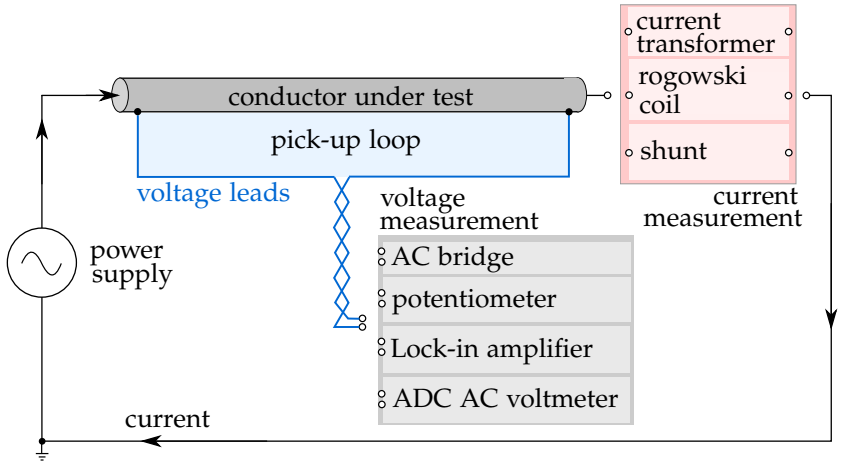

Figure 1.4: Overview of electrical methods for the AC loss measurement of power cables; the light blue rectangular area indicates the dimensions of the pick-up loop

1.2.3.2 *Calorimetric Method*

As *Joule losses* result in conductor heating, one can derive the conductor resistance from temperature changes. This method is referred to as the calorimetric approach. Figure 1.5 shows an exemplary measurement circuit. In this case, for an accurate loss calculation one needs accurate temperature measurements, a sufficient sample length and thermal insulation[9] at the ends to avoid temperature dissipation along the cable axis. Moreover, the exact value of thermal conductivity of the insulation and multiple temperature sensors along the CUT are required [Cig05, p. 52; Sch+15a].

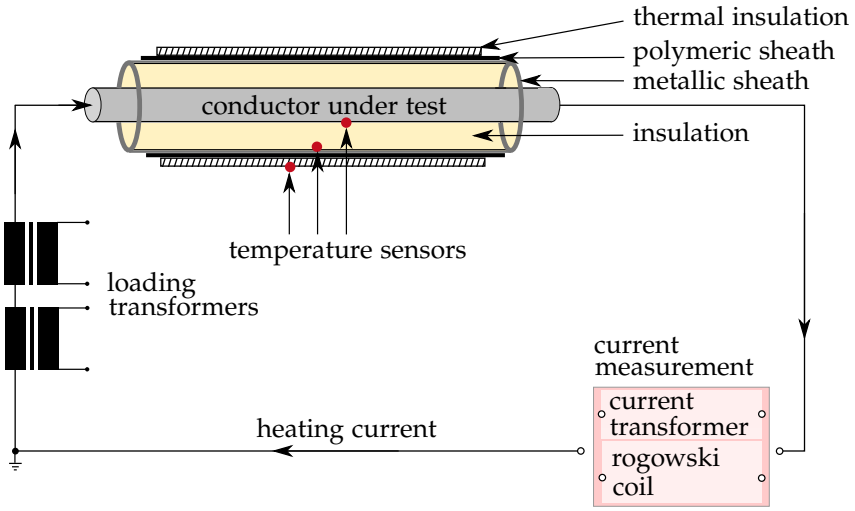

Figure 1.5: Schematic drawing of the calorimetric method for AC loss measurements of power cables; typically multiple temperature sensors are applied along the conductor axis [Cig05, p. 52]; here, the temperature sensors are attached on the surface of: CUT, conductor insulation and thermal insulation

According to [Cig05, p. 51] the AC resistance of the CUT can be calculated by:

$$R_{\mathrm{AC}} = \frac{\Delta T}{\|\underline{I}\|^2 \cdot R_\lambda} \quad . \tag{1.11}$$

In the equation above, ΔT is the temperature drop across the conductor insulation or thermal insulation in K and R_λ is the specific thermal resistance in K m/W of the material between both temperature measurement points (e.g.: conductor insulation or thermal insulation). As sheath currents generate losses as well, which influence the temperature measurement, prior to measurement one has to consider how to electrically connect the sheath or remove it if necessary.

1.2.3.3 *Comparison of Electrical and Calorimetric Method*

Table 1.2 shows a comparison of the electrical and calorimetric method. It shall be pointed out that some limitations depend on the cable and conductor properties. Others are of practical nature rather than physical limitations (e.g.: measurement of multiple frequencies). Larger conductor cross sections generally lead to smaller AC resistances and for a given current, less conductor heating and a smaller voltage drop. The latter

9 A thermal insulation is optional but can speed up bringing the conductor into its thermal steady-state.

increases the demand for an accurate voltage measurement for the electrical method. Less conductor heating also makes it more difficult to bring the cable into a thermal steady state condition when using the calorimetric method. Linear power conductors—no use of non-linear materials (e.g.: diamagnetic materials such as iron)—have a current independent AC resistance. Using smaller currents is more cost-efficient and does not require special connectors designed for larger currents. In addition, the use of smaller currents can be advantageous if non-linear materials are in proximity to the measurement circuit. Saturation in non-linear materials caused by large magnetic fields could make the measurement current-dependent. On the other side, larger test currents allow AC resistance measurements at operating temperature and increase the magnitude of voltage drop over the CUT, which can be advantageous.

Table 1.2: Comparison of electrical and calorimetric measurement method for AC loss determination of power cables

method	advantage	disadvantage
Electrical Methods	· fast preparation and measurement · currents $< 10\,\mathrm{A}$ possible · measurement of multiple frequencies possible · very short sample lengths measurable	· pick-up loops susceptible to parasitic electromagnetic fields · susceptible to thermoelectric voltages
Calorimetric Methods	· no pick-up loops · loss measurement at operating temperature possible	· time consuming to bring the cable into thermal steady-state (hours up to days) · large currents are necessary to heat up the cable (kA range) · larger logistical effort necessary

In the end it depends on the user to choose an appropriate measurement technique. In any case, the user should be informed about possible measurement errors and limitations of the applied measurement technique. Due to its inherent advantages—short preparation time enabling a cost-efficient measurement of the AC resistance at multiple frequencies—the electrical method with an ADC sampling voltmeter is used in this thesis.

1.2.3.4 *Similar Measurement Techniques*

It is reasonable to check for similar electrical measurement methods, where small voltage drops are measured, to profit as much as possible from available knowledge during this investigation. Therefore the next section lists some methods, which also focus on the measurement of small voltages.

ACPD A four-point alternating current potential drop (ACPD) measurement is a non-destructive technique used to determine properties of conductive materials such as thickness, electrical conductivity, magnetic permeability and the size of cracks in samples [BB07, p. 817]. A typical measurement probe of this method is shown in Figure 1.6.

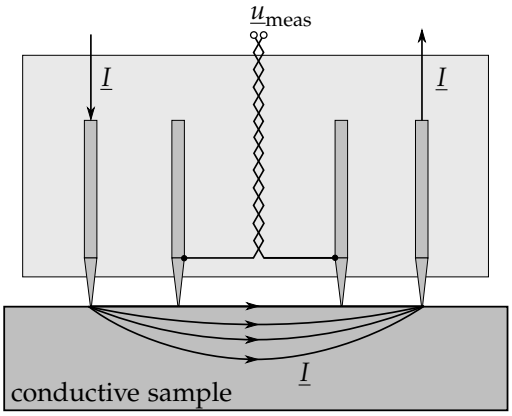

Figure 1.6: Schematic drawing of the ACPD method with test current $\underline{I}$ and *measured* voltage $\underline{u}_{\text{meas}}$ (own drawing based on [BB07, Fig. 1])

A small time-harmonic current—usually in the range of some ampere—is injected into the sample at a frequency of some kHz. From the voltage drop measured with two additional electrodes and an accurate mathematical model, one can derive the sample's electrical parameters. Even though AC brings along difficulties in the measurement, it can be the preferred choice compared to direct current potential drop (DCPD) measurements. In large, highly conductive samples, the voltage drop caused by the DCPD method can be too small for an accurate measurement. When using the ACPD method, the current flow is restricted to a small area beneath the surface. The tendency of the current to flow primarily near the surface is called *skin effect* and is further discussed in Chapter 3. Preventing the current to flow homogeneously through the whole sample cross section reduces the available cross section for the current and hence results in a larger voltage drop. Thereby the measurement accuracy is increased. Choosing the DCPD method, one would have to increase the magnitude of the current to increase the voltage drop, which can result in unwanted sample heating, changing the sample's properties [Mat10]. Theory and recommendations from researches of this technique—especially for contacting voltage lead wires and the positioning of the pick-up loops—are reconsidered in Chapter 4.

CURRENT SHUNTS Another application where an accurate voltage measurement is necessary is in current shunts. A current shunt—also called resistance standard—is a low resistance, low inductance circuit element with an accurately known resistance and high temperature stability. Some low inductance current paths used in shunt designs are shown in Figure 1.7.

Current shunts are mostly made of manganin, which is an alloy with a very low temperature coefficient α_T of only $10 \times 10^{-6}/\text{K}$ [RSF93, p. 2.26]. The principle of current measurements with a current shunt is based on keeping the *measured* inductance as small as possible to reduce phase angle errors [LSW04, p. 2]. Nevertheless, to achieve a sufficient voltage drop, one has to form a current path with significant resistance. Pick-up loops in cur-

rent shunts—designed to capture a minimum of magnetic flux—will also be reconsidered in Chapter 4. Basic considerations for current shunts can be found in [Sil30; WS70; Bey86, p. 317; Sch10, p. 179]. The design of a current shunt and the position of the voltage lead wires strongly depend on the application and is in detail described in [Sil30; Sch10; Cal13, p. 191].

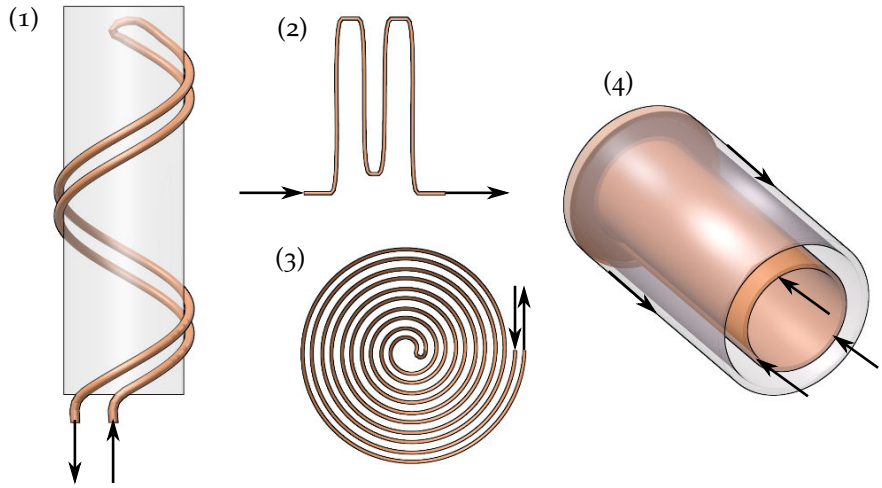

Figure 1.7: Exemplary low inductance current paths for resistance standards; (1), (2) & (3) show bifilar windings to reduce external magnetic fields; (4) shows a coaxial setup, where—in case of perfect concentricity—magnetic fields are only present inside the conducting domains and between inner and outer tube; the arrows indicate the direction of current flow $\underline{I}$

OTHER INVESTIGATIONS Additional insights related to interpretation of voltage signals and magnetic field distributions in close vicinity to complex conductors are obtained from measurements of superconductor and also reconsidered in Chapter 4.

1.3 MOTIVATION AND GOAL OF THIS THESIS

Joule losses due to the AC resistance of a power cable conductor mainly limit the current carrying capacity of a cable system. Therefore—to increase efficiency and decrease the overall costs of a cable system—it is vital to reduce the AC resistance as much as possible [DM07]. To lower AC losses in the conductor, which add up to inevitable DC losses, special conductor designs are used. For HV power cables with cross sections larger than 1000 mm^2, segmented conductors—also called *Milliken type* or *M-type* conductors—are used [Nex11]. Their construction is described in detail in Section 3.2.

AC loss determination of segmental conductors by measurement started with their first use in the mid of the 20th century. Some often cited references listing results for different *M-type* designs are [Sal48; Wis48; ME49; MBH51; BM68; CMR77].

As shown previously, some values are embedded in the recent IEC standard. These values have been obtained empirically. Nevertheless, AC losses of identical designs can vary from manufacturer to manufacturer and even from cable to cable depending on manufacturing quality and stability. This is depicted in Table 1.3. Designs which should have an identical AC resis-

tance according to the IEC standard show significant variations in their resistance ratios at 50 Hz. An extensive collection of published AC resistances of *Milliken* conductors can be found in Appendix A.1. In addition to that, new optimized conductor designs, variations in the manufacturing processes and conductor cross sections reaching up to 3500 mm^2 demand for reliable ways to access the *Joule losses* of such conductors. Hence, to accurately determine AC losses, measurements are the preferred choice [IEC14, p. 5]. As recommended by CIGRE Working Group B1.03 this test could be performed when the cables are type tested [Cig05, p. 52]. Often, the customer demands a proof of conductor performance by an acceptance test anyway. Accurate characterization of the used conductor is also of great importance as subsequent ampacity calculations often depend on the AC resistance measurement. Imprecise measurements can cause wrong thermal dimensioning of a cable or complete cable system. At worst this results in irreparable damage of equipment.

Table 1.3: Collection of some published R_{AC}/R_{DC} ratios for *Milliken* conductors (no *proximity effect*); A is the conductor cross section; T is the temperature of the conductor in °C; in [DM07] measurement results including *proximity effect* are shown[10]

A in mm^2	conductor material	design/ insulation	f in Hz	T in °C	R_{AC}/R_{DC}	reference
1600	Cu	blank	50	20	1.23	[Cig05, p. 14]
1600	Cu	blank	50	20	1.04	[CMR77, Dis]
2000	Cu	blank	50	20	1.24	[Cig05, p. 14]
2000	Cu	blank	50	20	1.495	[RSS11a]
2000	Cu	blank	50	80	1.16	[Joa98, p. 55]
2000	Cu	blank	50	80	1.23	[Joa98, p. 55]
2000	Cu	enameled	50	20	1.04	[Cig05, p. 14]
2000	Cu	enameled	50	90	1.04	[DM07]
2000	Cu	oxidized (hp)	50	80	1.137	[Joa98, p. 55]
2000	Cu	oxidized (lp)	50	80	1.086	[Joa98, p. 55]
2500	Cu	oxidized (hp)	50	80	1.23	[Joa98, p. 57]
2500	Cu	oxidized (lp)	50	80	1.152	[Joa98, p. 57]

Table 1.2 displayed advantages and disadvantages of different available measurement methods. Because of inherent advantages of electrical methods—especially when using fast ADC sampling voltmeters—multiple measurement systems have been developed at the Department of High Voltage Engineering engineering of *Technische Universität Berlin*. The first version was presented in [SKP11a]. A recent successor version—used for measurements in this thesis—is described in Section 2.2. To make use of the advantages given by the electrical method, one has to thoroughly revise the measurement circuit. Measurements of electrical quantities on complex conductors are related to many theoretical consideration and practical limitations. Due to the nature of non-conservative electric fields at AC, the

10 The k_s factor could not be calculated in most cases because often the DC resistance or lengths was not available. Moreover, if no frequency was given, the typical power frequency of the country, where the investigation was performed was assumed. If no temperature was given in the reference, then 20 °C was used. "Dis" in the reference stands for discussion, "hp" stands for high pressure (mechanically) and "lp" for low pressure.

voltage measurement becomes a complex task, which is to be understood completely to avoid the introduction of measurement errors.

Therefore, the goal of this work is the theoretical discussion and practical application of the electrical measurement method using ADC sampling voltmeters to accurately determine AC losses of complex conductor designs. When set up, performed and interpreted correctly, the electrical method makes the evaluation of recent HV power cable design much more efficient compared to all other recently available measurement methods. Even though the focus lies on AC losses, inevitable some remarks and recommendations about the measurement of DC losses are also given.

2 METHODOLOGY

> The first principle is that you must not fool yourself...
> and you are the easiest person to fool.
> *Richard Feynman*

The purpose of this chapter is to provide the reader with definitions of used technical terms and material parameters. Additionally, the used measurement system is characterized in detail with the aim of making the results more transparent and reproducible. The accuracy of the used measurement system is determined afterwards and it is shown how measurement values are interpolated and corrected to different temperatures. At the end, the tool used for numerical simulations and basic simulation principles are presented.

2.1 DEFINITIONS

To allow better understanding for the reader, in the following some important synonyms and technical terms used throughout this work are described. This helps to prevent confusion in complex theoretical considerations and searching for previously defined terms.

2.1.1 *Synonyms*

Table 2.1 shows the used synonyms in this thesis to improve understanding.

Table 2.1: Synonyms used throughout this thesis

expression	used synonym(s)
analytical solution	explicit solution, exact solution, closed-form solution
end effect	*terminal effect*
in-phase component	real part of the component
in-plane component	vector component into the paper plane
Joule heating	*resistive heating*, *ohmic heating*
measured losses/resistance	*apparent* losses/resistance
Milliken conductor	*Milliken type* conductor, segmental conductor, segmented conductor, *M-type* conductor
out-of-phase component	imaginary part of component, quadrature component
voltage lead wires	voltage leads
stranding	twisting, pitching
strand	wire

2.1.2 *Technical Terms*

Table 2.2 shows the used terms in this thesis to improve understanding.

Table 2.2: Important technical terms used in this thesis

term	short explanation
annulus	a ring-shaped selection (e.g.: annulus of wires refers to wires with the same distance to the center)
blank wire	a wire without insulation
cable core	geometric center of a cable
core conductor	the central conductor in *M-type* conductors, which is solid or stranded but not segmented
core wire	the innermost single wire of a bundle or segment
current crowding	for conductors with corners, the current distribution also depends on the sharpness of these corners under AC (Section 3.1.3.10)
CUT	*conductor under test*; this is the conductor of interest and in most cases the inner conductor of a cable
eddy current	a general term to refer to circular flowing induced currents
edge effect	refers to the influence of the sharpness of corners on the current distribution (e.g.: in rectangular conductors; also see *current crowding*)
enameled wire	a wire with a thin insulation made of coating usually of some µm thickness
end effect	refers to a change of field quantities due to a change of conductor geometry or properties at the end of a sample
go circuit	is a circuit where two or more conductors are connected in parallel
in-phase magnetic field	magnetic field components, which have the same phase as the overall current $\underline{I}$, which generates them; induces inductive (quadrature/out-of-phase) voltage components in the pick-up loop
layer	collection of wires; in stranded conductors this refers to wires in one annulus
lay length	for stranded conductors, this is the distance where every wire completed one helically turn around the center of rotation
measured/apparent ...	losses, voltage or resistance is that value indicated by the measurement system but does not necessarily have a physical meaning for the CUT
out-of-phase magnetic field	magnetic field components, which are 90° phase-shifted to the total current $\underline{I}$, which generates them; induces resistive (in-phase) voltage components in the pick-up loop
normalized	all values are divided by the maximum value

oxidized wire	a wire with a thin, breakable oxide insulation; formed naturally on aluminum and copper wires at ambient air or by additional processing of copper wires
pick-up loop	a loop formed by voltage lead wires, CUT and measurement system together, which is susceptible to electromagnetic induction
return circuit	is a circuit, where the return conductor for the current path is included
segment	pie shaped conductor bundle formed by mechanical compression used in *M-type* conductors
segment core	center of a conductor segment (at the position of the core wire)
stranding	helically arranging wires around the center of a conductor to increase mechanical stability of bundled conductors
true/real ...	losses or resistance of the CUT; physical meaning is linked to *Joule heating*
voltage tap-offs	contact points of voltage leads on the CUT
virtual measurement	measurement performed in the finite element method (FEM) simulation; it delivers the same value, which would be measured in reality with the ADC AC voltmeter

2.2 USED MEASUREMENT SYSTEM

Even though the most important resistance values are those at DC and at operating frequency, which is 50 Hz or 60 Hz, measurements in this investigation are typically performed in the frequency range from 0 Hz to 300 Hz. This offers some advantages over other methods. First, frequency variable measurements enable the noiseless interpolation of the resistance at 50 Hz or 60 Hz. Second, the measurement circuit can be evaluated more thoroughly when using a conductor, where the analytical solution is available. As parasitic effects on the pick-up loop will increase with frequency, one can benchmark different measurement circuits more easily at higher frequencies, where some of these effects become more significant. Third, AC resistance determination at higher frequencies can give insights into the impact on losses from harmonics. Moreover, as shown in Section 3.1.2.6 the AC resistance of a conductor or a set of conductors remains unchanged at higher frequencies, if the geometric dimensions are scaled accordingly. Theoretically, this creates the opportunity to investigate some effects in large conductors on smaller downscaled conductor samples with increased frequency as the resulting AC resistance will be identical.

The measurement cycle is automated, taking only a few minutes for 15 measurements in the frequency range from 0 Hz to 300 Hz. The maximum measurement frequency is limited to approximately 1000 Hz. The measurement system was first presented in [SKP11a] and also later in [SKP11b; Sch+12; Sch+14; Sch+15a; Sch+15b]. It is shown in Figure D.1.

2.2.1 *Setup of the Measurement System*

A schematic drawing of the measurement system is shown in Figure 2.1. It basically consists of a signal generator (1), a power amplifier (2), a current shunt (3), two ADCs synced by a common clock (4) and a data processing unit. The signal generator provides a frequency variable, sinusoidal current, which is then amplified. The power amplifier delivers a test current with a maximum rms of 11 A. The small test current prevents typical high voltage power cables from heating up. To access losses at operating temperature, the *measured* values have to be adjusted to or ideally be obtained at operating temperature in a climate chamber. Over the high resistance entrances of the ADCs, the voltage is measured and the current and voltage signals are sent to the data processing unit. Only the base frequency is evaluated using FFT algorithms.

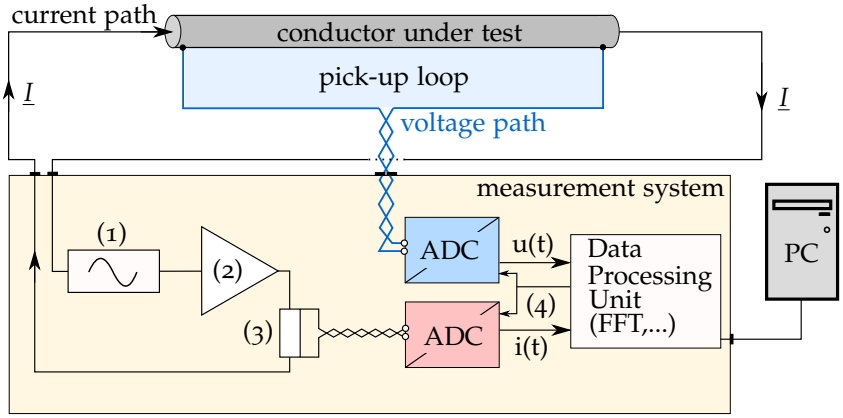

Figure 2.1: Schematic drawing of the used measurement system (yellow box); (1) variable frequency voltage source; (2) power amplifier; (3) current shunt; (4) sync clock

With test currents of only a few ampere, sample lengths down to a few meters only and cross sectional sizes reaching over 2500 mm^2, the voltage measured by the ADC lies in the µV range.

2.2.2 *Accuracy of the Measurement System*

ERROR OF THE MEASUREMENT SYSTEM The resistance is calculated from the measurement of current and voltage. Hence, its accuracy depends on the accuracy of these measurements. The current measurement is performed by an ADC voltmeter on a resistance shunt. The voltage signal is directly measured by an ADC sampling voltmeter. Instead of assessing the accuracy of every involved part separately, it was obtained by the following procedure:

1. The accuracy of the DC measurement was found by performing measurements on a calibrated 1 mΩ current shunt [bur15] with a guaranteed accuracy of ±0.02 %.

2. With the maximum deviation obtained by these measurements, the DC resistance of a 10 mΩ coaxial impulse current shunt was determined within a certain range. This coaxial current shunt remains to act like a pure DC resistance in the measurable frequency range (up to approximately 1000 Hz) [HIL17].

3. Afterwards, AC measurements were performed on this manually calibrated coaxial shunt and therefrom the relative maximum error of R_{AC}—called $v_{R_{\mathrm{AC}}}$—which is caused by the measurement system, was computed for every frequency and different confidence intervals.

Having performed a significant number of measurements combined with the assumption that the error is normally distributed, the standard deviation σ_{sd} can be calculated. The shaded areas in Figure 2.2 and Figure 2.3 show the confidence interval $3\sigma_{\mathrm{sd}}$ and $2\sigma_{\mathrm{sd}}$ plotted over different frequency ranges. A $3\sigma_{\mathrm{sd}}$ confidence interval means that in $\approx$ 99.73 % of the cases, the real value lies within this interval around the value indicated by the measurement system. A $2\sigma_{\mathrm{sd}}$ confidence interval relates to $\approx$ 95.45 %.

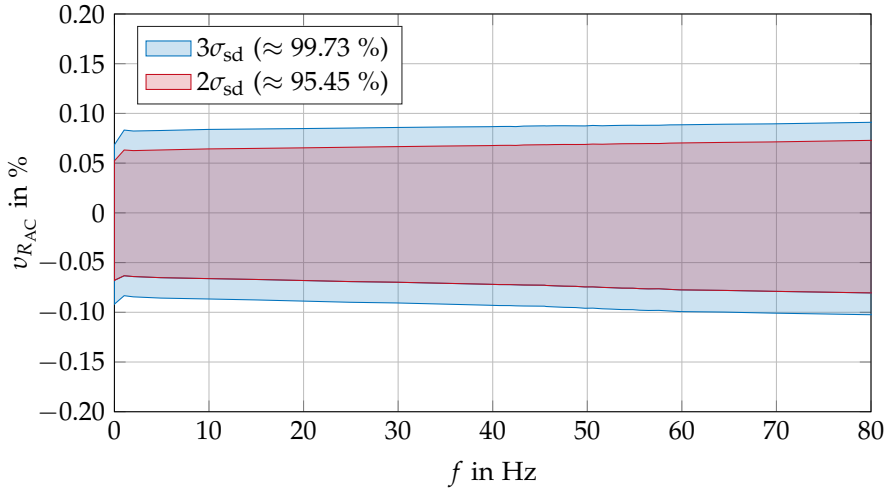

Figure 2.2: Relative maximum error $v_{R_{\mathrm{AC}}}$ of the measurement system with the blue and red surfaces indicating $3\sigma_{\mathrm{sd}}$ and $2\sigma_{\mathrm{sd}}$ confidence intervals up to 80 Hz

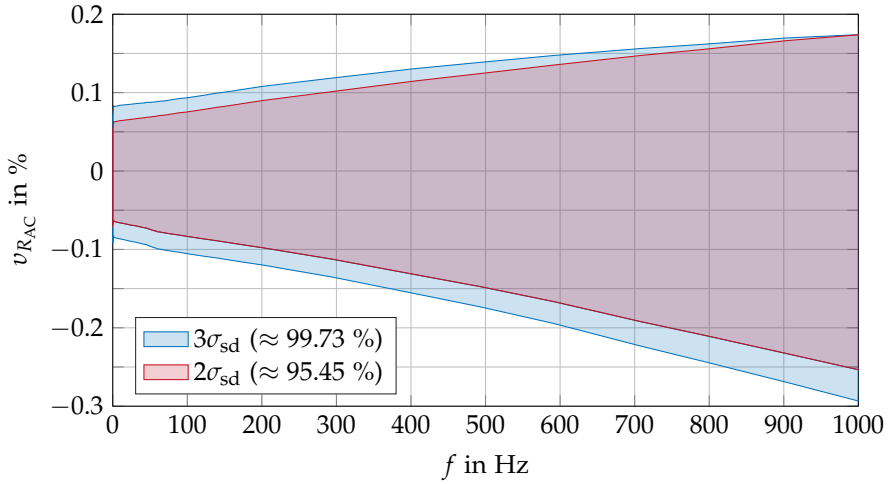

Figure 2.3: Relative maximum error $v_{R_{\mathrm{AC}}}$ of the measurement system with the blue and red surfaces indicating $3\sigma_{\mathrm{sd}}$ and $2\sigma_{\mathrm{sd}}$ confidence intervals up to 1000 Hz

It can be seen that at the most important frequencies of 0 Hz and 50 Hz the deviation of the real value to the value shown by the measurement will be less than $\pm$0.1 % for a $3\sigma_{\mathrm{sd}}$ confidence interval. When losses or resistances

change from 0 Hz to 50 Hz, the deviation of the *measured* value, for conductor sizes investigated in this thesis, is typically much larger than the error of the measurement system. Hence, this measurement system satisfies the accuracy requirements for the following investigations.

ERROR OF THE TEMPERATURE MEASUREMENT For the temperature measurements a calibrated PT100 sensor of tolerance class A is used [GSG]. In combination with the temperature measurement device [GHM], the maximum error of the temperature measurement in the temperature range of $-18.5\,°C$ to $55.5\,°C$ is $\pm 0.06\,K$. With the temperature coefficient of copper (defined next section), this results in a maximum relative error in the temperature measurement of $v_T \approx \pm 0.02$ %. The annual drift of the PT100 sensor is given with $0.005\,K/annum$.

ERROR OF THE LENGTH MEASUREMENT For straight unbend conductors and cables, the length measurement is performed with a laser range finder, whose accuracy is $\pm 2\,mm$ [Too13]. For cables with slight bends a standard tape measure is used, which was backchecked with the laser device and found to have no deviation from the displayed value of the laser range finder at a length of 1 m. Hence, the accuracy of the length measurement remains $\approx \pm 2\,mm$ and is generally defined as $v_l = \pm 100\ \% \cdot 2\,mm / l_{meas}$, where l_{meas} is the measuring length in m. Note that the k_s value is sensitive to errors in length measurements as it takes the DC resistance in Ω/m as an input argument. Great care must be taken as—for example—a length measurement error of only 1 cm over a total length of 5 m, relates to an error of 0.2 % of the k_s value, which is already larger than the maximum relative error of the measurement system. Nevertheless, often only the resistance ratio is analyzed to see the qualitative behavior of a conductor at AC. Here, an identical absolute deviation at DC and AC will not influence the results.

ERROR DUE TO EMFS When measuring large conductors with small test currents, as done with the available measurement system, the resulting voltage lies in the micro volt range. Hence, when junctions between dissimilar metals are present (e.g.: aluminum CUT and copper voltage lead wires) thermal electromotive forces (emfs) can arise, which can influence the *measured* voltage. When temperature gradients are present in the measurement setup, thermal emfs due to *Seebeck* or *Thomson effect* can arise at junctions. Even though no temperature gradients are present, thermal emfs can arise when current flows over a dissimilar metal junction. This so-called *Peltier heating* can increase the temperature gradients at the junction and can then cause emfs by Seebeck effect [WS70, p. 841; Row06, pp. 1-2]. To prevent thermal emfs in measurements, the DC value is obtained by a bipolar measurement. As the direction of existent thermal emfs only depends on temperature distribution, taking the average value of a bipolar measurement—as also automatically done at AC—averages out the influence of these emfs [Tek16, pp. 3-6; Bür95, p. 3].

OVERALL ERROR OF THE MEASUREMENT EQUIPMENT The maximum overall error v_o in percent of the used equipment is the sum of the different errors discussed above. This assumption can be made if the errors are independent of each other. Measuring absolute resistances at AC and DC includes the error of the measurement system, the error of temperature and length

measurement. In sum, regarding the $3\sigma_{\mathrm{sd}}$ confidence intervals for 50 Hz, it amounts to

$$v_{R_{\mathrm{AC}}}(50\,\mathrm{Hz}) + \quad v_T \quad + \quad v_l \quad = v_o \ , \tag{2.1}$$

$$(\pm 0.10\ \%) \quad + (\pm 0.02\ \%) + \left(\pm \frac{100\ \% \cdot 2\,\mathrm{mm}}{l_{\mathrm{meas}}}\right) = (\pm 0.12\ \%) + \ldots \left(\pm \frac{100\ \% \cdot 2\,\mathrm{mm}}{l_{\mathrm{meas}}}\right). \tag{2.2}$$

When observing the resistance ratio only, the error of length measurement vanishes and the relative overall error at 50 Hz is $v_o = (\pm 0.10\ \%) + (\pm 0.02\ \%) = \pm 0.12\ \%$.

Error bars are not plotted in this thesis for the sole reason that variations on the vertical axis plotted over the horizontal axis are in all cases much larger than the error bars. In other words, the error bars are too small to be displayed clearly.

Another detailed uncertainty analysis for a very similar measurement system can be found in [RSS11a].

2.3 MATERIAL PROPERTIES USED IN SIMULATIONS AND CALCULATIONS

Table 2.3, provided by IEC standard 60287-1-1:2006, shows material parameters for metals used in electrical conductors.

Table 2.3: Electrical parameters of common conductor materials used in simulations and calculations according to IEC 60287-1-1:2006 [IEC06b, p. 59]

material	conductivity σ in MS/m at 20 °C	temperature coefficient α_T in 1/K at 20 °C
aluminum	≈ 35.38	4.03×10^{-3}
copper	≈ 58.00	3.93×10^{-3}

These values are used in every calculation and numerical simulation in this thesis. If not stated otherwise, the simulations and calculations are performed at a temperature of 20 °C. Copper conductors used for electrical applications are typically made of Cu-ETP-1, Cu-OF-1 or Cu-OFE. Depending on type and manufacturing quality, the actual conductivity of a conductor can slightly vary [Deu17]. For aluminum conductors EN AW-E Al99,5 is the widest used conductor material [Kam11, p. 678].

In the temperature range of interest (1 °C to 100 °C), using a linear approximation for the temperature correction is valid for both materials [KAF04, p. 2; Kam11, p. 678][1].

1 In [Sjö13] different temperature coefficients for copper conductors for AC and DC were measured. This effect can possibly be attributed to the change of insulation properties in complex conductors as predicted by [Gra79, p. 102].

2.4 PROCESSING OF MEASURED DATA

To avoid interferences caused by equipment operated at power frequency, direct measurements at these specific frequencies—50 Hz, 60 Hz and their harmonics—are avoided. Moreover, to make measurements comparable with other labs, it is necessary to scale the measurements obtained at an arbitrary temperature to the reference temperature of 20 °C. The processing of measurement data is shown in the following.

2.4.1 *Interpolation of Measurement Data*

As the resistance at 50 Hz or 60 Hz is not directly measured due to possible interferences caused by nearby equipment operated at power frequency, this value has to be interpolated. Multiple measurements at frequencies close to this value allow for accurate fitting of the *measured* resistance at 50 Hz or 60 Hz.

To fit the measurement data, the functions recommended by IEC standard 60287-1-1:2006/AMD1:2014 (Equation (1.6) to Equation (1.9)) are used in combination with a least root-mean-square deviation algorithm. The x_s value enables piecewise application of these function to certain frequency ranges.

Even though more accurate, this method requires at least two measurements at different frequencies to enable a fitting for the desired frequency value at 50 Hz or 60 Hz. With the used measurement system described previously, measurements at multiple frequencies can be easily performed.

2.4.2 *Temperature Correction of Measurement Data*

In most cases, the grid operator is interested in the losses of the cable under maximum loading conditions. The allowed permanent temperature under maximum loading conditions for HV power cables with polymeric insulation is typically limited to 90 °C. As one advantage of electrical methods is the use of small test currents, measurements will typically not be performed at the maximum operating temperature. If not performed in a climate chamber, the measurement is performed at room temperature, which typically is 20 °C ± 10 °C. For the sake of comparability, the resistance has to be extrapolated to 20 °C or 90 °C. Even though often used for extrapolation, Equation (2.3) is only valid for DC.

$$R_{\mathrm{DC},0} = \frac{R_{\mathrm{DC},T}}{1 + \alpha_T (T - T_0)} \quad . \tag{2.3}$$

The reason is that the conductivity of a conductor changes with temperature. It also directly influences *skin effect* losses. For example, with increasing temperature, the conductivity of copper decreases, therefore additional *skin effect* losses decrease and hence, the $R_{\mathrm{AC}}/R_{\mathrm{DC}}$ ratio decreases as well. Changing the temperature thus results in a stretching (correction to higher temperatures) or compression (correction to lower temperatures) of the resistance ratio curve plotted over the frequency. In other words, the resistance ratio at a certain frequency will not be the same at different conductor temperatures. AC loss mechanisms as *skin effect* are further

described in Chapter 3. In the equations above, $R_{DC,0}$ is the conductor's DC resistance in Ω/m at the desired reference temperature T_0 (e.g.: 20 °C or 90 °C) and $R_{DC,T}$ is the conductor's DC resistance in Ω/m obtained at measurement temperature T (e.g.: 23 °C). Values for α_T can be taken from the previous section.

Nevertheless, according to the *Principle of Similitude*—introduced later in Section 3.1.2.6—the resistance ratio of a proportionate conductor geometry only depends on the ratio of frequency to DC resistance. Hence, when alternating the DC resistance (by changing the conductivity through higher or lower temperatures), one needs to adjust the frequency to remain the same resistance ratio. A disunited temperature scaling factor T_{SF} is introduced and can be calculated by:

$$T_{SF} = \frac{R_{DC,0}}{R_{DC,T}} = \frac{1}{1 + \alpha_T (T - T_0)} \quad . \tag{2.4}$$

T_{SF} is used to generate the new frequency f_0 and resistance R_0 at reference temperature T_0:

$$f_0 = f_T \cdot T_{SF} \quad , \tag{2.5}$$

$$R_0 = R_T \cdot T_{SF} \quad . \tag{2.6}$$

f_0 in Hz is the frequency value for the resistance R_0 at reference temperature T_0. f_T in Hz is the original measurement frequency at measurement temperature T and R_T is the originally *measured* resistance in Ω/m at T.

Figure 2.4 gives an example of how temperature scaling works by using the *Principle of Similitude*. The object under investigation is a tubular copper conductor with inner radius 1 cm and outer radius 2 cm. The red curve shows the analytical solution at 28 °C (see Equation (3.41)). The markers show the resistance values at 0 Hz, 49 Hz and 51 Hz. The blue curve plots the corrected resistance curve to the desired reference temperature T_0 using the method introduced above. As expected, the DC resistance is lower at 20 °C but due to the higher conductivity, AC losses increase slightly faster compared to 28 °C. Resistance R_0 plotted over the adjusted frequency vector f_0 is identical to the analytical solution directly obtained at the reference temperature T_0 = 20 °C—dashed yellow line—which is plotted for verification. Note that the scaling changed the position of the frequency markers and the markers now give the AC resistance at frequencies other than the original 49 Hz and 51 Hz. If one would only use Equation (2.3) for the whole curve—DC and AC values—one would only shift the original red curve downwards. This negative offset however would not coincide with the blue and yellow curve as at the original larger measurement temperature, the increase in AC losses appeared slower.

Calculating the k_s factor with the help of the recent standard directly assumes that the measurement is performed at the desired temperature of evaluation (exactly 20 °C or 90 °C), which is typically not the case. Even though more accurate than extrapolations using Equation (2.3), this method requires either two measurement values at different frequencies to enable a fitting for the desired frequency value at 50 Hz or 60 Hz; or calculating the necessary measurement frequency from the current measurement temperature in advance, so that scaling to the desired reference temperature

directly outputs the resistance at 50 Hz or 60 Hz. Multiple frequencies can easily be measured with the used measurement system described in the next chapter. Using Equation (2.3) presents a worst-case, as it does not involve the decrease in AC losses due to lower conductivity at higher temperatures. Nevertheless, it does not represent the real behavior and resistance of a conductor.

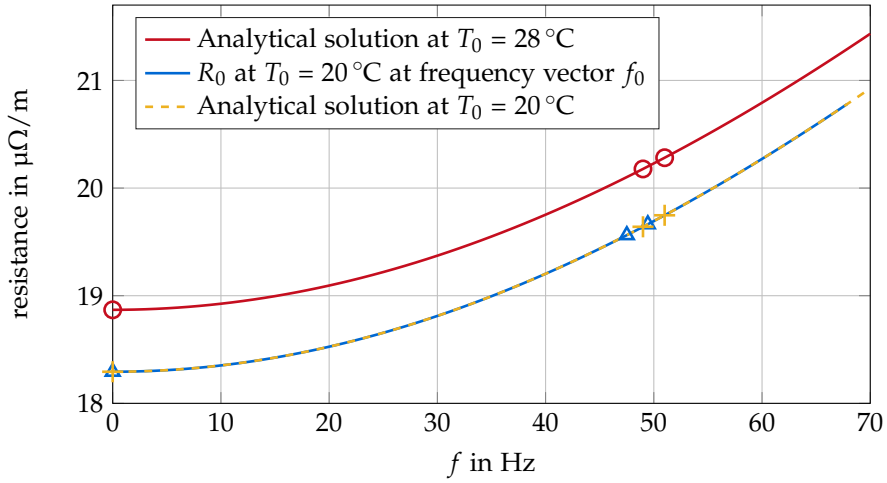

Figure 2.4: Use of *Principle of Similitude* for temperature correction on a tubular conductor; markers in red and yellow are at frequency values 0 Hz, 49 Hz and 51 Hz; blue markers are at these frequencies times T_{SF} (the curve needs to be moved downwards and compressed along the horizontal axis when downscaling temperature values)

This method of temperature correction is limited to the case, where factors influencing the AC resistance *do not* vary with temperature (e.g.: insulation properties of single strands in complex conductors,...). It should be noted that according to [Gra79, p. 102], it is possible that the performance of a *Milliken* conductor indeed varies at much higher temperatures, as this can affect insulation properties of the single strands.

The measurements performed in this thesis are all performed close to room temperature (20 °C ± 10 °C). As there is no significant change expected in insulation capability of enameled or oxidized wires in *M-type* conductors from room temperature to exactly 20 °C, using the principle above will then deliver the *true* conductor losses at 20 °C.

2.5 APPLIED SIMULATION TECHNIQUE

Even though the FEM is elaborated and extensively described in the literature—for the sake of completeness—a short introduction is given at this point.

2.5.1 *Fundamentals of the Used Simulation Program*

Throughout this work the *AC/DC module* of *Comsol Multiphysics 5* is used[2]. The applied physics interface depends on the field quantities, which shall be obtainable after simulation. Table 2.4 shows, which field quantities are calculated in the different physics interfaces.

2 *Comsol Multiphysics* is a numerical software package to simulate physics-based systems and can be found at www.comsol.com (visited on 21/11/2017).

Table 2.4: *Comsol Multiphysics'* solvers for *eddy current* simulations applicable for investigations in this thesis; explanation of the symbols follows

physics interface	calculated field quantities
magnetic field physics interface (*mf* interface)	$\boldsymbol{J}, \boldsymbol{B}$
magnetic and electric field physics interface (mef interface)	$\boldsymbol{J}, \boldsymbol{B}, \boldsymbol{E}, \boldsymbol{A}, V$

Even though the accuracy of the simulations would be sufficient using the quasi-static approximation (discussed in Section 3.1.2.2), including displacement currents in the frequency domain equations does not result in additional computational costs [Com13, p. 256]. Therefore, simulations in the frequency domain include displacement currents[3]. The magnetic and electric field (mef) interface without gauge fixing is used in this work as it calculates the relevant field quantities by keeping hardware expense relatively small.

When neglecting moving conductors and additional external currents, the governing equations in *Comsol Multiphysics'* mef physics interface become the following.

$$\nabla \cdot \boldsymbol{J}_\mathrm{t} = 0 \tag{2.7}$$
$$\nabla \times \boldsymbol{H} = \boldsymbol{J}_\mathrm{t} \tag{2.8}$$
$$\boldsymbol{B} = \nabla \times \boldsymbol{A} \tag{2.9}$$
$$\boldsymbol{E} = -\nabla V - \mathrm{j}\omega \boldsymbol{A} \tag{2.10}$$
$$\boldsymbol{J}_\mathrm{t} = \sigma \boldsymbol{E} + \mathrm{j}\omega \boldsymbol{D} \tag{2.11}$$

The nabla operator ∇ is defined in Appendix C. Bold symbols denote vectorial phasors (vectors with complex amplitude). $\boldsymbol{J}_\mathrm{t}$ is the total current density including the displacement current, $\boldsymbol{H}$ is the magnetic field intensity in $\mathrm{A/m}$, $\boldsymbol{B}$ is the magnetic flux density in $\mathrm{Vs/m^2}$, $\boldsymbol{A}$ is the magnetic vector potential in $\mathrm{V\,s/m}$, V is the electric scalar potential in V, j is the imaginary number and $\boldsymbol{D}$ is the electric displacement field in $\mathrm{A\,s/m^2}$. The magnetic vector potential $\boldsymbol{A}$ and the electric scalar potential V are the dependent variables in simulations with the mef physics interface [Com13, p. 6].

Equations (2.7) to (2.11) can be used to build a system of two linear equations: by using Equation (2.8) and Equation (2.10) in Equation (2.11)

$$\nabla \times \boldsymbol{H} = \sigma(-\nabla V - \mathrm{j}\omega \boldsymbol{A}) + \mathrm{j}\omega \boldsymbol{D} \quad . \tag{2.12}$$

Using constitutive relation from Equation (3.5) then leads to

$$\nabla \times \boldsymbol{H} = \sigma(-\nabla V - \mathrm{j}\omega \boldsymbol{A}) + \mathrm{j}\omega \varepsilon_0 \varepsilon_\mathrm{r} \boldsymbol{E} \tag{2.13}$$

where $\boldsymbol{E}$ is substituted by Equation (2.10)

$$0 = -\sigma \nabla V - \mathrm{j}\omega\sigma \boldsymbol{A} + \mathrm{j}\omega \varepsilon_0 \varepsilon_\mathrm{r}(-\nabla V - \mathrm{j}\omega \boldsymbol{A}) - \nabla \times \boldsymbol{H} \tag{2.14}$$

3 Nevertheless, explicitly modeling non-conductive, non-magnetic materials as conductor insulation and providing their electric permittivity is neglected, as only magnetic fields are analyzed outside of conductors.

and substituting $\boldsymbol{H}$ with *constitutive relation* from Equation (3.6) and then $\boldsymbol{B}$ with Equation (2.9) leads to

$$\begin{aligned} 0 = &-\sigma\nabla V - \mathrm{j}\omega\sigma\boldsymbol{A} + \mathrm{j}\omega\varepsilon_0\varepsilon_\mathrm{r}(-\nabla V - \mathrm{j}\omega\boldsymbol{A})\ldots \\ &- \nabla\times(\mu_0^{-1}\mu_\mathrm{r}^{-1}(\nabla\times\boldsymbol{A}))\ . \end{aligned} \tag{2.15}$$

This equation can be rearranged to:

$$\begin{aligned} 0 = &(\mathrm{j}\omega\sigma - \omega^2\varepsilon_0\varepsilon_\mathrm{r})\boldsymbol{A} + \nabla\times(\mu_0^{-1}\mu_\mathrm{r}^{-1}(\nabla\times\boldsymbol{A}))\ldots \\ &+ (\sigma + \mathrm{j}\omega\varepsilon_0\varepsilon_\mathrm{r})\nabla V\ . \end{aligned} \tag{2.16}$$

A second independent equation can be derived by inserting Equation (2.11) in Equation (2.7)

$$0 = \nabla\cdot(\sigma\boldsymbol{E} + \mathrm{j}\omega\boldsymbol{D}) \tag{2.17}$$

and then using Equation (3.5) and Equation (2.10)

$$0 = \nabla\cdot(\sigma(-\nabla V - \mathrm{j}\omega\boldsymbol{A}) + \mathrm{j}\omega\varepsilon_0\varepsilon_\mathrm{r}\boldsymbol{E})\ . \tag{2.18}$$

From replacing $\boldsymbol{E}$ by Equation (2.10) follows

$$0 = \nabla\cdot(\sigma(-\nabla V - \mathrm{j}\omega\boldsymbol{A}) + \mathrm{j}\omega\varepsilon_0\varepsilon_\mathrm{r}(-\nabla V - \mathrm{j}\omega\boldsymbol{A}))\ , \tag{2.19}$$

which can be rearranged to

$$0 = -\nabla\cdot((\mathrm{j}\omega\sigma - \omega^2\varepsilon_0\varepsilon_\mathrm{r})\boldsymbol{A} + (\sigma + \mathrm{j}\omega\varepsilon_0\varepsilon_\mathrm{r})\nabla V)\ . \tag{2.20}$$

By numerically solving Equation (2.16) and Equation (2.20) simultaneously for $\boldsymbol{A}$ and V, the electromagnetic fields can be calculated. Here, ε_0 is the permittivity of vacuum in As/(Vm), ε_r is the electric permittivity and μ_r is the magnetic permeability. On the boundaries of the calculation domain the tangential component of the magnetic vector potential and the normal component of the current density is set to zero (the latter except for the CUT's cross section). The excitation for the current flow through the CUT is implemented via a "Terminal Node" on the surface of the CUT's cross section. It sets

$$\int_C \boldsymbol{J}_\mathbf{t}\cdot\vec{n}\cdot\mathrm{d}\vec{A} = \boldsymbol{I}\ , \tag{2.21}$$

where subscript C indicates the boundary of the CUT's cross section, $\boldsymbol{I}$ is the overall current specified by the user and $\vec{n}$ is the normal component to the CUT's surface.

As it drastically increases computation time, only when it is necessary to directly access and evaluate the magnetic vector potential $\boldsymbol{A}$ or the electric scalar potential V in the simulation domain, a *Gauge Fixing Node* for the vector potential is applied in *Comsol Multiphysics*. This forces the magnetic vector potential to be source-free:

$$\nabla\cdot\boldsymbol{A} = 0\ . \tag{2.22}$$

This is necessary to get a unique and numerically stable solution and is done by adding an additional potential variable $\Psi_0 = 1\,\mathrm{A/m}$ to the equations above. As only the gradient of Ψ_0 is used in the equations, the absolute value is of no significance [Com13, p. 177].

In *Comsol Multiphysics*, the calculated fields in time-harmonic simulations are phasors and not actual physical fields. By default, the phasor is displayed at $time = 0$ [Com13, p. 25]. Any field components shown in figures in this thesis show the field quantity at that reference phase of the total current at 0°. Some fields can contain both: real and imaginary components at that phase.

2.5.2 *Basics of the FEM*

Analytical solving Equation (2.16) and Equation (2.20) can be extremely difficult even for simple geometries. It is much more efficient to approximate these partial differential equations (PDEs) and hence, find an approximation of the real solution [Bar06, p. 95; Com16b]. The FEM is only one of several approaches to discretize and solve the relevant PDEs in a computer model.

In general, the following steps are taken when solving a problem with the FEM:

I. Subdivision of the calculation domain:
After the user has finished the model building process—creating the geometry, assigning materials, defining the excitation and boundary conditions (BCs)—the calculation domain is first subdivided into a so-called mesh. In case of a 1D model (a line), this line is divided into multiple line segments. For low frequency simulations most solvers use triangles for 2D and tetrahedrons for 3D geometries. Nevertheless, much more possibilities to subdivide the domain are available and sometimes more appropriate even in low frequency applications[4].

II. Generation of interpolation functions:
Next, the interpolation functions—also called basis functions or shape functions—are chosen that shall approximate the governing PDE. The order of this function plays a major role in the solution process and the accuracy of the results. The appropriate order primarily depends on the problem relevant PDEs and expected results. For example: in case of a Poisson-type PDE—a second-order PDE—*Comsol Multiphysics* recommends an interpolation function also of second order [Fre16]. Moreover, in most single physics simulations[5] *Comsol Multiphysics* recommends to use first order (linear) or second order (quadratic) elements [Fre16]. Just like an adaptive mesh, adaptive element orders can greatly increase the accuracy of the simulation. Nevertheless, one should bear in mind that the higher the element order, the more degrees of freedom (DOF) exist for each element. With more DOF the computational effort to solve the same problem with an identical mesh is also larger.

4 For example: In *Comsol Multiphysics* the user can add "Boundary Layers" near the surface of a conductor to increase the resolution of severe *skin effect*/steep field gradients.
5 Simulations were no coupling of different physical phenomena is performed.

III. Construction of the equation system:
Subsequently, a system of equations is built. *Comsol Multiphysics* uses the *Galerkin method*—also called residual weighting formulation—as a discretization method [Com15a, p.185]. With the *Galerkin method*, one can numerically approximate the solution of a PDE. When solving the linear system in step IV one can calculate the residual, which displays the deviation to the true solution from the present solution [Baro6]. The residual provides information about the accuracy of the solution of the algebraic equation system. In combination with an error estimator, which keeps the *discretization error* small one can find an approximate solution of the governing PDEs.

IV. Implementation of the BCs & solution of the equation system:
After embedding the BCs, the equation system can be solved to calculate the unknown functions (the functions that approximate the PDE). This approximation must fulfill all BCs.

2.5.3 *FEM Errors and Simulation Principles*

In general there are multiple sources of errors occurring in the FEM:

- *Modeling error*
  Converting a complex physical system into a mathematical model is always a simplification of the real setup, ignoring model specific details, material properties and other physical effects [Baro6, p. 95].

- *Discretization/geometrical error*
  Describes the approximation of the real geometry using a finite number of elements. This error can be reduced if the number of elements used to approximate the geometry or the element order of the basis functions are increased [MG07, p. 200; Com15a, p. 1283]. Most commercial FEM tools have automated error estimators, which can help to reduce the error for example by *adaptive mesh refinement*.

- *Numerical errors*
  Summarizes *Round off errors* due to the limited number of digits available in digital systems, *Integration errors* and *Matrix conditioning errors*. All of them are generally assumed to be negligible [Com15a, p. 908].

To reduce these errors and, if possible, reduce simulation time as well, hereafter some general rules of thumb are listed that were considered in simulations[6]:

- first, the user should check for general errors in the model with a coarse mesh (correct assignment of excitations, BCs and materials),

- observe if the solution converges with a step-by-step refining mesh (mesh refinement study or mesh convergence study) [Fre16],

- use the geometry's symmetry whenever possible by applying BCs (*Dirichlet* BC[7] or *Neumann* BC[8]),

6 Additional notes on mesh refinement, post-processing and handling singularities can be found in [Com14; Com15b; Com16a].
7 This is also called magnetic insulation or perfect electric conductor (PEC).
8 Also referred to as perfect magnetic conductor (PMC).

- if the analytical solution to the problem is known: optimize the model in regard to the analytical solution to increase accuracy[9],
- if the analytical solution is *not* known: refine the mesh and alternate the BD[10] until the subsequent solution does not vary more than 1 % from the previous one,
- use at least two linear elements per *skin depth* δ [Com13, p. 50] (see Section 3.1.2.5 for the explanation of *skin depth*),
- if possible use the "Infinite Element Domain" feature, which allows close boundaries and thus a reduction of the calculation domain without influencing the fields inside the calculation domain [Com15a, p. 324],
- avoid small geometric features if possible and necessary,
- as recommended by *Comsol Multiphysics*: use default element order (second order) for single physics simulations [Fre16],
- to improve convergence—if necessary—one can apply a *Gauge Fixing Node* in the mef physics interface,
- reduce the *discretization error* by using *adaptive mesh refinement*,
- for the DC resistance evaluation in the frequency domain of the mef *solver* a frequency of 0.001 Hz is applied, as 0 Hz is not allowed in the frequency domain; this leads to nearly identical results compared to the stationary *electric currents (ec)* solver; even for large conductor cross sections with severe *skin effect* (e.g. copper solid with a cross section of 2500 mm^2) the deviation of the resistance at 0.001 Hz to the resistance at 0 Hz is negligible. Nevertheless, since the stationary solver only solves for V and not for V and $\boldsymbol{A}$ like the *mef* solver, more computational effort is needed for calculating the DC resistance in the *mef* solver.

2.6 AVAILABLE METHODS TO DETERMINE THE AC RESISTANCE OF MILLIKEN CONDUCTORS

For investigating the AC resistance of *Milliken* conductor, there are 3 main approaches, which can be used and should be combined as far as possible.

The first is basic analytical calculations for simple conductor cross section. Therefrom some conclusions can be drawn about the general dependency of AC resistance on cross section, conductivity, frequency and so on. An extensive collection of available analytical solutions for the AC resistance calculation of different cross sections is presented in Section 3.1.3. Moreover, algorithms using approximations of these analytical formulas can be used. An overview of existing calculations methods for *Milliken* conductors is shown in Table 3.1.

The second approach comprises numerical simulations such as the FEM. Numerical simulations are powerful tools to assess more complicated

9 For example: increasing the boundary distance (BD) from the CUT. One should bear in mind that the magnetic insulation BC represent a hollow PEC cylinder (the return path for the current if no other return conductor is defined).

10 The success of this routine of course depends on model and BC.

structures. Nevertheless, their application is also limited due to constraint hardware resources or because some conductor properties, such as manufacturing quality of the single wires, are not known in advance.

The third approach is the measurement—both calorimetric and electrical—, which is generally not constricted to the complexity of the conductor, when properly performed. It is the goal of this work to recommend a measurement setup and procedure for the electrical method, which delivers a measurement value as close as possible to the *true* resistance of the *Milliken* conductor.

Combining the available tools and back-checking them against each other, will indicate a value, which is close to the *true* value. Figure 2.5 shows the different methods and their applicability to the problem of AC resistance of complex conductors.

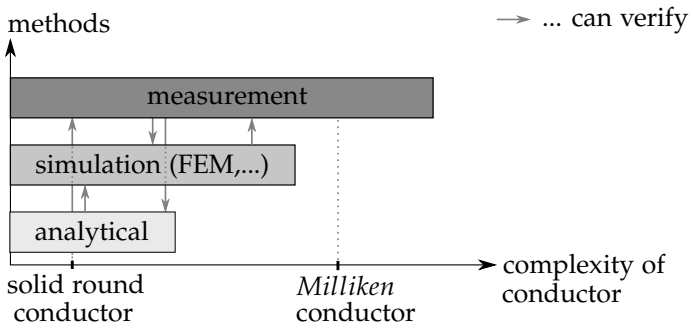

Figure 2.5: Available methods for the AC resistance determination of conductors and their applicability concerning the complexity of the conductor geometry

Figure 2.6 shows the excellent compliance of all three approaches for the simple case of a solid round conductor. The FEM and measurement can directly be verified by the analytical solution, which is described later in Equation (3.33).

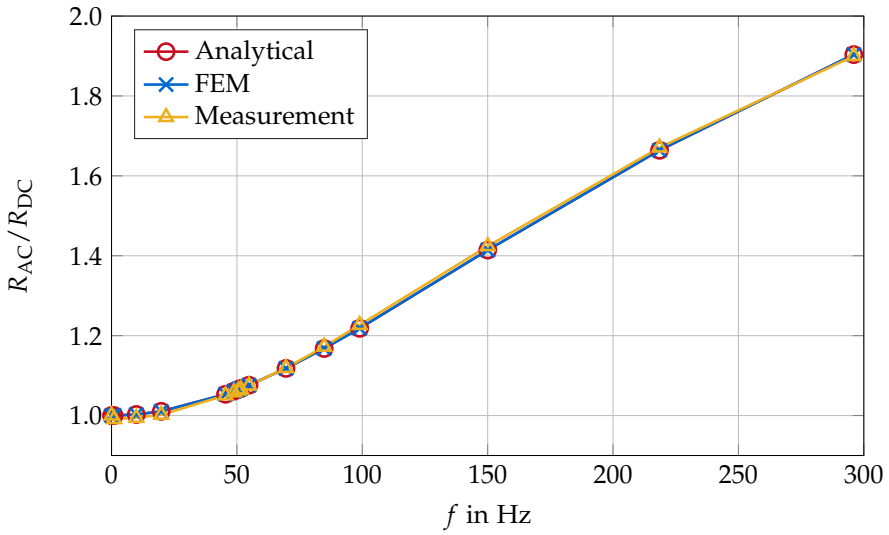

Figure 2.6: Comparison of analytical calculation, FEM simulation and measurement of a solid cylindrical aluminum conductor showing good agreement between all methods

These results show that the measurement method and the FEM are generally able to obtain accurate results. Chapter 4 highlights what one should bear in mind, when performing a measurement on a more complex conductor such as a *Milliken* conductor.

3

THEORY OF ALTERNATING CURRENT LOSSES IN ELECTRICAL CONDUCTORS

Study the past
if you would divine the future.
Confucius

The purpose of this chapter is to lead the reader through the history, important principles and formulas of AC losses in electrical conductors. Moreover, a brief description of the development of power cable conductors is given, ending with a description of recent power cable conductor designs with large cross sections.

3.1 SKIN EFFECT AND PROXIMITY EFFECT

The following section presents a detailed review of important historical developments and theoretical works on AC losses, in particular *skin* and *proximity effect*. *Skin* and *proximity effect* losses have been the topic of numerous past researches. Analyzing as much available work as possible, puts the following research in Chapter 4 on a solid foundation. The emphasis is placed on the comprehension of basic principles of AC loss mechanisms. Moreover, to the best knowledge of the author, the most complete collection of analytical formulas for *skin* and *proximity effect* in electrical conductors is presented.

3.1.1 *History of Important Discoveries and Exact Formulas*

Today *skin* and *proximity effect* losses are well understood. Nevertheless, the development of a basic comprehension of the underlying principles and of analytical formulas describing these effects has a long and rich history, which is in detail presented in the following. The term analytical (also called: exact or explicit) means that the solution is not restricted to a certain range of the involved parameters (e.g.: frequency, ...). A formula is still considered "analytical" even if the involved geometric series are infinite.

MID-19TH-CENTURY: The concept of *conservation of energy* is already well understood and established. In the years following, the idea of the *continuity of energy* becomes more prominent [Naho2, p. 115].

1873: James Clerk Maxwell publishes *"A treatise on electricity and magnetism vol. I* [Max73a] & *vol. II* [Max73b]*"*. In [Max73b, p. 291] Maxwell is the first to predict an uneven current distribution in a wire cross section in case of currents with varying intensity.

1884: Oliver Heaviside[1] is the first to state the direction of the energy flow around a wire [Hea84; Naho2, p. 118]. Only a little later that year, John Henry Poynting extensively describes the energy transfer in the dielectric surrounding a conductor with a worked-out mathematical

1 All of Heaviside's works cited below can be found in his *"Electrical Papers vol. I* [Hea92] & *vol. II* [Hea94]*"*.

background [Poy84][2]. One year later, Heaviside verifies Poynting's results in [Hea85].

1886: Even though the existence of the *skin effect* was already known to a few theorists like Maxwell, Horace Lamb and Heaviside [Jor82, p. 123], its thorough investigation started with the presidential address of David Edward Hughes for the *Society of Telegraph Engineers and Electricians* in January 1886 [Hug86]. Hughes measured differences in the resistance of conductors exposed to DC and pulsed currents [Yav11, p. 192]. Ignoring Maxwell's contribution to imbalances in current distribution in a conductor from his second treatise, he misinterpreted the measurement results[3]. Hughes misapprehension led to a deeper investigation of the *skin effect* phenomena, especially by Heaviside in April [Hea86c] and June [Hea86a]. His contribution from June shows the first use of Bessel functions to assess the current density in wires with circular cross sections. Moreover, by using the Bessel functions Heaviside derived the analytical formula for the resistance of a tubular conductor having a concentric tubular return conductor [Hea86b]. The return conductor is placed far enough as to not influence the current distribution of the inner tube [Hea86b; DW24]. Also in that year, Lord Rayleigh (named John William Strutt until 1873) presented a formula for the *skin effect* in an infinitely wide strip [Str91, p. 486; KLP15].

1889: Evaluating the Bessel functions without numerical methods or computers was a problem at that time. Lord Kelvin (called William Thomson until 1892) therefore rewrote the Bessel function, splitting it up in its real and imaginary part and provided tables for the calculation of those. That is the reason why the real and imaginary parts of the Bessel function are called Kelvin functions today [Smi14]. Using the Kelvin functions Lord Kelvin first provided the analytical formula to calculate the resistance ratio of conductors with circular cross sections in [Tho89, p. 35].

1891: J. Swinburne first calls the phenomenon of an uneven current distribution caused by AC: *skin effect* [KLP15].

1892: In the third edition of *"Maxwell's treatise vol. II"*, released 13 years after Maxwell's death, the analysis of *skin effect* in an isolated conductor with circular cross section was completed by John Joseph Thomson [Max92, p. 324].

1905: To simplify calculations, instead of using the unevenly distributed currents in the conductor for loss determination, P. Boucherot proposes to use an equivalent, smaller imaginary shell with a constant current distribution [Duc83, p. 7]. This concept is known as *skin depth* today and described in more detail in Section 3.1.2.5.

1909: Alexander Russell presents the analytical solution for a concentric tubular conductor having a solid inner conductor as a return [Rus09]. Moreover since 1909, first measurements of the *skin effect* in conductors are possi-

2 Russian physicist Nikolay Alekseevich Umov described the motion of mechanical energy in elastic and liquid media in 1874. Because of that, in Russian literature the Poynting vector is sometimes also referred to as Umov-Poynting vector [TT14, p. 147].

3 Hughes looked at the terms resistance and inductance as independent properties of the wire during the current onset. In fact they are a function of the current density in the wire [Nah02, p. 196].

ble with the rise of wireless communication systems, making accurate high-frequency AC sources available [Smi14].

1911: First theoretical considerations and measurements on *skin effect* in conductors of rectangular cross section are presented by Hiram Wheeler Edwards in [Edw11] and a little later in 1916 by A. Press in [Pre16].

1915: Extensive measurements of *skin effect* in different conductor types were published by A. E. Kennelly et al. in [KLP15] and one year later in [KA16].

1921: According to [Dwi23b; Mea25], John Renshaw Carson provided the first analytical formula to calculate the AC resistance of a solid conductor of circular cross section in close proximity to an identical parallel conductor (later referred to as: *proximity effect*) [Car21].

1922: Charles Manneback derives a new method to attack *skin effect* problems, which result in integral equations [Man22]. This method together with the *Poynting Vector* was later used to obtain more analytical solutions and avoid complicated Bessel function integrals at the same time [Dwi23b]. A similar approach was previously conducted by Harvey L. Curtis in 1920 [Cur20].

1923: Herbert Bristol Dwight presents another analytical solution to an isolated tubular conductor [Dwi23a]. In comparison to Heaviside, Dwight uses the Kelvin functions, which could be easily evaluated at that time compared to the Bessel functions used by Heaviside. Moreover, in contrast to Heaviside he derived the equations from an isolated tube [DW24].

1925: Sallie Pero Mead provides the analytical formula to calculate the AC resistance of a tubular conductor in close proximity to an identical parallel tubular conductor [Mea25]. Moreover, Chester Snow analytically describes the *proximity effect* in two non-identical adjacent solid round wires [Sno25].

1929: Conductors with rectangular cross sections have been investigated before and unsuccessful attempts have been made to obtain the analytical solution for the resistance by Heaviside, Lord Kelvin, Lord Rayleigh and others. More theoretical work on the calculation of AC resistance and *current crowding*[4] in isolated rectangular conductors is presented by J. D. Cockcroft [Coc29].

1937: A deeper investigation on losses in rectangular conductors was inspired by the extensive measurement data presented by S. J. Haefner in [Hae37]. Also this year John Daley presents an approach where one can analytically calculate the current distribution in an isolated rectangular conductor, if the BC of the differential equation—the surface current density—is obtained by measurement [Dal37; Dal39].

1940: The first entirely analytical solution to isolated rectangular and elliptical conductors is given by Hans-Georg Groß in [Gro40]. It is not well-known, as the given solution does not converge fast and required consid-

4 For conductors with edges, the current distribution also depends on the sharpness of these edges. This is called *current crowding* or *edge effect* [KA16].

erable numerical exploitation. Moreover, this work was only published in German language [Sil67].

1966: An iterative method to compute *eddy current* problems in conductors is introduced by Jiří Lammeraner and Miloš Štafl in [LŠT66, p. 166]. It is limited to the case of constant permeability. Even though this method has no inherent limitation, its practicability is often limited as higher order coefficients can become complex very fast. Nevertheless, it is useful if the accuracy of first order results is adequate as in [HR15].

1979: Analytical solutions to *skin* and *proximity effect* problems in various cross sectional shapes and also in case of transient excitation are presented by Matthias Ehrich in [Ehr79].

1980: In [HA80] and two years later in [AH82] Manfred Albach and Ludwig Hannakam show how to analytically solve a system of rectangular conductors in different geometric configurations including high permeable materials.

2007: An analytical solution for a system of an arbitrary number of rectangular conductors with arbitrary side ratios for AC and transient excitation is introduced by Lars Ole Fichte in [Fic07]. In 2004 the *eddy current* problem of a conducting rectangular conductor in an external magnetic field was given by Fichte in [FEK04].

2008: Ingo Manke et. al. optically determine the current density distribution due to *skin effect* in a solid conductor by using spin-polarized neutron radiography [Man+08].

2013: An alternative approach to access the analytical solution of *eddy current* problems for harmonic and transient excitations is proposed in [Sta+13]. This method can be advantageous as it does not use *Fourier Series* decompositions as usual but *space eigenfunction expansion*.

2015: Timothe Delaforge et. al. present a way to analytically solve the problem of an arbitrary number of parallel round wires in 2D [Del+15a; Del+15b].

2016: Cory James Liu derives the first analytical solution to the AC resistance of a bi-media solid cylindrical conductor in [Liu16, p. 79].

The investigation of the effect of alternating electromagnetic fields on the current distribution started 145 years ago. Theoretical studies on *eddy currents* yielded in a limited number of analytical formulas for mostly simple cross sectional shapes and conductor arrangements and a large number of approximate solutions for all kinds of geometries. Even though the analysis of complex integrals emerging from non-rotationally symmetric conductor cross sections is much easier with todays computational power and algorithms, using entirely numerical methods for *eddy current* analysis is often the preferred choice. The application of commercial software using numerical methods (such as the FEM) is more easily accessible to most engineers in comparison to sophisticated mathematical formulas and theories. Moreover, analytical methods are mostly limited to certain

geometries and BC, whereas commercial numerical tools are typically more flexible and often only limited by the computational resources available. Nevertheless, analytical solutions are sometimes necessary for verification of numerical methods and useful for understanding basic physical principles and relations of the parameters involved.

The evaluation of analytical formulas for solid circular conductors—involving Bessel functions—presented a challenge at the end of the 19th century. At the beginning of the 21st century—even with numerical methods and digital computers available—the numerical evaluation of some analytical formulas still required a considerable amount of computational power [Fico7, p. 113; LBV11].

3.1.2 *Theoretical Foundations*

To be able to tackle the theoretical questions and follow the line of thought in the next chapter, it is important to understand some basic theoretical concepts concerning *skin* and *proximity effect*. A short introduction is given subsequently.

3.1.2.1 *Maxwell's Equations*

Maxwell's equations describe electromagnetic phenomena at a macroscopic level. These equations state the fundamental relations between electromagnetic quantities. The complete Maxwell equations in the frequency domain in differential form are

$$\text{Ampère's Law:} \quad \nabla \times \boldsymbol{H} = \boldsymbol{J} + \mathrm{j}\omega \boldsymbol{D} \ , \tag{3.1}$$

$$\text{Faraday's Law:} \quad \nabla \times \boldsymbol{E} = -\mathrm{j}\omega \boldsymbol{B} \ , \tag{3.2}$$

$$\text{Gauss' Law (magnetic):} \quad \nabla \cdot \boldsymbol{B} = 0 \ , \tag{3.3}$$

$$\text{Gauss' Law (electric):} \quad \nabla \cdot \boldsymbol{D} = \varrho \tag{3.4}$$

with the *constitutive relations* of macroscopic linear material properties

$$\boldsymbol{D} = \varepsilon_0 \varepsilon_\mathrm{r} \boldsymbol{E} \ , \tag{3.5}$$

$$\boldsymbol{B} = \mu_0 \mu_\mathrm{r} \boldsymbol{H} \ , \tag{3.6}$$

$$\boldsymbol{J} = \sigma \boldsymbol{E} \ . \tag{3.7}$$

Above, ϱ is the electric charge density in $\mathrm{A\,s/m^3}$. Even though nonlinearities are not considered in this thesis, they are included here, as their influence is briefly described qualitatively in some passages. Another important equation in electrodynamics, taken from [Com13, p. 17], is the *equation of continuity*:

$$\nabla \cdot \boldsymbol{J} = -\mathrm{j}\omega\varrho \ . \tag{3.8}$$

3.1.2.2 *Quasistatic Approximation*

In this thesis typical frequencies dealt with in measurements and simulations are in the range from 0 to 10 kHz. The maximum geometric dimensions in both cases are limited to 1 km (e.g.: a cable on a drum). The calculation below follows [Sch13, p. VI.3] and shows, that the electric displacement field

$j\omega \boldsymbol{D}$ will—in any case—be much smaller than the conductor current density $\boldsymbol{J}$ and hence can be neglected in calculations.

$$|\boldsymbol{J}| \gg |j\omega \boldsymbol{D}| \tag{3.9}$$

$$|\sigma \boldsymbol{E}| \gg |\omega \varepsilon_0 \varepsilon_r \boldsymbol{E}| \tag{3.10}$$

$$1 \gg \frac{\omega \varepsilon_0 \varepsilon_r}{\sigma} \tag{3.11}$$

$$1 \gg \frac{2\pi \cdot 10 \times 10^3 \cdot 8.85 \times 10^{-12} \cdot 2.3}{58 \times 10^6} \tag{3.12}$$

$$1 \gg 2.2 \times 10^{-14} \qquad \text{Q.E.D.} \tag{3.13}$$

By using these typical parameters for the conductor and insulation of a cable, it is shown that one can simplify *Ampère's Law* to:

$$\nabla \times \boldsymbol{H} = \boldsymbol{J} \ . \tag{3.14}$$

A more detailed justification regarding the use of the magnetoquasistatic (MQS) approximation using wave propagation times in combination with the dimensions of the geometry of interest can be found in [Wil05]. This assumption is usually made for analytical calculations as it simplifies real 3D geometries to the more simple case of a 2D geometry. Then, the field quantities only vary in the cross section but not along the wire axis [Man22]. In other words, the MQS approximation assumes that the wave length of the electromagnetic wave traveling along the wire is much larger than the dimensions of the objects under investigation. This wave can therefore be regarded as a standing wave [Ehr79].

3.1.2.3 *Electromagnetic Fields & Energy Transport*

If the electric and magnetic fields are directly linked (e.g.: identical source of the fields) the *Poynting vector* $\boldsymbol{S}$ in $\mathrm{W/m^2}$ can be interpreted as the energy flux density [van07, p. 109] and describes the direction of energy flow by:

$$\boldsymbol{S} = \frac{1}{2} \boldsymbol{E} \times \boldsymbol{H}^* \ . \tag{3.15}$$

Conductors for wire-based energy transmissions act as a guideway for electromagnetic fields. The energy transfer from source to the load of the circuit takes place in the dielectric surrounding the conductor [Poy84; Hea94; Ski48, p. 134; Jac96; Leu05, p. 331; GG05, p. 111; van07; Yav11].

Even though a switch-on is much more complex, the following passages delivers a simplified explanation for what happens, when a power source is activated at one end of the power line: an electromagnetic wave—excited by the source—will propagate in the dielectric surrounding the conductor at a speed defined by the material properties of the dielectric. With the propagation of this wave, the current is set up at the conductor's surface by the displacement current in the dielectric. From there on, this current diffuses into the conductor and flows in the direction defined by the potential difference (pd) applied over both conductor terminals. The phase velocity of the diffusion (see Equation (3.19)) into the conductor depends on conductor properties such as conductivity, permeability and on the oscillation velocity of the exciting source—the frequency [ES01; ES03; Leh10, p. 398].

In case of static excitation, the current will eventually diffuse into the conductor completely and the current will be homogeneously distributed over the complete conductor cross section [Yav11, p. 195]. As the diffusion velocity is finite, in case of fast oscillating or transient sources, the current cannot penetrate into the conductor cross section completely before the direction of the electromagnetic field in the dielectric changes again. Moreover, due to *resistive losses* in the conductor, the magnitude of the penetrating fields decreases.

This limited penetration of electromagnetic fields—and hence currents—into the conductor, where only one conductor is present, is called the *skin effect* and is displayed in Figure 3.1 for a solid circular copper conductor. The term *skin effect* refers to the fact that the conductor current is largest at the surface—the "*skin*" of the conductor—and decreases towards its center. Figure 3.1 additionally shows that the phase of the current can be delayed strong enough, to let currents flow in the opposite direction in the center of the conductor, than the currents excited at the surface. In linear conductors the electric field is proportional to the current density as both quantities are linked by the conductivity (Equation (3.7)). As the conductor resistance is a property of the cross section available for current flow, it becomes evident that the electrical resistance is in fact a property depending on the frequency. Hence, a larger frequency causes an increased conductor resistance. Opposite to that, the internal inductance of a conductor decreases with higher frequencies, because less magnetic energy can enter the conductor. In general, ferromagnetic materials increase *skin effect*. With progressing saturation μ_r decreases and so does the *skin effect*. Electromagnetic fields will then penetrate the conductor more deeply [Duc83, p. 8].

If another conductor is brought into close proximity to this conductor, the electromagnetic wave, and with it the current density in both conductors, is distorted. This is called the *proximity effect* and is displayed in Figure 3.2. If both conductors build a *return circuit*, where both conductors carry the same current but in opposite direction, the electromagnetic wave is concentrated between both conductors (see Figure 3.4). If multiple conductors form a *go circuit*[5]—having currents of equal frequency and in the same direction—the wave is concentrated at the sides of the conductors facing away from each other (see Figure 3.5). In the case of two identical conductors, *proximity effect* losses are usually negligible if the distance between conductors exceeds five times the conductor radii [Mor13, p. 1253]. In special cases the *proximity effect* can even lower the AC resistance of a conductor in a *return circuit* as it can change the current density distribution in a way that the available cross section is increased compared to *skin effect* only [Coc29, p. 542]. For example the AC resistance decreases, when two thin conductor strips (broader sides facing each other) are brought closer together [Gra79, p. 49].

An alternative explanation for the *skin effect*—not using the physical phenomenon of electromagnetic field diffusion—was shown by Kennelly in [KA16, p. 548] and by A. Ducluzaux in [Duc83, p. 5] stating:

> "One explanation often put forward is that the inductance of the central filament of current in a conductor is higher than those of the peripheral filaments, this inductance being linked to the variation in the enveloped flux, which is itself a maximum for the central current filament.

5 In the simplest case they have of a coaxial return path.

In order to equalize the drops in inductive voltages between the various filaments, a higher current flows in the peripheral filaments. These different currents are thus more or less out of phase and their arithmetic sum is higher than the total measured current; as a result there are extra losses due to the *Joule effect*. This is equivalent to saying that the effective resistance is increased. In order to get a better quantitative idea of this *skin effect*, and of its implications, it is necessary to use the mathematical arguments developed by Lord Kelvin in 1889 [1][(1)] based on the propagation equations established by Maxwell a few years earlier."

3.1.2.4 *Visualization*

To improve the comprehension of the origin of *skin* and *proximity effect*—the electromagnetic field surrounding the conductor—some simple drawings and simulation results are given in the following. Figure 3.1 shows the current density and magnetic field due to *skin effect* in solid circular conductors.

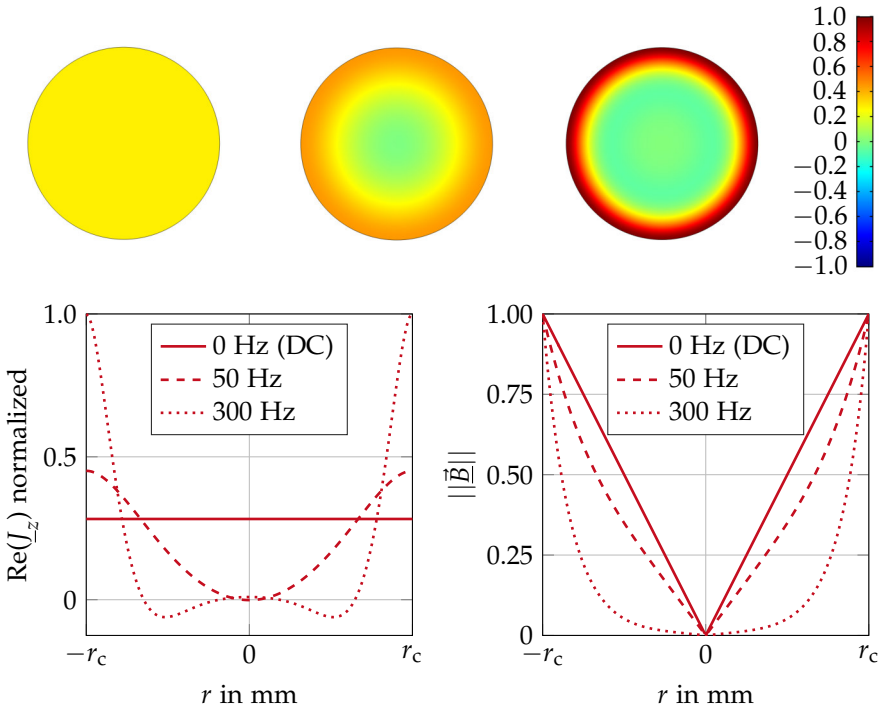

Figure 3.1: *Top*: normalized in-plane current density $\mathrm{Re}(\underline{J}_z)$ at 0 Hz (left), 50 Hz (middle) and at 300 Hz (right); *bottom*: normalized in-plane current density $\mathrm{Re}(\underline{J}_z)$ (left) and normalized magnitude of magnetic field (right) in the vertical center plane; the conductor radius r_c is 2.5 cm and the conductor material is copper; r is the radial coordinate and therefore the distance to the center of the cylindrical conductor; the symmetrical color legend is also valid for every other current density plot in this thesis

Even though two parallel conductors in a *go circuit* will have increased current density in the conductor parts furthest apart from one another (*proximity effect*, see Figure 3.2 right side), these conductors will attract each other (*inverse proximity effect*) [Duc83, p. 15].

The *inverse proximity effect* will exert a mechanical force F upon the conductors. This force—based on the *Lorentz Force Law*—depends on the current's magnitude, the length of parallel guidance and the magnitude of the magnetic field penetrating the conductors. However, it does not influence the

current distribution [Hea94, p.31]. In comparison to that, the *proximity effect* is independent of the current[6] and only depends on conductivity, frequency and geometrical parameters. The force effect of the *inverse proximity effect* can be understood by applying the *right-hand rule*. Figure 3.3 visualizes both phenomena.

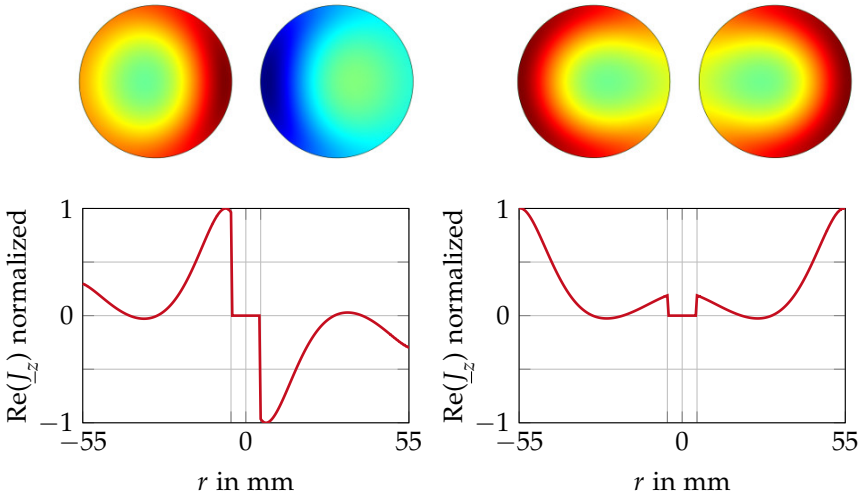

Figure 3.2: *Top*: normalized in-plane current density $\mathrm{Re}(\underline{J}_z)$ for a *return circuit* (left) and a *go circuit* (right); *bottom*: normalized in-plane current density $\mathrm{Re}(\underline{J}_z)$ for both arrangements in the center plane; copper conductors with $r_c = 2.5\,\mathrm{cm}$, $f = 50\,\mathrm{Hz}$ and distance d between both conductors set to 10 mm

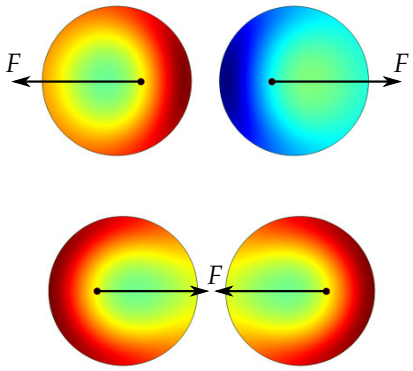

Figure 3.3: Mechanical force F and normalized in-plane current density $\mathrm{Re}(\underline{J}_z)$ in two parallel conductors in a *return circuit* (top) and *go circuit* (bottom) in accordance with [Duc83, p. 15]

Figure 3.4 to Figure 3.7 show the *Poynting vector* and other electromagnetic field quantities for different conductor arrangements. No *end effects* are present and the short-circuit between conductor and return conductor is located at the far left end of the circuit. Small differences in the field magnitudes along the conductor axis are caused due to the finite length of the simulation model. The scaling of the electric field and the *Poynting vector* is not the same in the dielectric and inside the conductor[7]. The

6 Assuming that no non-linear materials are present and thermal effects are neglected.

7 The magnitude of the electric field and the *Poynting vector* is much lower in the conductor than inside the dielectric for typical materials used in energy transmission systems.

simulations were performed for copper conductors of radius $r_c = 0.5\,\text{cm}$ at a frequency of 50 Hz. These simulations and drawings depend on different parameters of the setup and hence only give a schematic representation.

It can be shown that the reduction of the electromagnetic energy in the electromagnetic field surrounding the conductor, is equal to the power loss generated in the conductor itself [Heno7]. Hence, the *Poynting vector*—indicating the direction of energy flow—will have a component perpendicular to the conductor axis in the dielectric. Therefrom it follows that the electric field at the conductor's surface is not perfectly perpendicular to the surface if the conductor's resistance is not zero [Hea94, p. 95; vano7, p. 111]. In the presented low-loss cases (Figure 3.4 to Figure 3.7) this component in direction of the conductor axis—indicating the losses in the conductor—is much smaller than the component perpendicular to the conductor axes. The more lossy a conductor, the stronger the *Poynting vector* is skewed towards the conductor close to its surface and the more the electric field at the surface deviates from perpendicularity to the surface [Yav11, p. 168]. It does not matter if additional losses arise from a lower conductivity or from an increased frequency causing additional AC losses. In case of a single phase *return circuit* (Figure 3.4) the electric field at the conductor's surface would show an increasing deviation from perpendicularity for closer spacings for example.

Inside the conductor the *Poynting vector* will be nearly perpendicular to the conductor's surface, pointing directly at the conductor axis. It diminishes with progression to the center as the magnetic field decreases as well [Ski48, p. 134]. When penetrating into the conductor, the electromagnetic energy of the field is gradually transformed into heat, so-called *Joule heating* [Poy84, p. 351; Yav11, p. 167]. Deviations from perpendicularity to the surface are caused by non-perfectly insulating dielectrics causing the current to leave the conductor and hence creating small radial electric field components in the conductor [Mieoo]. In calculations this is typically neglected as the conductivity of typical conductors is usually much greater than that of typical insulators[8].

Additional conductive material in the dielectric (Figure 3.7) generates an additional sink for the *Poynting vector*. Energy will dissipate into heat in the conductive part (*proximity effect* losses) and reduce the energy received at the other conductor end. These losses are attributed to the main conductor and hence can be observed as an increase in resistance. Moreover, due to the distortion of the electromagnetic field caused by nearby conductive parts, the current density distribution differs even further from homogeneous distribution in the cross section. The AC resistance is smallest, when the current is homogeneously distributed over the complete available conductor cross section [Gra79, p. 32].

Note that in Figures 3.5 to 3.7 it is assumed that the return conductors (thin black lines) also exhibit losses. If that would not be the case, the *Poynting vector* would not be skewed in their direction.

8 In some early publications [TM93; Som99; Mieoo] non-perfectly insulating dielectrics are regarded.

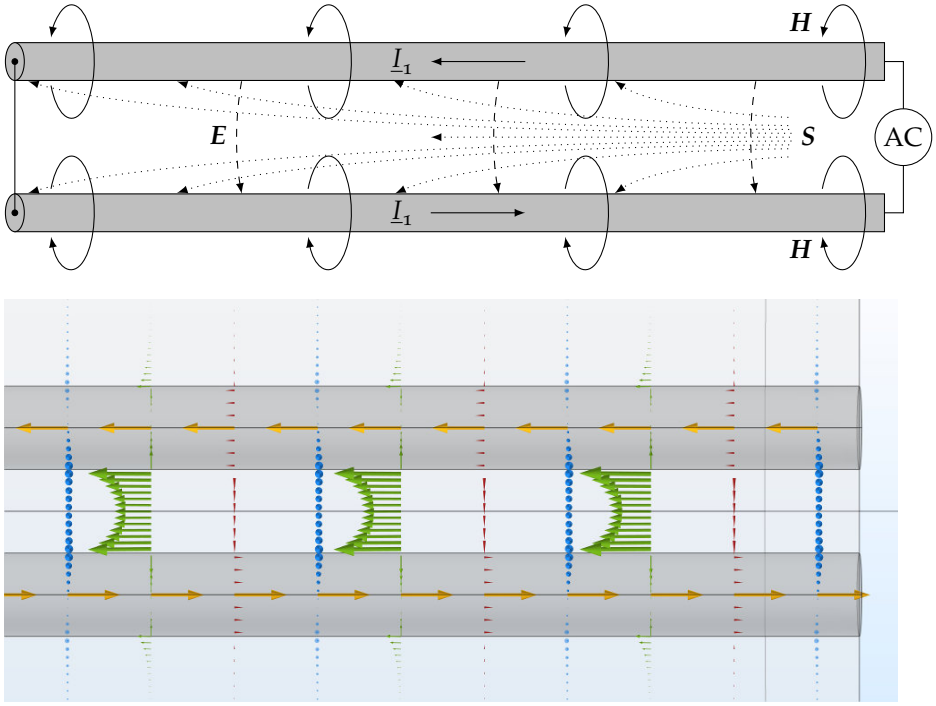

Figure 3.4: Energy flux density (dotted/green arrows), electric field (dashed/red cones), current density (yellow arrows) and magnetic field (solid line/blue arrows) in the midplane of a closely spaced single phase return circuit

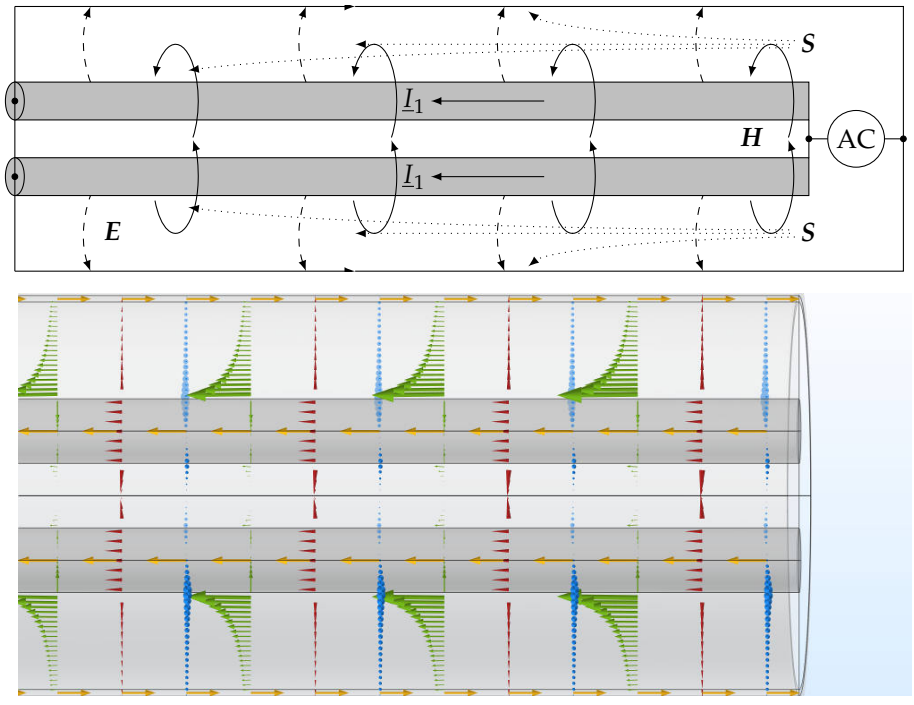

Figure 3.5: Energy flux density (dotted/green arrows), electric field (dashed/red cones), current density (yellow arrows) and magnetic field (solid line/blue arrows) in the midplane of a closely spaced go circuit with a coaxial return conductor

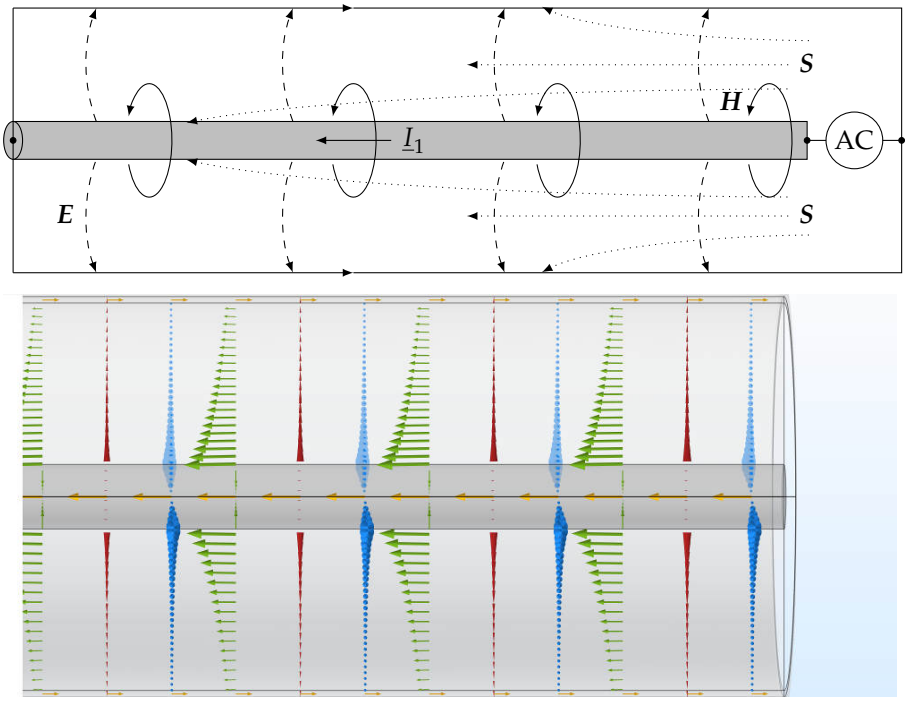

Figure 3.6: Energy flux density (dotted/green arrows), electric field (dashed/red cones), current density (yellow arrows) and magnetic field (solid line/blue arrows) in the midplane of a coaxial cable

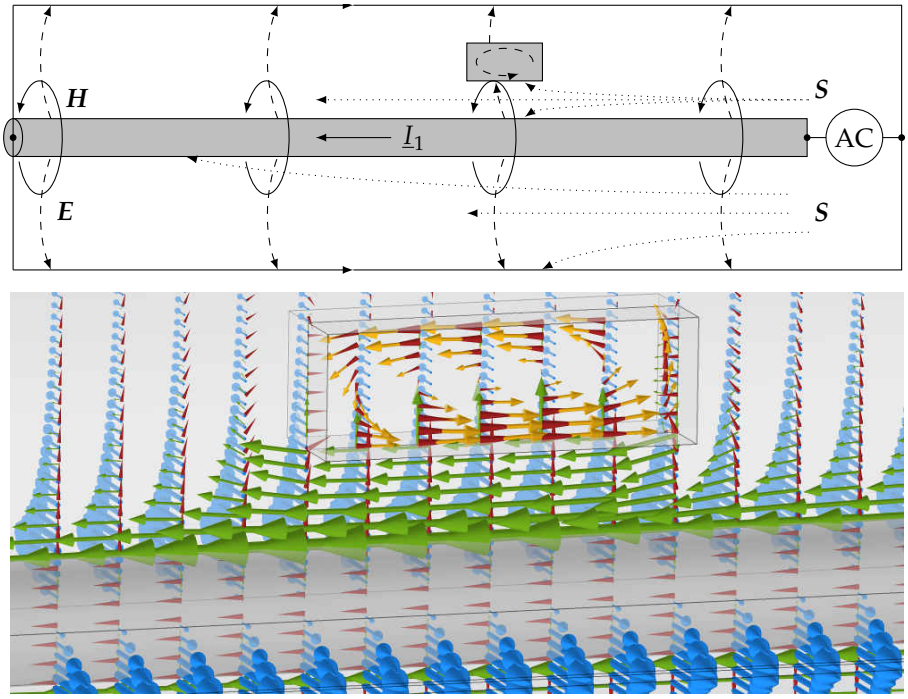

Figure 3.7: Energy flux density (dotted/green arrows), electric field (dashed/red cones), current density (yellow arrows) and magnetic field (solid line/blue arrows) in the midplane of a coaxial cable with additional conductive material in proximity

3.1.2.5 *Skin Depth and Diffusion Velocity*

The *skin depth* describes the thickness of an equivalent hollow conductor, whose DC resistance is equal to the AC resistance of the conductor of interest. In the MQS approximation—for *good* conductors—the *skin depth* depends on the conductivity of the material, the angular frequency and the magnetic permeability of the conductor and according to [JB68, p. 130] can be calculated by

$$\delta = \sqrt{\frac{2}{\sigma\ \mu_0 \mu_\mathrm{r}\ \omega}}\ . \tag{3.16}$$

Without restriction to *good* conductors, [Jor82, p. 130] shows that the *skin depth* is generally defined as

$$\delta = \frac{1}{\omega \sqrt{\frac{\mu_0 \mu_\mathrm{r} \varepsilon_0 \varepsilon_\mathrm{r}}{2} \left(\sqrt{1 + \frac{\sigma^2}{\omega^2 \varepsilon_0^2 \varepsilon_\mathrm{r}^2}} - 1 \right)}}\ . \tag{3.17}$$

At distance δ from the surface of a conductor, the current density has dropped to $\mathrm{e}^{-1} \approx 37\ \%$ of its peak value with e being the Euler number [RC18, p. 255]. In isolated round conductors the peak value is located at the conductor's surface. For copper at 50 Hz the *skin depth* is approximately 9.3 mm. The initial electromagnetic wave excited by the source will nearly propagate undamped in the dielectric (e.g.: air) but not inside the conductor [Leu05, pp. 229,231]. In the simplest case of an infinitively wide conducting half space the current density decays exponentially from surface to the center of the conductor [Kni16, p.12]. The current density at distance x from the surface of the conducting half space with surface current density $\underline{J}_\mathrm{s}$ given in $\mathrm{A/m^2}$ is governed by

$$\underline{J}_{x,\mathrm{AC}}(x) = \underline{J}_\mathrm{s}\ \mathrm{e}^{(-x/\delta)} \tag{3.18}$$

and shown in Figure 3.8. Moreover, the plot shows the equivalent conductor thickness—which is the *skin depth*—in shaded red.

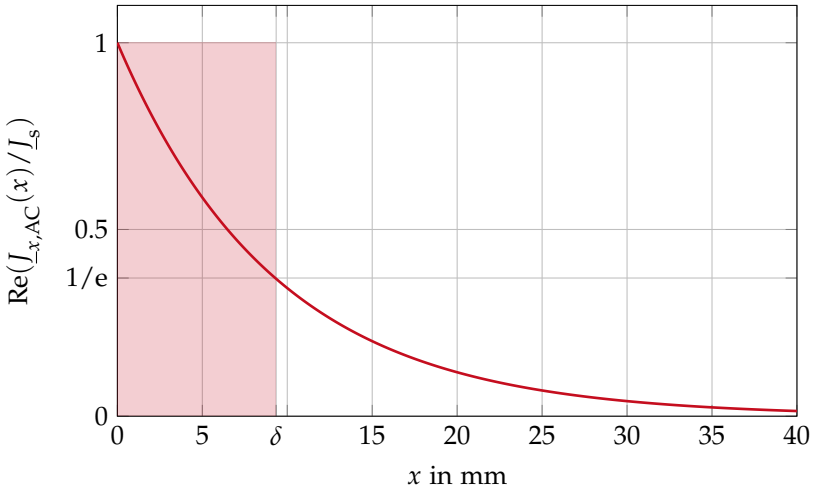

Figure 3.8: Real part of normalized current density decay in an infinitely wide copper half space at 50 Hz; the shaded red area represents the equivalent hollow conductor thickness

If the diameter of a conductor becomes larger than twice the *skin depth*, it is obvious that the conductor is uneconomical [DR30, p. 387]. This concept for loss calculation can be used if the thickness of the conductor and the radius of curvature is much greater than the *skin depth*. Moreover no rapid change of curvature radius is allowed around the conductor periphery [Ter43, p. 34].

The diffusion phase velocity—the speed of the electromagnetic wave—in the conducting medium is

$$v_{\text{diff}} = \omega \cdot \delta = \sqrt{\omega} \cdot \sqrt{\frac{2}{\sigma\, \mu_0 \mu_\text{r}}} \tag{3.19}$$

according to [LŠT66, p. 40; ES03]. For a copper conductor at 50 Hz the diffusion velocity reaches approximately 2.9 m/s. Equation (3.19) additionally shows that a PEC is a perfect obstructor and cannot absorb energy of the electromagnetic field as the electromagnetic field cannot diffuse into the conductor [Hea93, p. 328; Leh10, p. 407]. In that case the diffusion velocity will be zero and the PEC acts as a perfect guideway for the electromagnetic wave propagating along the conductor.

3.1.2.6 *Principle of Similitude*

The *Principle of Similitude* was first enunciated in 1918 by H. Dwight in [Dwi18, p. 1398] and shortly after followed by a mathematical proof by J. Slepian in the discussion to the same reference ([Dwi18, p. 1401]). The principle implies that a conductor or a set of conductors of a proportionate shape[9] and identical relative positions to one another, will have a fixed resistance ratio $R_{\text{AC}}/R_{\text{DC}}$ for a specific value of f/R_{DC}. In return, this means that curves plotted over f/R_{DC}, $\sqrt{f/R_{\text{DC}}}$ or parameters proportionate to the ratio f/R_{DC}, can be used to determine the resistance ratio at any frequency and conductivity for any proportionate conductor shape. In other words, the conductor resistance for a certain shape is a function solely depending on the frequency and conductivity (in case of isolated conductors). Hence, a parameter including the ratio of both quantities can be introduced [Hae37; Dwi47]. This is called the *Principle of Similitude parameter* (*pos parameter*). It is defined as

$$p = \sqrt{\frac{f}{R_{\text{DC}}}} \cdot 1 \times 10^{-3} \ , \tag{3.20}$$

and given in $\sqrt{\text{m}/(\Omega\text{s})}$. The arbitrary constant 1×10^{-3} is introduced to keep the value of this parameter in an easily traceable range for typical conductor properties dealt with in this thesis. For a wider use of results, one will rather plot curves for different conductor shapes or different relative positions over p and not over frequency f. From curves plotted over p, the results for different frequencies or conductivities can be deduced for any proportionate shape. For very large frequencies—where only surface currents are existent—the resistance ratio $R_{\text{AC}}/R_{\text{DC}}$ is linear proportional to $\sqrt{(f/R_{\text{DC}})}$ [Dwi47, p. 1]. These curves become straight lines when plotted over p (see Figure 3.9).

9 When scaling geometric dimensions all geometric ratios of the conductor cross sections have to remain constant (e.g.: for a tubular conductor the ratio of outer diameter to inner diameter). This equals zooming in or out of a setup without directly changing the geometry.

Figure 3.9 shows the general resistance curve for isolated solid cylindrical conductors. From this curve one can obtain the resistance ratio for every other conductor of proportional shape (for every desired frequency, conductivity and cross section).

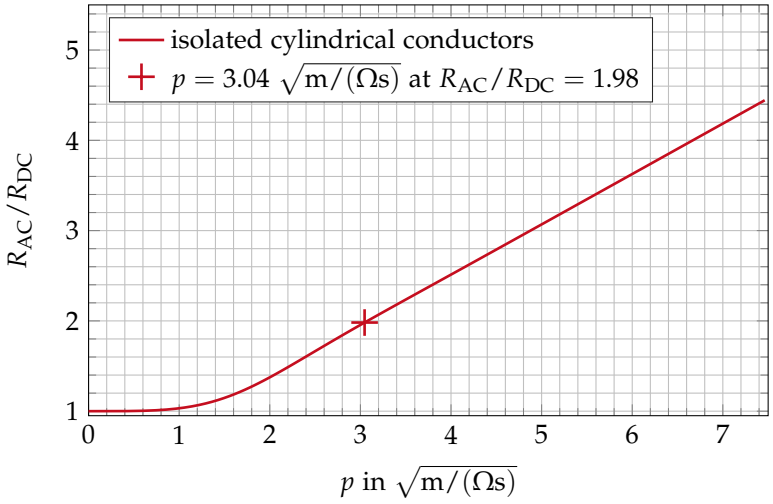

Figure 3.9: Characteristic resistance curve for isolated solid cylindrical conductors

For example: a solid cylindrical copper conductor with a cross section of $A = 3200\,\mathrm{mm}^2$, conductivity $\sigma = 58 \times 10^6\,\mathrm{S/m}$ and applied frequency $f = 50\,\mathrm{Hz}$, has a *pos parameter* of $p = 3.04\ \sqrt{\mathrm{m}/(\Omega\mathrm{s})}$ and is also marked in Figure 3.9. Figure 3.10 serves as a verification as it plots the resistance ratio for this specific conductor over the frequency and shows that the resistance ratio at 50 Hz is in fact 1.98, as predicted by Figure 3.9.

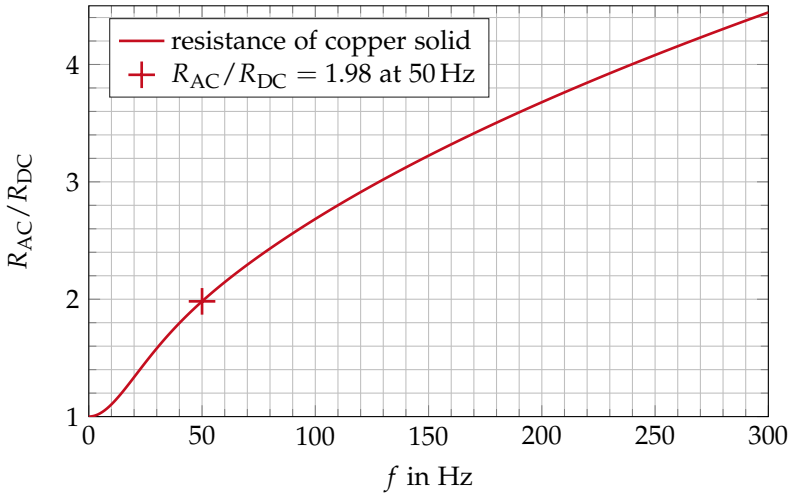

Figure 3.10: Resistance ratio plotted for the specific copper conductor with $A = 3200\,\mathrm{mm}^2$; the ratio matches the predicted value of Figure 3.9

In comparison to Figure 3.10 where the applicability of the absolute value is restricted to this conductor only, Figure 3.9 can predict the resistance ratio for any other conductor of proportional shape.

Another example, where *proximity effect* is included is shown in Figure 3.11. To get the same resistance ratio at half the frequency, one needs to linearly

scale all dimensions proportional to $1/p$ [DR30, p. 495]. Hence, when reducing the frequency to halve the value, increasing all dimensions by $\sqrt{2}$ will result in the same resistance ratio and current density distribution [BA69, p. 184][10].

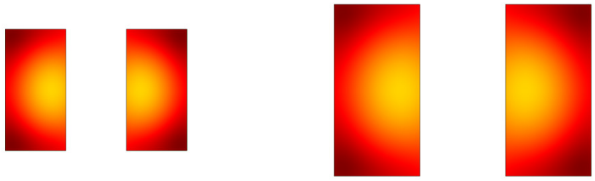

Figure 3.11: Normalized in-plane current density $\mathrm{Re}(\underset{\sim}{J})$ in two parallel copper bars; *left*: at $f = 50\,\mathrm{Hz}$; *right*: at $f = 25\,\mathrm{Hz}$ with dimensions (conductor height, conductor width and center-to-center distance) enlarged by $\sqrt{2}$; both arrangements have the same resistance ratio; note that both plots are independently normalized and hence do not have the same absolute current density

As suggested by Dwight this principle can be used for measurements on large conductors as well. As the voltage drop is decreasing with larger cross sections, one could alternatively increase the frequency and use a smaller conductor with proportional shape [Dwi18, p. 1398]. If all geometrical and material properties are known this could also be done for more complex conductor types.

To make for a wider application, plots where all factors of influence are known (e.g.: analytical curves) are plotted over the *pos parameter*. For the evaluation of measurements, the results are plotted over the frequency. As seen later, the exact properties of a *Milliken* design are not known in advance. Moreover, the plots will be unique as every setup and laboratory has a specific geometric configuration (position of conducting walls, floors, ...).

3.1.2.7 *Skin Effect and Energy Flow Analogies*

As previously explained, the current diffuses from the conductor's surface into the conductor. Physical analogues are similar processes governed by the same type of equation as the *skin effect*: the generalized diffusion equation

$$\frac{\partial \boldsymbol{F}}{\partial t} = a \frac{\partial^2 \boldsymbol{F}}{\partial x^2} \tag{3.21}$$

as taken from [ES01, p. 404]. $\boldsymbol{F}$ can for example stand for $\boldsymbol{E}, \boldsymbol{J}$ or $\boldsymbol{H}$.

First *skin effect* analogies were evicted by Heaviside already in 1892 in [Hea92, p.384] and later in [Hea94, p.182] and [Yav11, p.195]. Heaviside compared the diffusion of electromagnetic fields into a conductor to a pipe filled with water. In this case water represents the conductor, the pipe the dielectric and the velocity of the water represents the magnitude of the current density. If the pipe is accelerated along its axis—analogous to an electromagnetic wave propagating in the dielectric—due to the friction and its viscous character, the water inside the pipe will accelerate as well. Layers of water in direct contact with the pipe will be accelerated faster than water at the center of the pipe. This example remains sensible for both cases: DC

10 The reason is that the frequency is in the denominator of the root term for the *skin depth* calculation, which is connected to the current density and hence the resistance.

and AC excitation.

Henry Poynting used the liquid analog to describe the dissipation of field energy into the conductor. He compared the electromagnetic wave surrounding a conductor to a liquid, which transforms kinetic energy to thermal energy due to friction on the conductor's surface. In case of AC the losses appear to increase due to the change of direction of the fluid [Poy84].

Another powerful analog first presented by Lord Kelvin et. al. in 1890 is the temperature diffusion into a solid [TLJ90, p. 496]. In case of a change in temperature in the medium surrounding the solid, the temperature will only diffuse into the solid with a phase shift and damped amplitude. For example the alternating surface temperature on earth will only slowly diffuse into the soil and only to a limited amount.

3.1.3 *Review of Available Exact Formulas*

For middle range frequencies *skin effect* losses are not easily computed [Leh10, p. 410]. Whereas for very low frequencies the resistance is almost identical to the DC resistance and for very high frequencies one can use the *skin depth* concept. Large power cable conductors operated at power frequency are within this intermediate range. Hence, in the following, all conductor types that have an explicit formula for the resistance, inductance or current density are listed, to be independent of certain frequency ranges for AC resistance calculations. All analytical solutions are based on the MQS approximation and assume that no *end effects* are present[11] [Kni16]. If no return conductor is specified, its influence is neglected in the calculation (the conductor is isolated). Moreover, the current can only flow into the direction of the conductor axis and not radially. In other words, the dielectric surrounding the conductors is a perfect insulator and hence, only the z-components of the current density vector has a value different from zero.

For some important cross sectional shapes example plots are given. The exemplary current density distribution plots show the real part of the normalized in-plane current density $\mathrm{Re}(\underline{J}_z)$ at frequencies or dimensions, where severe *skin effect* occurs. Whereas the real part is linked to the AC resistance, the imaginary part or phase shifted components are directly linked to the internal inductance [Liu16, p. 34]. The color legend of the plots is again this of Figure 3.1. The *Matlab*[12] code to solve some of these analytical solutions can be found in Appendix B. The used *Bessel* and *Kelvin functions* are defined in Appendix C. In every case, only the real part of the current density is plotted, which represents the magnitude of the current. Resistance and inductance curves are plotted—according to the *Principle of Similitude*—over parameter p (except for the *Infinitively Wide Strip*, where no DC resistance value can be calculated).

In Section 3.1.5 characteristic resistance and inductance curves for different conductors are compared. Moreover, to get an impression of the current

11 The term *end effect* refers to current inhomogeneities caused by an inhomogeneous current injection into the conductor. Only true 2D problems are considered.

12 *Matlab* is a software provided by *MathWorks* and can be found at `www.mathworks.com` (visited on 08/12/2017).

density distribution in different conductor cross sections and arrangements, a large number of simulation results for the current density is given in Section 3.1.5 as well.

The formulas for the *Infinitively Wide Strip* (Section 3.1.3.1), for *Two Solid Cylindrical Conductors in Return Circuit* (Section 3.1.3.8) and the formulas for *Two Tubular Conductors in Return Circuit* (Section 3.1.3.9) have been derived at the beginning of the 20th century and therefore use the electromagnetic unit centimetre-gram-second (emu cgs) system. In these calculations all distances have to be given in cm, all surface areas in cm^2 and the conductivity in abmhos/cm.[13] The emu cgs of ω is identical to the SI unit. All other formulas in this work use the SI system of units.

In every case, conductivity σ depends on temperature T and temperature coefficient α_T as follows

$$\sigma = \frac{\sigma_0}{1 + \alpha_T (T - T_0)} \quad . \tag{3.22}$$

Typical values for the reference conductivity σ_0 at $T_0 = 20\,°C = 293.15\,K$ and for α_T have been displayed in Section 2.3. The curves will be plotted for copper conductors at 20 °C.

3.1.3.1 *Infinitively Wide Strip*

The conductor is infinitively expanded in x direction. The following formulas were taken from [KLP15, p. 2002]. Even though this is not a realistic conductor geometry, this was the first analytical formula for the AC resistance calculation presented in the literature. The formulas use the emu cgs.

GEOMETRY:

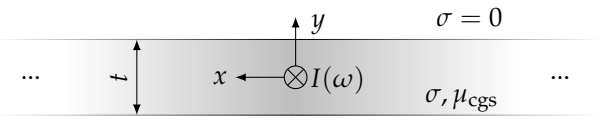

CURRENT DENSITY RATIO: The AC current density $\underline{J}_{z,\mathrm{AC}}(y)$ at coordinate y with regard to the current density at the surface of the strip $\underline{J}_{z,\mathrm{AC}}(y = t/2)$ is

$$\frac{\underline{J}_{z,\mathrm{AC}}(y)}{\underline{J}_{z,\mathrm{AC}}(y = t/2)} = \frac{\cosh(\underline{\alpha} y)}{\cosh(\underline{\alpha}(t/2))} \tag{3.23}$$

$$\text{with} \quad \underline{\alpha} = \sqrt{2\pi\sigma\mu_{\mathrm{cgs}}\omega} + \mathrm{j}\sqrt{2\pi\sigma\mu_{\mathrm{cgs}}\omega} \quad . \tag{3.24}$$

In the formulas above t is the thickness of the strip in m and cosh the hyperbolic cosine. μ_{cgs} is the dimensionless permeability in emu cgs and is exactly 1 for non-magnetic conductors.

13 Conversion of SI unit m to emu cgs cm is performed by a multiplication of the SI unit with 10^2. Conversion of SI unit m^2 to emu cgs cm^2 is performed by a multiplication of the SI unit with 10^4. Conversion of SI units S/m for the conductivity to abmhos/cm is performed by a multiplication of the SI unit with 10^{-11}. Permeability μ_{cgs} is dimensionless and exactly 1 for non-magnetic conductors [RWv94, p. 813]

RESISTANCE RATIO: The resistance ratio is defined as

$$\frac{R_{\mathrm{AC}}}{R_{\mathrm{DC}}} = \mathrm{Re}\left(\frac{\underline{\alpha} t}{2 \cdot \tanh\left(\frac{\underline{\alpha} t}{2}\right)}\right) , \tag{3.25}$$

whereby tanh is the hyperbolic tangent.

INTERNAL REACTANCE RATIO: As the definition of the DC resistance is not sensible in case of an infinitively wide strip the normalized internal reactance is given instead by:

$$\frac{L_{\mathrm{iAC}} \cdot \omega}{R_{\mathrm{DC}}} = \frac{X_{\mathrm{iAC}}}{R_{\mathrm{DC}}} = \mathrm{Im}\left(\frac{\underline{\alpha} t}{2 \cdot \tanh\left(\frac{\underline{\alpha} t}{2}\right)}\right) . \tag{3.26}$$

L_{iAC} is the AC internal inductance per-unit length in H/m, X_{iAC} is the AC internal reactance per-unit length in Ω/m and Im takes the imaginary part of the expression.

EXAMPLE PLOTS: Plots for a copper strip with a thickness $t = 2\,\mathrm{cm}$. From left to right: normalized y coordinate over magnitude (real part) of current density ratio at frequency $f = 50\,\mathrm{Hz}$, plot of resistance and reactance ratio over frequency f.

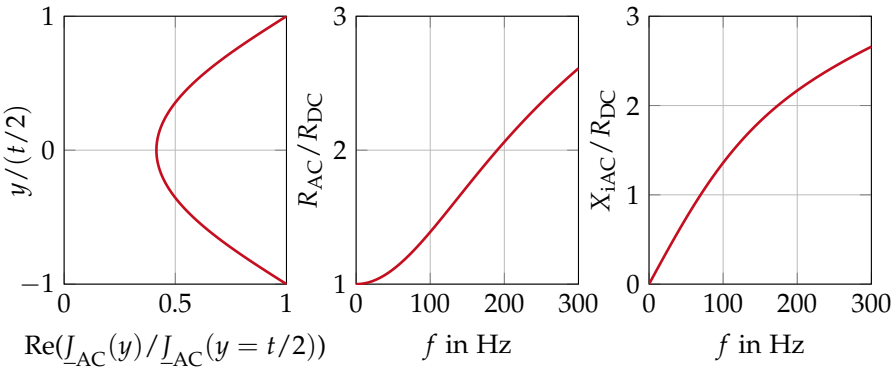

3.1.3.2 *Solid Cylindrical Conductor*

The formulas using the Bessel functions were taken from [Wee81, p. 38], whereas the formulas with the Kelvin functions and their derivatives are taken from [Kni16, p. 8] and [McL55, p. 158].

GEOMETRY AND EXEMPLARY AC CURRENT DENSITY:

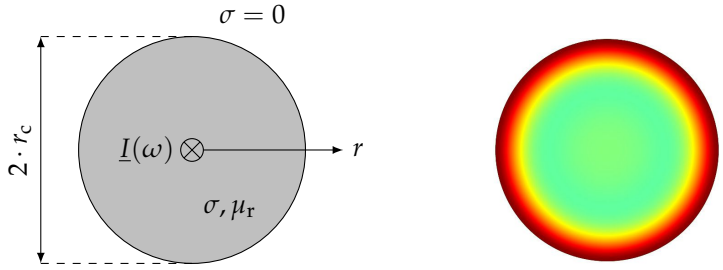

CURRENT DENSITY: The DC current density $J_{z,\mathrm{DC}}$ in $\mathrm{A/m^2}$ is:

$$J_{z,\mathrm{DC}} = \frac{I}{\pi r_\mathrm{c}^2} \quad . \tag{3.27}$$

In case of ACs, the current density also depends on the radial distance r to the center of the wire by

$$\underline{J}_{z,\mathrm{AC}}(r) = \frac{\underline{m}\, \underline{I}}{2\pi r_\mathrm{c}} \frac{\mathrm{J}_0(\underline{m} r)}{\mathrm{J}_1(\underline{m} r_\mathrm{c})} \tag{3.28}$$

$$\text{with} \quad \underline{m} = \sqrt{-\mathrm{j}\omega\mu_0\mu_\mathrm{r}\sigma} = (1-\mathrm{j})\sqrt{\frac{\omega\mu_\mathrm{r}\mu_0\sigma}{2}} = (1-\mathrm{j})\frac{1}{\delta} \tag{3.29}$$

or alternatively using the Kelvin functions

$$\underline{J}_{z,\mathrm{AC}}(r) = \frac{\underline{I}k}{2\pi r_\mathrm{c}} \left[\frac{\mathrm{ber}_0(kr) + \mathrm{j}\cdot\mathrm{bei}_0(kr)}{\mathrm{bei}_0^{'}(kr_\mathrm{c}) - \mathrm{j}\cdot\mathrm{ber}_0^{'}(kr_\mathrm{c})} \right] \tag{3.30}$$

$$\text{with} \quad k = \sqrt{\omega\mu_0\mu_\mathrm{r}\sigma} = \mathrm{Re}(\underline{m})\cdot\sqrt{2} \quad . \tag{3.31}$$

Above, r_c is the conductor radius and J_ν is the Bessel function of the first kind and ν^{th} order. Moreover, ber_ν, bei_ν, $\mathrm{ber}_\nu^{'}$, $\mathrm{bei}_\nu^{'}$ are the Kelvin functions, which are the real and imaginary parts of the Bessel function of the first kind and ν^{th} order: J_ν. The apostrophe indicates their derivatives.

RESISTANCE RATIO: The DC resistance per-unit length of a solid cylindrical conductor is

$$R_\mathrm{DC} = \frac{1}{\sigma\cdot\pi r_\mathrm{c}^2} \quad . \tag{3.32}$$

The resistance ratio of a cylindrical conductor is

$$\frac{R_\mathrm{AC}}{R_\mathrm{DC}} = \mathrm{Re}\left[\frac{\underline{m} r_\mathrm{c}}{2} \frac{\mathrm{J}_0(\underline{m} r_\mathrm{c})}{\mathrm{J}_1(\underline{m} r_\mathrm{c})} \right] \tag{3.33}$$

$$= \frac{kr_\mathrm{c}}{2} \left[\frac{\mathrm{ber}_0(kr_\mathrm{c})\mathrm{bei}_0^{'}(kr_\mathrm{c}) - \mathrm{bei}_0(kr_\mathrm{c})\mathrm{ber}_0^{'}(kr_\mathrm{c})}{(\mathrm{ber}_0^{'}(kr_\mathrm{c}))^2 + (\mathrm{bei}_0^{'}(kr_\mathrm{c}))^2} \right] \quad . \tag{3.34}$$

INTERNAL INDUCTANCE RATIO: The internal inductance ratio is

$$\frac{L_\mathrm{iAC}}{L_\mathrm{iDC}} = \frac{R_\mathrm{DC}\cdot 8\pi}{\omega\mu_\mathrm{r}\mu_0} \cdot \mathrm{Im}\left[\frac{\underline{m} r_\mathrm{c}}{2} \frac{\mathrm{J}_0(\underline{m} r_\mathrm{c})}{\mathrm{J}_1(\underline{m} r_\mathrm{c})} \right] \tag{3.35}$$

$$= \frac{R_\mathrm{DC}\cdot 8\pi}{\omega\mu_\mathrm{r}\mu_0} \cdot \frac{kr_\mathrm{c}}{2} \left[\frac{\mathrm{ber}_0(kr_\mathrm{c})\mathrm{ber}_0^{'}(kr_\mathrm{c}) + \mathrm{bei}_0(kr_\mathrm{c})\mathrm{bei}_0^{'}(kr_\mathrm{c})}{(\mathrm{ber}_0^{'}(kr_\mathrm{c}))^2 + (\mathrm{bei}_0^{'}(kr_\mathrm{c}))^2} \right] . \tag{3.36}$$

The internal inductance at DC per-unit length in H/m from [Mor13, p. 1253] is independent of r_c and defined as

$$L_\mathrm{iDC} = \frac{\mu_\mathrm{r}\mu_0}{8\pi} = \frac{\mu_\mathrm{r}\cdot 10^{-7}}{2} \quad . \tag{3.37}$$

EXAMPLE PLOTS: From left to right: real part of normalized current density over normalized r coordinate at frequency $f = 50\,\mathrm{Hz}$ for a solid cylindri-

cal copper conductor with $r_c = 2\,\text{cm}$ and plot of resistance and inductance ratio over the *pos parameter* p.

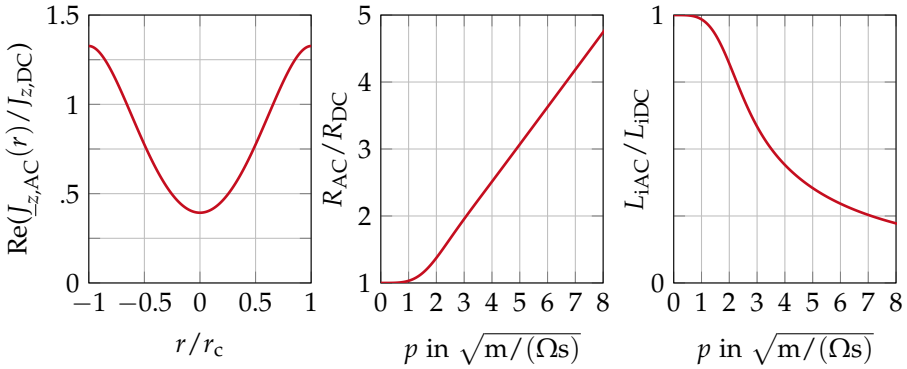

3.1.3.3 *Tubular Conductor*

The analytical formulas for tubular conductors are taken from [Mor13]. The formula for the inductance ratio was corrected accordingly (typo in [Mor13, p. 1255]).

In detail described by [LBV11], large complex Bessel function arguments can lead to numerical instabilities in the evaluation of the Bessel function. Approximate formulas proposed in [VBS09] are recommended, if large complex Bessel function arguments appear. They show to be of high accuracy and numerically stable [LBV11]. Alternatively, precalculated numerical results for large function arguments can directly be taken from [MY04].

GEOMETRY AND EXEMPLARY AC CURRENT DENSITY:

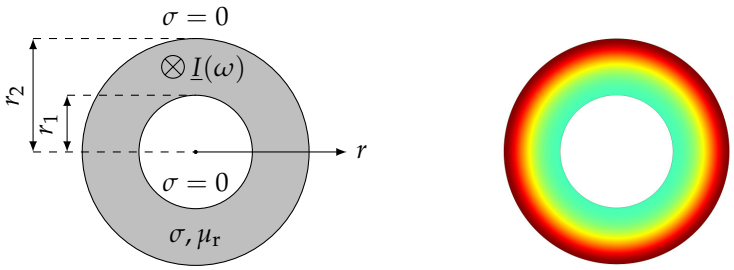

CURRENT DENSITY: The DC current density for a tubular conductor is

$$J_{z,\mathrm{DC}} = \frac{I}{\pi(r_2^2 - r_1^2)} \quad . \tag{3.38}$$

The AC current density at coordinate r is

$$\underline{J}_{z,\mathrm{AC}}(r) = \underline{J}_{z,\mathrm{AC}}(r_2)\left[\frac{\mathrm{J}_0(\underline{m}r)\mathrm{Y}_0'(\underline{m}r_1) - \mathrm{J}_0'(\underline{m}r_1)\mathrm{Y}_0(\underline{m}r)}{\mathrm{J}_0(\underline{m}r_2)\mathrm{Y}_0'(\underline{m}r_1) - \mathrm{J}_0'(\underline{m}r_1)\mathrm{Y}_0(\underline{m}r_2)}\right] \quad , \tag{3.39}$$

where $\underline{J}_{z,\mathrm{AC}}(r_2)$ is the current density at the conductor's surface [Mor13]. Y_ν is the Bessel function of the second kind and order ν. To the best knowledge of the author, $J(r_2)$ cannot be computed analytically.

RESISTANCE RATIO: The DC resistance per-unit length of a tubular conductor is

$$R_{\mathrm{DC}} = \frac{1}{\sigma \cdot \pi (r_2^2 - r_1^2)} \quad . \tag{3.40}$$

The resistance ratio of a hollow conductor is calculated as

$$\frac{R_{\mathrm{AC}}}{R_{\mathrm{DC}}} = \mathrm{Re}\left[\frac{\mathrm{j}k(r_2^2 - r_1^2)}{2r_2} \cdot \ \ldots \right. \\ \left. \frac{(\mathrm{ber}_0(kr_2) + \mathrm{jbei}_0(kr_2)) - \underline{C}(\mathrm{ker}_0(kr_2) + \mathrm{jkei}_0(kr_2))}{(\mathrm{ber}_0'(kr_2) + \mathrm{jbei}_0'(kr_2)) - \underline{C}(\mathrm{ker}_0'(kr_2) + \mathrm{jkei}_0'(kr_2))}\right] \tag{3.41}$$

$$\text{with } \underline{C} = \frac{\mathrm{ber}_0'(kr_1) + \mathrm{jbei}_0'(kr_1)}{\mathrm{ker}_0'(kr_1) + \mathrm{jkei}_0'(kr_1)} \quad . \tag{3.42}$$

INTERNAL INDUCTANCE RATIO: The internal inductance ratio is given by the following equation.

$$\frac{L_{\mathrm{iAC}}}{L_{\mathrm{iDC}}} = \frac{R_{\mathrm{DC}}}{\omega \cdot L_{\mathrm{iDC}}} \cdot \mathrm{Im}\left[\frac{\mathrm{j}k(r_2^2 - r_1^2)}{2r_2} \cdot \ \ldots \right. \\ \left. \frac{(\mathrm{ber}_0(kr_2) + \mathrm{jbei}_0(kr_2)) - \underline{C}(\mathrm{ker}_0(kr_2) + \mathrm{jkei}_0(kr_2))}{(\mathrm{ber}_0'(kr_2) + \mathrm{jbei}_0'(kr_2)) - \underline{C}(\mathrm{ker}_0'(kr_2) + \mathrm{jkei}_0'(kr_2))}\right] \quad , \tag{3.43}$$

whereby the internal inductance per-unit length at DC is

$$L_{\mathrm{iDC}} = \frac{\mu_{\mathrm{r}}\mu_0}{2\pi}\left[\frac{r_1^4}{(r_2^2 - r_1^2)^2} \ln\left(\frac{r_2}{r_1}\right) - \frac{3r_1^2 - r_2^2}{4(r_2^2 - r_1^2)}\right] \quad . \tag{3.44}$$

EXAMPLE PLOTS: From left to right: real part of normalized current density over r coordinate at frequency $f = 50\,\mathrm{Hz}$ for a solid tubular copper conductor with $r_1 = 1.25\,\mathrm{cm}$ and $r_2 = 2.5\,\mathrm{cm}$ (simulated) and plot of resistance and inductance ratio over p for $r_2/r_1 = 2$.

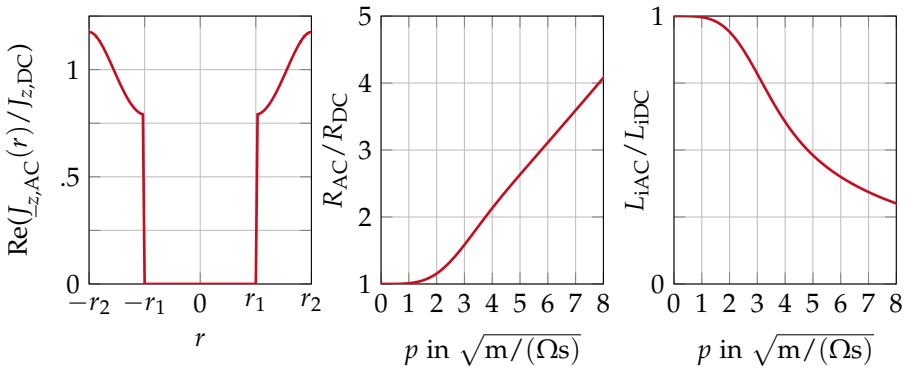

3.1.3.4 *Coaxial Cable in Return Circuit*

The overall impedance of a coaxial cable, where current flows in one direction in the inner conductor and returns in the concentric tubular conductor is given in [Mro03, p. 161] and [MS13, p. 140]. The following equations for the resistance and inductance per-unit length are taken from [Mro03, p. 161].

GEOMETRY AND EXEMPLARY AC CURRENT DENSITY:

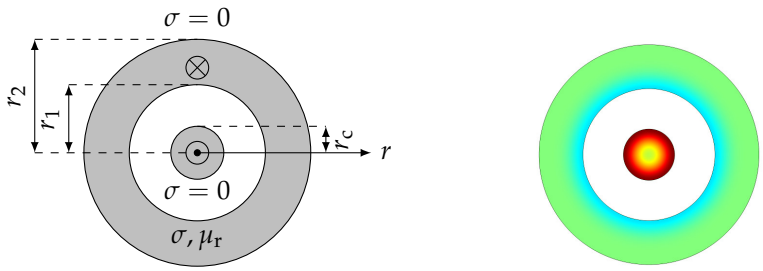

Even though the *proximity effect* forces the current to oppose *skin effect* in the outer tube and concentrate on the inner side instead, the current density deviates even stronger compared to an isolated tubular conductor at the same p. This results in AC losses in the outer tube, which are larger than those of an isolated tubular conductor alone.

RESISTANCE RATIO: The DC resistance per-unit length is

$$R_{\mathrm{DC}} = \frac{1}{\sigma\pi r_{\mathrm{c}}^2}\left[1 + \frac{r_{\mathrm{c}}^2}{r_2^2 - r_1^2}\right] \tag{3.45}$$

and the resistance ratio is given by

$$\frac{R_{\mathrm{AC}}}{R_{\mathrm{DC}}} = \mathrm{Re}\left[\frac{\underline{\gamma} r_{\mathrm{c}}(r_2^2 - r_1^2)}{2(r_2^2 - r_1^2 + r_{\mathrm{c}}^2)} \cdot \ldots \right.$$
$$\left. \left[\frac{\mathrm{I}_0(\underline{\gamma} r_{\mathrm{c}})}{\mathrm{I}_1(\underline{\gamma} r_{\mathrm{c}})} - \frac{r_{\mathrm{c}}}{r_1} \cdot \frac{\mathrm{I}_0(\underline{\gamma} r_1)\mathrm{K}_1(\underline{\gamma} r_2) + \mathrm{K}_0(\underline{\gamma} r_1)\mathrm{I}_1(\underline{\gamma} r_2)}{\mathrm{I}_1(\underline{\gamma} r_1)\mathrm{K}_1(\underline{\gamma} r_2) - \mathrm{K}_1(\underline{\gamma} r_1)\mathrm{I}_1(\underline{\gamma} r_2)}\right]\right]. \tag{3.46}$$

In the equations above and in the following

$$\underline{\gamma} = \sqrt{\mathrm{j}\omega\sigma\mu_0\mu_{\mathrm{r}}}\ , \tag{3.47}$$

I_ν is the modified Bessel function of the first kind and ν^{th} order and K_ν is the modified Bessel function of the second kind and ν^{th} order.

INTERNAL INDUCTANCE: The internal AC inductance is given by the following equation.

$$L_{\mathrm{iAC}} = \mathrm{Im}\left[\frac{\underline{\gamma}}{2\pi r_{\mathrm{c}}\sigma\omega} \cdot \ldots \right.$$
$$\left. \left[\frac{\mathrm{I}_0(\underline{\gamma} r_{\mathrm{c}})}{\mathrm{I}_1(\underline{\gamma} r_{\mathrm{c}})} - \frac{r_{\mathrm{c}}}{r_1} \cdot \frac{\mathrm{I}_0(\underline{\gamma} r_1)\mathrm{K}_1(\underline{\gamma} r_2) + \mathrm{K}_0(\underline{\gamma} r_1)\mathrm{I}_1(\underline{\gamma} r_2)}{\mathrm{I}_1(\underline{\gamma} r_1)\mathrm{K}_1(\underline{\gamma} r_2) - \mathrm{K}_1(\underline{\gamma} r_1)\mathrm{I}_1(\underline{\gamma} r_2)}\right]\right] \tag{3.48}$$

3.1.3.5 *Concentric Tubular Conductor with an Inner Solid Return Conductor*

In comparison to the previous formulas, the following calculation shows the analytical solutions for the resistance and inductance of the outer tubular conductor alone, even though the solid inner conductor is present and used as the return. Hence, the *Geometry and Exemplary AC Current Density* is identical to the one shown in the previous section (Section 3.1.3.4). The solution was first given in emu cgs by [Rus09] in 1909. The formula below is

given in SI units[14]. The following formulas expand over multiple lines and are terminated by a full stop.

RESISTANCE RATIO: The AC resistance ratio is

$$\begin{aligned}\frac{R_{\mathrm{AC}}}{R_{\mathrm{DC}}} = \frac{r_c(r_2^2 - r_1^2)k}{4(r_c^2 - r_1^2 + r_2^2)G_1(kr_c)} \cdot \ldots \\ \Big[\big(\mathrm{ber}_0(kr_c)\mathrm{bei}_0'(kr_c) - \mathrm{bei}_0(kr_c)\mathrm{ber}_0'(kr_c)\big) + \\ \mathrm{bei}_0'(kr_c)\big(\Xi_3\mathrm{ber}_0(kr_1) + \Xi_4\mathrm{bei}_0(kr_1) + \Xi_1\mathrm{ker}_0(kr_1) + \Xi_2\mathrm{kei}_0(kr_1)\big) - \\ \mathrm{ber}_0'(kr_c)\big(\Xi_3\mathrm{bei}_0(kr_1) - \Xi_4\mathrm{ber}_0(kr_1) + \Xi_1\mathrm{kei}_0(kr_1) - \Xi_2\mathrm{ker}_0(kr_1)\big)\Big].\end{aligned} \tag{3.49}$$

The formula above is extended over four lines.

INTERNAL INDUCTANCE: The DC inductance is

$$L_{\mathrm{iDC}} = 2\mu' \log\frac{r_1}{r_c} + \frac{\mu}{2} + \frac{2\mu r_2^4}{(r_2^2 - r_1^2)^2}\log\frac{r_2}{r_1} - \mu\frac{3r_2^2 - r_1^2}{2(r_2^2 - r_1^2)} \tag{3.50}$$

and the inductance at AC is

$$\begin{aligned}L_{\mathrm{iAC}} = 2\mu' \log\frac{r_1}{r_c} + \frac{2\mu}{kr_cG_1(kr_c)} \cdot \ldots \\ \Big[\big(\mathrm{ber}_0(kr_c)\mathrm{ber}_0'(kr_c) + \mathrm{bei}_0(kr_c)\mathrm{bei}_0'(kr_c)\big) + \\ \mathrm{ber}_0'(kr_c)\big(\Xi_3\mathrm{ber}_0(kr_1) + \Xi_4\mathrm{bei}_0(kr_1) + \Xi_1\mathrm{ker}_0(kr_1) + \Xi_2\mathrm{kei}_0(kr_1)\big) + \\ \mathrm{bei}_0'(kr_c)\big(\Xi_3\mathrm{bei}_0(kr_1) - \Xi_4\mathrm{ber}_0(kr_1) + \Xi_1\mathrm{kei}_0(kr_1) - \Xi_2\mathrm{ker}_0(kr_1)\big)\Big].\end{aligned} \tag{3.51}$$

The formula above is extended over four lines as well. In these formulas μ is the product of magnetic permeability of the conductors times the vacuum permeability. μ' is the product of magnetic permeability of the space between the conductors times the vacuum permeability. Functions G_1 to G_3 and Ξ_1 to Ξ_4 are defined in Appendix C.4.

3.1.3.6 *Bi-Media Conductor*

The analytical solution for a solid bi-media conductor was first derived in [LCK15] and [Liu16] as it can be of practical relevance for new power cable conductor designs. The basic idea is to combine two materials with different conductivities (e.g.: copper and aluminum) and put the material of lower conductivity in the conductor center to reduce the *skin effect* in these parts. The following formulas were taken from [Liu16, pp. 76-79]. The *Matlab* code for the calculations can be found in the appendix of [Liu16].

14 A big thank you to my student assistant Nick Wieczorek for translating this formula from the original **emu cgs system** to SI units and working out the constants and arguments of the involved functions.

GEOMETRY AND EXEMPLARY AC CURRENT DENSITY:

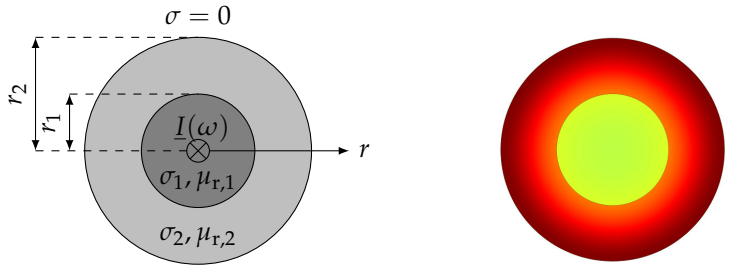

CURRENT DENSITY: The current density can be calculated by

$$\underline{J}_{z,\mathrm{AC}}(r) = \frac{\mathrm{J}_0(\underline{n}_1 r)}{\frac{\sigma_1}{\sigma_2}\left(\frac{\mathrm{J}_0(\underline{n}_2 r_1) + c\mathrm{H}_0(\underline{n}_2 r_1)}{\mathrm{J}_0(\underline{n}_2 r_2) + c\mathrm{H}_0(\underline{n}_2 r_2)}\right)} \quad , \tag{3.52}$$

$$\text{with} \quad \underline{n}_n = (1+\mathrm{j})\frac{1}{\delta_n} \quad , \tag{3.53}$$

$$c = -\frac{\mathrm{J}_1(\underline{n}_1 r_1)\mathrm{J}_0(\underline{n}_2 r_1) - (\underline{n}_2/\underline{n}_1)\,\mathrm{J}_0(\underline{n}_1 r_1)\mathrm{J}_1(\underline{n}_2 r_1)}{\mathrm{J}_1(\underline{n}_1 r_1)\mathrm{H}_0(\underline{n}_2 r_1) - (\underline{n}_2/\underline{n}_1)\,\mathrm{J}_0(\underline{n}_1 r_1)\mathrm{H}_1(\underline{n}_2 r_1)} \quad . \tag{3.54}$$

In the equations above, index n relates to the medium. In the inner medium $n = 1$ and for the outer medium $n = 2$. Hence, $\underline{n}_1$ is the function argument of medium 1, $\underline{n}_2$ is the function argument of medium 2, δ_1 is the *skin depth* in medium 1 and δ_2 is the *skin depth* in medium 2, σ_1 is the conductivity of medium 1 and σ_2 is the conductivity of the outer medium, medium 2. H_ν is the Hankel function (or Bessel function of the third kind) of order ν. The current density and magnetic field intensity was also derived in [Mro03, p. 146] before.

RESISTANCE RATIO: The DC resistance per-unit length is

$$R_{\mathrm{DC}} = R_{\mathrm{DC},1} || R_{\mathrm{DC},2} = \frac{1}{\sigma_1 \pi r_1^2 + \sigma_2 \pi (r_2^2 - r_1^2)} \quad , \tag{3.55}$$

where $||$ indicates a parallel connection. The resistance ratio is

$$\frac{R_{\mathrm{AC}}}{R_{\mathrm{DC}}} = \frac{\pi r_1^2 (\sigma_1/\sigma_2) + \pi(r_2^2 - r_1^2)}{\mathrm{Re}\left(2\pi \int_0^{r_1} r \underline{J}_{z,\mathrm{AC}}(r)\mathrm{d}r + 2\pi \int_{r_1}^{r_2} r \underline{J}_{z,\mathrm{AC}}(r)\mathrm{d}r\right)} \quad . \tag{3.56}$$

INTERNAL INDUCTANCE: No explicit formula for the DC internal inductance is given in [Liu16]. One can alternatively use the analytical formulas for the DC inductance of a solid circular conductor (Equation (3.37)) and for a tubular conductor (Equation (3.44)). The internal inductance at AC is

$$L_{\mathrm{iAC}} = \frac{\pi r_1^2 + \pi(r_2^2 - r_1^2)}{\omega\ \mathrm{Im}\left(2\pi \int_0^{r_1} r \underline{J}_{z,\mathrm{AC}}(r)\mathrm{d}r + 2\pi \int_{r_1}^{r_2} r \underline{J}_{z,\mathrm{AC}}(r)\mathrm{d}r\right)} \cdot R_{\mathrm{DC}} \quad . \tag{3.57}$$

3.1.3.7 *Two Identical Solid Cylindrical Conductors in a Go Circuit*

As soon as multiple conductors are involved, the solution often contains a summation. The reason is that the current distributions in each conductor depends on the currents distribution in the adjacent conductor. Until the equilibrium state is reached, the current densities will influence each

other [Dwi23b, p. 853]. The more general case of two unequal conductors was analytically solved by Chester Snow in 1925 in [Sno25, p. 327] but will not be shown here because of its complexity. To the best knowledge of the author this is also the only reference, where the current density for two solid parallel conductors is calculated analytically [Sno25, p. 326].

Multiple references for the analytical solution of the resistance ratio for two identical conductors can be found in the literature. For example in [Dwi23b, p. VIII] in emu cgs or in [KA94] in SI units. As the latter is commonly used nowadays, the following analytical solution originates from this reference. The AC and DC resistance accounts for one conductor only. Exemplary current density distribution is shown later in Figure 3.13.

GEOMETRY:

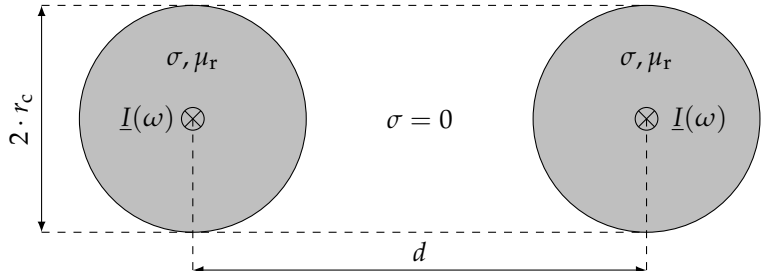

RESISTANCE RATIO: The resistance ratio for one conductor is

$$\frac{R_{\mathrm{AC}}}{R_{\mathrm{DC}}} = \mathrm{Re}\left(\mathrm{j}\omega\mu_0\mu_\mathrm{r}\sigma\pi r_\mathrm{c}^2\left[2\pi\underline{Q}_0\left\|M_0\right\|^2\ldots + \sum_{n=1}^{\infty}\left(\frac{\pi r_\mathrm{c}^{2n}}{n}\left\|\underline{M}_n\right\|^2\left(1-\underline{Q}_n^*\right)\cdot\left(1+\underline{Q}_n\right)\right)\right]\right) \quad , \tag{3.58}$$

where * denotes the complex conjugate, $\|\ldots\|$ takes the norm of the expression and

$$M_0 = \frac{1}{2\pi} \quad , \tag{3.59}$$

$$\underline{M}_1 = -\frac{M_0}{d}\left[1+\left(\frac{r_\mathrm{c}}{d}\right)^2\underline{Q}_1+\left(\frac{r_\mathrm{c}}{d}\right)^4\underline{Q}_2+\left(\frac{r_\mathrm{c}}{d}\right)^4\underline{Q}_1^2+\ldots\right] \quad , \tag{3.60}$$

$$\underline{M}_2 = -\frac{M_0}{d^2}\left[1+2\left(\frac{r_\mathrm{c}}{d}\right)^2\underline{Q}_1+\ldots\right] \quad , \tag{3.61}$$

$$\underline{M}_3 = -\frac{M_0}{d^3}+\ldots \quad , \tag{3.62}$$

$$\underline{Q}_0 = \frac{-\mathrm{J}_0(\underline{z}_0)}{\underline{z}_0\cdot\mathrm{J}_1(\underline{z}_0)} \quad , \tag{3.63}$$

$$\underline{Q}_n = \frac{\mathrm{J}_{n+1}(\underline{z}_0)}{\mathrm{J}_{n-1}(\underline{z}_0)} \quad , \tag{3.64}$$

$$\underline{z}_0 = \mathrm{j}r_\mathrm{c}\sqrt{\mathrm{j}\omega\mu_0\mu_\mathrm{r}\sigma} \quad . \tag{3.65}$$

Symbol d is the center-to-center distance of both conductors. According to [KA94] using three harmonics gives results of sufficient accuracy.

INTERNAL INDUCTANCE RATIO: The internal inductance at AC is

$$L_{\mathrm{iAC}} = \mathrm{Im}\left(\mathrm{j}\mu_0\mu_\mathrm{r}\left[2\pi\underline{Q}_0\left\|M_0\right\|^2 + \sum_{n=1}^{\infty}\left(\frac{\pi r_\mathrm{c}^{2n}}{n}\left\|\underline{M}_n\right\|^2\left(1-\underline{Q}_n^*\right)\cdot\left(1+\underline{Q}_n\right)\right)\right]\right) \tag{3.66}$$

and with the internal DC inductance from Equation (3.37) the inductance ratio becomes

$$\frac{L_{\mathrm{iAC}}}{L_{\mathrm{iDC}}} = \mathrm{Im}\left(\mathrm{j}8\pi\left[2\pi\underline{Q}_0\left\|M_0\right\|^2 + \sum_{n=1}^{\infty}\left(\frac{\pi r_\mathrm{c}^{2n}}{n}\left\|\underline{M}_n\right\|^2\left(1-\underline{Q}_n^*\right)\cdot\left(1+\underline{Q}_n\right)\right)\right]\right). \tag{3.67}$$

3.1.3.8 *Two Identical Solid Cylindrical Conductors in Return Circuit*

The analytical solution was first presented by Carson in [Car21, p. 625] and in an alternative form by Dwight in [Dwi23b, p. VII]. A general solution to the current density can be found in formula (39) in [Dwi23b]. The formulas use the emu cgs [Car21, p. 626] and are valid for non-magnetic conductors only. Exemplary current density distribution is given later in Figure 3.13.

GEOMETRY:

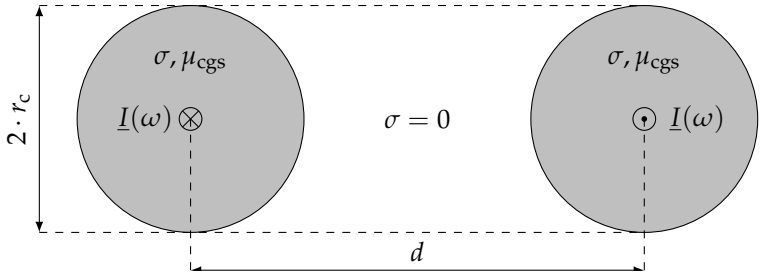

RESISTANCE RATIO: The resistance ratio is

$$\frac{R_{\mathrm{AC}}}{R_{\mathrm{DC}}} = R_{\mathrm{AC,C}}\sigma\pi r_\mathrm{c}^2\cdot\left[1+\frac{1}{2}\sum_{n=1}^{\infty}\left\|\underline{h}_n\right\|^2\frac{u_n v_n' - u_n' v_n}{u_0 v_0' - u_0' v_0}\right] \tag{3.68}$$

$$\text{with}\quad R_{\mathrm{AC,C}} = \frac{1}{r_\mathrm{c}}\sqrt{\frac{\mu_{\mathrm{cgs}}\omega}{\pi\sigma}}\cdot\frac{u_0 v_0' - u_0 v_0}{u_1^2+v_1^2}\ , \tag{3.69}$$

$$\underline{h}_n = p_n\frac{\mathrm{J}_1(\underline{\xi})}{\mathrm{J}_{n-1}(\underline{\xi})}\cdot\left(1-2n\frac{k_\mathrm{k}^2}{s^{n-1}}\frac{\mathrm{J}_1(\underline{\xi})}{\underline{\xi}\mathrm{J}_0(\underline{\xi})}\right)\ , \tag{3.70}$$

$$u_n + \mathrm{j}v_n = \mathrm{J}_n(\underline{\xi}) = \mathrm{J}_n(b_\mathrm{b}\mathrm{j}\sqrt{\mathrm{j}})\ , \tag{3.71}$$

$$u_n' + \mathrm{j}v_n' = \frac{\mathrm{d}}{\mathrm{d}b_\mathrm{b}}\mathrm{J}_n(b_\mathrm{b}\mathrm{j}\sqrt{\mathrm{j}})\ , \tag{3.72}$$

$$\underline{\xi} = b_\mathrm{b}\mathrm{j}\sqrt{\mathrm{j}}\ , \tag{3.73}$$

$$b_\mathrm{b} = r_\mathrm{c}\sqrt{4\pi\sigma\mu_{\mathrm{cgs}}\omega}\ , \tag{3.74}$$

$$k_\mathrm{k} = \frac{r_\mathrm{c}}{d}\ , \tag{3.75}$$

$$s = 2\cdot\frac{1-\sqrt{1-(2k_\mathrm{k})^2}}{(2k_\mathrm{k})^2}\ , \tag{3.76}$$

$$p_n = (-1)^n 2k_\mathrm{k}^n s^n\ . \tag{3.77}$$

$R_{AC,C}$ is the AC resistance of one isolated conductor. In SI units it is equal to Equation (3.33). As indicated by the emu cgs, for this resistance and inductance calculation, r_c and d have to be given in cm, μ_{cgs} is 1 for non-magnetic conductors and σ is given in abmhos/cm. The calculated resistance is that of one conductor only. The resistance of one conductor in a *go circuit* is lower than that of a one conductor in a *return circuit* with the same geometrical dimensions and electrical parameters. Moreover, losses in addition to the *skin effect* losses—*proximity effect* losses—only depend on the ratio of conductor radius and center-to-center distance and can reach an upper limit [Car21, p. 609].

INTERNAL INDUCTANCE The AC internal inductance is

$$L_{iAC} = \operatorname{Im}\left(\frac{\underline{Z}_0}{\omega}\left(1+\sum_{n=1}^{\infty}(-1)^n\left(\frac{h_n \mathrm{J}_n(\underline{\xi})}{\mathrm{J}_0(\underline{\xi})}\right)\right)\right) \tag{3.78}$$

$$\text{with}\quad \underline{Z}_0 = \frac{2\mathrm{j}\mu_{cgs}\omega}{\underline{\xi}}\frac{\mathrm{J}_0(\underline{\xi})}{\mathrm{J}_0'(\underline{\xi})}\ . \tag{3.79}$$

$\underline{Z}_0$ is the analytical AC internal impedance per-unit length (Ω/m) of an isolated solid conductor.

3.1.3.9 *Two Identical Tubular Conductors in Return Circuit*

The following solution for a return circuit is taken from [Mea25], where it was first derived. The formulas use the emu cgs. The calculated values are those of one tubular conductor of the circuit. Exemplary current density distribution is given in Figure 3.13. The analytical solution for the AC resistance of two tubular conductors in a *go circuit* is given in [Ehr79, p. 169]. Approximations for both cases are presented in [Dwi45, pp. 207-209].

GEOMETRY:

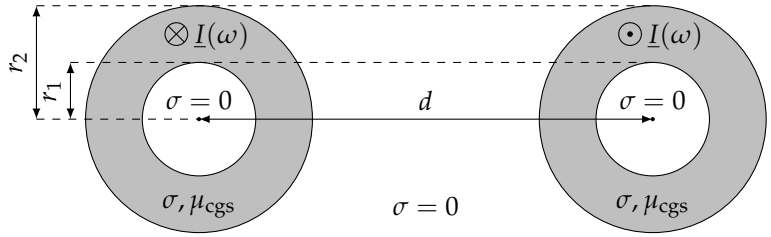

RESISTANCE RATIO: The resistance ratio is

$$\frac{R_{AC}}{R_{DC}} = \operatorname{Re}\left[\frac{2\mathrm{j}\mu_{cgs}\omega\sigma\pi(r_2^2-r_1^2)}{\underline{\Gamma}}\cdots \cdot\left[\frac{\underline{N}_0(\underline{\Gamma})}{\underline{N}_0'(\underline{\Gamma})}+\frac{1}{2}\sum_{n=1}^{\infty}\|\underline{o}_n\|^2\frac{\underline{N}_n(\underline{\Gamma})}{\underline{N}_0'(\underline{\Gamma})}\cdot\left(\frac{\underline{N}_n'(\underline{\Gamma})}{\underline{N}_0'(\underline{\Gamma})}\right)^*\right]\right]\ , \tag{3.80}$$

$$\text{where}\quad \underline{N}_n(\underline{\Gamma}) = \mathrm{J}_n(\underline{\Gamma}) - \frac{\mathrm{J}_{n+1}(\underline{\zeta})}{\mathrm{Y}_{n+1}(\underline{\zeta})}\mathrm{Y}_n(\underline{\Gamma})\ , \tag{3.81}$$

$$\underline{N}_n'(\underline{\Gamma}) = \mathrm{J}_n'(\underline{\Gamma}) - \frac{\mathrm{J}_{n+1}(\underline{\zeta})}{\mathrm{Y}_{n+1}(\underline{\zeta})}\mathrm{Y}_n'(\underline{\Gamma})\ , \tag{3.82}$$

$$\underline{\zeta} = r_1\sqrt{4\pi\sigma\mu_{cgs}\omega}\cdot\mathrm{j}\sqrt{\mathrm{j}}\ , \tag{3.83}$$

$$\underline{\Gamma} = r_2\sqrt{4\pi\sigma\mu_{\mathrm{cgs}}\omega}\cdot\mathrm{j}\sqrt{\mathrm{j}}\ , \tag{3.84}$$

$$\|\underline{\varrho}_n\|^2 = \frac{u_1^2+v_1^2}{u_{n-1}^2+v_{n-1}^2}\cdot\left\|\frac{1+\underline{\lambda}_0\mathrm{Y}_1(\underline{\Gamma})/\mathrm{J}_1(\underline{\Gamma})}{1+\underline{\lambda}_n\mathrm{K}_{n-1}(\underline{\Gamma})/\mathrm{J}_{n-1}(\underline{\Gamma})}\right\|^2\cdots \cdot p_n^2\left(1+\frac{2n\underline{g}k_{\mathrm{k}}^2}{s^{n-1}}\right)\ , \tag{3.85}$$

$$\underline{g} = \frac{\sqrt{2}}{r_2\sqrt{4\pi\sigma\mu_{\mathrm{cgs}}\omega}}\cdot\frac{w[u_1(u_0+v_0)-v_1(u_0-v_0)]}{u_0^2+v_0^2}\cdots \cdot\frac{-q[u_1(u_0-v_0)+v_1(u_0+v_0)]}{u_0^2+v_0^2}\ , \tag{3.86}$$

$$w+\mathrm{j}q = \frac{1+\underline{\lambda}_1\mathrm{Y}_1(\underline{\Gamma})/\mathrm{J}_1(\underline{\Gamma})}{1+\underline{\lambda}_1\mathrm{Y}_0(\underline{\Gamma})/\mathrm{J}_0(\underline{\Gamma})}\ , \tag{3.87}$$

$$\underline{\lambda}_n = -\frac{\mathrm{J}_{n+1}(\underline{\zeta})}{\mathrm{Y}_{n+1}(\underline{\zeta})}\ . \tag{3.88}$$

Functions u and v are already defined in Equation (3.71) but with $\underline{\xi}$ being replaced by $\underline{\Gamma}$. k_{k} is defined in Equation (3.75) but with r_2 replacing r_{c}. Variable p_n is already defined in Equation (3.77) and s is defined in Equation (3.76).

INTERNAL INDUCTANCE: Accordingly, the internal AC inductance can be calculated to be

$$L_{\mathrm{iAC}} = \mathrm{Im}\left[\frac{2\mathrm{j}\mu}{\underline{\Gamma}}\left[\frac{\underline{N}_0(\underline{\Gamma})}{\underline{N}_0'(\underline{\Gamma})}+\frac{1}{2}\sum_{n=1}^{\infty}\|\underline{\varrho}_n\|^2\frac{\underline{N}_n(\underline{\Gamma})}{\underline{N}_0'(\underline{\Gamma})}\cdot\left(\frac{\underline{N}_n'(\underline{\Gamma})}{\underline{N}_0'(\underline{\Gamma})}\right)^*\right]\right]\ . \tag{3.89}$$

3.1.3.10 *Solid Rectangular Conductor*

An analytical solution to the AC resistance of a rectangular conductor was given approximately 50 years after the analytical solution to a conductor of circular cross section. It was first presented in [Gro40] and later in [Ehr79; Fic07]. The reason is that for non-circular conductors, the current density varies around the circumference. This means that the BC, which is necessary to solve the related PDEs, is not available. Instead of using PDEs—as done for circular conductors—the attempt was made to solve integral equations, where the BC is already included [Ehr79, p. 5]. Specialized mathematical methods and considerable numerical effort, which is necessary to solve these integral equations, were not applied to this problem until 1940 by Hans-Georg Gross [Gro40, pp. 241,242; Sil67]. Because of its complexity, solving these integrals still presented a challenge with the computational power and numerical methods available 2007 [Fic07, p. 131][15]. Moreover, for conductors with edges, the current distribution also depends on the sharpness of these edges. This is called *current crowding* or *edge effect* [KA16].

As the scope of this work is limited, the analytical solution is not given. Some resistance ratio curves for specific side ratios are shown in Section 3.1.5. Rectangular conductors are listed here, as they are still of rele-

15 Earlier, the high frequency resistance for rectangular conductors (although possible for any conductor shape) was approximated with an electrostatic field analog. At very high frequencies the magnetic field lines cannot enter the conductor and become parallel to the surface. These field lines are identical to the equipotential lines, when looking at the rectangular conductor as an electrode of an electrostatic capacitance problem [Coc29, p. 534; Jac34, p. 433; Gro40, p. 241; Dwi47, p. 550; LŠT66, p. 215].

vance in today's energy transmission systems (e.g.: bus bar systems in substations, rotating machines,...).

GEOMETRY AND EXEMPLARY AC CURRENT DENSITY

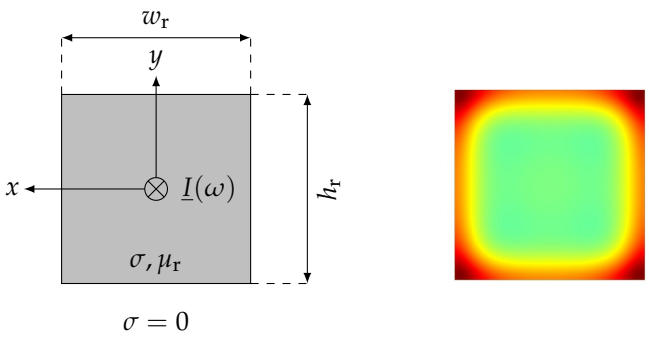

3.1.3.11 *Two Solid Cylindrical Conductors in a Go Circuit in Another Tubular Conductor*

Another analytical formula is presented in [KAA95]. It takes the losses in two parallel wires in a *go circuit* in a lossy coaxial return conductor into account. Different sized inner conductors can be calculated including non-rotational symmetric arrangements. Similar to the solution of a rectangular conductor, it is too complex to be shown here.

3.1.3.12 *Solid Circular Conductors in 3-phase Systems*

Analytical solutions for solid cylindrical conductors in a 3-phase system exist for triangular (trefoil) spacings and conductors in flat spacing. The solutions are given in [Dwi23b, p. 857] and for triangular arrangement also in [Cos36]. The solutions are also far too complex to be shown here. The exemplary current density is shown in Figure 3.13.

3.1.3.13 *Solid Circular Conductors in 3-phase Systems in a Sheath*

A very recent analytical formula for a 3-phase cable systems with cable sheaths can be found in [Bri+16]. Similar to the previous 3-phase system case, the solution is too extensive to be presented in this work.

3.1.4 *Overview of Approximate Formulas*

Before the rise of digital computers, the analytical computation of solutions was complicated and can—in some cases—still be challenging today [Fic07, p. 131]. Hence, approximations for the resistance of different conductors can be found in numerous references. In the following, some important references for different conductor designs are listed.

In [Coc29; Arn38; Sil67; GSR05; Pay16] approximate solutions for rectangular conductors can be found. Further investigations showed that the accuracy of the approximation found in [Pay16] seems to increase with larger p values. An approximation for thin conductor strips can be found in [Ern17, p. 238]. Dwight presents numerous approximation in [Dwi23a] and later more in [Dwi45]. Amongst others, approximations for thin tubes and cables with sheaths are included. A. Arnold and V. T. Morgan show approximations for elliptical conductors in [Arn46; Mor13]. Arnold also

shows an approximation for *three-phase systems* in [Arn41a]. In [Mor13] a simplified formula for helically-stranded (steel-cored) conductors is given. Humberto et. al. give approximate formulas for *skin effect* in power transmission lines [Gat+14a].

Today, approximate solutions for simple geometrical shapes as rectangles, ellipses and tubes are only of academic interest as the FEM enables a much faster and more precise evaluation of losses for these shapes.

3.1.5 *Comparison of Different Conductor Shapes*

Resistance ratio plots according to the *Principle of Similitude* for solid cylindrical conductors, a regular octagon, tubular conductors with three radii ratios and rectangular conductors with three different side ratios are plotted in Figure 3.12. The results are obtained by FEM simulations.

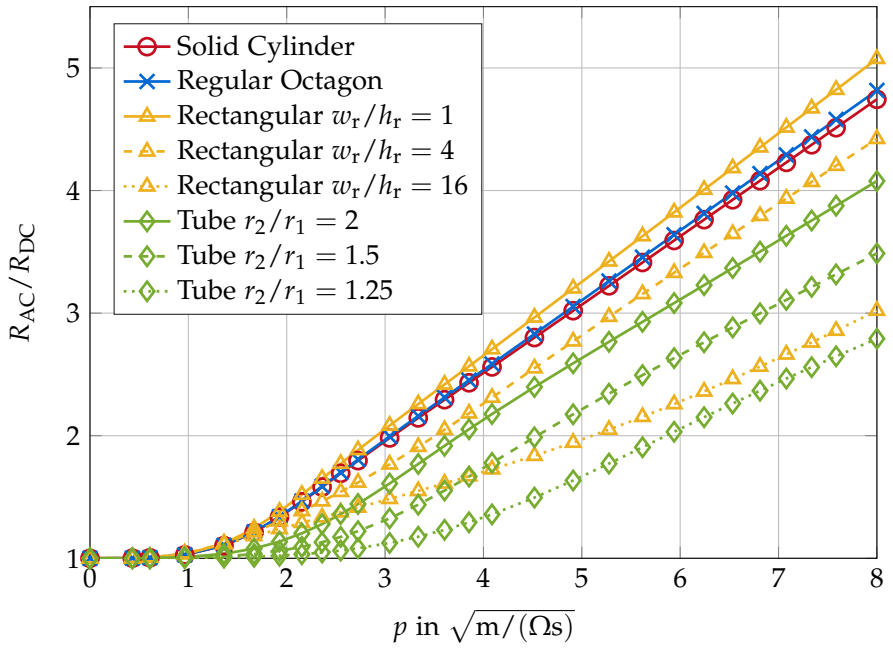

Figure 3.12: Comparison of R_{AC}/R_{DC} ratios of different conductor shapes; the results coincide with the measurement results given in [FG33] (as different units were used, $P = p \cdot \sqrt{8\pi/10}$)

A solid cylindrical conductor has the smallest *circumference to cross section ratio* (a circle can be seen as a polygon with an infinite number of corners). When remaining the cross sectional area, with a decreasing number of corners, the circumference increases (this is only true for a lower limit of 4 corners). Equilateral polygon conductor cross sections with with a smaller *circumference to cross section ratio* show larger *skin effect* losses. Rectangular conductors with larger side ratios show smaller *skin effect* losses. The radius ratio for a tube is $1 < r_2/r_1 < \infty$. For r_1 approaching r_2 the conductor gets thinner. For smaller r_1 it becomes more similar to a solid conductor. As also seen in Figure 3.12 the analytical solution of a solid is hence only a special case of the analytical solution of a tubular conductor.

Although these observations give some insights into the origin of AC loss mechanisms, this is not further investigated here. More curves—including

proximity effect—can for example be found in [Dwi45; Gra79]. The current densities at AC and severe *skin effect* for various conductors and conductor arrangements are shown in Figure 3.13.

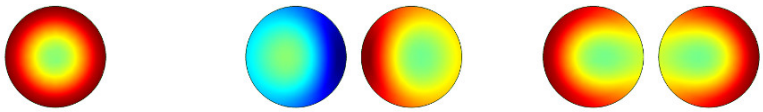

(a) From left to right: solid cylindrical conductor, two solid cylindrical conductors in *return circuit* and two solid cylindrical conductors in a *go circuit*

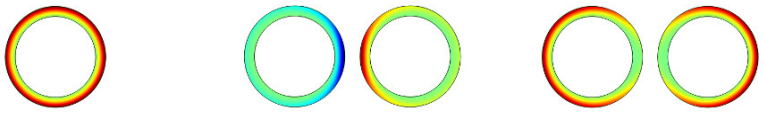

(b) From left to right: hollow cylindrical conductor, two hollow cylindrical conductors in *return circuit* and two hollow cylindrical conductors in a *go circuit*

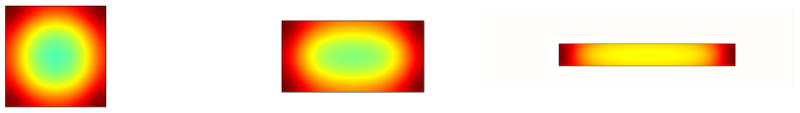

(c) From left to right: rectangular conductor with side ratio $a/b = 1$; 0.5 and 0.125

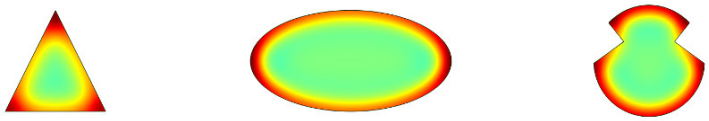

(d) From left to right: triangular conductor, elliptical conductor and a typical contact wire profile of the *Deutsche Bahn*

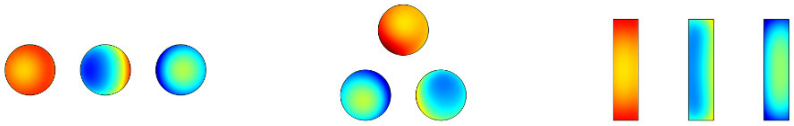

(e) 3-phase systems (left to right: L1-L2-L3 at phase 0°) from left to right: in planar formation, in trefoil formation (L1 on top, L2 right, L3 left side); bus bar system

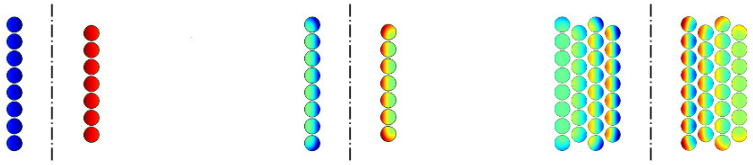

(f) From left to right: a seven turn single-layer coil in cross-sectional view at DC, a seven turn single-layer coil in cross-sectional view at AC and a multi-layer coil in cross-sectional view at AC; the dash-dot lines show the central axes of the coils

Figure 3.13: Normalized in-plane current density $\mathrm{Re}(\underline{J}_z)$ in case of severe *skin* and *proximity effect* for different conductor geometries/systems

3.2 HIGH VOLTAGE POWER CABLE CONDUCTORS

3.2.1 *Stranded Conductors*

Power cable conductors have a circular cross section because it provides the best trade of between *skin effect* losses and surface area (see Figure 3.12). The first affects the operating costs, the latter affects the degree of insulation expenditure and hence the costs of the complete cable. Moreover, circular conductors are generally more easy to handle and also provide an homogeneous electric field distribution in the dielectric surrounding the conductor.

At the beginning of the 20th century, *skin effect* losses were not a problem as the cross sectional areas were comparatively small. With an increase in power transmission capacity, the cross sections were increased to allow for higher current carrying capacities. As larger cross sections resulted in larger AC resistances (Equation (3.33)) and became harder to manufacture and bend, cable manufactures investigated new designs. Subdividing a conductor to single uninsulated wires (also called strands) increases flexibility and eases up the manufacturing process. Nevertheless, such a conductor will have nearly the same AC resistance as a single solid cylindrical conductor with identical cross section [KA16, p. 554; Gra79, p. 98]. However, increased strand spacing (increased wire to wire distance) generally decreases the AC resistance. This seems obvious, as larger spacings decrease *proximity effect* between the wires [KA16, p. 554; SPW15].

For mechanical reasons: if single wires are used, they are helically stranded (also called: spiraling or twisting). That means they form spirals around the conductor axis. The layers—collection of wires in the same annulus—can be stranded unidirectional (all layers spiraled in the same direction) or bidirectional (alternating the spiral direction from layer to layer—also called contradirectional or alternately reversed spiraling). Assuming the single strands are insulated from one another, spiraling slightly lowers the AC resistance and reactance of the conductor compared to a solid conductor with the same DC resistance [Zab53, p. 601][16]. Stranding conductors destroys the symmetry and also adds a radial electric field component (inside the strands) and a magnetic field component in direction of the conductor axis. Multiple conducting parts also introduce higher order Bessel functions in calculations [Dwi23a]. This can also be observed in measurements in [Fer92; Ros+11]. To the best knowledge of the author, no analytical solution for 3D stranded conductors is given in the literature. Recently, an approximate calculation method for the *spirality effect* was proposed in [DZW14]. As a conclusion what can be said about stranded conductors is:

- Conductors with stranded insulated wires have a lower AC resistance compared to a conductor of equal DC resistance [Zab53, p. 601]. This effect increases with smaller lay lengths [DZW14].
- Unidirectional stranding lowers AC losses more than bidirectional stranding [Zab53, p. 601; DZW14].

16 For unidirectional stranding the AC resistance is slightly lower and the internal inductance is slightly higher compared to bidirectional stranding [Zab53, p. 601; DZW14]. As unidirectional stranding creates an increase of longitudinal flux, it results in an increased reactance [Zab53; Gra79, p. 106].

- This *spirality effect* can become significant at power frequencies for typical conductors [DZW14].
- Increased distance between single strands lowers AC losses [KA16, p. 543; SPW15].
- *Proximity effect* can be lowered when using insulated stranded conductors [SSW35, p. 325] (also see Table 4.2).
- Depending on the interwire insulation, the DC resistance of a stranded conductor increases with shorter lay lengths due to the longer helical strand paths [Gra79, p. 99].
- Stranded conductor bundles with a circular overall cross section appear to be the worst-case, as they have the largest per-unit losses compared to every other bundle shape [Mur89, pp. 118,119].
- Stranding blank wires, which have direct contact with each other, can result in a larger AC resistance with shorter lay lengths [KLP15, p. 1980; Dwi45, p. 221].

3.2.2 *Milliken Conductors*

To significantly reduce AC losses for conductors with copper cross sections larger than 1000 mm^2, *Milliken type* conductors are typically used [Nex11][17]. Figure 3.14 shows a *Milliken* conductor in cross-sectional view.

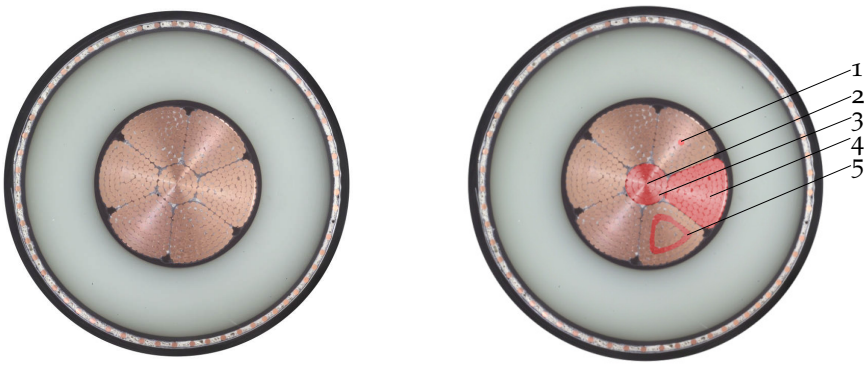

Figure 3.14: Cable with *Milliken* conductor in cross-sectional view (right: important parts highlighted in red); (1) segment core/single strand; (2) cable core; (3) core conductor; (4) pie shaped segment; (5) a layer in a segment; courtesy of *Südkabel GmbH*

The *Milliken* design was first proposed by Humphreys Milliken in a patent in 1933 [Mil33] and later extended by a second patent of H. Milliken in 1940 [Mil40]. Multiple patents for the manufacturing and improvement of *Milliken type* conductors followed [LR61; Kat71; Tak88; Bra90; BD99; WW10]. The basic principle of this design is to transpose the single strands in a conductor in a way, that the total induction in each of them is the same. In other words, every single strand has to occupy each position in the complete cross section for the same distance. This guarantees—in theory—that the current has no preferred path and the phase and magnitude is identical in each strand [Gra79, p. 101][18]. This is done by splitting the conductor into pie

17 Using aluminum as conductor material, *Milliken type* conductors are usually applied for cross sections larger than 1200 mm^2.

18 At DC the magnitude of the current can also vary in different layers and strands due to the different helical current path lengths affecting a layer's DC resistance.

shaped segments[19](usually 5 to 6), which are insulated from one another. Every segment is a pie shaped wire bundle, consisting of multiple—originally concentric—layers. Single strands should have a contact resistance between them, many times greater than the resistance of one turn of this strand along the cable to prevent currents from freely flowing between single strands and crossing to different layers. Because of the different size of available contact surface this contact resistance is expected to be different for uni- and bidirectional stranding and may vary over the life time of the cable due to long-term oxidation, bending and mechanical stress [Gra79, p. 98]. As interwire insulation cannot be guaranteed, different layers are typically also insulated from one another [WW10]. Even though blank (uninsulated) copper wires are sometimes used as well, for this principle to work efficiently, oxidized or enameled copper wires are the preferred choice. Aluminum strands rapidly oxidize by themselves, when exposed to air [BM11]. Copper wires do too, but are sometimes also treated with flames to build a stronger oxide layer. As the layers of one segment are twisted around the segment core, all strands in one layer will carry the same current. Every layer in a segment will nearly have the same geometrical center (also center of mass), which is close to the segment core. Hence, the total induction for every layer is the same. For mechanical reasons and to homogenize additional *proximity effect* losses—caused by other conductors in close proximity—over all segments, the segments are twisted around the cable core as well. The reason why AC losses are still measured in practice (for example in [Joa99; DM07]) are:

- The insulation of the single wires is not perfect and can be damaged by mechanical force upon the segments during manufacturing, reeling and unreeling [Gra79, p. 98]. According to [Arn41b, p. 55] the relative interwire conductivity can reach values of up to 80 % of the conductor material and more for mechanical treated, insulated conductors.
- At larger cross sections, nearly no current will flow in the core conductor as the strands never get to the periphery of the conductor and therefore have their geometrical center at the conductor center. It can be reasonable to remove the core conductor for a better resistance ratio, because—as *skin effect* is an electromagnetic field diffusion process—current can flow into the opposite direction in the core conductor, increasing losses (compare Figure 3.1).
- The geometrical centers of the layers of one segment do not exactly coincide. Layers with their geometrical center closer to the conductor center will carry less current.
- Even though small, *skin effect* losses occur in the single strands as well. The strand diameter should therefore be as small as possible.
- The flower shape of the complete conductor should rather be a perfect circle. Due to practical restrictions this is not possible.
- Assuming all strands have the same total induction, one still has to balance the DC resistance of the single wires, which depends on the length and hence on the pitch (or lay length) of the layers, to create an ideal conductor.

19 For that reason, *Milliken type* conductors are also referred to as *segmented* conductors.

Additional measures to reduce AC losses in *Milliken type* conductors have been given in a patent by Heinrich Brakelmann [Bra90] and by Volker Waschk and Dag Willén in [WW10]. The first suggests using different lay lengths for the same layers in different segments to outbalance the induction in between both by reducing the mean distance between both layers. The latter suggests (similar to H. Milliken second patent [Mil40]) the use of at least two non-conducting strands (e.g.: plastic strands) in a layer to prevent circular currents in one layer and force the current in each strand to remain on its helical path. In [Joa99] it is claimed that *skin effect* losses can almost be completely avoided even with the use of bare wires, when a conductive shell made of high permeability material is placed around the conductor at regular intervals. Due to the best knowledge of the author, this method is not used in *Milliken type* conductors under operation. It was reported that reduced *skin effect* losses also lower *proximity effect* losses [Gra79, p. 105]. Later, in Section 4.2 this statement is further discussed. Different levels of strand insulation and mechanical loads on the segments were investigated in [BM68].

As argued previously, even for simpler shapes no analytical solution is available. Due to its complex shape and lack of knowledge over multiple manufacturing parameters (e.g.: condition of the strand insulation, shape of strand cross sections...) an analytical solution for *Milliken type* conductors is not available [Cig05, p. 21]. Even if it could be derived, its suitability would strongly depend on the knowledge of all material and manufacturing parameters. According to [Liu16], the most detailed calculation method for AC losses in segmented conductors available at the moment is given in [Sug81] with adjustments suggested by [Cig05]. Another recent calculation method is presented in [SK08]. Table 3.1 provides an overview of some calculation methods to approximate the AC resistance of complex conductors[20].

Prior to *segmented* conductors for power cables, a *skin effect* reduced power conductor design for electric machinery has been patented in 1913 by Ludwig Roebel using a similar principle [Roe15]. *Roebel bars* or *Roebel cables* are composed of multiple insulated flat rectangular conductors, alternating their position in the complete conductor cross section to homogenize the current distribution, while still maintaining an overall rectangular cross section. Deeper investigations concerning *skin effect* in *Roebel cables* can for example be found in [LŠT66, p. 120; ZGS13].

Even for linear conductors, the magnitude of the current can influence the AC resistance. The conductivity depends on the temperature, which in turn depends on the current. Uneven current distribution due to *skin effect* can heat up the periphery of a conductor and create a radial temperature gradient. Even in case of large radial temperature gradients (e.g.: for aluminum conductor steel reinforced (ACSR) used for overhead lines), the influence on the AC resistance can be neglected [Liu16, p. 5]. For stranded conductors, it was said that the interwire conduction—affecting the performance—can change with temperature [Gra79, p. 102]. If this is true, extrapolating

20 The method names stand for: TL→ Teilleiterverfahren, PEEC→ Partial Element Equivalent Circuit (also see [Ros18]), MCA→ Multiconductor Cell Analysis, Litz→ Litz Wire Method, Flux→ Flux Method, MF→ Magnetic Field Method (also see [ADS99] for the last two methods)

measurement values obtained at different temperatures can lead to errors.

Additional information concerning the mechanical construction of stranded and segmental conductors can be found in [Gan16].

Table 3.1: Overview of some calculation methods and their features available for the AC resistance calculation of complex cable conductors

	method					
features	TL [Joa99]	PEEC [Zha+14]	MCA [Ben07]	Litz [SZ14]	Flux [Mat+83]	MF [Sug81]
contact resistances	√	√	√	-	-	√
R_{DC} increase by stranding	√	√	*pos.*	√	√	√
non-identical segments	√	√	-	*pos.*	-	-
core conductor	√	√	*pos.*	√	-	-
pitch of layers	√	√	√	√	√	-
different sized strands	√	√	*pos.*	*pos.*	-	-
mechanical compression	*pos.*	*pos.*	√	≈	-	≈

√ .....implemented ≈ ...simplified
pos. ...possible but not implemented - .....not implemented

4

RECOMMENDATIONS FOR ALTERNATING CURRENT LOSS MEASUREMENTS OF HIGH VOLTAGE POWER CABLES

Advances are made by answering questions.
Discoveries are made by questioning answers.
Bernhard Haisch

The purpose of this chapter is to clarify how AC voltmeters work and what they actually measure. Subsequently, the role of complex magnetic fields is evaluated thoroughly with an emphasis on *M-type* conductors. After that, a list of possible sources of influence, which can occur during electrical measurements is given. These influences are then evaluated quantitatively for commonly used measurement setups. Finally, a recommendation for the procedure and measurement setup best suited for *Milliken* conductors is provided. At the end of this chapter the foundation for accurate AC loss measurements on any conductor type is present, which enables the accurate characterization of different *M-type* conductors in Chapter 5.

4.1 THEORY OF AC LOSS MEASUREMENTS

Throughout the last century there have been numerous discussions on the difference between the basic concepts of pd, induced emf and voltage [Moo70; Kle81][1]. Blurry definitions and generalizations caused misunderstandings, which were discussed in multiple references [Eri68b; Eri68a; Pag77; VML11]. In the following, it is made clear, which term has to be used in what case. Table 4.1—in accordance with [VML11]—shows the nomenclature used throughout this work.

In Equation (4.1) voltage u_{ab} only depends on position and magnitude of the electric charge distribution. At DC the voltage for a closed loop (Equation (4.3)) is zero as the prevailing field is conservative (also called static or irrotational field). At DC the voltage is always independent of the chosen integration path between two points a and b. In Equation (4.2) voltage $\underline{u}_{ab}$ depends on position and magnitude of the electric charge distribution and also on the induced emf $\underline{\varepsilon}_i$, whose power comes from alternating electromagnetic fields and/or the relative motion of conductors with regard to the prevailing electromagnetic fields, which can be regarded as being the same. In closed loops the contribution of pd ΔV vanishes and the voltage is identical to the induced emf (see Equation (4.4), which is *Faraday's Law* of induction). Time-varying fields are also called non-conservative as the induced voltage in a loop depends on the integration path, which is defined by the loops contour C. Therefrom follows that the *measured* voltage between two points a and b, which are called voltage tap-offs, can be ambiguous and depend on the position of the measurement device. This is discussed in detail in the next sections.

1 As an example: many references misleadingly use the term *potential* lead wires instead of voltage lead wires or voltage tap-offs in case of AC.

Table 4.1: Definition of voltage u for DC and AC separately for closed and open loops analogously to [VML11]

	voltage definition at DC	voltage definition at AC
open loop	$u_{ab} = \Delta V = \int_a^b \vec{E} \cdot \mathrm{d}\vec{s}$ (4.1)	$\underline{u}_{ab} = \Delta V + \underline{\varepsilon}_\mathrm{i} = \int_a^b \underline{\vec{E}} \cdot \mathrm{d}\vec{s}$ (4.2)
closed loop	$u_{aa} = \Delta V = \oint_C \vec{E} \cdot \mathrm{d}\vec{s} = 0$ (4.3)	$\underline{u}_{aa} = \underline{\varepsilon}_\mathrm{i} = \oint_C \underline{\vec{E}} \cdot \mathrm{d}\vec{s} = -\frac{\mathrm{d}}{\mathrm{d}t} \iint_A \underline{\vec{B}} \cdot \mathrm{d}\vec{A}$ (4.4)
	· V is the electric scalar potential in V and ΔV is the pd $V_a - V_b$ (often: $\Delta\varphi$)	· $\underline{\varepsilon}_\mathrm{i}$ is the induced emf in V
	· only at DC the pd is identical to voltage u	· only in closed loops at AC the induced emf is identical to $\underline{u}$
	· source of V: distribution of electrical charges	· source of $\underline{\varepsilon}_\mathrm{i}$: varying electromagnetic fields and/or moving conductors

Note that in every case the voltage can be defined as the integral (line or loop) of the total electric field intensity [VML11, p. 2].

4.1.1 *Measurements with AC Voltmeters*

There were numerous discussions on what an high impedance voltmeter actually measures under AC. These debates started in the late 1960s [Moo69; Kle81; Rei82; Rom82; Pet84; LZ95; Nic05; VML11] and are partly still being discussed in the 21st century in greater detail [Bos08][2].

Figure 4.1 shows the voltage measurement circuit of an electrical measurement system using an ADC AC voltmeter on a solid cylindrical conductor. Sinusoidal conductor current $\underline{I}$ is injected into the conductor at frequency $f > 0\,\mathrm{Hz}$. If the surrounding dielectric has negligible conductivity compared to the CUT, then $\underline{\vec{J}}$ will only have a z-component. The pick-up loop area A_L, enclosed by curve C is located in the y-plane and is build of CUT, voltage leads with their resistances R_VL and the voltmeter with the internal measurement resistance R_im. The perpendicular extension of the voltage leads from the CUT's surface is d_VL and the distance between a and b on the conductor's surface is measurement length l_meas. Directions of vector boundary elements $\mathrm{d}\vec{s}$ on curve C follow the application of the *right-hand*

2 These debates arose from what was often referred to as "a paradox in electrodynamics", where two identical voltmeters connected to the same two points, would deliver different result. Also powerfully demonstrated by Walther Lewin in his lecture *Complete Breakdown of Intuition* [Lew02] and in [HM89, p. 10.0.1]. With the definitions of the preceding sections this paradox can be resolved easily.

rule on vector area elements $\mathrm{d}\vec{A}_\mathrm{L}$. The internal measurement resistance R_im is usually in the range of some MΩ to draw only negligible current—internal measurement current $\underline{i}_\mathrm{im}$—from the test circuit[3]. The resistances of the thin metallic voltage lead wires are usually much smaller than R_im. Recollect, all vectors and complex quantities are rms values.

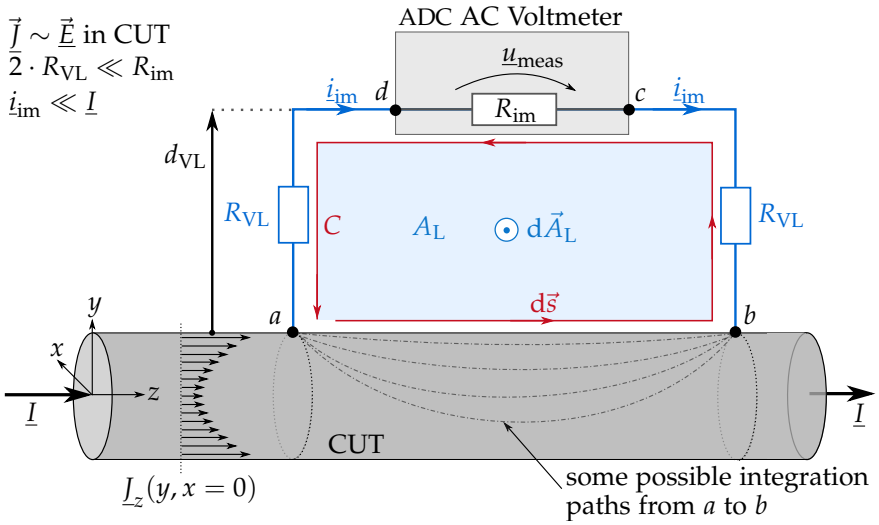

Figure 4.1: Schematic drawing of the voltage measurement circuit (blue rectangle) in electrical AC loss measurements on a solid cylindrical CUT (gray cylinder) using an ADC AC voltmeter (light gray rectangle)

A voltmeter's reading is proportional to the total electric field intensity over its internal impedance [LZ95, p. 88]. Starting from *Faraday's Law* of induction in integral form for non-moving conductors in Equation (4.5) with the notation given in Figure 4.1, one can derive the total electric field intensity in the voltmeter (Equation (4.10)), through Equation (4.5) to Equation (4.10).

$$-\frac{\mathrm{d}}{\mathrm{d}t}\iint_{A_\mathrm{L}} \underline{\vec{B}} \cdot \mathrm{d}\vec{A}_\mathrm{L} = \oint_C \underline{\vec{E}} \cdot \mathrm{d}\vec{s} \tag{4.5}$$

By subdividing C:

$$-\frac{\mathrm{d}}{\mathrm{d}t}\iint_{A_\mathrm{L}} \underline{\vec{B}} \cdot \mathrm{d}\vec{A}_\mathrm{L} = \int_a^b \underline{\vec{E}} \cdot \mathrm{d}\vec{s} + \int_b^c \underline{\vec{E}} \cdot \mathrm{d}\vec{s} + \int_c^d \underline{\vec{E}} \cdot \mathrm{d}\vec{s} + \int_d^a \underline{\vec{E}} \cdot \mathrm{d}\vec{s} \tag{4.6}$$

and with:

$$\int_a^b \underline{\vec{E}} \cdot \mathrm{d}\vec{s} \;\wedge\; \int_c^d \underline{\vec{E}} \cdot \mathrm{d}\vec{s} \gg \int_b^c \underline{\vec{E}} \cdot \mathrm{d}\vec{s} \;\wedge\; \int_d^a \underline{\vec{E}} \cdot \mathrm{d}\vec{s}\ , \tag{4.7}$$

$$\int_c^d \underline{\vec{E}} \cdot \mathrm{d}\vec{s} = -\int_d^c \underline{\vec{E}} \cdot \mathrm{d}\vec{s}\ , \tag{4.8}$$

$$\underline{u}_\mathrm{meas} = \int_d^c \underline{\vec{E}} \cdot \mathrm{d}\vec{s} = \underline{i}_\mathrm{im} \cdot R_\mathrm{im}\ , \tag{4.9}$$

the *measured* voltage is:

$$\underline{u}_\mathrm{meas} \approx \int_a^b \underline{\vec{E}} \cdot \mathrm{d}\vec{s} + \frac{\mathrm{d}}{\mathrm{d}t}\iint_{A_\mathrm{L}} \underline{\vec{B}} \cdot \mathrm{d}\vec{A}_\mathrm{L}\ . \tag{4.10}$$

3 In the used measurement system R_im is the input impedance of the ADC used for the voltage measurement (compare Figure 2.1).

Note that the measurement system uses the total current $\underline{I}$ through its internal measurement shunt to calculate the *measured* resistance

$$R_{\text{meas}} = \frac{1}{l_{\text{meas}}} \text{Re}\left(\frac{\underline{u}_{\text{meas}}}{\underline{I}}\right) \quad . \tag{4.11}$$

The *measured* inductance is obtained by:

$$X_{\text{meas}} = \frac{1}{l_{\text{meas}}} \text{Im}\left(\frac{\underline{u}_{\text{meas}}}{\underline{I}}\right) \quad . \tag{4.12}$$

Both quantities are given in Ω/m. Equation (4.5) to Equation (4.10) are valid if no additional thermal, chemical or mechanical emfs are present in the circuit [Pag77, p. 979]. The result coincides with *Lenz's law*, which states that the induced emf will drive a current whose magnetic field will counteract its source field. Lately, Alain Bossavit showed that bringing voltage lead wires with finite conductivity close to the measurement circuit will typically not influence the results [Bos08]. From Figure 4.1 and Equation (4.10) it can be seen that any magnetic flux through surface A_{L} affects the measured voltage $\underline{u}_{\text{meas}}$. At DC the time derivative will vanish and the measured voltage will be purely resistive. At AC an additional voltage caused by the magnetic flux through surface A_{L} will be measured. According to *Faraday's Law* of induction, this induced voltage is 90° phase-shifted, in regard to the phase of the magnetic field, which creates it. Thus, the measured voltage can become a complex quantity at AC. Note that the contribution of the electric field to the *measured* voltage can also be complex at AC.

As the electric field varies inside the conductor due to *skin effect*, the question of: "Which of the infinitive possible integration paths of the electric field from a to b inside the conductor is the *true integration path*?" should be raised. This question and the influence of magnetic fields in electrical measurements is discussed in the next section.

4.1.2 *The Role of Outer Out-of-Phase Magnetic Fields*

COMPLEX MAGNETIC FIELDS IN ELECTRICAL MEASUREMENTS At DC, even though the current density can also vary in the cross section (e.g.: due to severe bending, corners,...), the integration along the electric field along any convenient path from voltage tap-off a to b will—by definition in Equation (4.1)—lead to the *true* voltage drop.

At AC the current density is not the same in the whole conductor cross section. Due to *skin* and *proximity effect* it varies in magnitude and phase at different locations inside the cross section. Subdividing the current density into filamentary currents (similar to the black arrows in the CUT in Figure 4.1) makes the following line of argument more easy to follow. The total conductor current $\underline{I}$ is obtained by integrating over all these current filaments.

The diffusion of the electromagnetic field from outside of the conductor into the conductor results in an increasing phase displacement of current filaments towards the conductor center[4]. Every filamentary current produces

4 Note that due to superposition of all current filaments, the annulus in phase with the total conductor current $\underline{I}$ is found beneath the surface at AC.

a magnetic field due to *Ampère's Law*, whereby all of them contribute to the overall magnetic field surrounding the conductor by superposition. The magnetic field produced by a current filament will have the same phase as the current filament. As the current filaments differ in phase, the magnetic fields generated by different filaments will differ in phase as well. Magnetic field components, which are in-phase with the total conductor current $\underline{I}$ are called real or in-phase components. Magnetic field components that are not in phase with the total conductor current $\underline{I}$ are called imaginary, quadrature or out-of-phase magnetic field components.

From *Faraday's Law* of induction it can be concluded that real magnetic field components through surface A_L will generate 90° phase-shifted induced currents in loop C due to the time-derivation in *Faraday's Law*. The phase shift is relative to the reference phase of the total current $\underline{I}$. Hence, imaginary magnetic fields captured by surface A_L will induce currents that are either 0° or 180° phase-shifted. This is shown in a phasor diagram in Figure 4.2.

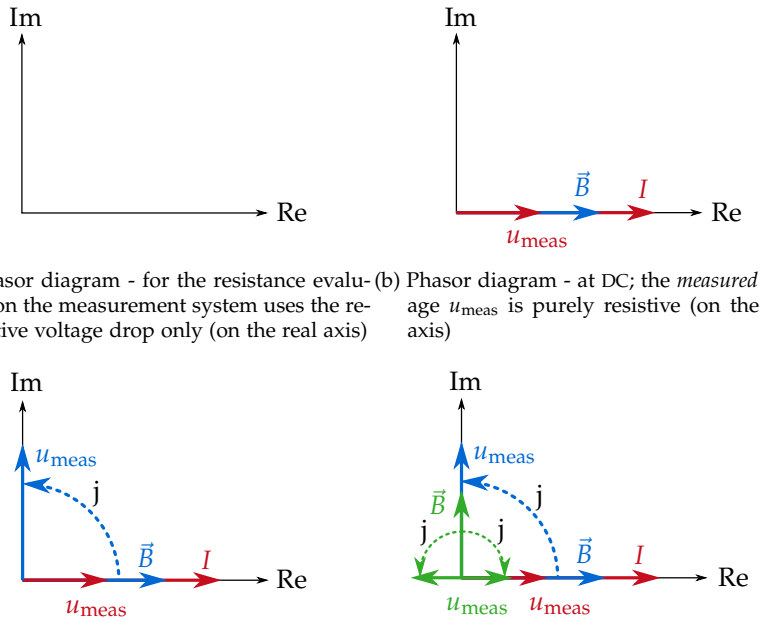

(a) Phasor diagram - for the resistance evaluation the measurement system uses the resistive voltage drop only (on the real axis)

(b) Phasor diagram - at DC; the *measured* voltage u_meas is purely resistive (on the real axis)

(c) Phasor diagram - at AC for rotationally symmetric conductors; the total voltage is composed of an imaginary and a real part; the *measured* voltage is complex

(d) Phasor diagram - at AC for non-rotationally symmetric conductors, where outer imaginary magnetic field components exist in the pick-up loop

Figure 4.2: Phasor diagrams of electrical measurements at DC and AC for different setups; I is the excitation current; the colors links, which *measured* voltage drop u_meas is caused by which current and which magnetic field component; the total *measured* voltage is the vector sum of the single voltage drops; j symbolizes the phase-shifted induction; for simplification, the real $\vec{B}$ only inductively induces a voltage (a cable typically has a resistive-inductive behavior); imaginary magnetic field components induce a voltage component in-phase (in positive real axis) or in anti-phase (negative real axis direction) depending on their orientation relative to the pick-up loop

Therefore, out-of-phase magnetic field components captured in the pick-up loop, generate an in-phase[5] current through the measurement system, which results in an in-phase voltage drop over R_im. As the measurement system evaluates this resistive voltage drop to obtain the resistance of the

5 In the following in-phase relates to the general affect on the real voltage drop. As put forward above out-of-phase magnetic fields can also cause anti-phase voltage signals.

CUT, the *measured* resistance is directly affected by out-of-phase magnetic fields penetrating surface A_L.

The out-of-phase magnetic field components in and near different conductor cross sections are displayed in Figure 4.3.

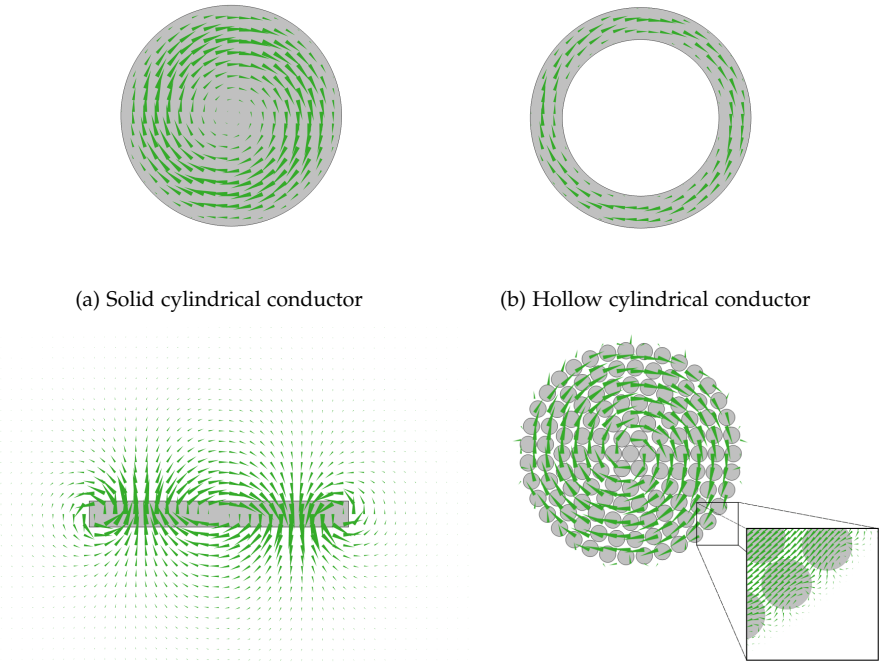

(a) Solid cylindrical conductor

(b) Hollow cylindrical conductor

(c) Rectangular conductor

(d) Stranded conductor

Figure 4.3: Out-of-phase magnetic field components (green cones) in and near different conductor cross sections (gray); the influence of the return conductor is neglected

For *rotationally symmetric current density distributions*—only present at rotationally symmetric conductor cross sections of uniform conductivity and without *proximity effect* (e.g.: Figure 4.3a and Figure 4.3b)—the superposition of all filamentary currents leads to an absence of out-of-phase magnetic fields outside of the conductor cross section. The reason for that is, all current filaments in an annulus are identical and hence every annulus of filamentary currents has its geometric center at the conductor center. Due to superposition, externally, the conductor acts as a single current filament in-phase with the total conductor current, having its geometric center at the conductor center [Tay70]. The cross section and current density of a rectangular conductor (see Figure 3.13) is not rotationally symmetric. Therefore, out-of-phase magnetic field components exist outside of the conductor (see Figure 4.3c). For the stranded conductor in Figure 4.3d twisting of the layers is not included. Nevertheless, the field distribution would nearly look identical despite additional small axial magnetic field components[6]. As the current density is close to being rotationally symmetric, there is only little imaginary flux leakage outside the conducting domains. At this point it should be noted that imaginary magnetic field components can also arise from other sources in a measurement setup. *Eddy currents* in nearby metal framework are 90° phase-shifted to current $\underline{I}$ that excited them in the first

6 The ratio of axial (in direction of z-axis) magnetic field component to magnetic field components in x- or y-direction, depends on the pitch and is small in typical conductor designs.

place. Hence magnetic fields generated by these *eddy currents* will be out-of-phase related to this initial current $\underline{I}$ and affect the *measured* resistance if captured in the pick-up loop. These additional losses will also be analyzed in following sections.

INTEGRATION PATH OF ELECTRIC FIELD INSIDE THE CONDUCTOR

Concerning the integration path of the electric field inside the conductor from voltage tap off a to b, it can be shown with Figure 4.4 that every possible integration path inside the conductor results in the same voltage as obtained from the surface voltage drop (line integral of the electric field at the conductor surface).

$$C_\mathrm{o} = C_1 + C_{2,\mathrm{o}} + C_{3,\mathrm{o}} + C_{4,\mathrm{o}} \qquad \sigma \approx 0 \rightarrow \underline{E}_{x,y,z} > 0$$
$$C_\mathrm{i} = C_1 + C_{2,\mathrm{i}} + C_{3,\mathrm{i}} + C_{4,\mathrm{i}}$$

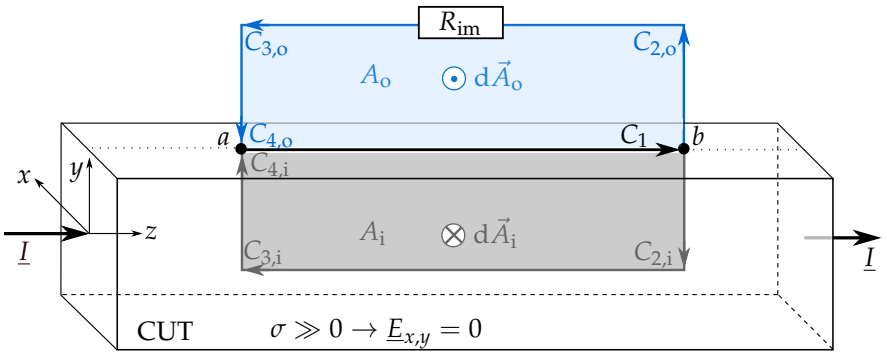

Figure 4.4: Schematic drawing of a rectangular conductor and possible inner and outer loops; inner contour C_i spans surface A_i (gray surface) and outer contour C_o spans surface A_o (blue surface); annotations belong to the arrow-heads

For a solid cylindrical conductor this surface voltage drop divided by the total current enclosed by this surface is by definition the AC resistance [GP04]. With *Faraday's Law* and the assumption that there is no radial electric field component inside the conductor[7] one can conclude:

$$-\frac{\mathrm{d}}{\mathrm{d}t}\iint_{A_\mathrm{i}} \underline{\vec{B}} \cdot \mathrm{d}\vec{A}_\mathrm{i} = \oint_{C_\mathrm{i}} \underline{\vec{E}} \cdot \mathrm{d}\vec{s} \tag{4.13}$$

$$\longrightarrow -\frac{\mathrm{d}}{\mathrm{d}t}\iint_{A_\mathrm{i}} \underline{\vec{B}} \cdot \mathrm{d}\vec{A}_\mathrm{i} - \int_{C_{3,\mathrm{i}}} \underline{\vec{E}} \cdot \mathrm{d}\vec{s} = \int_{C_1} \underline{\vec{E}} \cdot \mathrm{d}\vec{s} = \int_a^b \underline{\vec{E}} \cdot \mathrm{d}\vec{s} \tag{4.14}$$

Every possible path inside the conductor together with the magnetic flux captured in the loop that is formed by this path, leads to the same voltage drop as present at the surface between a and b. Hence, in the analysis of a problem, any convenient path between a and b together with A_i can be chosen. Contact points a and b are defined by the position of the voltage lead loop. Hence, contacting the voltage tap-offs of a and b around the conductor circumference will not affect the results for single conductors. For multiple insulated conductors, such as stranded conductors, the effect of contacting multiple strands will be explained later. Figure 4.3a can be used for an illustrative example. When changing the depth of the integration path from surface into the conductor, not only does the electric field along inner path $C_{3,\mathrm{i}}$ vary, but also the inner loop A_i formed inside the conductor,

7 This can be assumed, when the conductivity of the surrounding dielectric is much smaller than that of the conductor.

which captures more or less imaginary magnetic flux changes. The electric field and magnetic flux density compensates each other as *Faraday's Law* has to be fulfilled at all times.

The same is valid for outer loop C_o. Line integral over $C_{3,o}$ together with the flux captured by A_o will always be equal to the surface voltage drop along C_1. Nevertheless, only the line integral over $C_{3,o}$ is obtained by the measurement system, as shown earlier in Equation (4.10), which can make the voltage measurement position-dependent at AC.

PAST INVESTIGATIONS ON COMPLEX MAGNETIC FIELDS Basically, one can distinguish between *true* losses in the conductor and *measured* losses. *Measured* losses are also called *apparent* losses. The aim is to find a measurement setup, where the *measured* losses are as close as possible to the *true* conductor losses. The *true* losses are those caused by *Joule heating* in the CUT and which will also be measured with the calorimetric method. They are caused by the resistive characteristic of a conductor and are increased by *skin* and *proximity effect* at AC. *Measured losses* can diverge from the *true* conductor losses due to the influence of imaginary magnetic fields and non-rotationally symmetric surface current densities, directly affecting the electric field intensity integral of Equation (4.10).

The importance of complex outer magnetic fields was already detected in 1930 by Dannatt and Redfearn [DR30, p. 492]. It was shown that complex magnetic fields have to be measured to obtain the *true* losses, when *proximity effect* is present. Different voltage lead positions, capturing sufficient magnetic flux, have been analyzed and were compared to obtain the *true* conductor losses of a busbar system. These methods were called *2-wattmeter* and *3-wattmeter methods*. Later in 1948, different *apparent* losses were attributed mainly to geometrical parameters of the setup in [Sal48, p. 1392]. E. H. Salter reported in 1949 that losses of close metal framework are not included in the measurement, as long as the voltage loop is sufficiently small to not capture magnetic stray fields caused by them [Sal49]. The same is concluded in the discussion to [Sal48, Discussion]. Expanding the voltage loop over a cable's sheath will include losses from the sheath in the *measured* value (see Section 4.2.2.3). This is in accordance with the explanation put forward above combined with the out-of-phase magnetic field distribution in hollow conductors (Figure 4.3b). Moreover, in this discussion E. E. Hutchings recommends enlarging the voltage loop to 50 times the conductor spacing to account for the *true* losses in 3-phase systems [Sal48, Discussion]. In 1970, R. L. Jackson [Jac70]—and J.E. Taylor in the corresponding discussion [Tay70]—tackled this topic again including a more detailed analysis with lumped circuit elements.

In the same year—1970—the important role of complex magnetic fields was first brought up and analyzed in the superconductor community for superconducting tapes. Here, the electrical method of AC loss determination—as used in this work—is often referred to as the *transport method*. For superconductors, John R. Clem was the first to point out the position-dependency of the *measured* voltage for rectangular conductors in [Cle70]. In 1995 A. M. Campbell recommended a larger voltage loop to capture sufficient magnetic flux to account for the *true* losses independent of the voltage tap-off positions around a tape's circumference [Cam95]. Three years later, P.

Dolez showed that if the radial extension of the voltage loop is three times the conductor strip's wider side, the deviation to the *true* losses is smaller than 1 % [Dol+98]. In 2005 an analytical model for these false loss voltage signals was developed in [GFŠ05]. This allows a correction to the *true* losses by averaging the values obtained by numerous voltage leads attached homogeneously around the conductors circumference at a certain distance to the conductor. A sophisticated combination of spiral and rectangular arrangement of voltage loops to access *proximity effect losses* of superconductors in flat formation separately was given in [Tsu+05]. Investigations on the influence of voltage lead position are still ongoing up to this day for specially designed superconductors [Ryu+13; RL16].

CONCLUSION Although known to some members in the high voltage cable measurement community, the effects of imaginary magnetic fields have often been neglected and were not investigated sufficiently during electrical AC resistance measurements to guarantee reproducible results. This also raises the question of reproducibility of measurements performed on complete cable drums. Moreover, often solid cylindrical copper conductors—where the analytical solution is known—are used to benchmark a measurement circuit. This can be problematic as this conductor type does not necessarily exhibit the same effects as the CUT, which is measured subsequently. For example: placing the voltage leads on the surface of a solid cylindrical conductor will result in measuring the *true* losses. Using this result to prove the accuracy of the setup will lead to errors, when exchanging the cylindrical solid with a rectangular conductor and retaining the same measurement setup (voltage leads attached to the surface). Hence, the benchmark of a measurement system and setup has to consider the effects of the CUT, which is measured afterwards. Preliminary investigations on necessary voltage loop size for the CUT need to be included in the benchmark of a setup.

With rising importance of accurate AC loss determination, the analysis of out-of-phase magnetic fields in and around *Milliken* conductors is more important than ever. This work intends to give recommendations for AC resistance measurements based on cumulative knowledge from past researches in different fields of AC loss measurements in combination with state-of-the-art FEM simulations and measurements on *Milliken* conductors. It should be noted that—to the best knowledge of the author—no investigation on a compromise between sufficient voltage loop size (to capture enough complex magnetic field for the *true* losses) versus a voltage loop as small as possible (to reduce the effect of external stray fields and decrease the reactive voltage drop) was performed for *Milliken* conductors until now. This is tackled in Section 4.1.4.

Prevailing imaginary magnetic field components are directly linked to the imaginary components of the electric field inside the conductor and can be seen as an equivalent according to *Ampère's Law*. Out-of-phase electric field components in the conductor are caused by AC losses, more precisely *skin* and *proximity effect*. Hence, imaginary magnetic fields contain information about AC losses. In case of conductors with a rotationally symmetric current density, e.g.: isolated *skin effect* in a solid circular conductor, imaginary magnetic fields are present in the conductor only. Attaching the voltage leads to the surface of the conductor therefore already includes the information

about the total AC losses. In all other cases the imaginary magnetic field and hence the information about AC losses is present in and in the surrounding of the conductor. To include the AC losses in the measurement, one therefore has to expand the pick-up loop above the conductor's surface. This is further investigated in Section 4.1.4 and demonstrated in Section 4.2.2.3.

Another consequence of the considerations above is that one can easily set up a measurement circuit, where one can measure a decreasing resistance with increasing frequency. Using a conductor within a tubular return conductor, the current density at AC will be similar to that shown in Section 3.1.3.4. In the outer hollow conductor the current density increases on the inner side due to *proximity effect*, whereas it decreases at the outer side. As the current density is directly linked to the electric field, attaching the voltage tap-offs and lead wires at the outer surface of the hollow conductor, will show a declining resistance. This is due to a decreasing surface current density on the outer surface of the tubular conductor with increasing frequency.

From this chapter it should be clear that observing a position-dependency of the measurement result at AC indicates asymmetric distributions of electromagnetic field quantities such as current density and magnetic fields in the measurement setup.

4.1.3 *Development of an Analogous Simulation Model*

As it is now clear what is actually being measured by an AC voltmeter, a simulation model can be build to easily assess different measurement setups in advance. With a comparison of what the measured values should look like (FEM simulation) and how the actual measurement values do look like (measurement), one can gain further insides and analyze additional sources of influence in different setups. Moreover, accurate simulation models where all parameters are known enable the investigations of different influences.

As discussed in detail in Section 2.5, *Comsol Multiphysics* is used for FEM simulations. From the preceding arguments it can be seen that there is a difference between *true* losses/resistance of the conductor, which arises from *Joule heating* and *measured* losses/resistance, which arises from the *measured* voltage through the voltmeter. *Comsol Multiphysics* allows the direct implementation of equations. To calculate the *true* conductor resistance, the definition of the resistance that is always valid is implemented: the volume integration of the loss density divided by the real part of the total current squared (Equation (1.1) and Equation (1.4)). As the excitation in the simulations is a current source and gives the reference phase, the current has no imaginary component and hence taking the real part is not necessary here. In the mef physics interface this is done in the "Results" tab by a "volume integration node" with $mef.Qh/\underline{I}^2_{\mathrm{rms}}$. Value $mef.Qh$ is internally defined in *Comsol Multiphysics* as the volumetric loss density (electromagnetic) p_{V} in $\mathrm{W/m^3}$. Value $mef.omega$ is internally defined as the angular frequency ω in $\mathrm{s^{-1}}$.

Rebuilding the measurement system in the simulation is called *virtual* measurement. To include the *virtual* measurement in the simulation, both

summands of the *measured* voltage from Equation (4.10) have to be implemented. Depending on the model and purpose, the line for the electric field integral and the surface of the magnetic field surface integral are either explicitly modeled and defined under "Definitions"→"Component Couplings"→"Integration" or retrospectively defined under "Data Sets" as "Parametric Curves/Surfaces". For this *virtual* measurement the integration path of the electric field line integral is put on the conductor's surface.

When investigating multiple parallel conductors (also stranded conductors with insulated wires), for the calculation of the AC resistance from the *virtual* measurement, the total current $\underline{I}$ through all conductors is used, even though the voltage tap offs are only attached to one conductor or strand. The reason for that is that in reality the actual measurement system also only measures the overall current through the shunt in the measurement system. Figure 4.5 shows the implementation of *true* losses and *virtual* measurement in *Comsol Multiphysics*.

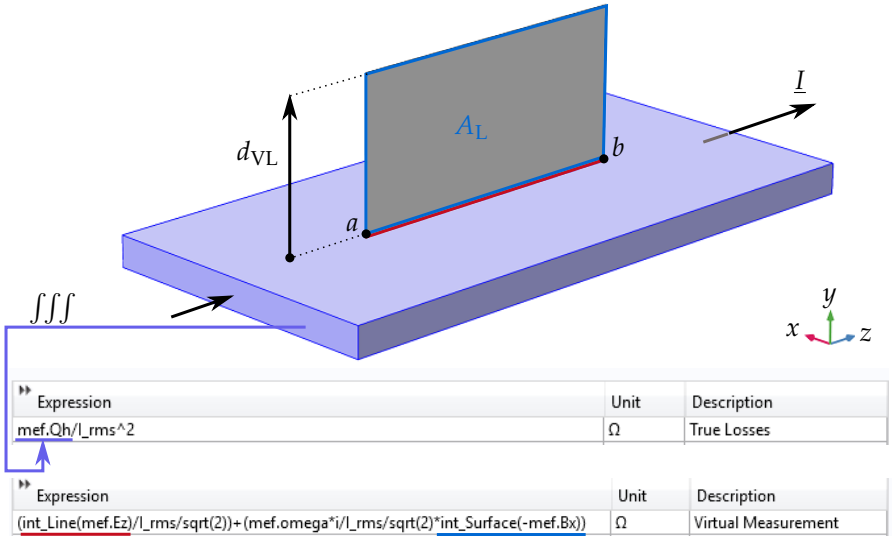

Figure 4.5: Rectangular CUT (lavender), voltage loop A_L (gray with blue border in the yz-plane) and the equations implemented in *Comsol Multiphysics*; int_Line and int_Surface are priorly defined line and surface integrals; I_rms is identical to $\underline{I}$

In Figure 4.5, note that because the current flows in positive z-direction, the vector area element $\mathrm{d}\vec{A}_L$ points in negative x-direction, which results in a sign reversal in the surface integral evaluation. Also recollect that the devision by $\sqrt{2}$ is necessary because *Comsol Multiphysics* calculates phasor quantities. The values obtained by the implemented equations are divided by the conductor length afterwards to obtain the resistance per-unit length. The final values obtained by this method are called R_{virt} in the following.

4.1.4 *Measurement of Complex Conductors*

The principles and observations noted above are now transferred to complex conductor cross sections. It shall be answered what losses are measured with extended pick-up loops on closely spaced parallel conductors such as stranded conductors with insulated wires or *Milliken* conductors. Moreover, a minimum for the radial extension of the voltage leads $d_{VL,min}$ is defined for rectangular, stranded and segmental conductors. This guarantees that

sufficient magnetic flux is captured by the pick-up loop, to account for the *true* losses of the CUT.

RECTANGULAR CONDUCTORS First, measurements and simulations are performed on a rectangular conductor, seen in Figure 4.6.

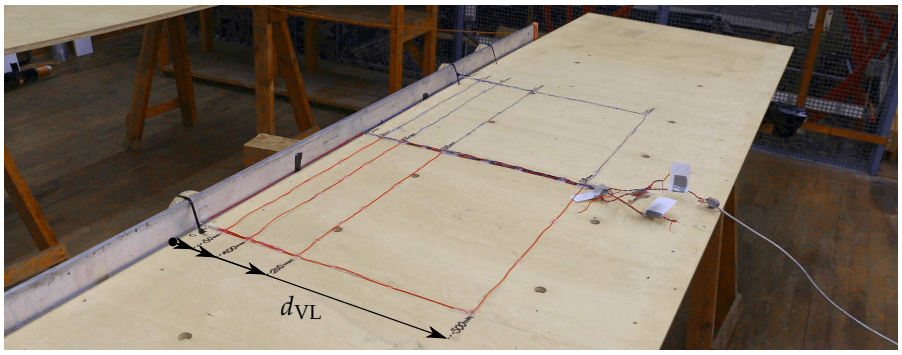

Figure 4.6: Rectangular aluminum CUT (gray on the left side) and setup of voltage leads (red & blue) for the investigation on a rectangular aluminum conductor on its broad side; single return conductor placed 2 m apart

The conductor under investigation is an aluminum bar with a cross section of 10 mm × 100 mm and a *measured* conductivity of $\sigma_0 = 34.10\,\mathrm{MS/m}$. The *true* AC resistance at 110.37 Hz obtained by FEM is $R_{true} = 37.24\,\mu\Omega/\mathrm{m}$. Figure 4.7 shows the *true* resistance, the *measured* resistance and the *virtual* resistance, which is ideally identical to R_{meas}.

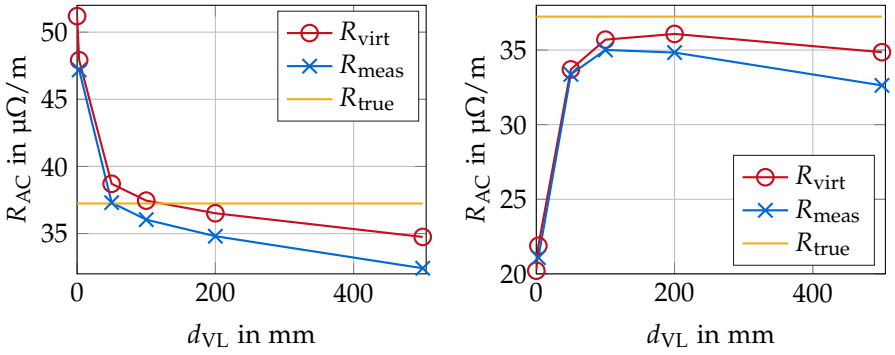

Figure 4.7: Resistances obtained by the measurement and *virtual* measurement on the rectangular aluminum conductor for different voltage lead extensions d_{VL} at 20 °C and 110.37 Hz; *left:* pick-up loop located at the center of narrow side; *right:* pick-up loop located at the center of broad side (as seen in Figure 4.6); in the setup the CUT was rotated and the pick-up loop remained in the same place

Two important observations can be made from the plots:

- First, the results do not perfectly converge against the *true* resistance. At 3 × 100 mm = 300 mm the deviation was expected to be lower than 1 % as discussed earlier.
- Second, the plots show convergence into the direction of R_{true} from opposite sides.

First, perfect convergence requires a surrounding free of other conductive parts. The effect seen above can be attributed to a steel fence 2 m apart from the CUT (see Figure D.2). Even though the true electrical parameters of this fence are unknown, adding a thin iron wall at the specified distance

in the simulation with $\sigma_0 = 11.2\,\mathrm{MS/m}$ and $\mu_r = 1000$ did qualitatively reproduce the curves obtained by the measurement (as seen in Figure 4.7)[8]. Removing the fence from the simulation shows perfect convergence against R_{true}. P. Dolez claimed that with a $d_{\mathrm{VL}} = (3\times$ the sample's wider side) will keep the error below 1 % for strip conductors [Dol+98]. In the case of the aluminum CUT above, simulations at 50 Hz showed that a $d_{\mathrm{VL}} = (2\times$ the sample's wider side) $= 200\,\mathrm{mm}$ will already give an AC resistance with a deviation below 1 % from R_{true}. Again, this is only valid if the surrounding is free of additional conductive parts. Nevertheless, FEM simulations of a hypothetical triangular conductor show that it can be necessary to increase the radial pick-up loop extension to even more than 3 times the maximum 2D conductor dimension to reach a deviation of less than 1 %. As this influence is based on the magnitude of out-of-phase magnetic field components, which in return depends on the current distribution, it should be clear that $d_{\mathrm{VL,min}}$ also depends on the frequency.

Second, the reason for convergence from opposite sides lies in the current density distribution in rectangular conductors with severe *skin effect*. It is larger than the average surface current density on the narrow side and smaller than the average surface current density on the broad side (see Figure 3.13). For small d_{VL} the influence of the line integral of the electric field is much larger than that of induced magnetic fields, which completely vanishes at $d_{\mathrm{VL}} = 0$. Hence, the current density, which is linked to the surface electric field by the conductivity, dictates the direction of convergence.

Helically winding the voltage leads around the conductor's circumference at its surface will not result in the *true* losses at AC either. The average surface current density of a conductor, which would be obtained then, does not necessarily relate to its overall losses. Nevertheless, for larger spacings of d_{VL} this can be advantageous compared to averaging the results of multiple lead arrangements. Helical wound pick-up loops are discussed again at a later point in this work.

STRANDED CONDUCTORS The question of what is measured with the electrical method in stranded conductors with insulated wires was already put forward by [Gra79, p. 105]. Already in 1930 it was reported that no difference can be measured when contacting the voltage leads to a single insulated strand or to multiple wires of a stranded conductor [DR30, p. 1392]. Figure 4.8 shows a section of a CUT, which is a stranded conductor with 19 $(1 + 6 + 12)$ perfectly insulated wires. The surrounding air was used as an insulator. Whereas the outer layer has a slight right-hand pitch along the conductor axis z, the inner layer—composed of six strands—is not twisted[9]. The current density and out-of-phase magnetic field components are shown in a cross section.

Figure 4.9 shows the resistances and reactances obtained by the *virtual* measurement. Note that not every position of d_{VL} is realizable in reality due to space occupied by other strands. It can be seen that the R_{virt} and X_{virt} are symmetrical to the true axis of the complete bundle, which is located

8 Note that due to the single return conductor outer fields are present in the complete measurement setup and produce *eddy currents* in nearby metallic objects.

9 The reason is the simpler definition of integration path and parametric surface in the the *virtual* measurement performed in *Comsol Multiphysics*.

at $d_{VL} = -3.37\,\text{mm}$. Due to almost perfect rotational symmetry in the current density distribution, this is in line with the arguments above.

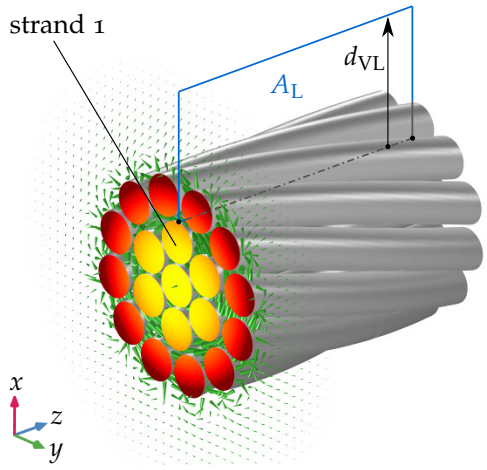

Figure 4.8: Absolute magnitude of current density $||\boldsymbol{J}||$ and out-of-phase magnetic fields between strands (green cones; logarithmic scaling) in a stranded conductor with perfectly insulated wires; current flows in positive z-direction voltage leads are attached to the top side of untwisted strand 1 building loop A_L: the dash-dotted line shows the integration path on the top side of strand 1

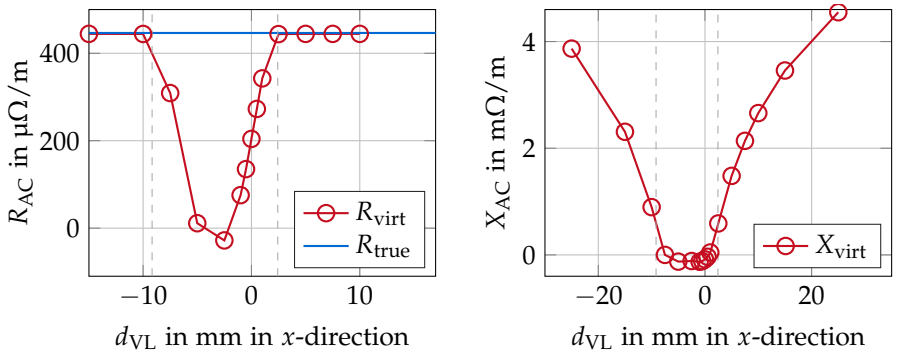

Figure 4.9: Resistance and reactance obtained by the *virtual* measurement for different voltage lead extensions d_{VL}; the vertical dashed gray lines indicate the outer dimensions of the stranded conductor; the simulation was performed at 2000 Hz to provoke severe *skin effect* in the small bundle with strand radii of 1.09 mm

Most important, at AC the resistance R_{virt}, which would also be obtained by a measurement, rapidly converges against the *true* resistance of the complete conductor bundle with increasing radial pick-up loop extension d_{VL}. This is illustrated in another example in Appendix A.2. As seen from Figure 4.9 the *true* resistance is nearly directly reached on the surface of the bundle. The reason for that is the almost perfect rotational symmetry in the current density distribution of the stranded conductor (compare Figure 4.3d). Nevertheless, this investigation is based on the assumption that the voltage tap-offs are connected to the same strand in the bundle at both voltage tap-offs a and b. Guaranteeing that can be challenging in reality for complex conductors. For the moment, it can be concluded that with a $d_{VL,min} = d_{CUT}$, sufficient complex magnetic field will be captured for typical stranded conductors with nearly perfect rotational symmetry.

Here d_{CUT} is the overall conductor diameter.

The same is valid for DC. If the voltage tap-offs a and b are both connected to the same strand, the resistive drop over this parallel connection of multiple insulated strands will deliver the *true* DC resistance.
Further discussions and requirements for the above made statements for both—AC and DC—are described in more detail in Section 4.2.3 and Section 4.2.4.

For the moment, the simulations above showed that electrical methods are generally able to measure the desired target quantity—AC losses of a complete conductor bundle with insulated strands—under certain conditions. In the following, a value for one of these conditions, which is the necessary minimum radial extension of pick-up loop $d_{\mathrm{VL,min}}$, is analyzed for the most important conductor type in this thesis: a *Milliken* conductor.

MILLIKEN CONDUCTORS In *Milliken* conductors, the geometric design parameters influencing the current density and hence magnetic field distribution show large variations in dimension. For example: the thickness of strand insulation lies in the µm range and the lay length of segments is a couple of m. To calculate the real current density in such a conductor a true 3D simulation is required. Despite the fact that some parameters involved (quality of strand insulation,...) are not known and likely vary along the conductor, even with state-of-the art commercial tools and current hardware, such a simulation seems to be out of reach.

Figure 4.10 shows a collection of possible current distributions in *M-type* conductors obtained by 2D simulation. As the real current density in such a *M-type* conductor cannot be known for certain, these imprinted current densities are educated guesses, based on expertise of different experts and cable manufacturers. On first sight it can be seen that expectations vary strongly.

This was achieved by remodeling a real 2500 mm^2 *Milliken* conductor cross section with 540 insulated, deformed strands in *Blender*[10]. The 2D model was then transferred to *Comsol Multiphysics*. By explicitly specifying the conductivity of each layer and using a current source as excitation, the current density was imprinted. Figure 4.10a, Figure 4.10d and Figure 4.10f were simulated at 50 Hz, to include the influence of real *skin effect* in the simulation as well. Figure 4.10b, Figure 4.10c and Figure 4.10e were simulated at 0.01 Hz. Simulations at 0.01 Hz guarantee that the desired or expected current density is not influenced by real *skin effect* in the simulation. But, a frequency greater than 0 Hz also makes out-of-phase magnetic fields, which directly depend on the enforced current distribution, accessible.

Figure 4.10a gives an impression on how the current density of an unoptimized *Milliken* conductor with blank strands could look like. When interwire conductivity is relatively large—opposite to insulated or oxidized strands—a segment will nearly act as a single bulk conductor. The effect of stranding will nearly vanish and full *skin effect* losses appear in the conductor. For large conductor dimensions as shown here, at 50 Hz the

10 *Blender* is a free modeling and render software package by *Blender Foundations* and can be found at www.blender.org (visited on 21/11/2017).

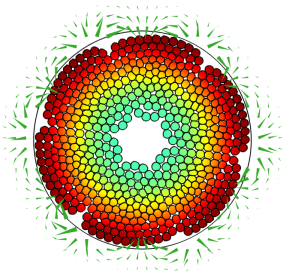

(a) Exemplary current density I (worst-case: blank strands) @50 Hz

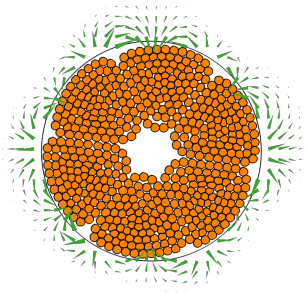

(b) Exemplary current density II (ideal conductor: $\boldsymbol{J}$ completely balanced)

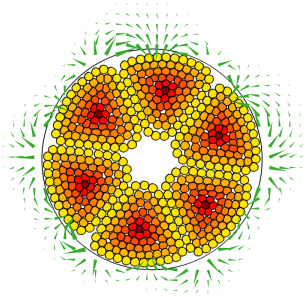

(c) Exemplary current density III (outer layers with larger resistance)

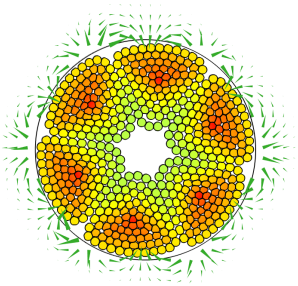

(d) Exemplary current density IV (III including *skin effect*) @50 Hz

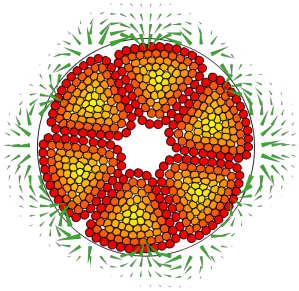

(e) Exemplary current density V (III inversed: *skin effect* in segments as in [Cig05, p. 37])

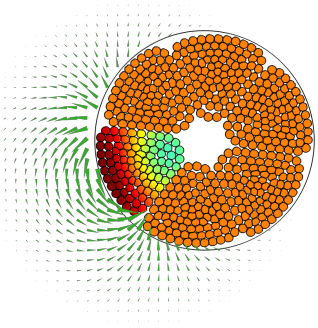

(f) Exemplary current density VI (II including a damaged segment) @50 Hz

Figure 4.10: Possible normalized in-plane current densities $\mathrm{Re}(\underline{J}_z)$ at 50 Hz in *Milliken* conductors and out-of-phase magnetic field components (green cones); a real conductor cross section of 2500 mm^2 without central conductor is shown

current can already flow back in the opposite direction at the conductor center (also compare current density at 300 Hz in Figure 3.1). Hence, it is reasonable from a certain cross section and up, to exclude the central conductor as seen in this example. Having a central conductor or not, will nearly have no influence on the outer out-of-phase magnetic field distribution as the central conductor is close to being rotationally symmetric and therefore does not produce outer out-of-phase magnetic fields (compare to Figure 4.3d).

Figure 4.10b shows an ideally AC current distribution in a *Milliken* conductor. A completely homogenized current density would result in the lowest possible losses. Note that such an ideal design would not only require to balance the *eddy currents* in all layers but also requires to balance the DC resistances of different layers (due to their lay lengths). Figure 4.10c assumes that the current distribution at AC primarily depends on the layers resistance, which increases outwards in this case. In Figure 4.10d the same conductivity for each insulated layer is preset but the simulation was performed at 50 Hz to show the superimposed influence of *skin effect*. Figure 4.10e shows a conductor, where every segment acts like a separate solid with *skin effect*. In Figure 4.10f an ideal conductor with a mechanically damaged segment is shown. This damage results in electrically connected strands, which cause full *skin effect* in this segment. Except for Figure 4.10f, the current density remains quite periodically and nearly rotationally symmetric in all cases. Therefore, the distribution of outer out-of-phase magnetic field components is confined to a small region near the surface only. As the asymmetry is largest in Figure 4.10f, imaginary magnetic fields leak out to a larger extent compared to all others.

Even though the direction of the magnetic field is comparability, quantitatively comparing the outer out-of-phase magnetic fields was not done here and is may not even sensible. Although there is a risk of capturing the fields of other metallic parts, a *convergence-check* of the *measured* resistance is recommended before the measurement. Nevertheless, from the estimated current densities and measurements performed on *Milliken* conductors, it is expected that the *measured* resistance typically converges fast with increasing d_{VL}. Similar to the stranded conductor, $d_{\mathrm{VL,min}} = d_{\mathrm{CUT}}$ is expected to deliver results with a deviation < 1 % to the *true* conductor resistance. Recollecting that the conductor segments also rotate around the cable core should additionally help in lowering the position-dependency, when the measuring length is in range of the segment lay length—which usually ranges from 1 m to 3 m—or larger. Additional investigations supporting some of the previous statements in this section are given in Appendix A.2.

4.2 IDENTIFICATION OF SOURCES OF INFLUENCE ON AC LOSS MEASUREMENTS

In the previous section it was made clear what exactly is being measured using the electrical measurement method. In this section it is shown, what sources of influence exist and how significant they are in different, commonly used measurement setups. For the following investigations it is important to analyze the worst-case scenario for current distribution asymmetries in setups caused by *proximity effect*. In numerical simulations it is investigated, if a solid or stranded CUT has more *proximity effect* losses in an

identical setup. Therefore, two conductors with the same total cross section next to a close return conductor are compared under AC. The first CUT is a small stranded copper conductor and the second CUT is a solid cylindrical copper conductor. Both come with a arbitrary total cross section of approximately 71 mm^2 and a length of 10 cm. The stranded conductor consists of a core wire, an inner layer with 6 wires and an outer layer with 12 wires. The wires' diameters are 2.18 mm with a perfect insulation of 100 µm on each wire. The lay length of both layers coincides with the total model length of 10 cm. The stranding of insulated wires results in a larger DC resistance of the stranded conductor compared to the solid CUT. The return conductor is identical to the second CUT and has a center-to-center distance of 1.5 cm to both CUTs. As shown in Section 3.1.2.6, increasing the frequency gives the same qualitative result as increasing conductor dimensions. Hence, the frequency at AC is set to 700 Hz to observe severe *skin* and *proximity effect* for these comparatively small stranded conductors. Figure 4.11 shows the current density in both cases under AC. Table 4.2 compares the additional losses due to *proximity effect*.

Figure 4.11: Normalized in-plane current density $\mathrm{Re}(\underline{J}_z)$ under AC of both CUTs next to a closely spaced return conductor (right sides): *left:* stranded CUT; *right:* solid CUT

Table 4.2: Comparison of severe *skin* and *proximity effect* in a stranded conductor with insulated strands and in a solid conductor

	stranded conductor	solid conductor
R_{AC}/R_{DC} at 700 Hz isolated (*skin effect* only)	1.20	1.22
R_{AC}/R_{DC} at 700 Hz next to the close solid return (*skin* and *proximity effect* Figure 4.11)	1.22	1.37

At first sight, it can be seen that *skin effect* losses are slightly reduced in the stranded conductor. This was already explained in [SPW15, p. 4] and is due to the larger distance between single strands, which in turn reduces *proximity effect* between all strands. Moreover, even though—because of the packing density of the single wires—the distance between the surface of the stranded CUT and return is smaller than the distance between the surface of the solid CUT and return conductor, the *proximity effect* caused by the solid return conductor is smaller in the stranded case. The current density in the stranded conductor is nearly unaffected by the close return conductor. The reason is that exactly one complete lay length (10 cm) was simulated, exposing every wire in the outer layer to the same *proximity effect* losses over one complete lay length. Therefore, no preferred current path in the outer layer exists and the current is the same in all outer layer wires. Nevertheless, the current density—even though the same in every wire of

the outer layer—is slightly affected by the return conductor, resulting in small additional losses. It was also observed that the *proximity effect* losses in the return conductor were slightly lower, when being positioned next to the stranded conductor. These results also verify the claim made by [SSW35, p. 325], stating that bundled conductors with insulated wires have lower *proximity effect* losses compared to solid conductors or stranded conductors with blank wires touching each other[11].

It can be concluded that the worst-case scenario, where the current density is affected the most by other conductors, is a solid conductor. As many high voltage power cables nowadays have cross sections up to 2500 mm^2—even though larger cross sections are already available—and AC losses increase for larger conductivities, in the following investigations the CUT will be a 2500 mm^2 solid cylindrical copper conductor. The reference DC resistance $R_{\mathrm{DC,Ref}}$ for that conductor is approximately 6.897 µΩ/m. According to Equation (3.33) the reference AC resistance $R_{\mathrm{AC,Ref}}$ at 50 Hz (isolated conductor with *skin effect* only) is approximately 12.260 µΩ/m. These reference resistances are the *true* resistances and are desired to be measured.

True losses in the CUT due to nearby conducting materials should be avoided in the measurement setup as they are not present under operating condition of the cable. Conducting materials near the measurement setup can be divided into return conductor influences and influences from nearby metal framework. For both cases, the most common setups are analyzed in the following.

4.2.1 *Additional True Losses due to Proximity Effect*

Another conductor close to the CUT will distort the electromagnetic field of the CUT and can destroy the rotational symmetry[12]. At this point only the real change of conductor losses is evaluated and not the influence on the integration path of the electric field intensity due to varying surface current densities. The appropriate choice of pick-up loop location when significant *proximity effect* is present is discussed in Appendix A.

In the following, *proximity effect* due to return conductors and due to nearby conducting metal framework is distinguished.

4.2.1.1 *Influence of Different Return Conductor Configurations on True Losses*

Figure 4.12 shows a set of commonly used return conductor arrangements used for electrical measurements. Moreover, the exemplary current density is shown for small center-to-center spacings d. For *Setup IV* and *Setup V*, d is the distance to the inner side of the return. The CUT—2500 mm^2 solid copper cylinder—is presented in gray and the return conductors in dark gray. *Setup I* uses an identical conductor as a return conductor. *Setup II* uses a smaller copper return conductor with a cross section of 240 mm^2.[13] In *Setup III* two identically spaced return conductors are used, which are

11 Note that this is only the case if the length of the stranded conductor is much greater than the lay length of the layers or a whole multiple of the lay lengths, as in this example.

12 The only exception is a perfectly concentric tubular return conductor, which does not destroy the symmetry of current density distribution and therefore does not influence the AC resistance.

13 This rather arbitrary cross section was taken from [Ols+99], where measurements with *Setup III* were performed.

located in the same vertical plane as the CUT. Both are made of copper with a cross section of 240 mm^2 each. *Setup IV* and *V* use a coaxial current return, which represent typical cable sheaths. Both sheaths are concentrically arranged. The solid sheath of *Setup IV* is made of aluminum with an overall cross section of 600 mm^2. The copper wire sheath of *Setup V* consists of 69 homogeneously arranged strands and has an overall cross section of 257 mm^2. The sheath cross sections of *Setup IV* and *V* are kept constant, when varying d.[14] *Setups I* and *II* are usually referred to as *single return method*, *Setup III* as the *symmetrical method* and *Setup IV* and *V* are commonly called *sheath* or *shield return methods*.

Whereas *Setup I* and *II* are the most straight forward approaches to set up a current return path, *Setup III* was successfully used in AC resistance measurements of superconductors before [Ols+99]. When using an appropriate d (round about 5 cm to 7 cm), *Setup IV* and *V* become typical power cable configurations. Returning the measurement current via cable sheath was first shown in [BM68] and later also in [CMR77; Fro05; SKP11a].

Figure 4.13 shows additional *proximity effect* losses relative to the isolated conductor losses (*skin effect* only) in the CUT at 50 Hz for different setups and return conductor spacings d.

As no additional losses appear in case of perfect concentric return conductor arrangements (*Setup IV* and *V*), the more realistic case of slightly asymmetrical (indicated by (a)) return conductors were simulated as well[15]. Therefore, the CUT in *Setup IV* and *V* was shifted 2 mm from the geometric center of the outer return conductor. This can be seen as a worst-case scenario, because high voltage power cable manufactures have to abide an eccentricity of the insulation smaller than 10 % for high voltage cables over 150 kV according to IEC 62067. As eccentricity is calculated from the difference between maximum and minimum insulation thickness divided by the maximum insulation thickness, a possible shift of the inner conductor is allowed to reach up to 1.58 mm for a 30 mm insulation. *Setup III* can also quickly become asymmetric in reality, both electrically and geometrically. In the model this is achieved by setting up one return conductor at distance d and the other at distance $d + 3$ cm. Moreover, in *Setup III* unbalanced return conductor currents ($0.45 \cdot \underline{I}$ in one return and $0.55 \cdot \underline{I}$ in the other closer spaced return conductor) are included. The results where obtained by a 2D FEM simulation in *Comsol Multiphysics*.

It can be seen from Figure 4.13 that using minimum distance d_{min}, where the additional *true* losses are lower than 0.1 %, can easily be reached in practice. For *Setup I* and *II*, d_{min} is approximately 1 m, for *Setup III* d_{min} is about 20 cm[16] and for *Setups IV* and *V* d_{min} is automatically reached in typical cable constructions. Hence, *proximity effect* losses can easily be prevented in all setups.

14 These are typical construction parameters of high voltage power cables, even though screen wire configuration and sheath geometry strongly depend on short-circuit specifications and can therefore vary strongly (refer to IEC 60949).

15 For *Setup IV* the reason is that in case of a perfect concentric setup, the rotational symmetry of the electromagnetic wave traveling between inner and outer conductor is not distorted and hence the current distribution remains the same in both conductors, even though the electromagnetic field is confined to a smaller region. For *Setup V* the additional losses are only approximately zero and decrease with increasing number of wires in the sheath [HR15].

16 This coincides with the distances used in [Ols+99], which are in the range of 20 cm to 40 cm.

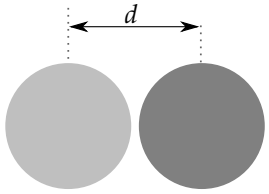

(a) *Setup I* - configuration

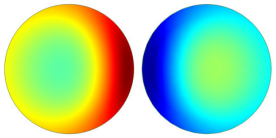

(b) *Setup I* - current density

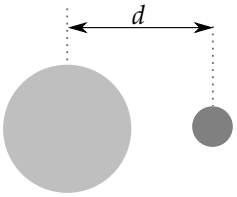

(c) *Setup II* - configuration

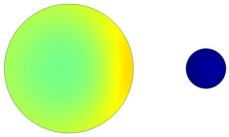

(d) *Setup II* - current density

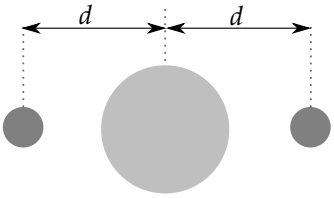

(e) *Setup III* - configuration

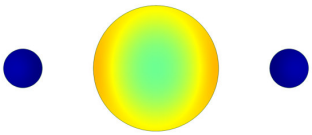

(f) *Setup III* - current density

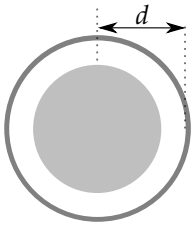

(g) *Setup IV* - configuration

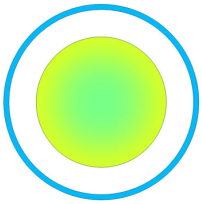

(h) *Setup IV* - current density

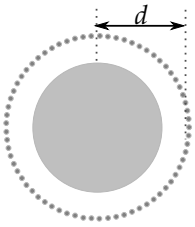

(i) *Setup V* - configuration

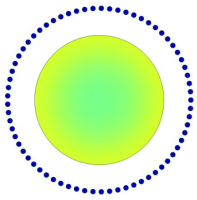

(j) *Setup V* - current density

Figure 4.12: Different commonly used return conductor configurations in electrical measurements and exemplary normalized in-plane current densities $\mathrm{Re}(\underset{\sim}{J}_z)$ in case of severe *proximity effect*; the CUT is marked in gray; return conductor($\widetilde{\mathrm{S}}$) in dark gray

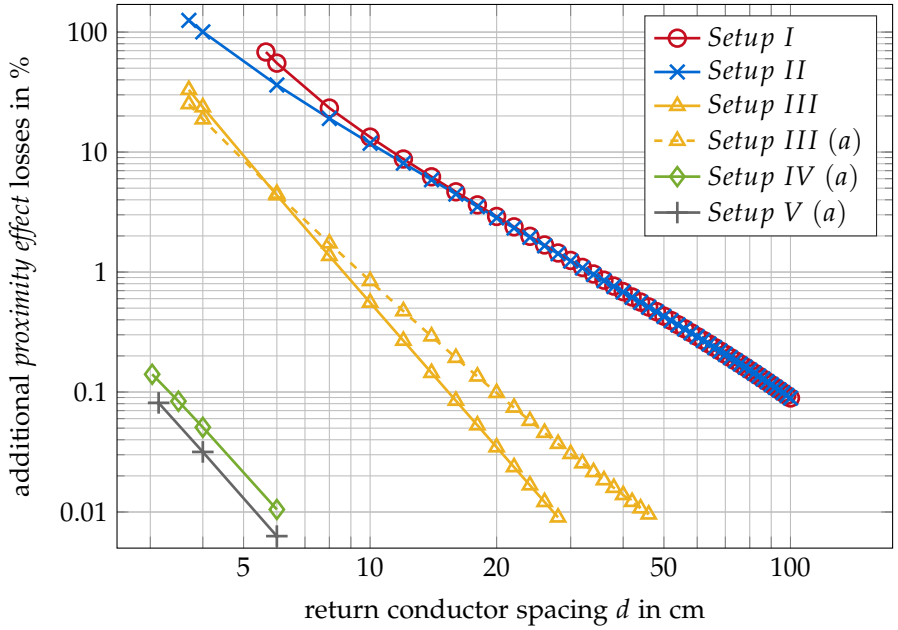

Figure 4.13: Log-log plot of additional losses in the CUT caused by the return conductor(s) at 50 Hz for different return conductor configurations

4.2.1.2 *Influence of Nearby Metal Framework on True Losses*

In most cases, laboratories are not free of additional conductive parts. Often reinforced concrete with steel reinforcing bars (rebars) is used during the construction of a building. An electromagnetic compatibility test chamber presents an extreme case, building a completely closed conductive surrounding. Moreover, shelves and other equipment can be a source of influence. In these cases conductive and also magnetic materials can be present in close proximity to the measurement setup resulting in additional *true* losses in the CUT due to *proximity effect*. Return conductor placement, distance, geometry, grounding condition and material composition—affecting electric and magnetic properties—of conductive parts nearby, vary from laboratory to laboratory. As there is no standard example, below only some examples of completely conductive laboratory floors influencing the CUT's current density due to *proximity effect* are presented.

Figure 4.14 shows the investigated geometric configuration and the exemplary current density in case of a closely spaced metallic ground. Here, the influence of the return conductor is neglected completely. The metallic floor has a width of 4 m and thickness t. Copper (Cu) and *soft iron* (Fe) are used as ground materials in this investigation. The electrical parameters of *soft iron (with losses)*—a predefined material in *Comsol Multiphysics*—are: $\sigma = 11.2\,\mathrm{MS/m}$ and $\mu_\mathrm{r} = 100$ in the linear range, when applying test currents of $\underline{I} = 11\,\mathrm{A}$.

Figure 4.15 displays the influence of different hypothetical laboratory floor geometries and materials on the CUT's *true* losses. Again, typical arrangements found in the literature can easily exceed the necessary minimum distance of 0.5 m to solid conductive parts and hence will not have considerable influence upon the *true* losses in the CUT.

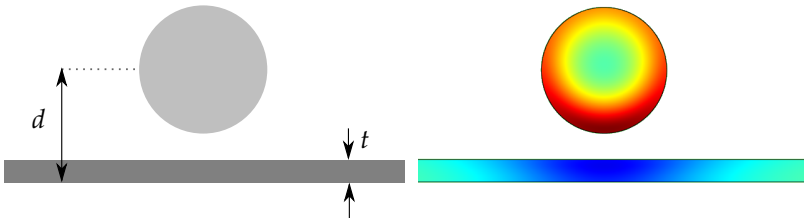

(a) *Setup VI* - configuration (b) *Setup VI* - current density

Figure 4.14: Configuration of CUT and nearby metal framework and exemplary normalized in-plane current densities $\mathrm{Re}(\underline{J}_z)$ in case of severe *proximity effect*; the CUT is marked in gray; metallic floor in dark gray; influence of the return conductor is neglected completely

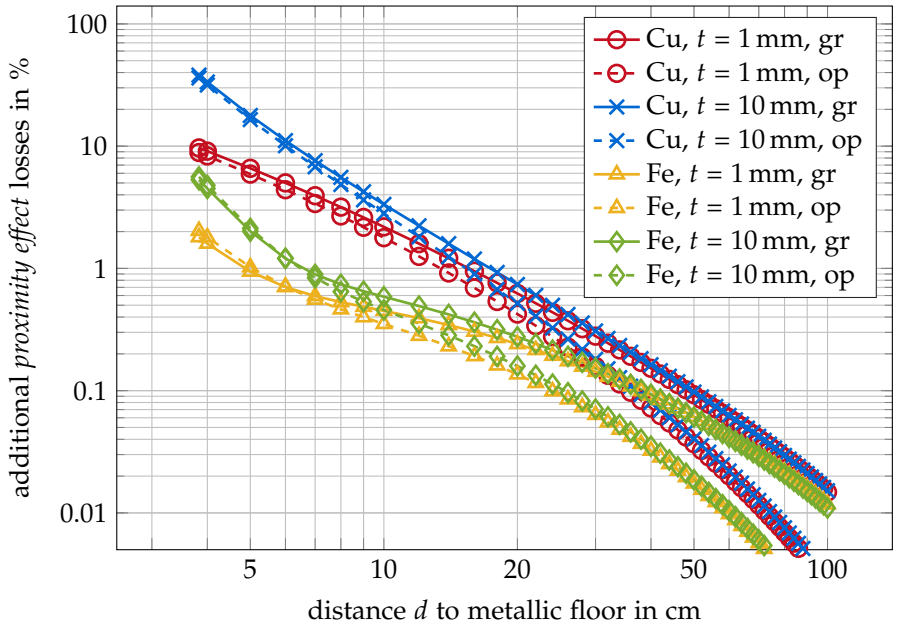

Figure 4.15: Log-log plot of additional losses in the CUT caused by a solid metallic floor at 50 Hz for different geometric, electric and magnetic properties of the floor; op = both sides of metallic floor open ended (not grounded); gr = both sides of metallic floor grounded; Cu indicates copper and Fe indicates *soft iron*

This section made clear, which distances to possible conductive floors or walls could be necessary to not significantly influence the *true* losses of the CUT. In the investigated practical setups the influence is well below 0.1 % and therefore of no significance. Nevertheless, one should bear in mind to keep these unwanted losses as low as possible when setting up a measurement circuit. Ideally there should not be any additional conductive materials nearby at all.

In the next chapter the more significant influence of return conductor configuration and metal framework on the *measured* losses is evaluated.

4.2.2 *Additional Apparent Losses Caused by the Position of the Voltage Pick-Up Loop*

Measured—also called *apparent*—losses are directly influenced by the surface current density near the voltage tap-offs and complex magnetic fields as argued previously. In this section, the influence of the different *Setups* and different pick-up loop positions on the *measured* losses are investigated. The asymmetries for *Setups III* to *V* are identical to those defined in the previous section. Afterwards, the influence of a metallic laboratory floor is shown. Typical voltage lead wires have cross sections much smaller than that of the CUT. In addition to that, they do not draw significant current. Hence, they will not lead to noticeable additional *true* losses in the CUT. Explicitly modeling the voltage leads in the FEM simulations is therefore neglected.

4.2.2.1 *Influence of Different Return Conductor Configurations on Apparent Losses*

Figure 4.16 shows the direction of in-phase and out-of-phase magnetic fields for every setup in case of close return conductor spacings. Nevertheless, with the knowledge obtained by the previous section, the return conductor(s) are set at the minimum distance d_{min}. In *Setup IV* and *V* d is set to 5 cm, which is close to a typical high voltage cable geometry. For *Setups III*, *IV* and *V* only the asymmetrical configurations were investigated, as they are more relevant in practice. Figures 4.17 to 4.21 show the deviation of the resistance obtained from the *virtual* measurement to the *true* losses of the CUT. The *true* resistance relates to that of isolated *skin effect* losses. Keeping this deviation between *apparent* and *true* resistance as small as possible in an electrical measurement, presents the main challenge.

In the different setups, *right* stands for the pick-up loop extended in positive x-direction, *top* for that pick-up loop extended in positive y-direction, *left* for that pick-up loop extended in negative x-direction and *bottom* for that pick-up loop extended in negative y-direction. Due to symmetry, the *bottom* configuration and the *top* configuration are identical in every setup. Note that in case of perfect symmetry in *Setup III*, *IV* or *V*, another symmetry plane in the yz-plane is present and the *right* and *left* setups would also deliver identical results. *AVG* is the value obtained by taking the average of all other setups: $(top + right + bottom + left)/4$. In *Setup IV* and *V*, depending on the voltage loop the sheath is located at $d_{\mathrm{VL}} \approx 2.1\,\mathrm{cm}$ to 2.3 cm.

Figures 4.17 to 4.21 also present values for the reactance to resistance ratio in different setups, as it can influence the phase angle measurement. The accuracy of phase angle determination is limited and depends on the used equipment. The *measured* phase angle can be calculated by: $\arctan(X/R)$ and with an increasing *measured* reactance asymptotically approaches 90°. One should bear this influence in mind and compensate the inductive part of the *measured* voltage signal, if necessary.

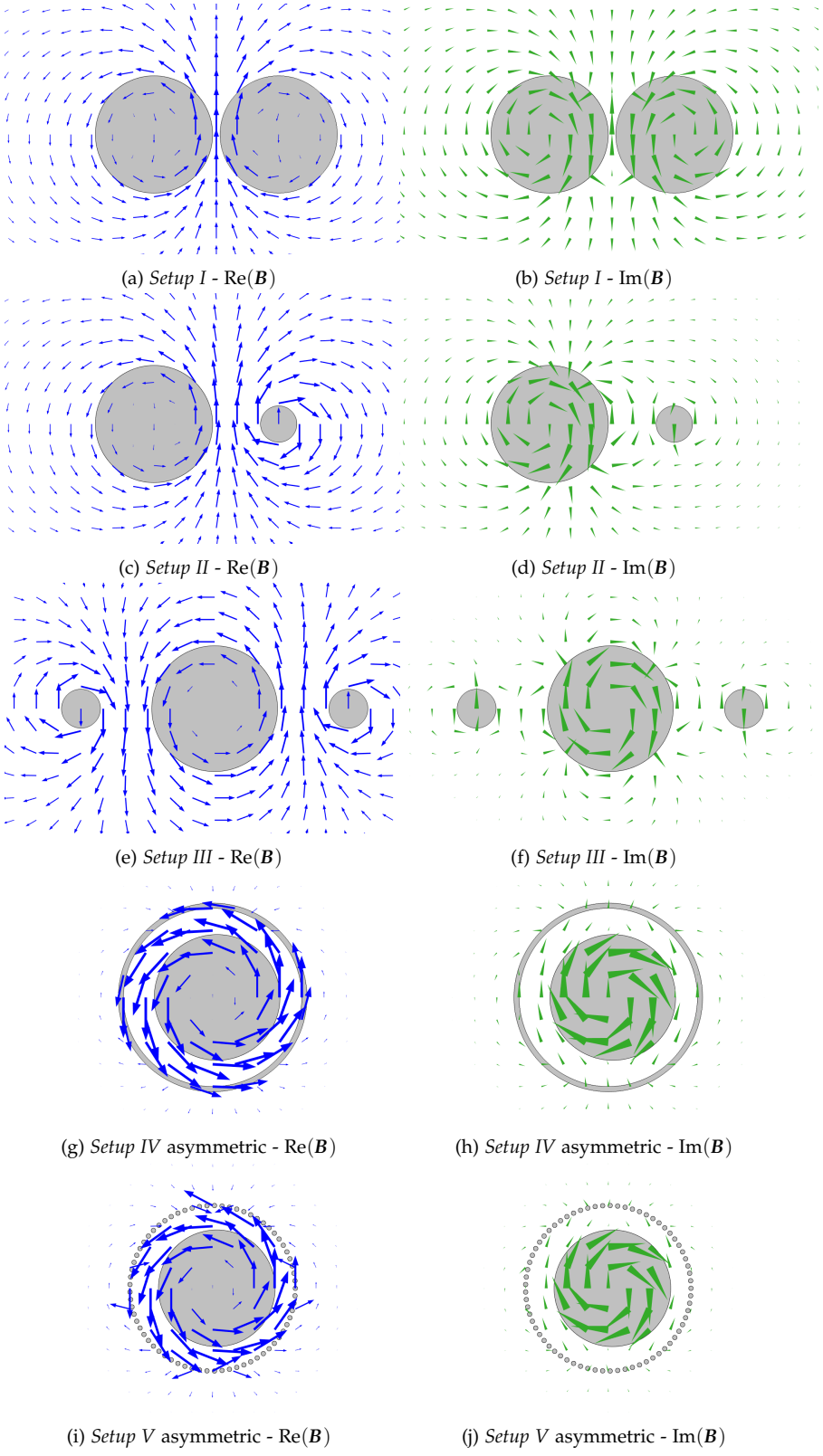

(a) *Setup I* - Re($\boldsymbol{B}$)

(b) *Setup I* - Im($\boldsymbol{B}$)

(c) *Setup II* - Re($\boldsymbol{B}$)

(d) *Setup II* - Im($\boldsymbol{B}$)

(e) *Setup III* - Re($\boldsymbol{B}$)

(f) *Setup III* - Im($\boldsymbol{B}$)

(g) *Setup IV* asymmetric - Re($\boldsymbol{B}$)

(h) *Setup IV* asymmetric - Im($\boldsymbol{B}$)

(i) *Setup V* asymmetric - Re($\boldsymbol{B}$)

(j) *Setup V* asymmetric - Im($\boldsymbol{B}$)

Figure 4.16: Direction of in-phase (blue arrows, left) and out-of-phase (green cones, right) components of the magnetic field for different closely spaced return conductor configurations; for better visibility the plot is scaled logarithmically; the fields in each plot are scaled differently and hence do not provide information about the absolute magnitude of the magnetic fields; in the CUT the current flows out of the paper plane, in the return conductors the current flows into the paper plane

SETUP I

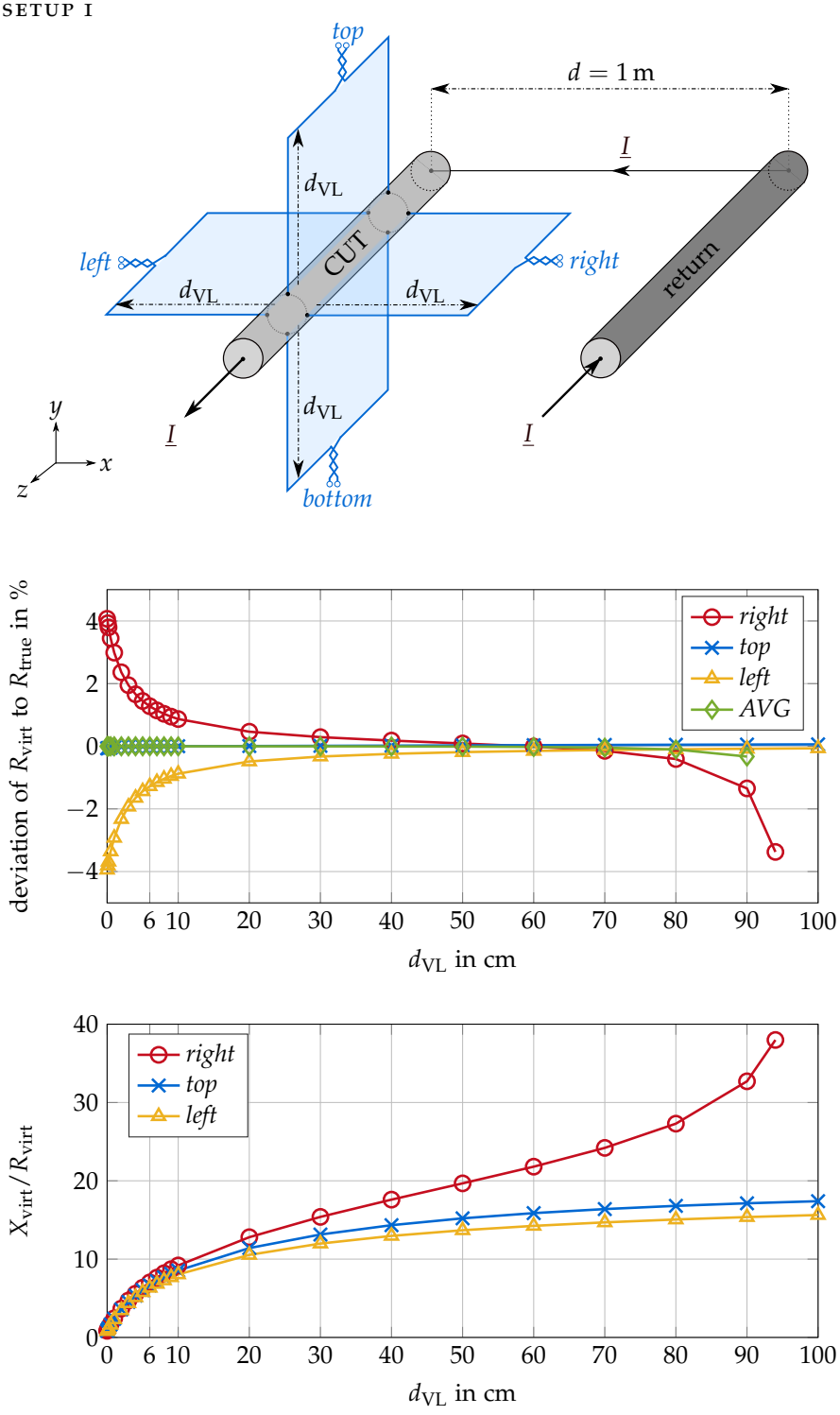

Figure 4.17: FEM simulation of *Setup I* at 50 Hz: *top*: deviation of R_{virt} to R_{true} (isolated *skin effect*) in % over d_{VL}; *bottom*: ratio of reactance to resistance over d_{VL}

RECOMMENDATION When using *Setup I*, it is recommended to exploit the symmetry of the setup and position the voltage loop on the *top* or *bottom* side of the CUT at $d_{\text{VL,min}}$.

SETUP II

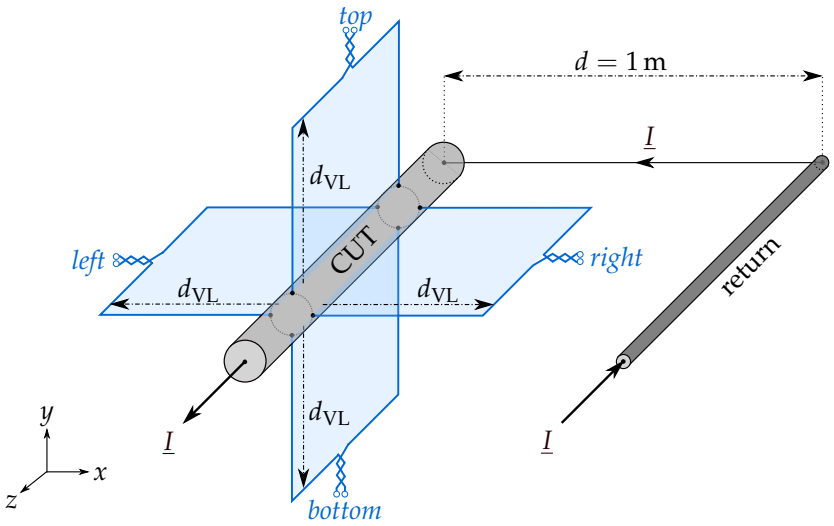

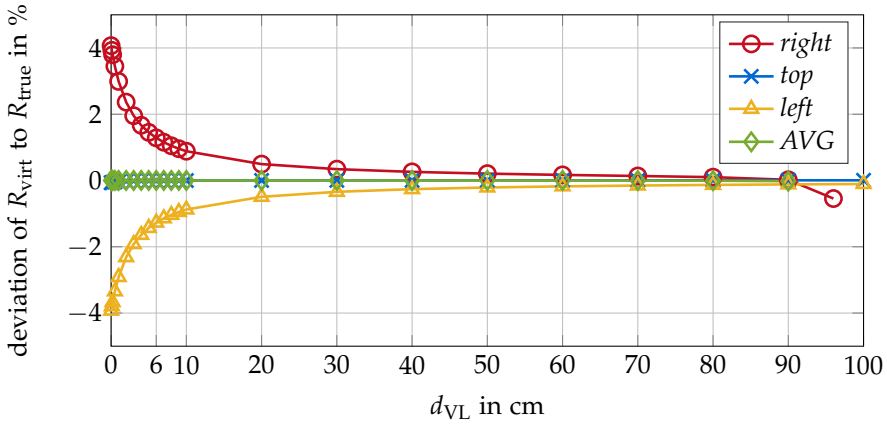

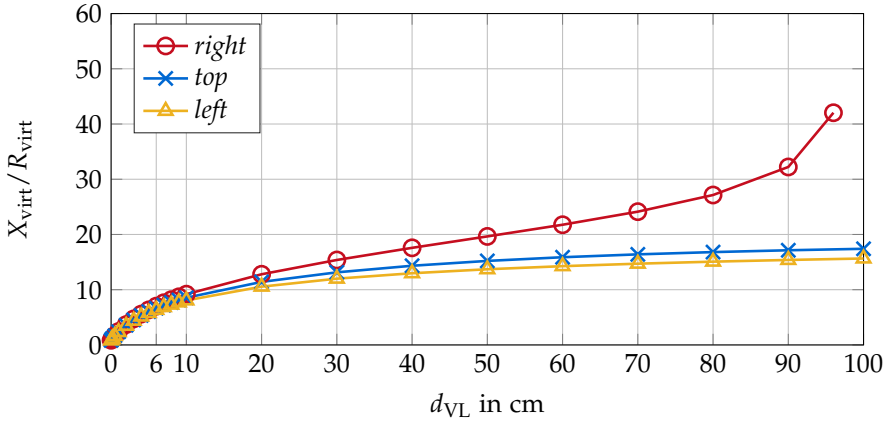

Figure 4.18: FEM simulation of *Setup II* at 50 Hz: *top*: deviation of R_{virt} to R_{true} (isolated *skin effect*) in % over d_{VL}; *bottom*: ratio of reactance to resistance over d_{VL}

RECOMMENDATION When using *Setup II*, it is recommended to exploit the symmetry of the setup and position the voltage loop on the *top* or *bottom* side of the CUT at $d_{\text{VL,min}}$.

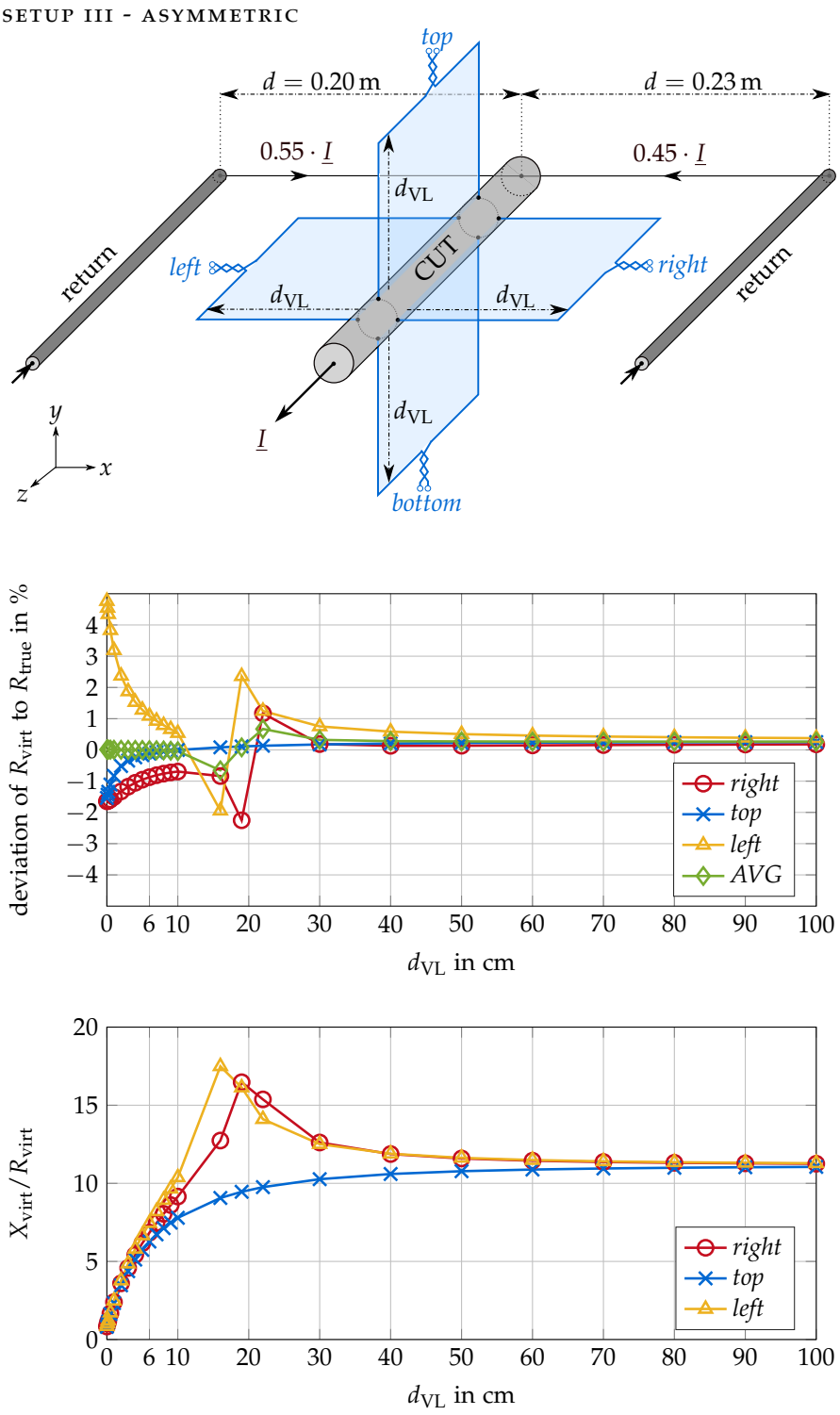

Figure 4.19: FEM simulation of *Setup III asymmetric* at 50 Hz: *top*: deviation of R_{virt} to R_{true} (isolated *skin effect*) in % over d_{VL}; *bottom*: ratio of reactance to resistance over d_{VL}

RECOMMENDATION When using *Setup III*, it is recommended to exploit the symmetry of the setup and position the voltage loop on the *top* or *bottom* side of the CUT at $d_{\text{VL,min}}$.

SETUP IV - ASYMMETRIC

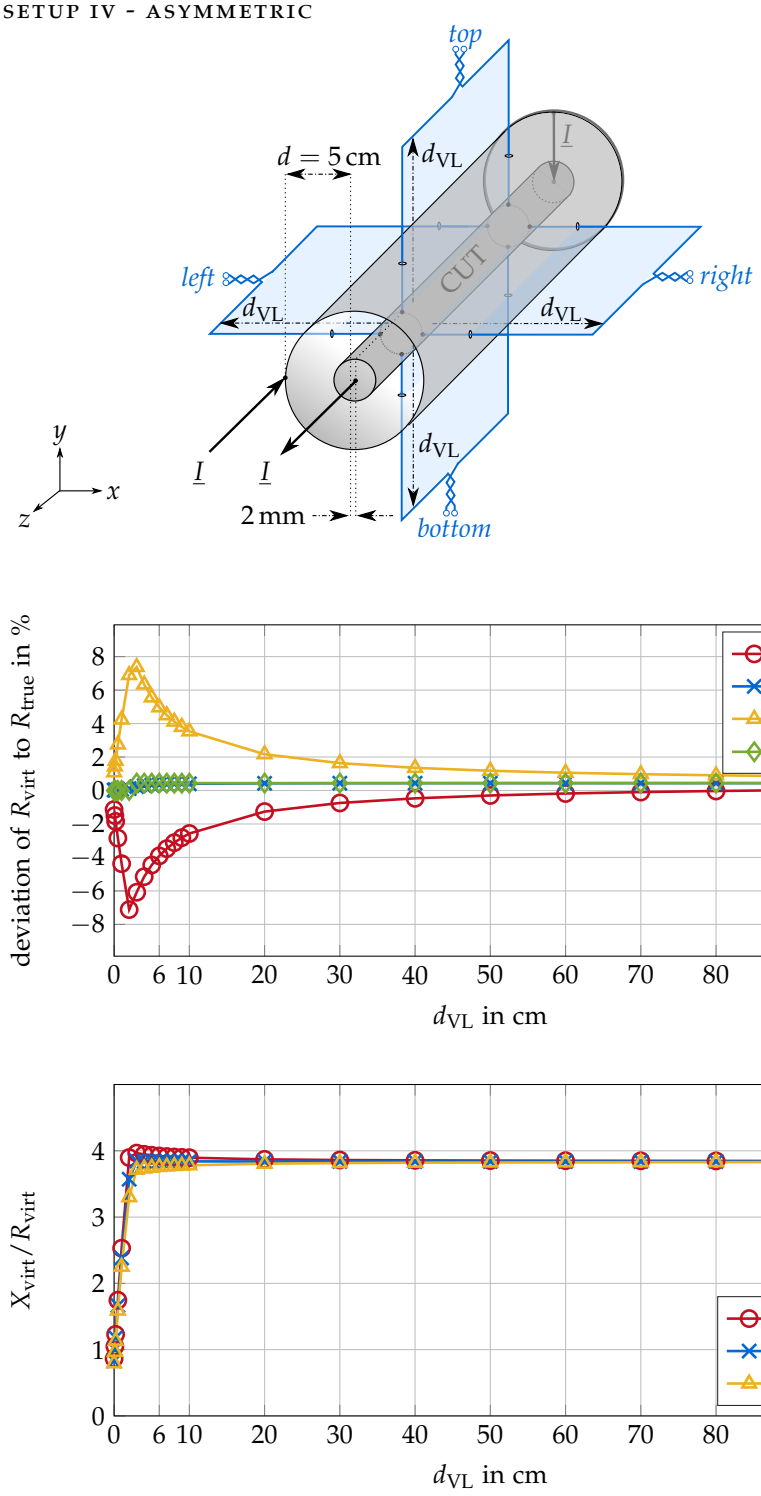

Figure 4.20: FEM simulation of *Setup IV asymmetric* at 50 Hz: *top*: deviation of R_{virt} to R_{true} (isolated *skin effect*) in % over d_{VL}; *bottom*: ratio of reactance to resistance over d_{VL}

RECOMMENDATION When using *Setup IV*, it is recommended to take the average of at least 4 evenly distributed voltage loop configurations all located at the sheath's or cable's surface.

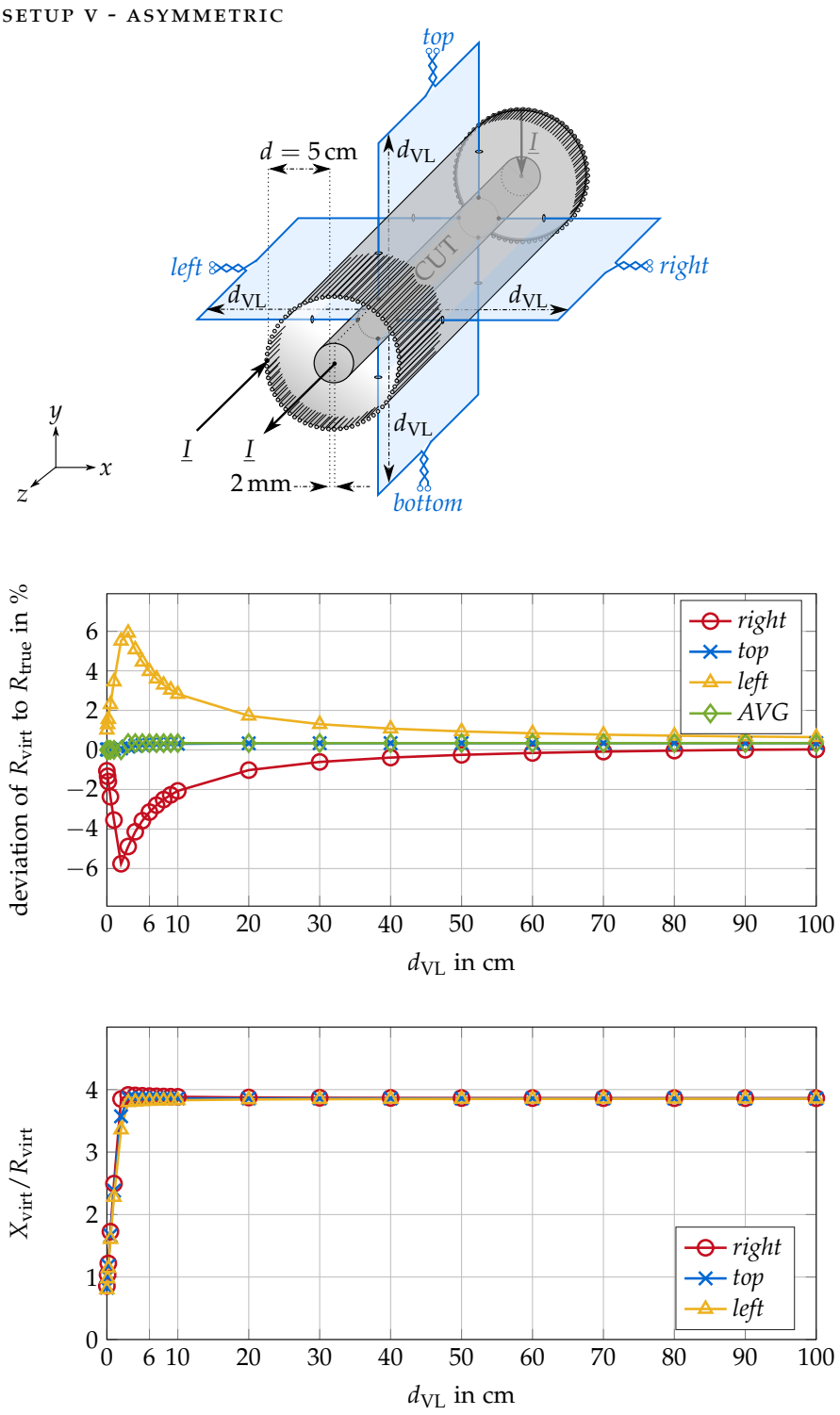

Figure 4.21: FEM simulation of *Setup V asymmetric* at 50 Hz: *top*: deviation of R_{virt} to R_{true} (isolated *skin effect*) in % over d_{VL}; *bottom*: ratio of reactance to resistance over d_{VL}

RECOMMENDATION When using *Setup V*, it is recommended to take the average of at least 4 evenly distributed voltage loop configurations all located at the sheath's or cable's surface.

CONCLUSION The results obtained by FEM simulations clearly indicate a position-dependency of the *measured* resistance and reactance. Even though the influence on *true* losses was set below 0.1 % in the setups, the influence on *measured* losses reached values up to 7 %. For every loop, the *measured* resistance—obtained by *virtual* measurement—converges against the *true* resistance within 1 % accuracy for increasing loop size.

As discussed earlier, in case of a 2500 mm^2 *Milliken* conductor the minimum radial voltage loop extension should be equal to the conductor diameter, which is in the range of 50 mm to 70 mm. The average of $d_{\mathrm{VL,min}} = 6\,\mathrm{cm}$ is taken for the following evaluations.

Choosing the *top* or *bottom* pick-up loop in *Setup I* or *Setup II* results in a deviation of *measured* to *true* resistance close to zero. The reactance to resistance ratio is 6.65 at 6 cm.

Choosing the *top* or *bottom* pick-up loop in *Setup III* results in a deviation of *measured* to *true* resistance of approximately -0.12 %. The reactance to resistance ratio is 6.27. Even at $d_{\mathrm{VL}} = 1\,\mathrm{m}$ the error amounts to only 0.25 %.

Averaging the results obtained by 4 pick-up loops evenly distributed around the sheath's surface in *Setup IV* results in a deviation of *measured* to *true* resistance of approximately 0.44 % directly above the sheath. When extending the voltage leads over the sheath, they capture a negligible amount of sheath losses as discussed later. The *top* and *bottom* lead wire configurations converge more rapidly against the deviation of 0.44 % than the pick-up loops located *right* and *left* of the CUT. The reactance to resistance ratio lies between 3.76 and 3.92 for the different loops.

Averaging the results obtained by 4 pick-up loops evenly distributed around the sheath's surface in *Setup V* results in a deviation of *measured* to *true* resistance of approximately 0.34 % directly above the sheath. This also includes sheath losses. The reactance to resistance ratio lies between 3.82 and 3.90 for the different loops. If possible and $d_{\mathrm{VL}} \geqq d_{\mathrm{VL,min}}$ still holds, one can avoid capturing sheath losses by locating the voltage lead wires beneath the sheath's surface—on its inner side.

The influence observable at smaller loop sizes can be reduced, when increasing the return conductor spacing or decreasing asymmetry, even though this is sometimes not feasible in practice. Nevertheless, these idealized simulations neglect the influence of the current feed line and additional metal in proximity to the setup. Moreover, perfectly placing the voltage leads in the symmetry planes or on *top*, *bottom*, *right* or *left* side of the CUT is hard in reality. Deviations from symmetry will introduce additional errors in real setups.

From this investigation alone it seems that *Setup I*, *II* and *III* are the most convenient and easiest to build. Nevertheless, all setups have to be checked for their susceptibility to deviations from symmetry and also on the influence of nearby conductive parts. This is done exemplarily in the next section.

At this stage it can already be concluded that it is advantageous to know and use the symmetry of each setup. For the *sheath return method* multiple

voltage lead loops should be used, as the asymmetry is not known in most cases[17]. Averaging the results obtained by 4 or more evenly distributed pick-up loops around the conductor's circumference gives very good results in all setups. Surprisingly—in the *sheath return methods*—only the out-of-phase magnetic field components seem to leak out to a significant amount still influencing the *measured* resistance at larger d_{VL}. The reactance is nearly unaffected by larger loop sizes. This would make these methods less prone to external asymmetries caused by conductive components.

4.2.2.2 *Influence of Nearby Metal Framework on Apparent Losses*

For *Setup I*, *II* and *III* the *top* pick-up loop seemed to present a reasonable choice. For the *sheath return method* the average has to be taken. In Figure 4.22 the influence of a metallic floor is demonstrated for these voltage loop arrangements. From Figure 4.15 it was concluded that a grounded copper plate represents the worst case. Nevertheless, the more realistic case of a thickness of $t = 1\,\mathrm{mm}$ is chosen here. The width of that plate is again 4 m and it is located at $d = 1\,\mathrm{m}$ beneath the conductor.

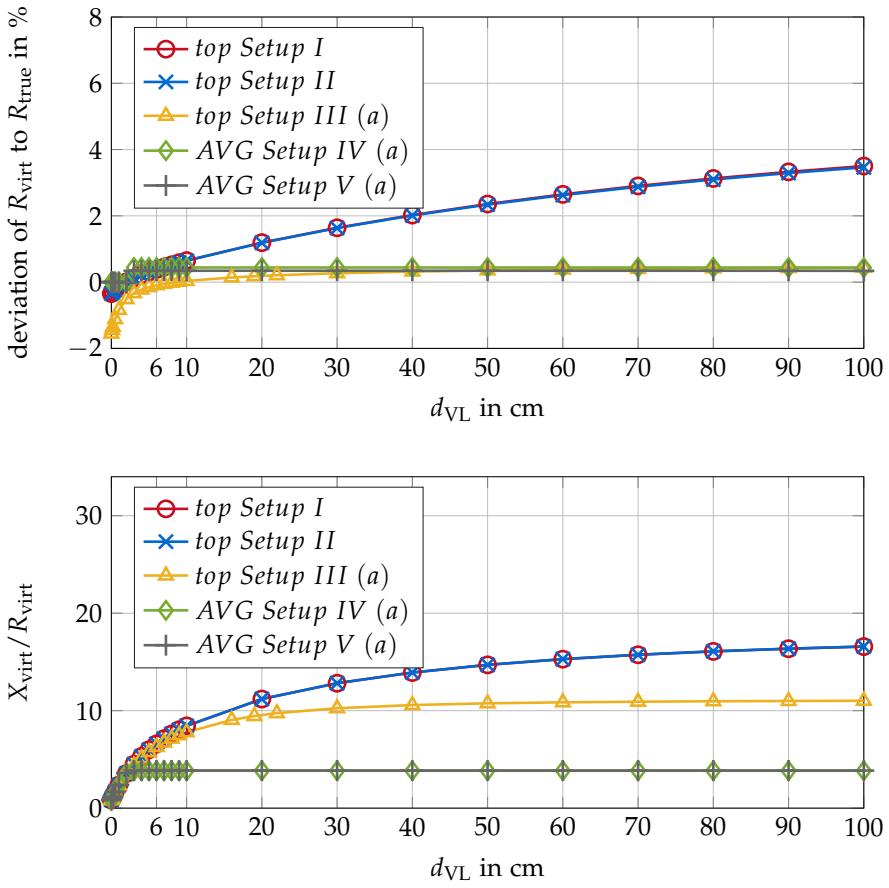

Figure 4.22: FEM simulation of all setups at 50 Hz with a thin copper plate 1 m beneath the CUT; *top*: deviation of R_{virt} to R_{true} (isolated *skin effect*) in % over d_{VL}; *bottom*: ratio of reactance to resistance from simulation over d_{VL}

17 Helically winding the voltage lead wires around the circumference at distance $d_{\mathrm{VL,min}}$ is likely another alternative to easily perform a measurement with the *sheath return method* and only one pick-up loop. This however was not investigated in theory but included in the measurements in Chapter 5.

CONCLUSION Setup *I* and *II* show the biggest influence of the copper plate upon the *measured* resistance for larger d_{VL}. The reason is that such large return conductor spacings cause a much wider magnetic field distribution in the surrounding, which in turn then interferes stronger with the conductive ground plate. This can also be seen in the reactance to resistance ratio plots. It is important to point out that the influence on other pick-up loops in these setups (*right* and *left*) is even larger. An asymmetric conductive ground relative to the pick-up loop will therefore have a more significant impact on the *measured* values.

Setup III, *IV* and *V* are nearly not affected by the metallic ground plate and show errors below 0.5 % even for larger spacings. Nevertheless, other asymmetries (metallic shelfs,...) could affect *Setup III* more than the *sheath return methods*, as they produce nearly no in-phase magnetic field components outside of the return conductor. As there are too many geometrical and electrical parameters involved, this example's only purpose is to raise awareness for the influence caused by other metallic parts, instead of directly assessing and comparing different setups.

4.2.2.3 *Influence of Variable Sheath Construction Parameters on Apparent Losses*

When extending the pick-up loop over the cable sheath, the magnetic field inside the sheath will be included in the pick-up loop. At AC it is complex (see Figure 4.16h and Figure 4.16j) and induces a voltage in the pick-up loop, which causes the measurement of additional losses. Figure 4.23 shows the additionally *measured* resistance in asymmetric *Setup IV*. The red, blue and yellow curves show that exact increase in *measured* resistance, which appears when extending the pick-up loop from beneath to above the sheath's surface. The results are nearly identical for asymmetric *Setup V*. In the following investigations, the pick-up loops are located at the same places as in the previous sections.

It can be seen from Figure 4.23 that the *true* losses of CUT and sheath are much larger than the additionally *measured* losses. In the worst case—*left* pick up loop—at 50 Hz the additionally *measured* losses due to the sheath only amount to 0.13 %. The influence on the *measured* resistance directly arises from the out-of-phase magnetic fields in the sheath, which in turn are directly linked to its AC losses. As AC losses are small for typical sheath geometries—because of their tubular geometry and usually small thickness—the influence on the *measured* resistance is negligible in most cases at 50 Hz.

Symmetric *Setup IV* delivers results in the same magnitude but without a position-dependency. In the symmetric case the out-of-phase magnetic field components are only present in the sheath (similar to Figure 4.3b). Regarding the sheath, subtracting the DC resistance from the *true* AC resistance would directly deliver the curve for the additionally *measured* resistance. One can therefore conclude that in the symmetric case: the total out-of-phase magnetic field solely includes the information about total additional AC losses. Interestingly there are slumps at specific frequencies in the *right* pick-up loop. They arise from specific parameter combinations and are not further investigated here.

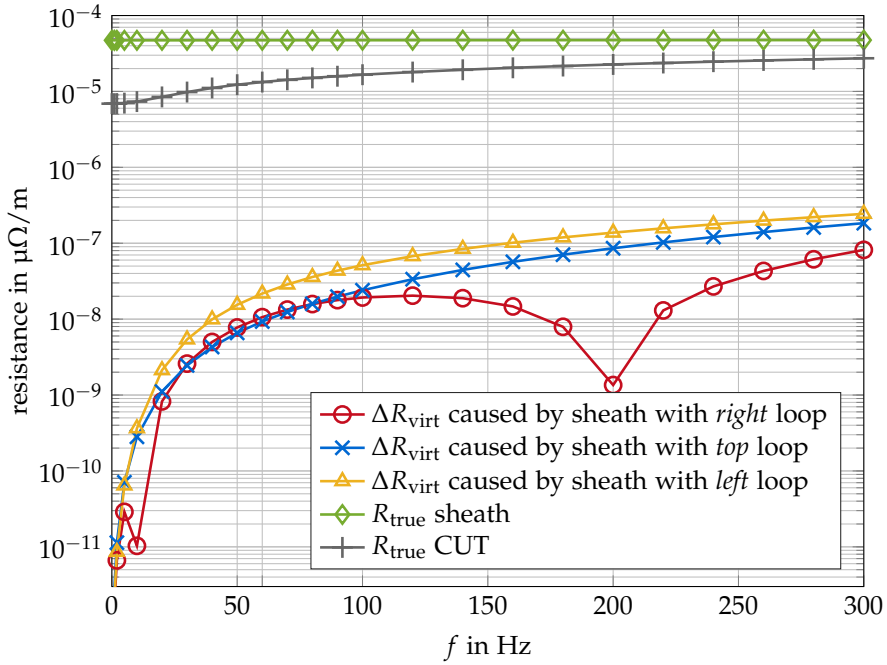

Figure 4.23: FEM simulation of asymmetric *Setup IV*: absolute influence—of the sheath only—on the *measured* resistance plotted up to 300 Hz; also the *true* resistance of CUT and sheath is shown; the *bottom* configuration is again identical to the *top* configuration

Even though the additional losses captured at that point when extending the pick-up loop over the sheath are typically negligible[18], variable sheath construction parameters can still heavily influence a measurement. Their influence on out-of-phase magnetic field distribution in the setup is shown in the following.

As there are too many variable parameters to be investigated in this work alone, a combination of worst cases is analyzed. For the thin solid aluminum sheath in *Setup IV*, in addition to the asymmetry caused by the CUT and the sheath not being perfectly concentric, the sheath can also have a varying thickness. The thickness of the sheath at $d_{\text{min}} = 5\,\text{cm}$ with the sheath cross section of $600\,\text{mm}^2$ is 1.87 mm. This thickness will be varied by 50 %, resulting in a thickness of $1.5 \cdot 1.87\,\text{mm}$ on the right side and $0.5 \cdot 1.87\,\text{mm}$ on the left side of the CUT. The geometry, resulting fields and results of the simulations are shown in Figure 4.24 and Figure 4.25.

A varying thickness of the sheath geometry results in 2 % more *true* losses in the inner CUT, compared to the isolated *skin effect* losses of $12.260\,\mu\Omega/\text{m}$. From Figure 4.25 it can also be seen that there is a tremendous increase in position-dependency in the measurement setup. This is due to the increased amount of AC losses in the sheath and therefore stronger out-of-phase magnetic field components in its vicinity. The stationary value of the average of all pick-up loops is −1 % percent. Another calculation with 20 % instead of 50 % varying thickness, showed the same qualitative behavior, but with maximum deviations in the range of −10.8 to 10.9 %.

18 This statement does not necessarily relate to steel wire armored cables.

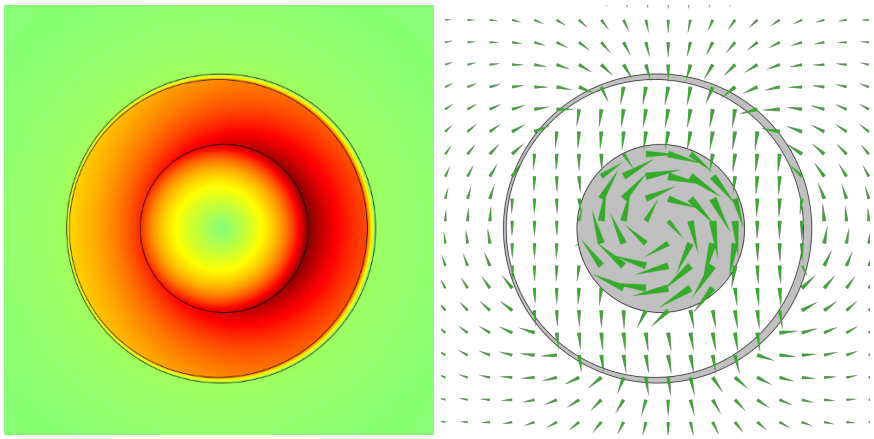

(a) *Setup IV* - $||\boldsymbol{B}||$ (b) *Setup IV* - $\mathrm{Im}(\boldsymbol{B})$

Figure 4.24: Magnitude and out-of-phase magnetic field of asymmetric *Setup IV* with varying sheath thickness of 50 %

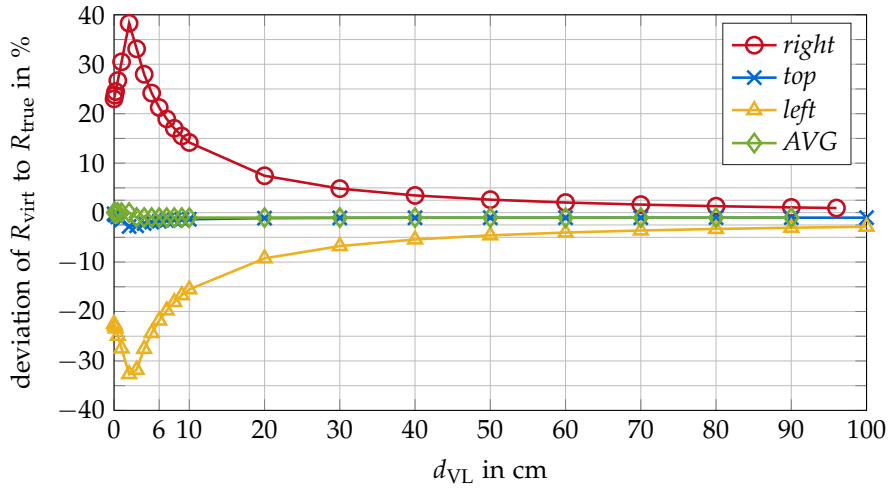

Figure 4.25: FEM simulation of *Setup IV*: influence of varying sheath thickness of 50 % on the *measured* resistance at 50 Hz; the deviation to the isolated *skin effect* resistance of the inner CUT is given for different pick-up loop sizes and locations; *bottom* is identical to *top*

For the copper wire screen the circumferential distribution of the single wires can be inhomogeneous. This is achieved by shifting every second wire by 4°, rotating one wire to the center right side and rotating one wire further away from the center left side. Note that the symmetry is broken and the *bottom* pick-up loop will no longer deliver identical results compared to the *top* pick-up loop. When considering short measurement length with the *sheath return method*, one could also assume an asymmetric current distribution in the sheath wires due to a non-ideal short-circuit at the end of the cable. The geometry, resulting fields and results of the simulations are shown in Figure 4.26 and Figure 4.27.

The inhomogeneous circumferential distribution of the copper sheath wires increases the *true* AC losses of the inner CUT by only 0.02 % compared to the isolated *skin effect* losses of 12.260 µΩ/m. In other words, the inhomogeneous distribution of sheath wires does not alter the AC losses significantly compared to the case of homogeneous distribution. In line with this obser-

vation, it can be seen from Figure 4.27 that the maximum deviation is in the lower percent range and even lower compared to the homogeneous distribution of sheath wires. The stationary value for the average of all pick-up loops is 0.26 %. Again, in this case—if the measuring length is much larger or an integer of the lay length of the wire screen—the position-dependency of the measurement will likely be reduced, as this equals an averaging.

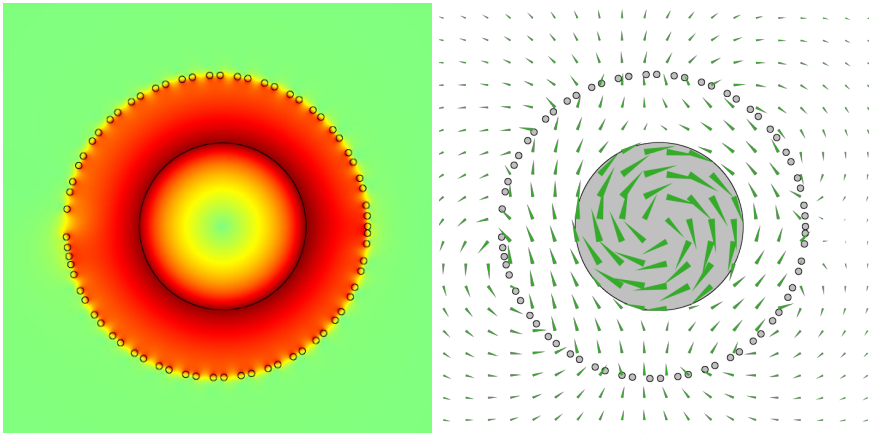

(a) *Setup V* - $||\boldsymbol{B}||$ (b) *Setup V* - $\mathrm{Im}(\boldsymbol{B})$

Figure 4.26: Magnitude and out-of-phase magnetic field of asymmetric *Setup V* with inhomogeneously distributed sheath wires

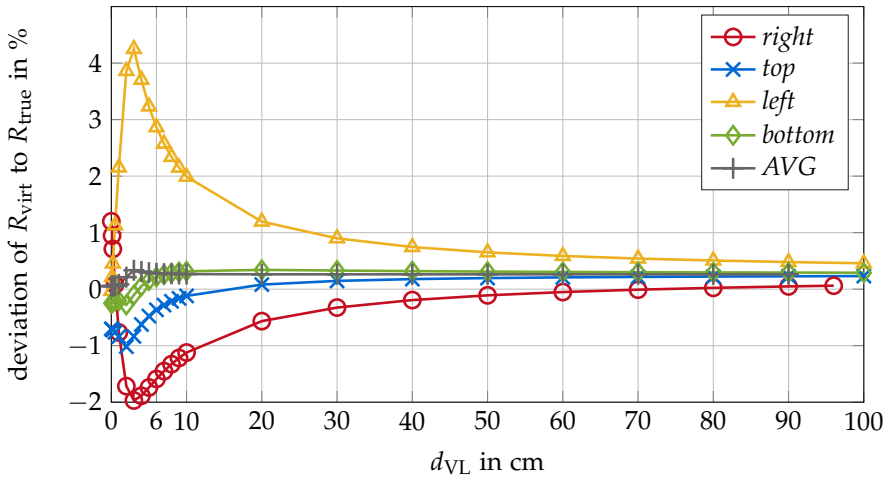

Figure 4.27: FEM simulation of *Setup V*: influence of inhomogeneous distribution of sheath copper wires on the *measured* resistance at 50 Hz; the deviation to the isolated *skin effect* resistance of the inner CUT is given for different pick-up loop sizes and locations

Even though, the examples above present rather extreme cases—at least for the solid aluminum sheath—one can derive the following conclusions from these investigations:

- Variations in the sheath geometries, whether inevitably caused by construction or by drumming or further handling the cable, can result in additional asymmetries in the setup. In turn they can influence the measurement to a certain degree, which depends on the AC losses in the sheath and the asymmetry.

- Inhomogeneities in the sheath wire distribution seem to have less impact on the measurement, than variations in thickness for solid sheaths.

The results of this chapter also coincide with observations made previously in [Suc14]. These stated that additional losses—only measured, when cables with solid sheaths are drummed—can possibly be attributed to the fact that asymmetries in the sheath current distribution are much more significant in solid sheaths than in cables with sheath wires. Drumming a cable with a solid sheath does not only give a preferred path for the current to flow, which is at the inner side of the cable drum[19], but can also give rise to mechanical induced variations in the solid sheath geometry. These asymmetries produce much more out-of-phase magnetic fields in the cables vicinity and can cause more *proximity effect* losses on a drum.

4.2.2.4 *Influence of Additional Measurement Setup Factors on Apparent Losses*

When setting up a measurement, additional possible influences on the *measured* resistance can arise from the setup due to practical restrictions. Some of them are discussed in the following. The purpose of these investigations is to give further insights into possible error sources by presenting some basic examples.

CURRENT TRANSITION AT VOLTAGE TAP-OFF POSITION In *Setup IV* the CUT uses a tubular aluminum conductor as the current return. If the CUT is part of a cable and the tubular return is the cable sheath, one has to cut open a window in the sheath and insulation to reach the surface of the CUT with the voltage tap-offs. This gap or window has to be bridged by the current return path to keep the circuit closed. This bridging is referred to as *current transition* and displayed in Figure 4.28. Depending on how the *current transition* is realized, it can affect the measurement. Of course this effect depends on the overall measurement length and becomes more critical as the measurement length decreases.

The following simulation results account for a total measuring length l_{meas} of 1 m at 50 Hz. Moreover, d is chosen as 5 cm as previously, d_{VL} as 6 cm and attached in the center of the window. The aluminum sheath cross section is again 600 mm^2 and the setup is symmetric to focus on the effect of *current transition* alone. The *current transition* is realized by a copper wire with a cross section of approximately 19.6 mm^2 in a transition window of 10 cm length.

The simulated deviation to the isolated *skin effect* resistance, which would be measured in case of a perfectly concentric *current transition*—neglecting the small additional losses caused by the sheath—amount to:

- 13.2 % for *top*,
- −5.7 % for *right* (which is identical to *left* due to symmetry),
- 4.6 % for *bottom*,
- 1.6 % for the *AVG* of all pick-up loops.

19 This is due to the fact that the side of the sheath facing the drum center presents a shorter and hence less resistive path for the current.

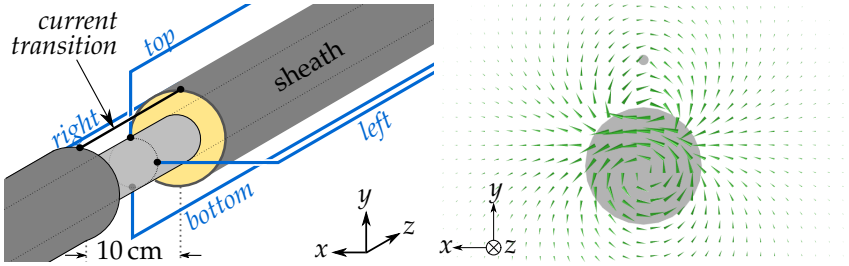

(a) Simulation setup; note that the pick-up loops location (in the coordinate system) is consistent to the setups analyzed previously

(b) Out-of-phase magnetic fields at voltage tap-off position; the viewer looks in direction of the z-axis, which is also the direction of the current in the CUT

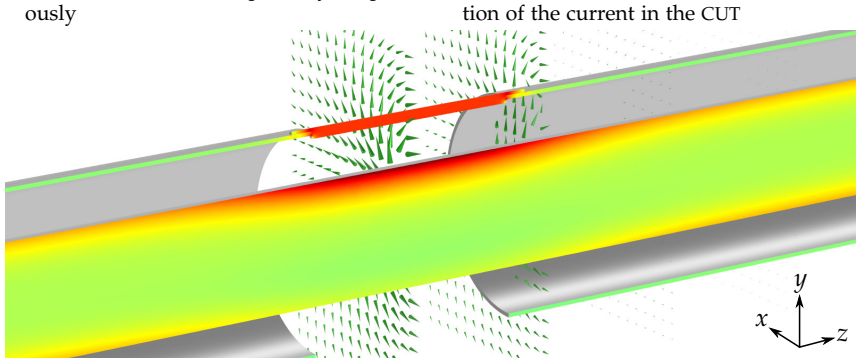

(c) Cut view of resulting outer out-of-phase magnetic fields at different positions along the conductor axis and $||\boldsymbol{J}||$ in CUT and sheath (scaled differently); this picture shows both: *skin effect* only (at the left and right end of the CUT) and *proximity effect* at the position of *current transition*

Figure 4.28: The *current transition* remains in the same *top* position; again the 4 pick-up loops (*right*, *top*, *left*, *bottom*) around the circumference are deployed and attached to the CUT's surface

Figure 4.28c and additional evaluations also show that the influence of the out-of-phase magnetic fields upon the loops rapidly decreases behind the *current transition*. Also, it is interesting to note that its influence after the *current transition* acts in a way that decreases the effect of the *current transition*. In other words, the outer out-of-phase magnetic fields have an opposite direction after the *current transition* than at the place of the *current transition*.

Recollect that a perfectly concentric *current transition* would have no influence. In that case only the out-of-phase magnetic fields in the sheath would affect the *measured* resistance as discussed in the previous section. In the investigated setup the outer out-of-phase magnetic fields affecting the *measured* resistance, again arise from the rotational asymmetry in the current distribution—due to the *current transition*—in and close to the window. To avoid these effects one should try to achieve a *current transition* as concentric as possible. This can—for example—be achieved by using two half shells to form another tubular conductor enclosing the gap (see Figure D.3b). Nevertheless, even then one would need to drill holes in the sheath to reach the CUT with the voltage lead wires, which affect the current distribution in it and may influence the measurement. This is shown in the next paragraph.

It has been found that the *current transition* can heavily influence the results and should be considered or avoided in a measurement setup. The influence on *measured* resistance will decrease with increasing measuring length l_{meas}.

DRILL HOLES IN A TUBULAR RETURN CONDUCTOR Again symmetric *Setup IV* is considered as guiding the voltage leads through a wire screen or any other non-solid sheath does not present a challenge. Drilling holes is only practical, if the there is no insulation between CUT and tubular return conductor. Figure 4.29 shows the influence of a small drill hole with a diameter of 5 mm on the current density in the sheath.

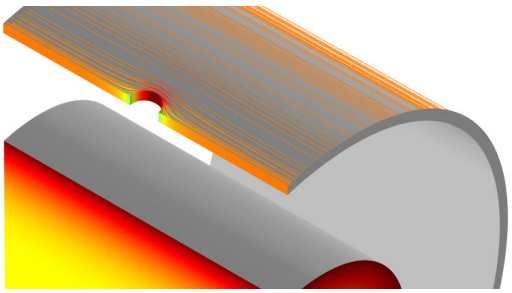

Figure 4.29: Cut view of *Setup IV* with a drilled hole in the sheath; $||\boldsymbol{J}||$ in CUT and sheath (scaled differently) and current streamlines in the sheath are shown

As concluded by the previous section, the influence depends on the ratio of asymmetry (drill hole dimension) to measurement length l_{meas}. As this ratio is typically very small, no significant influence is expected upon the results by drilling small holes in the sheath. Moreover, the investigation of asymmetric sheath wire distribution indicated only negligible influences of small irregularities in the sheath geometry.

SHORT-CIRCUIT AT THE END OF SAMPLE When making a connection from CUT to return conductor, one introduces additional magnetic field components. These are in-phase and eventually out-of-phase components. Taking *Setup I* as an example, in 2D one would not have magnetic field components in direction of the axis of CUT or return conductor. A short-circuit at the end connecting both would introduce these components. Depending on distance and position of the pick-up loop it can affect the measurement. This is no problem for the previously favored *top* or *bottom* pick-up loops in *Setup I*, *II* and *III* as their surface normal is perpendicular to all magnetic field components introduced by the short-circuit. Even though one should keep this effect in mind when analyzing a setup, the influence of the short-circuit can easily be diminished. As the magnitude of the magnetic fields is proportional to the reciprocal of the distance from the short-circuits surface, setting the distance from the pick-up loop to the short-circuit much larger than d_{VL} will rapidly decrease the influence. This condition is easy to achieve in every setup and laboratory and is therefore not further investigated here.

A similar, much more relevant question on how far the current injection has to be placed apart from the voltage tap-offs is addressed in Section 4.2.3.

4.2.2.5 *Further Notes on Influences on Apparent Losses Due to the Pick-Up Loop Location*

Another important fact open for investigation is the influence of deviations from symmetry, which could have a large impact on the *measured* value. Moreover, as pointed out previously, when benchmarking a measurement setup with a known reference conductor, one should consider influences

by the subsequently measured CUT. What needs to be avoided is directly applying the setup used for the reference conductor to the CUT without further considerations (e.g.: how does $d_{\mathrm{VL,min}}$ change, how does the magnetic field of the CUT influence the surrounding compared to the fields of the reference conductor,...).

Moreover, some other variational geometric parameters of the cable or the CUT could be checked for their influence, more specifically the ovality of the CUT or complete cable. Some exaggerated impressions of manufacturing-depend fluctuations in cable geometry are shown in Figure 4.30.

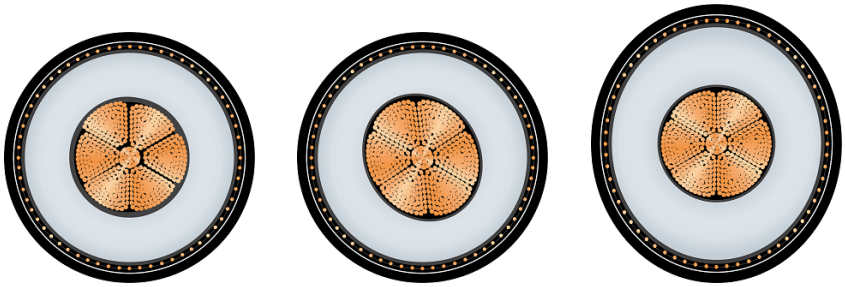

(a) Displaced segments (b) Oval inner conductor (c) Oval cross section

Figure 4.30: Exaggerated illustration of possible cable geometry fluctuations due to the manufacturing process of the cable; courtesy of *Südkabel GmbH*

4.2.3 *Influence of Current Contact System and Resulting Current Homogenization*

The current distribution in combination with its resistivity determines the *true* losses of a conductor. They are lowest when the current density in a cross section is completely homogeneous [Gra79, p. 32]. The current injection into a conductor can enforce current distributions and therefore influence its *true* losses. This is called *end effect* or *terminal effect*. In an electrical measurement its influence on the *measured* resistance depends on:

- the type of contact/contact system (e.g.: how much of the cross section is connected to the current injection, how good is the connection,...),
- geometrical and electrical parameters of the CUT and measurement setup (e.g.: conductivity, applied frequency, strand insulation,...)
- distance from current injection to the voltage tap-offs of the pick-up loop.

In the measurement it is desired that the current density in the measured section is identical—representatively—to the current density in most parts of the conductor under operation[20]. In a long cable a steady current distribution in the cross section is expected along the majority of the overall length. Thus, the current density in the measured section should not be influenced by any *end effects* either, to give results of practical relevance. Moreover, it is desired that the practical expense to set up the connections at both ends of the cable is as low as possible. This expenditure also

20 Note that this only refers to the distribution and not the magnitude of the current density as only linear conductors are considered, where the AC resistance does not depend on the magnitude of the current.

depends on the magnitude of the test current—which is small with the measurement system used in this work—but can be much larger using other equipment and hence result in specially designed connectors as in [MBD15].

In the following, some references including theoretical considerations and measurements regarding stranded conductors are given. It is followed by a short FEM investigation of a small stranded conductor including different types of current injections. At the end, based on these preceding investigations, practical measures are discussed.

4.2.3.1 *Past Work and Theoretical Considerations*

A very early remark on the current homogenization in conductors is made by J. C. Maxwell, when considering the measurement of small resistances:

> "At a short distance from the extremities the current becomes sensibly uniform." [Max73a, p. 405].

It is clear that this general statement depends on multiple factors as noted above, especially on the quality of the electrical contact connecting the current path (also called current leads) to the CUT. Extensive studies on electrical contacts in general can—for example—be found in the "Electric Contacts Handbook" [Hol58] and in [Vin16]. These analyze the influence of temperature, mechanical stress and different contact types such as sliding, switching and stationary contacts, whereas only the latter is of relevance in this work. Analytical solutions for the current homogenization in conductors can be found in [HM76; BM86; MS13, p. 112; ZL13]. More recent and advanced works on long-term behavior of different contact systems are found in [Gat+14b; Gat+16] for example.

One study, which focused on the current homogenization in stranded conductors at DC is [Bür95] by Jens Bürkner. The goal here was to accurately measure the contact resistance between a connector and a stranded conductor. In this case it is also necessary that the measurement is not influenced by inhomogeneous current distributions caused by the electrical contact between the connector and the following stranded conductor. This problem is schematically displayed in Figure 4.31.

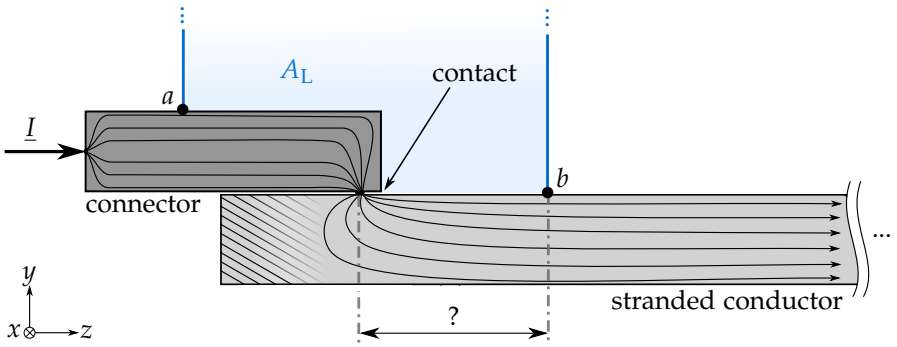

Figure 4.31: Current homogenization at DC after a punctiform contact based on [Bür95, Bild 2.1]; *a* marks the first voltage tap-off; the necessary distance to second voltage tap-off *b* on the stranded conductor was investigated in [Bür95]

For the DC measurement the author concluded that there are 3 possible countermeasures against inhomogeneous current distributions, caused by this contact:

1. One can take the measurement at a position, far enough apart from the contact, where the current density is homogeneous in the cross section. In stranded conductors, this distance depends on the contact resistance between the single strands in the bundle. This distance approaches zero if the strands have a contact resistance, which is much lower than the resistance along the strand (extreme case is a solid conductor) and approaches infinity, if the contact resistance is much larger than the resistance of the strand. For example: in case of an ACSR the minimum necessary distance ranged from 0.9 m to 9 m. For an aluminum single-core cable this distance was much lower with 0.9 m to 1.8 m, due to the mechanical forces by the insulation, which decreased the contact resistance between strands [Bür95, p. 13].

2. Another option is to equalize the current density in a cross section by short-circuiting all wires. Setting up a low resistance contact between all wires forces the current density to homogenize faster. For a small 7-strand cable this was achieved by connecting an additional low resistive wire ring around the periphery of the bundle [Bür95, p. 16].

3. The last option is to perform a measurement on every single strand in the cross section and then calculating the average value [Bür95, p. 20]. This is not feasible for *M-type* conductors, which can easily contain more than 500 strands.

From these results it follows that one needs to have a current injection as homogeneously as possible or may give the current a certain distance to homogenize in the cross section. Therefore, some FEM examples are displayed in the following to get an impression on how current homogenization can occur in stranded conductors with insulated strands. As argued previously, due to small test currents of only a few A, no rise in conductor temperature is expected, if the CUT is a power cable. Thus, the effect of temperature is neglected in the following simulations[21].

Concerning the voltage tap-offs, a deeper discussion on how to optimally connect them at AC and DC is given in Section 4.2.4.

4.2.3.2 *FEM Simulations*

Concerning solid and tubular conductors, previous FEM simulations in [SPS16] showed that current homogenization along the conductor axis appears rapidly. In a solid circular 2500 mm^2 copper CUT, independent of the position of punctiform current injection into the cross section, the current density around the conductor's circumference deviates no more than 0.4 % compared to that of a homogeneous injection after 15 cm, which is slightly below 3 times the conductor diameter. This recommendation of necessary length for current homogenization being at least $3 \cdot d_{CUT}$, is used again later in this work. Generally, the necessary length for current homogenization becomes shorter with increasing frequency and conductivity. Another more general statement for solid conductors at DC is given by [Bür95, p. 6] and states that at a distance of approximately 0.75 times the width of the conductor, the current density is nearly identical in the whole cross section.

21 Nevertheless, of course small temperature gradients could arise at constriction resistances at the contact points.

In the following investigation, these studies are extended to the case of a stranded copper CUT composed of 19 $(1 + 6 + 12)$ perfectly insulated strands, again with a total cross section of 2500 mm^2 and a rms test current of $\underline{I} = 1$ A. Every wire has a perfect insulation of 100 µm thickness. The first layer has a lay length of 25 cm and the second, outer layer has a lay length of 50 cm. Again, the excitation is realized by a current source at a frequency of 50 Hz. Generally, in addition to possible contact resistances between strands, at AC the current distribution is also affected by *proximity effect*. For DC, behind the current injection[22] the current density is only further affected by the contact resistances between strands.

Figure 4.32 shows 3 different setups and the current densities at AC in the center plane of the model. In the first setup, a homogenized current injection is realized by a solid copper plate at both ends of the CUT. The losses produced by this current distribution serve as the desired reference losses. Here, the losses at 50 Hz are calculated to 12.56 µW/m.[23] The second setup realizes the current insertion with a ring, connecting all strands of the outer layer exclusively. The third simulation model shows an extreme case, where only the central wire is connected to the current path of the measurement circuit at both ends. The overall length of every model is 42 cm and the losses are evaluated in a 1 cm long section at the center of the model.

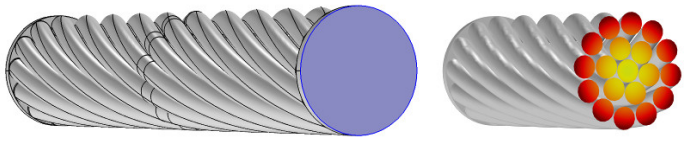

(a) Homogeneous current injection (desired reference)

(b) $||\boldsymbol{J}||$ 21 cm behind current injection in case of homogeneous contact

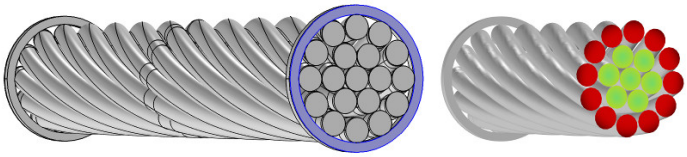

(c) Current injection via ring in the outer layer only

(d) $||\boldsymbol{J}||$ 21 cm behind current injection in case of a ring contact

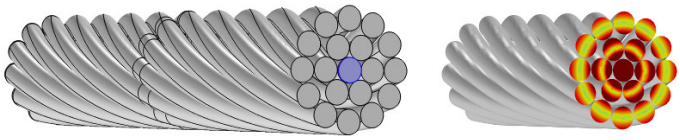

(e) Current insertion into central wire only (worst-case scenario)

(f) $||\boldsymbol{J}||$ 21 cm behind the current injection in the central wire only

Figure 4.32: The blue areas indicate the terminal, where the current is injected; the maximum current densities in all figures are normalized to the maximum value of Figure 4.32b; note that therefore in Figure 4.32f the current density in the central wire is off the chart, as it is approximately 10 times larger than the maximum current density in the other plots; the terminal at the opposite side (not shown) is identical

22 Current injection refers to the connections of the current path to the CUT on both sides of the conductor. Observations and conclusion drawn are therefore also valid for both sides if not noted otherwise. Current injection is therefore equal to the current extraction on the opposite side.

23 This is slightly larger than the losses by a solid CUT with 12.26 µW/m as stranding can increase the absolute resistance due to longer current paths.

The homogeneous current injection in Figure 4.32b shows the desired current density in the bundle[24]. Figure 4.32d shows a larger deviation from homogeneity in the cross section compared to the homogeneous case. Currents in the outer layer will set up *eddy currents* in the inner layer and central wire. These *eddy currents* are not part of the test current and only cause additional losses. They flow in one direction at one part of a strand and in the opposite direction on the other side of a strand. The injected current has to flow over the outer layer only, which in turn increases the overall losses to about 13.39 µW/m. Similar thereto, Figure 4.32f shows the current density at AC, if the current is only injected into the central wire. *Eddy currents* are excited in the 2 adjacent layers. Forcing this constant current through only 1/19 of the cross section (central wire only) results in losses of 147.64 µW/m.

These results make the problem with insulated wires clearer: on one hand, it is desired to have a perfect insulation of the single wires to reduce AC losses in the *Milliken* design. On the other hand, this would require the completely homogeneous injection of the test current in the cross section to have a representative current distribution (Figure 4.32b) in a measurement.

In practice, depending on the manufacturing quality and effort put into the insulation of the single strands, it is likely that some low resistive contacts between strands are present. The number and quality of these interwire contacts clearly depend on multiple parameters from exact conductor design to manufacturing processes and can be affected by further handling of the cable also (drumming, heating, ...). Table 4.3 includes some examples, where contacts between strands have been included in the 19 wire stranded conductor with a current injection into the central wire only. Note that the boundary condition at the opposite side affects the current homogenization in the simulation as well. For the contacts to show any significant effect, it was assumed here that the complete cross section is grounded at the side opposite from injection.

Table 4.3 shows the following: concerning the homogeneous current injection (I.) it can be seen that the DC resistance is larger compared to a solid copper CUT with the same overall cross section ($R_{\mathrm{DC,Ref}} = 6.897\,\mu\Omega/\mathrm{m}$). The reason is that the path the current has to follow is longer in the layers due to the helical winding. Nevertheless, the resistance ratio of 1.64 is smaller than that of a solid conductor with 1.77 at 50 Hz. For the injection via a ring into the outer layer (II.), the resistance ratio is smallest because the current distribution at DC is already similar (mostly in the outer layer) to the current density enforced by *skin effect* at AC. An injection into the central wire only (III.) results in the largest absolute losses. At DC they are approximately 19 times larger compared to the homogeneous case because only 1/19 of the cross section is used. Setting up small conductive contacts between central wire and all 6 wires of the inner layer and 6 "contacts" between the strands of this first layer and the 6 strands of the outer layer (IV.), which directly face the 6 strands of the first layer, reduces losses significantly. Note that losses are still larger because in the remaining strands of the outer layer, which have no direct contact with the current path, *eddy currents* are

24 In theory, losses could be lowered by balancing the injected current in the layers with the impedance caused by their AC and DC resistance, to have a completely uniform current density in the cross section. This however does not relate to any case of practical relevance.

excited. Two "contacts" (V.) are much better because in this special case all strands of the second layer are connected to the current path and therefore participate in transporting the test current, hence reducing losses.

Homogenization appears nearly instantly behind highly conductive contact points. Then the distance to the voltage tap-offs would nearly play no role. If the conductivity of the contact is lower than that of the conductor material, the necessary distance for current homogenization directly depends on the ratio of longitudinal strand resistance to contact resistance. Then, longer samples might be necessary as the resistance of the contact remains constant, while the longitudinal resistance increases with conductor length. An increased distances between injection and voltage tap-off can also help as it is likely that more contact points are present between the strands. This increases current flow over the contact points, which in turn improves current homogenization. The influence of this resistance ratio was analyzed for DC in more detail in [Bür95].

Table 4.3: Comparison of different configurations in the 42 cm long 19 strand bundle; "contacts" relate to a contact surface of 1 mm × 0.5 mm between central wire and all strands of the first layer and 6 equal transitions between first and second layer, where strands directly face each other

configuration	losses at DC in µW/m	losses at AC in µW/m	losses AC/DC
I. homogeneous current injection, all wires perfectly insulated (reference) (Figure 4.32a)	7.65	12.56	1.64
II. current injection in layer 2 only, all wires perfectly insulated (Figure 4.32c)	12.17	13.39	1.10
III. current injection into central wire only, all wires perfectly insulated (Figure 4.32e)	131.82	147.64	1.12
IV. current injection into central wire only, "contacts" 4.25 cm after injection with a conductivity of $1 \cdot \sigma_{Cu}$	24.08	43.53	1.81
V. current injection into central wire only, 2 "contacts": 4.25 cm & 8.5 cm after injection with a conductivity of $1 \cdot \sigma_{Cu}$	8.46	12.94	1.53
VI.current injection into central wire only, 2 "contacts": 4.25 cm & 8.5 cm after injection with a conductivity of 1 MS/m (this is equal to the resistance caused by a strongly oxidized copper surface [BM11])	41.20	46.29	1.12

4.2.3.3 *Practical Considerations*

Due to practical limitations, one wants to keep the necessary length from current injection to voltage tap-off as short as possible. Thus, current homogenization has to be established as fast as possible along the conductor axis. Therefore, in a conductor with insulated wires one needs to establish a contact over the whole cross section at both ends of the specimen. To achieve that, one could use copper braids, low-melting solders or some other kind of conductive contact gel at both terminals, which reaches every wire in the cross section. Special designs with many needles pushing against the cross section reaching every single strand would be a proper way to achieve a homogeneous current injection.

Figure 4.33 shows the contact system used by *TU Berlin* in the measurements of *Milliken* conductors. It uses a simple copper weave to reach as many of the insulated strands as possible. Even thought not all strands will be reached, the procedure described in the next section shows why it works, if the conductor is further processed.

Figure 4.33: Simple current contact system used by *TU Berlin* for *Milliken* conductors; a copper braid is used on the inside to increase the contact area

Even though the exact way of current injection was not described, in [Sjö13], where the CUT was a 2000 mm^2 *Milliken* conductor with bare wires and 20 m length, it was observed that the influence of the *end effect* is already below 0.5 % at a distance of 20 cm from the current injection and not present at all after 60 cm. As no further information about the contact system at the terminals was given, this example only gives some ideas about current homogenization.

4.2.3.4 *Conclusion*

Current homogenization along a stranded conductor with insulated wires is either achieved by establishing a good contact to every single strand at both ends, or by having good electrical contacts between strands, which boost current homogenization along the conductor axis. Moreover, behind good electrical contacts and in solid conductors, current homogenization appears rapidly.

From the FEM simulations some conclusions regarding current homogenizations could be drawn. A lot is still open for investigation: e.g. homogenization in *M-type* designs, different contact resistances between strands and so forth. An important general statement concerning the

current injection, which can be derived from references and preceding investigations is that the current injection should be as homogeneously as possible, as one cannot rely on good electrical contacts between strands in *M-type* conductors with oxidized or enameled wires.

The important influence of voltage tap-off positioning is described in the next section.

4.2.4 *Placement of the Voltage Tap-Offs Including Conductor Preparation*

This section also serves as a conclusion of some observations and statements made previously in different sections. The placement of the voltage tap-offs is strictly linked to the question of current homogenization.

There are certain requirements about the positioning of the voltage tap-offs on *Milliken* conductors or conductors with insulated wires in general.

- At DC: To accurately measure the DC resistance between two points *a* and *b* in a complex conductor composed of multiple insulated parallel strands, one has to meet the following two requirements:
  1. The current distribution in this section has to be representative for the operating condition. This means that every strand in this sections between *a* and *b* has to take a part of the test current. The more parallel strands are available for the test current the fewer DC losses appear. This can be achieved by establishing at least one good electrical contact between all strands before voltage tap-off *a* and after voltage tap-off *b* or a completely homogeneously current injection. If a perfect injection cannot be guaranteed, the safest way to establish a good electrical contact between all strands is welding the conductor at both terminals. This enables quick current homogenization after the injection in this—now solid—conductor section. Alternatively, the insulation on the strands can be removed at both terminals followed by mechanically compressing all strands to enable good contact between them. Another alternative, which relies on interwire conductivity, is to give the current sufficient length along the conductor to homogenize in the cross section. The distance between voltage tap-offs and current injection then has to be increased. This of course does not guarantee that all strands have contact to the current path and can lead to the measurement of an increased DC resistance.
  2. One needs to assure that both voltage tap-offs, *a* and *b*, are attached to the same strand. If this is not the case, contact resistances between wires are included in the measurement. This is also achieved best when attaching the voltage tap-offs to the blank, solid section described by 1. (for example by welding). If not welded, it can be hard and lavishly to retrieve the same strand at the rear voltage tap-off *b*. Moreover, this strand is not necessarily located at the surface in *M-type* designs due to the twist of layers.
- At AC: The same requirements as for DC are necessary. As at DC, theoretically, it would be sufficient to contact the voltage tap-offs to one

individual strand only at both voltage tap-offs—assuming a representative current density is already established in the cross section—because the outer out-of-phase magnetic field components captured by the pick-up loop contain the information about AC losses of the complete conductor bundle (also see Appendix A.2)[25]. Again, from the practical side of view it is much safer to electrically connect all strands at the voltage tap-off positions by welding for example.

For both excitations, AC and DC, it is important that between the tap-offs a and b the conductor has to have the design it was intended to have: e.g. insulated wires for AC loss reduction. This guarantees that the increase of DC resistance, due to longer helically current paths in the single insulated wires, is measured correctly as it will occur under operation as well. At AC it will guarantee that the loss optimized *Milliken* design is measured. One possible and recommended way to connect the voltage tap-offs is shown in Figure 4.34.

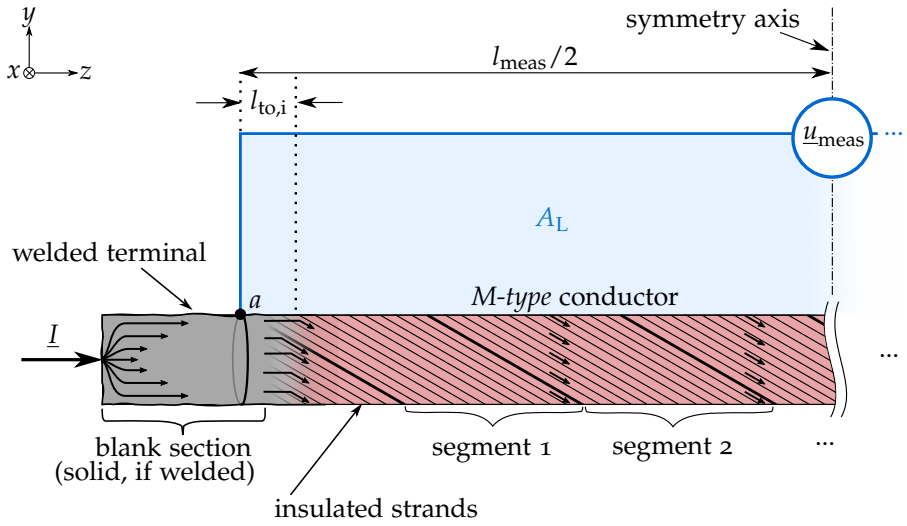

Figure 4.34: One possible way to position the voltage tap-offs at a and b on a *Milliken* conductor with insulated strands; only one end of the conductor is shown, voltage tap-off b is located on the far right side and connected identical to a; the gray shade indicates blank strands/conductor parts and the red area symbolizes insulated strands/conductor parts

Concerning the distance between voltage tap-off on the blank section and beginning of the insulated section—length $l_{to,i}$—one has to regard the following at DC and AC:

- On one hand, the connection between all strands should still be very good, so that the electric scalar potential is still constant in the cross section.
- On the other hand, $l_{to,i} \ll l_{meas}$ should hold, so that the representative conductor section (red shaded area in Figure 4.34) is mainly influencing the results. Due to removing the insulation of the strands at the terminals and voltage tap-off positions, at DC the local losses near the voltage tap-offs are smaller compared to the insulated section, because the current does not have to follow longer helical paths. At AC the local

25 As discussed earlier, this of course is only valid when $d_{VL} \geq d_{VL,min}$.

losses near the voltage tap-offs are larger, because this blank conductor section is not optimized and has therefore full AC losses compared to the optimized *Milliken* conductor design in the middle section.

This is schematically depicted in Figure 4.35. It shows simulation results at DC including the electric scalar potential and current density.

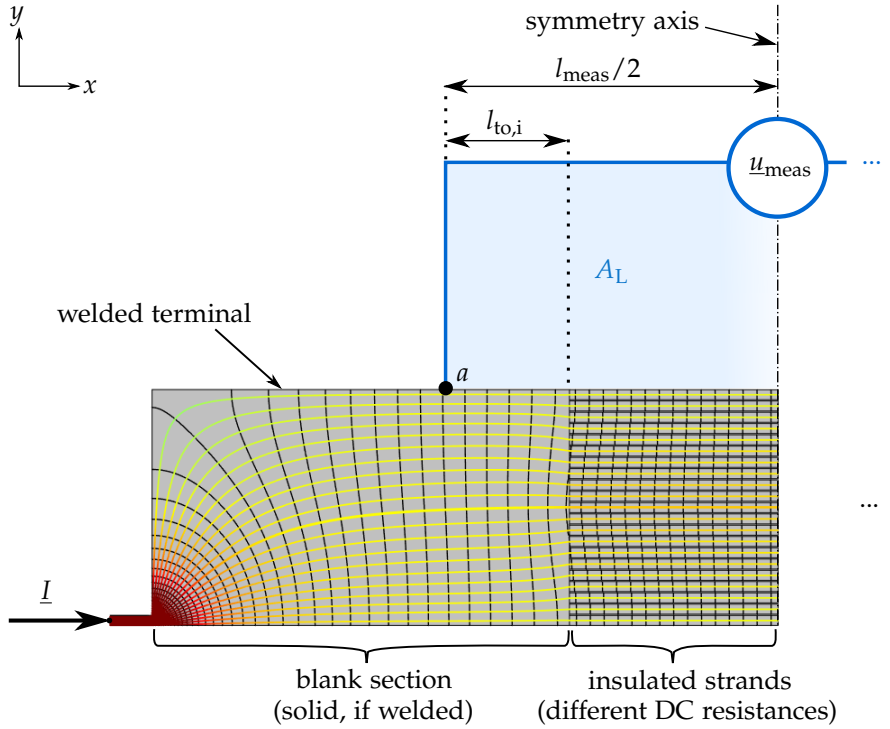

Figure 4.35: 2D DC FEM simulation of inhomogeneous current injection into the blank terminal of a conductor with perfectly insulated strands, which have different conductivities; recommended position of voltage tap-offs *a* and *b* (*b* is not shown, but identical to *a*) is indicated; current streamlines are color-coded according to the absolute current density and the equipotential lines are shown in black

It was made clear that a *Milliken* conductor has to be further processed for the succeeding measurement. All strands should have electrical contact if perfect current injection cannot be guaranteed. This is also valid for blank *Milliken* conductor designs as oxides can form on the strands and the segments are usually separated by thin tapes. In practice this can be achieved by one of the following ways:

- Welding the terminals of the cable, using thermite for example, to form a solid conductor as shown in Figure 4.34 and Figure 4.35 is likely the most reliable way to guarantee that all strands are electrically connected.
- Alternatively, one can remove the insulation of all single strands and mechanically compress the bundle to further decrease contact resistance between strands. This can be done by a conductive ring clamp or high current connector. The clamp should be conductive to equalize the electric scalar potential over all segments, which are typically insulated from one another by thin tape. Of course the tape can also be removed in the first place. Yet the clamp should not contain any ferromagnetic materials as this could locally increase losses at AC. In

case of enameled wires the insulation can be scraped off with a knife, be removed chemically or be removed with a sandblaster for example. In the case of oxidized strands, it can be sufficient to apply strong mechanical pressure to the individual wires, as the thin oxide layers on the strands then break open. Oxides on copper conductors can easily be removed by using a citric acid solution.

Both approaches of conductor preparation are relatively time-consuming. But it is recommended that the conditions put forward above are met, because one will likely still obtain a measurement result, if these preparations are not made, but a result, which likely includes contact resistances. The same conclusion was drawn by [BM11], where the authors developed a system to accurately determine the DC resistance of small insulated conductor bundles. From the practical side of view, independent of the chosen method, one should check the DC resistance with expectations. If the DC resistance is in agreement with the expectation, the chosen approach is adequate, as DC losses directly indicate the number of strands participating in current transport. If DC losses meet the expectation, the whole cross section is used and possible contact resistances included in the measurement are negligible. Even in enameled *Milliken* conductor designs it was observed that injecting the current in only one of the hundreds of strands in the cross section, shows good compliance with the calculated DC resistance if the voltage tap-offs are placed sufficiently far away (0.5 m to 2 m) from the injection, even though placed on the blank surface of an enameled section.

From this section it becomes clear that if all the above conditions for the voltage tap-offs are met, the current injection is not a critical part anymore. The reason is that current homogenization appears rapidly in solid, rather uninsulated conductors, which should be present at both terminals.

4.2.5 *Additional Sources of Influence Open for Investigation*

This section shortly lists additional possible sources of influence upon the measurement, which were not further investigated in this thesis. These points are discussed again later in Chapter 6.

MINIMUM MEASUREMENT LENGTH The AC resistance of a *Milliken* conductor is influenced by its 3D geometry, due to the twisting of the segments and layers. This is opposite to a solid cylindrical conductor for example, where every cross section along the conductor axis is identical and therefore making it a 2D problem.

The question should be raised at which length a sample used for a measurement shows the same behavior as the complete cable. When using a sample of only a couple of meters in length, the mutual induction between different insulated layers—which directly affects the current density in the layers—can be different compared to a much longer sample. An example for clarification: having a twisted pair cable with some space between both wires and both ends short-circuited, placed in an external alternating magnetic field, will induce a current in the single wires depending on the number of twists (also see [Ros18, Figure 2.4]). If the number of twists is an integer, the total induced current will be zero, because induced currents will cancel each other out. If the number of twists is not an integer, *eddy currents* will flow in the twisted pair cable and therefore change its

losses. Nevertheless, induced currents will successively decrease with an increasing number of twists. In a complex conductor, such as the *Milliken* conductor, the exact position of each strand towards each other strand, will likely not repeat (be the same again) in short samples. This lowest common multiple of the lay lengths of layers and segments—where the complete 3D geometry starts to repeat—will probably be larger than the measurement length as shown in the following example: [Joa98, p. 45] gives the lay lengths of a 2500 mm^2 *Milliken* conductor, where the segments and 2 of 3 layers are stranded. With the segment lay length of 2.15 m, a lay length of 0.29 m for the second and 0.33 m for the third layer, the lowest common multiple amounts to roughly 2000 m.[26] Theoretically, only after this distance all wires in a layer have been exposed to the same electromagnetic field distribution—caused by the other segments—and therefore have the same current density and AC losses. Despite this length being already larger than typical production lengths, having a sample of only a couple of meters in length will probably not show the exact same behavior compared to a longer cable.

The necessary minimum measurement length pertains all measurement methods equally, including the calorimetric approach. In the measurements performed in this thesis a measurement length of at least 5 m was tried to be realized. For typical designs this includes multiple segment lay lengths.

INFLUENCE OF DRUMMING OF THE CABLE Already in [Gra79, p. 98] it has been noted that the insulation of the single strands can be damaged by mechanical force upon the segments during manufacturing, reeling and unreeling. Damage caused by the manufacturing process will be visible in the measurement. Nevertheless, it is unknown if and how the performance of a cable with insulated strands is affected after the cable has been put on a drum and is again reeled off on site.

LONG-TERM BEHAVIOR Load cycles under operating condition of the cable can heat up the conductor of a power cable up to more than 90 °C. Heat can have a direct effect upon the surface of blank copper wires and on the electrical properties of insulation of the single strands as well. Moreover, heat-ups and cool-downs can have an indirect effect by inducing mechanical stress upon the segments and strands in a conductor. This in turn can influence the insulation properties of the strands by friction between different layers for example. Both effects should be studied. Due to these uncertainties it is questionable if the measurement value obtained at 20 °C for example can directly be corrected to higher temperatures.

26 Another example of a 2000 mm^2 *Milliken* conductor given in [Joa99] has a lowest common multiple of approximately 200 m.

4.3 RECOMMENDATIONS FOR AC LOSS MEASUREMENTS WITH THE ELECTRICAL METHOD: SETUP, CONDUCTOR PREPARATION AND PROCEDURE

This section provides a quick overview and uses all results obtained previously to recommend a setup and procedure with only little further explanation as this was already done for nearly all points previously.

4.3.1 *Conductor Preparation*

It is recommended to prepare the *Milliken* conductor in the following way:

1. In oxidized or enameled designs, the insulation of all strands at both terminals should be removed by welding or scraping it off for a length of $\geq 3 \cdot d_{\mathrm{CUT}}$. Alternatively chemical methods can be used as well. Then enable a good electrical connection between all strands and segments, for example by applying mechanical pressure.
2. Remove oxide layers (by using sandpaper for example):
   - from the cross section at both terminals to improve current injection into the CUT's cross section,
   - from the CUT's surface at the voltage tap-off positions (if it is not placed at the blank section at the terminals)
   - and also from the ends of the voltage lead wires themselves [HB81, p. 115][27].
3. Establish a conductive circumferential connection at the voltage tap-offs.
4. Connect the current path to the blank terminals as homogeneously as possible.

Next, the pick-up loops and return conductors have to be set up.

4.3.2 *Setup of Pick-Up Loops and Return Conductors*

In general one should avoid additional conductive parts, in which *eddy currents* can build up, as much as possible.

If it is certain that no additional conductors are nearby (including the laboratory floor, shelves,...) then using the *symmetrical return method* with one pick-up loop will deliver very accurate results. The *top* configuration is very robust against asymmetries from the return conductors. The recommended setup in this case is shown in Figure 4.36. The return conductor spacing should be larger than d_{min}, which is the case with $d = 0.5\,\mathrm{m}$ or larger.

In Figure 4.36 the sheath was removed, even though it was shown earlier that it will not influence the measurement significantly in typical sheath designs[28]. The insulated section of the *Milliken* conductor (middle section in red) has to be kept under the insulation, as the mechanical pressure of the insulation can influence the conductor performance. The distance from

27 Further information on films on electric contacts can be found in [Hol58, p. 27] for example.
28 Note that cables with special sheath designs or steel wire armored cables can be a special case and influence the measurement noticeable. This has to be checked in advance.

voltage tap-offs to the insulated part of the CUT should be much smaller than the overall measurement length. Current homogenization in the blank conductor sections at the terminals is sufficient after approximately three times the conductor diameter. In practice, current homogenization was often observed below this distance. This can also be checked back with FEM simulations in advance. To avoid the excitation of *eddy currents* in the surrounding as much as possible, the current feed line should be performed coaxially. This suppresses outer magnetic fields caused by this current path.

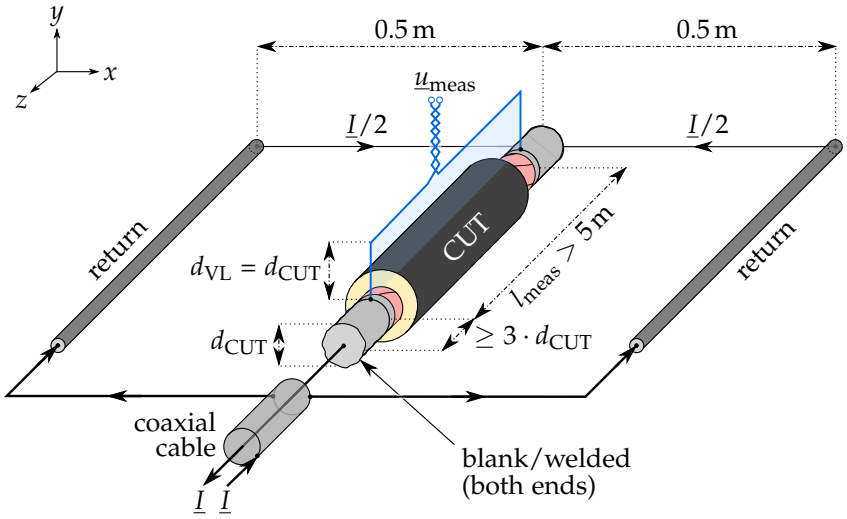

Figure 4.36: Recommended measurement setup for short *Milliken* conductor samples, if no other conductive parts are nearby; the still insulated section of the *Milliken* conductor is shaded in red; both ends of the CUT are prepared equally

When having additional conductive materials in the surrounding (including the laboratory floor, shelves,...) or if it is not known for sure, the average value (*AVG*) of at least 4 pick-up loops evenly distributed around the cables circumference at the same d_{VL} should be used. The generally recommended setup for an AC resistance measurement is shown in Figure 4.37.

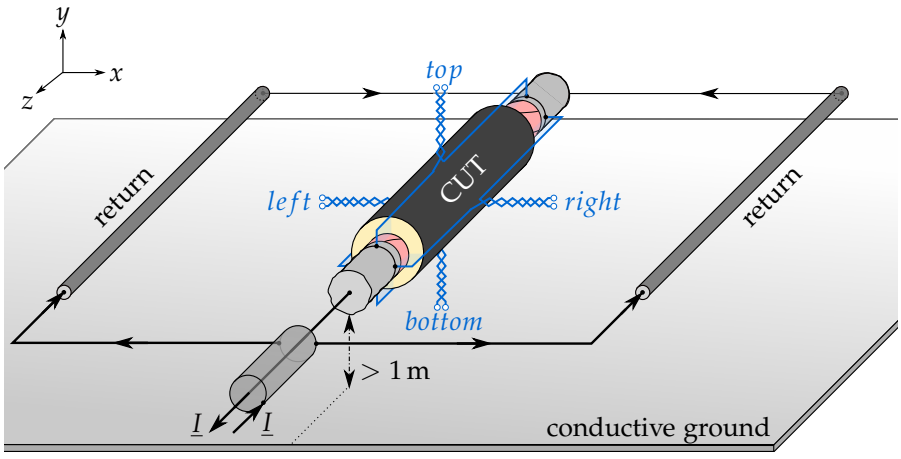

Figure 4.37: Generally recommended measurement setup for short *Milliken* conductor samples; the still insulated section of the *Milliken* conductor is shaded in red; both ends of the CUT are prepared equally; this setup is also robust with regard to asymmetries from the surrounding

The preceding investigations showed that averaging also reduces the necessary $d_{\mathrm{VL,min}}$. Hence, the pick-up loops can be attached at the surface of the cable. This will also reduce the phase angle of the measurement as well, which is advantageous[29]. Except for d_{VL} all other parameters are identical to those shown in Figure 4.36. For the sake of clarity they are not shown here again. One additional geometrical distance is defined, which is the spacing of the whole setup to a possible conductive ground or wall being at least 1 m. The reason for that is that the distance to the asymmetry should be as large as possible—even though the *AVG* is taken—and a distance of 1 m is easy to realize in practice. Moreover, as discussed earlier, if the DC resistance still meets expectations, one can reduce the distance between current injection and voltage tap-off or set up a more simple current injection and put the voltage tap-offs further away. The DC resistance shows if current homogenization in the cross section is already sufficient.

In general one should avoid conductive parts near the measurement circuit as far as possible. Moreover, if the *Milliken* conductor is exchanged against another CUT one should consider to adapt d_{VL}. Some additional remarks are put forward below:

- The voltage leads should be much thinner than the CUT to avoid an influence on the current distribution in the CUT. This can also be easily checked with FEM simulations in advance.
- Even though the terminals are welded, the current injection should be performed as homogeneously as possible.
- From the point the voltage lead wires first meet, they have to be twisted together very tightly to avoid further influence of alternating magnetic fields. Instead of connecting the voltage leads at the center of the CUT at $l_{\mathrm{meas}}/2$, the rear voltage lead wire can also be led along the CUT to the first voltage tap-off and from there on twisted with the second voltage lead wire and brought to the measurement system.
- Moreover, the circumferential connection for the voltage tap-offs should not be too thick to enable accurate length measurement.
- Both return conductors should not produce outer out-of-phase magnetic fields, therefore having a rotationally symmetric cross section.
- All pick-up loops should already be prepared before the first measurement to avoid influencing the setup (e.g.: unintentionally changing the voltage tap-offs,...), when setting up a new loop. Having all 4 loops prepared also helps in keeping the deviation of the measurement temperature between multiple measurements small, as one can switch the pick-up loop much faster.
- For the setup in general and for fixing connections and so on, tape or cable ties are recommended instead of conductive materials as clamps or other metallic parts.
- In case thermal emfs do play a role in a measurement (when no bipolar DC measurement is feasible or the test current is much larger and

29 From all previous results one can also conclude an hypothetical ideal setup: taking the average of numerous evenly distributed voltage leads (extreme case a thin tube) and having numerous evenly distributed return conductors spaced very far from the CUT (extreme case a tube with a very large inner diameter).

can heat up the CUT), one should use low thermal connections such as crimp connections and avoid dissimilar metal connections [HB81, p. 115].

4.3.3 *Measurement Procedure*

It is clear that the exact measuring procedure depends on the selected measuring instrument. Nevertheless, when performing the measurement one can stick to the following recommended procedure:

1. Check all connections for a good electrical contact.
2. Take the measurement length l_{meas}.
3. Meter the conductor temperature.
4. Conduct the bipolar DC measurement and use the average [RSS11b] (also see Section 2.2.2)[30].
5. Perform the AC resistance measurements: If the temperature of the CUT is not the desired temperature for the final resistance evaluation (typically 20 °C) then the measurement frequency has to be chosen in accordance with the temperature correction procedure (see Section 2.4.2). For example: if the copper CUT had a temperature of 15 °C, this would require a measurement frequency of 49.0175 Hz, if the resistance is to be evaluated at 20 °C for 50 Hz. In no case should the measurement be performed directly at 50 Hz or 60 Hz or their harmonics to avoid interferences. Even though the conductor temperature is exactly 20 °C, the AC resistance of 50 Hz or 60 Hz should be interpolated with at least 2 measurement values close to the desired frequency (see Section 2.4.1).
6. At the end, the temperature and DC resistance can be recorded again to make sure that no temperature drift occurred during the measurement.

4.4 ADDITIONAL INFORMATION REGARDING THE AC RESISTANCE MEASUREMENT ON COMPLEX CONDUCTORS

Some more important remarks about AC resistance measurements are given in the following sections.

4.4.1 *General Remarks Concerning Preceding Simulations*

Regarding the results put forward in this chapter one should keep the following in mind:

- The goal of the simulations was to point out the effect of different, possible influences in AC resistance measurements separately. Compared to real measurements, where often multiple sources of influence are present, their interplay is neglected in most cases. As there is no typical measurement setup or laboratory, it was not senseful to build unique setups, where multiple sources of influence are present and interact.

30 In general, every measurement value should be checked against expected values. The final resistance ratio can also appear reasonable while the absolute resistances deviate from expectations.

- When looking at the results, one should also bear in mind that the results account for the worst-case of a solid circular CUT with a cross section of 2500 mm^2.
- On the other side these idealized simulations had perfectly defined positions for the CUT, return conductors and pick-up loops, whose positions also vary in reality and hence influence the results. The influence of deviations from symmetry require further investigations.
- The results put forward are qualitatively also valid for 60 Hz. Losses in the CUT and the influences on the pick-up loops will generally be larger compared to 50 Hz.

4.4.2 *Additional Measurement Setups Used in the Literature*

Four more measurement setups were found in the literature, which have not been part of the previous extensive investigations due to the limited scope of this work. One is similar to the previously defined *Setup III*, but called the *asymmetric return method*. In comparison to the *symmetrical return method* the two return conductors are not placed in the same plane as the CUT. It was used in [Ols+99] for example. The other three of them are shown in Figure 4.38 and briefly discussed below.

In setup (1) the return conductor configuration is identical to the previously defined *Setup I*, consisting of an identical return conductor. The AC resistance of the sample is obtained by measuring the resistance between tap-offs c and d and subtracting the resistance obtained between voltage tap-offs a and b divided by two times the measuring length [CMR77]. The large pick-up loops will capture much in- and out-of phase magnetic field components. Therefore, no asymmetries as external conductors, metallic floors and so on should be in proximity to the setup. The phase angle measurement should also be very accurate.

Setup (2) uses a tubular return conductor and helically winds the rear voltage lead wire, which is split up, around the tubular return for an integer number of turns.

Setup (3) also uses one helically wound voltage lead wire. It is not clear from the reference [SK08], if this voltage lead is attached to the surface of the conductor or the cable, which makes the assessment hard. If the helically wound voltage loop is attached directly to the surface of the CUT and the current distribution is not rotationally symmetric (for example due to *proximity effect*), FEM simulations indicated that the measurement will note deliver the *true* losses of the conductor. This means that in case of helically wound pick-up loops $d_{\mathrm{VL,min}}$ also has to be larger than 0 for some conductors or arrangements.

Helically wound pick-up loops were not further investigated in theory, but some measurements using helically wound voltage loops will be shown in Chapter 5.

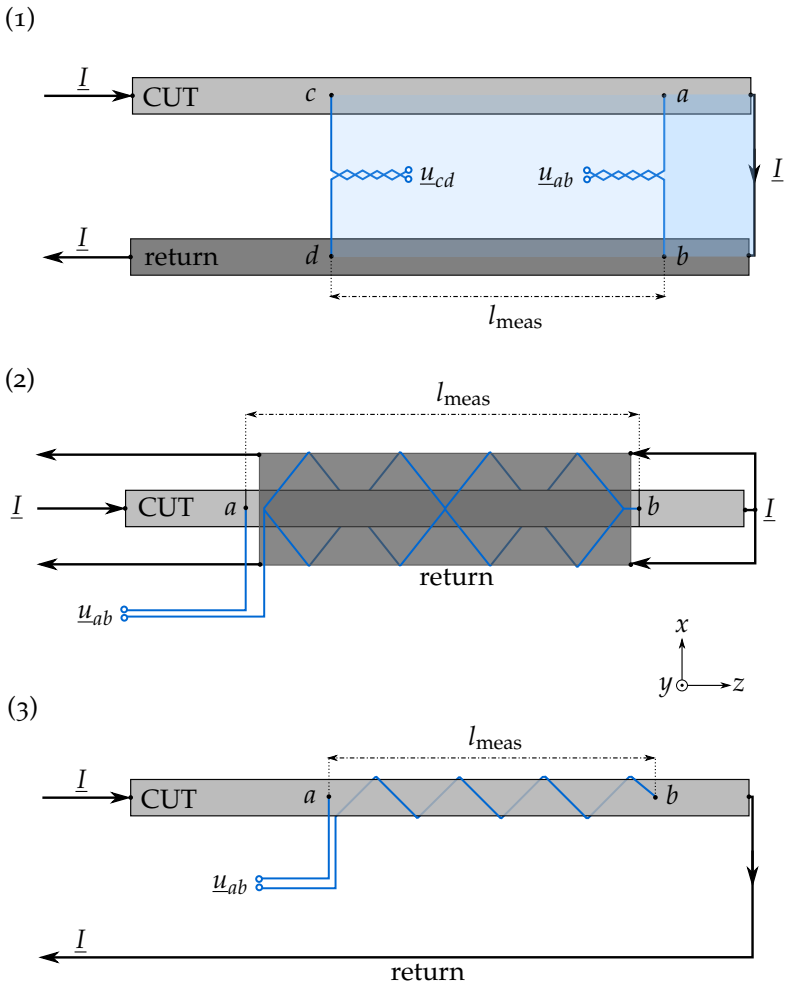

Figure 4.38: Additional pick-up loop setups for the AC resistance measurement of *Milliken* conductors found in the literature; (1) was presented in [BM68] and [CMR77]; (2) was presented in [RSS11b]; (3) was presented in [SK08]; the coordinate system is valid for all setups

4.4.3 *Resistance Measurement in Three-Phase Systems*

Measuring conductor losses of a three-phase system presents an even more complicated task for the electrical measurement. In [DR30; Sal48, pp. 1392-94; ME49, p. 825; Jac70; Tay70] it was shown that, if the pick-up loops attached to every phase capture sufficient complex magnetic fields, the average of all readings relates to the *true* losses of the system. Due to the out-of-phase magnetic field distribution, some readings can be negative, which does not present a limitation, if the average of all measurements is taken [ME49, p. 825]. Nevertheless, the necessary extension can exceed a couple of meters but of course depends on the conductor spacings and configuration [Jac70]. In return, larger loops can introduce *apparent* losses from surrounding conductive parts (floor,...) and can also significantly increase the phase angle. As previously done for different single-phase setups, today, the necessary radial voltage loop extension can easily be calculated by numerical simulations in advance. Trying to tackle these issues, [Tay70] discusses other voltage loop arrangements, which can reduce these errors in 3-phase arrangements. In 2005, [Tsu+05] discussed

how to separate the losses for each conductor using the electrical method with multiple sophisticated pick-up loop arrangements.

Concluding one can say that the electrical method is able to measure the AC resistance of a 3-phase system and that it is even possible to access the losses of each conductor individually.

5 MEASUREMENTS OF MILLIKEN CONDUCTORS

Whenever you find yourself on the side of the majority,
it is time to pause and reflect.
Mark Twain

In this chapter, the preceding results find their application in accurate measurements of different *Milliken* conductor designs. As some measurements were performed parallel to open investigations, not in all cases could all recommendations be applied. The influence of these neglected recommendations were further investigated and their effect was estimated to be small. This means that the results presented in the following are still expected to be close to the *true* values in these cases. At first, measurement curves for different conductor designs are plotted up to 100 Hz. Afterwards, all measurements are compared to the recent IEC standard and plotted up to 300 Hz. Moreover, helically wound voltage pick-up loops are compared to the recommended *AVG* setup to get empirical evidence about their applicability for *Milliken* conductors. Photographs of some measurement setups are shown in Appendix D.

For the k_s-factor estimation the interpolation recommended by the IEC standard in Section 2.4.1 was used. The plotted curves in the following use linear interpolation between the actual measurement values.

5.1 MEASUREMENT OF DIFFERENT CONDUCTOR DESIGNS

In the following, measurement results for different designs are shown. Note that *Milliken* conductors with the same design can vary in AC resistance, due to manufacturing quality and further design choices[1]. Whenever possible, these design parameters are provided for each sample.

The following measurements were performed close to room temperature and corrected to 20 °C and 90 °C with the method shown in Section 2.4.2.

5.1.1 *Aluminum Conductors*

SAMPLE AL Table 5.1 and Figure 5.1 show the results of the measurement of a 2000 mm², 6 segment aluminum *Milliken* conductor with a bidirectional pitch of layers. The diameter of the single strands is 2.4 mm. The welded section at both terminals was less than 1 cm long (see Figure D.4). Nevertheless, the voltage tap-offs were placed 2 m apart from the terminals to enable current homogenization. The DC resistance showed good agreement with the calculated value, which is an indicator for sufficient current homogenization. For this setup the *sheath return method* was used. The solid aluminum sheath had a thickness of 1.5 mm. The coaxial *current transition* is shown in Figures D.3a to D.3c. The conductor was placed close to the laboratory floor, which may contains conductive materials. Nevertheless,

1 This includes parameters such as number of segments, pitch of the layers in the segment (uni- or bidirectional), diameter of the single strands, design of core conductor and so on.

estimates from additional FEM simulations showed that no significant additional *true* losses do occur in the CUT—because only little magnetic field leaks out in this coaxial setup—and an influence on the *apparent* losses can also be avoided by using the *AVG* setup.

The *AVG* setup and the *helical* setup were used in this measurement. The voltage loops were placed on the surface of the cable in both cases, resulting in a d_{VL} of approximately 3.5 cm, which is similar to $0.6 \cdot d_{CUT}$. Recollect that the *AVG* setup allows a d_{VL} below $d_{VL,min}$.

Table 5.1: Temperature corrected resistance ratios of a 2000 mm², 6 segment aluminum *Milliken* conductor at 50 Hz, *measured* and IEC recommended k_s values; actual measurement temperature $T = 19.5\,°C$ to $19.9\,°C$; measurement length $l_{meas} = 7.945\,m$

setup of pick-up loops	R_{AC}/R_{DC} at 20 °C	R_{AC}/R_{DC} at 90 °C	k_s (measured)	k_s (acc. to IEC)
AVG (average of 4 loops)	1.070	1.037	0.43	0.25
Helical (2 turns)	1.056	1.030	0.38	0.25

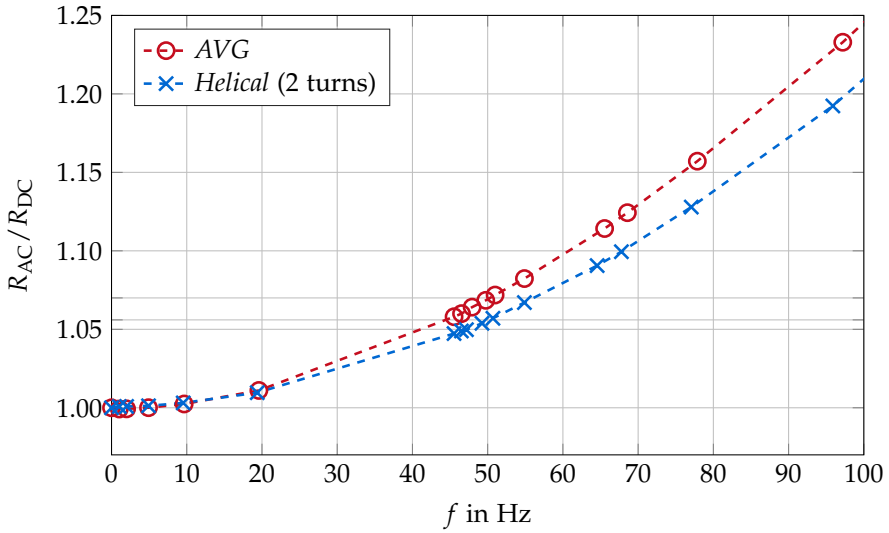

Figure 5.1: Resistance ratio curves for a 2000 mm² aluminum *Milliken* conductor at 20 °C for 2 different voltage pick-up loop setups; the corresponding resistance ratios at 50 Hz are marked on the vertical axis as well

According to the *AVG* setup, the ratio of AC to DC resistance at 50 Hz and 20 °C is 1.07. The resulting k_s factor of 0.43 is larger compared to the recommendation by the IEC standard. The result obtained by the *Helix* is lower but still significantly larger than the IEC value.

5.1.2 *Copper Conductors*

As described in detail in Section 3.2.2, the single strands of a copper *Milliken* conductor are either blank (untreated), oxidized or enameled. Blank copper strands can also oxidize over time, altering the performance of the CUT. In enameled designs either each strand is insulated or in some layers only every second strand is insulated. This is sufficient, as long as no two adjacent blank wires—also from different layers—have direct contact.Moreover, it is

expected that the insulation of the single strands of all designs and hence conductor properties can change, if the cable has been subjected to electrical or mechanical stress such as load cycles or drumming.

5.1.2.1 *Blank*

SAMPLE CU-B The results presented in Table 5.2 and Figure 5.2 correspond to a copper *Milliken* conductor manufactured by *Norddeutsche Seekabelwerke* (*NSW*)—a *General Cable* company—having blank strands with bidirectional pitch, 5 segments with lay lengths of 1.526 m and a total cross section of approximately 1773 mm^2 (3500 kcmil). The current connection to the CUT was established by high current connectors. The specially designed sheath is composed of a solid lead sheath and an additional layer of copper wires. This conductor was measured after a heat cycling test according to the recent IEC standard 62067. The conductor experienced 88 heat cycles in total, a maximum current of 3400 A and a maximum temperature of 105 °C.

Table 5.2: Temperature corrected resistance ratios of a blank 1773 mm^2, 5 segment copper *Milliken* conductor with blank strands at 50 Hz, *measured* and IEC recommended k_s values; actual measurement temperature T = 19.2 °C to 19.3 °C; measurement length l_{meas} = 8.41 m

setup of voltage pick-up loops	R_{AC}/R_{DC} at 20 °C	R_{AC}/R_{DC} at 90 °C	k_s (measured)	k_s (acc. to IEC)
AVG (average of 4 loops)	1.224	1.130	0.58	0.80
Helical (18 turns)	1.222	1.129	0.58	0.80

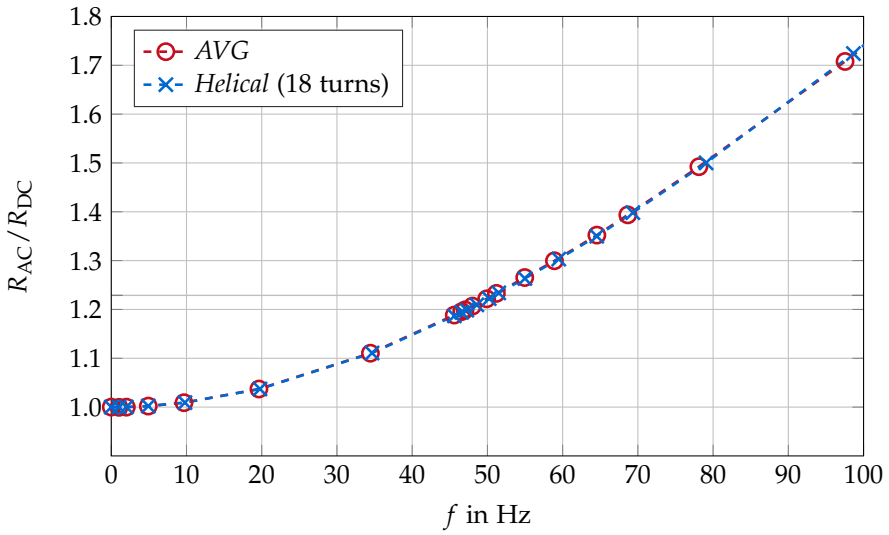

Figure 5.2: Resistance ratio curves for a blank 1773 mm^2 copper *Milliken* conductor at 20 °C for 2 different voltage pick-up loop setups; the corresponding resistance ratios at 50 Hz are marked on the vertical axis as well; *Courtesy of General Cable*

The actual measurement setup is shown in Figure D.5 and uses the *symmetrical return method*. *Eddy current* losses in the sheath caused only negligible additional *measured* losses (see Section 4.2.2.3). The CUT was located 46 cm above the laboratory floor. The distance d between CUT and the return conductors was 70 cm. The voltage loops were placed on the surface of

the cable resulting in a d_{VL} of approximately 4.6 cm, which is similar to $0.9 \cdot d_{CUT}$.

The measurement setup corresponds to that shown in Figure 4.37. It is interesting to note that the helically wound voltage loop delivered results with a deviation smaller than 0.1 % at 50 Hz compared to the *AVG* setup. This is much smaller than the deviation seen in Figure 5.1. A possible reason for that is the increased number of turns. The *helical* setup could then better compensate possible asymmetries along the cable axis, which may be present in the vicinity of the cable. At the same time, the distance to a possible source of asymmetry—the laboratory floor—was much larger than in the setup used for the aluminum *Milliken* conductor. Even though no further theoretical investigation were performed here, this gives some good insights and shows the possible potential of this method. The *helical* voltage loop should be wound in the opposite direction of the segment pitch. With that one can avoid having a constant relative position to the segment—and therefore not capture a possible asymmetric complex magnetic field distribution of the CUT—if pitch of the *helical* voltage loop and the segments are identical. Moreover, the number of turns should be an integer, to outbalance the induction from possible, nearby sources of influences.

What can also be seen from Table 5.2 is that the measured k_s is significantly lower than recommended by the IEC standard.

5.1.2.2 *Oxidized*

SAMPLE CU-O-1 Table 5.3 and Figure 5.3 show the results of the measurement of a 1200 mm², 6 segment copper *Milliken* conductor with unidirectional pitch and oxidized strands. The DC resistance showed good agreement to the calculated value. For this setup the *symmetrical return method* was used. The distance d between CUT and the return conductors was 70 cm. The solid aluminum sheath of the cable had a thickness of approximately 4 mm. The CUT was located 45 cm to 50 cm above the ground. The measured conductor had a solid copper core conductor with a diameter of 1.08 cm.

The voltage loops were placed on the surface of the cable resulting in a d_{VL} of 2.985 cm, which is similar to $0.7 \cdot d_{CUT}$. At both terminals the oxide layer was removed by a citric acid solution for a section of approximately 20 cm length. The measurement setup corresponds to that shown in Figure 4.37 having the voltage tap-offs placed approximately 15 cm behind the current injection.

Table 5.3: Temperature corrected resistance ratios of a 1200 mm², 6 segment copper *Milliken* conductor with oxidized strands at 50 Hz, *measured* and IEC recommended k_s values (Sample 1); actual measurement temperature $T \approx 20\,°C$; measurement length $l_{meas} = 12.775$ m

setup of pick-up loops	R_{AC}/R_{DC} at 20 °C	R_{AC}/R_{DC} at 90 °C	k_s (measured)	k_s (acc. to IEC)
AVG (average of 4 loops)	1.15	1.08	0.68	-
Helical (17 turns)	1.16	1.09	0.71	-

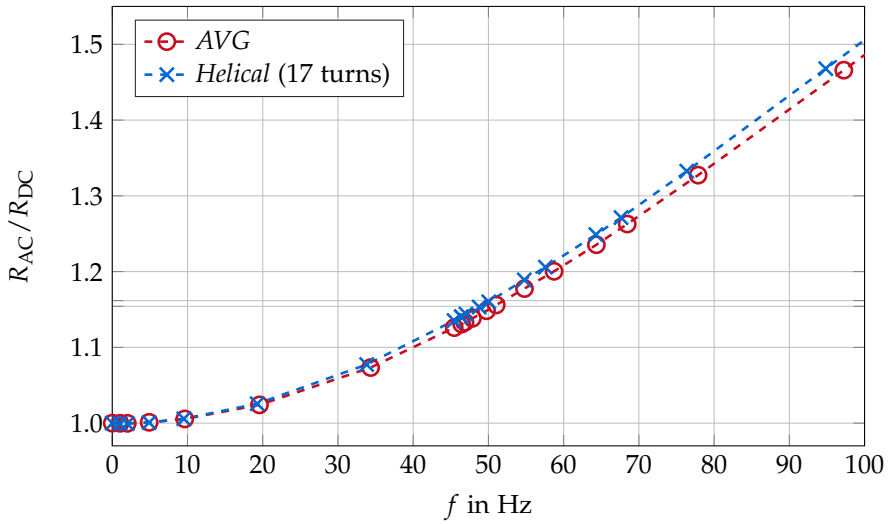

Figure 5.3: Resistance ratio curves of an oxidized 1200 mm² copper *Milliken* conductor at 20 °C for 2 different voltage pick-up loop setups (Sample 1); the corresponding resistance ratios at 50 Hz are marked on the vertical axis as well

SAMPLE CU-O-2 Table 5.4 and Figure 5.4 show the results of the measurement of a 2500 mm², 6 segment copper *Milliken* conductor with unidirectional pitch and a segment lay length of 1.4 m. All strands in the cross section are oxidized. The DC resistance showed good agreement to the calculated value. For this setup the *sheath return method* was used. The solid aluminum sheath had a thickness of 1.5 mm. The diameter of the single strands was 2.5 mm. The CUT was located 54 cm to 77 cm above the laboratory floor. The measured conductor had no core conductor.

The voltage loops were placed on the surface of the cable resulting in a d_{VL} of 4 cm, which is similar to $0.6 \cdot d_{CUT}$. The current connection to the CUT was established by high current connectors. The cable was led through 2 loading transformers (turned off), which could have slightly affected the outcome.

Table 5.4: Temperature corrected resistance ratios of a 2500 mm², 6 segment copper *Milliken* conductor with oxidized strands at 50 Hz, *measured* and IEC recommended k_s values (Sample 2); actual measurement temperature $T = 20.4\,°C$; measurement length $l_{meas} = 8.35\,m$

setup of pick-up loops	R_{AC}/R_{DC} at 20 °C	R_{AC}/R_{DC} at 90 °C	k_s (measured)	k_s (acc. to IEC)
AVG (average of 4 loops)	1.10	1.05	0.26	-
Helical (9 turns)	1.11	1.06	0.27	-

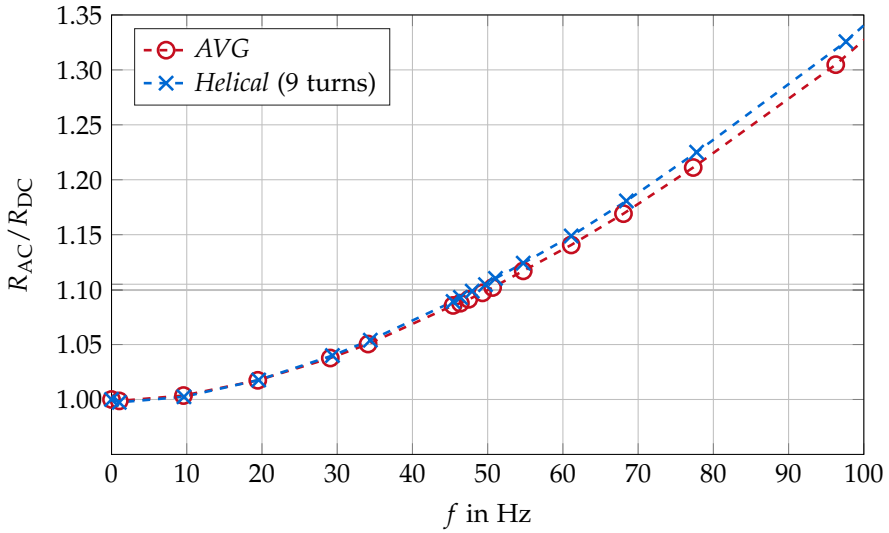

Figure 5.4: Resistance ratio curves of an oxidized 2500 mm² copper *Milliken* conductor at 20 °C for 2 different voltage pick-up loop setups (Sample 2); the corresponding resistance ratios at 50 Hz are marked on the vertical axis as well

SAMPLE CU-O-3 Table 5.5 and Figure 5.5 show the results of the measurement of another 2500 mm², 6 segment copper *Milliken* conductor with oxidized strands. Even though the oxide layers on the outer strands were only removed superficially on both terminals and the voltage tap-offs were only placed 15 cm behind the injection, the DC resistance showed good agreement to the calculated value. For this setup the *symmetrical return method* was used. The distance d between CUT and the return conductors was 70 cm. The CUT was located 45 cm to 50 cm above the ground. The measured conductor had a solid core conductor with a diameter of 1.36 cm.

The voltage loops were placed on the surface of the cable resulting in a d_{VL} of 3.52 cm, which is similar to $0.56 \cdot d_{CUT}$. The measurement setup corresponds to that shown in Figure 4.37.

Table 5.5: Temperature corrected resistance ratios of a 2500 mm², 6 segment copper *Milliken* conductor with oxidized strands at 50 Hz, *measured* and IEC recommended k_s values (Sample 3); actual measurement temperature $T \approx 20$ °C; measurement length $l_{meas} = 9.68$ m

setup of pick-up loops	R_{AC}/R_{DC} at 20 °C	R_{AC}/R_{DC} at 90 °C	k_s (measured)	k_s (acc. to IEC)
AVG (average of 4 loops)	1.43	1.27	0.63	-
Helical (16 turns)	1.46	1.29	0.65	-

In this measurement another configuration was tested, where all voltage lead loops of the *AVG* setup (*top*, *left*, *right*, *bottom*) have been connected at both ends. This configuration showed nearly identical results compared to the *AVG* setup. This should also be investigated in more detail in subsequent investigations, as one would then only need to perform one measurement instead of four separate measurements for the *AVG* setup.

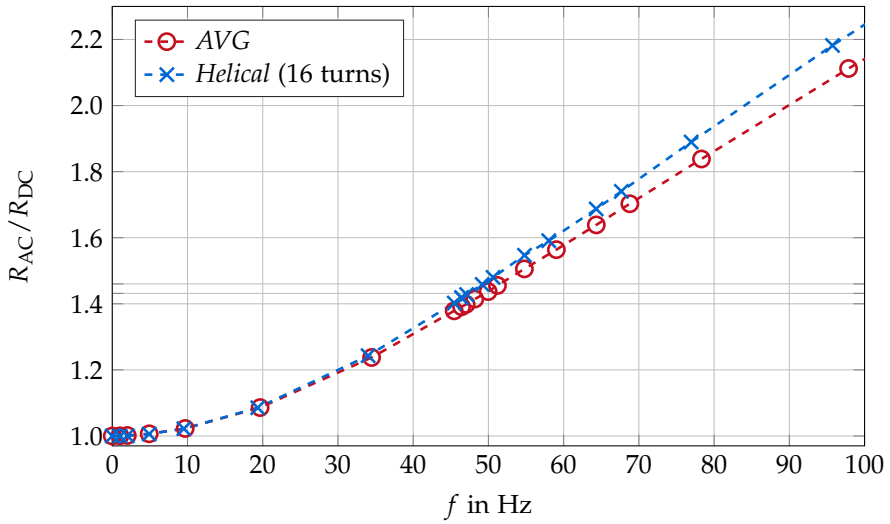

Figure 5.5: Resistance ratio curves of an oxidized 2500 mm² copper *Milliken* conductor at 20 °C for 2 different voltage pick-up loop setups (Sample 3); the corresponding resistance ratios at 50 Hz are marked on the vertical axis as well

5.1.2.3 *Enameled*

SAMPLE CU-E Table 5.6 and Figure 5.6 show the results of the measurement of a 2500 mm², 6 segment copper *Milliken* conductor with unidirectional pitch and enameled wires. The DC resistance showed good agreement to the calculated value. For this setup the *sheath return method* was used. The sheath consisted of a copper wire screen in combination with an aluminum sheath. The CUT was located at more than 1 m above the laboratory floor. The measured conductor had no core conductor.

The voltage loop was placed on the surface of the cable resulting in a d_{VL} of 3.9 cm, which is similar to $0.56 \cdot d_{CUT}$. At the time of the measurement it was not possible to perform the *AVG* setup. Moreover, the measurement length was only 3 m. The measurement setup corresponds to that shown in Figure 4.37 but only using one *helical* voltage loop.

Table 5.6: Temperature corrected resistance ratios of a 2500 mm², 6 segment copper *Milliken* conductor with enameled strands at 50 Hz, *measured* and IEC recommended k_s values; actual measurement temperature $T = 23.82\,°C$; measurement length $l_{meas} = 3\,m$

setup of pick-up loops	R_{AC}/R_{DC} at 20 °C	R_{AC}/R_{DC} at 90 °C	k_s (measured)	k_s (acc. to IEC)
Helical (4 turns)	1.220	1.126	0.38	0.35

The results show a slight upward deviation from the IEC standard. Nevertheless, the measurement length was only 3 m and as discussed in more detail in Section 4.2.5, it is questionable how the measurement length affects the results. Longer samples may perform differently.

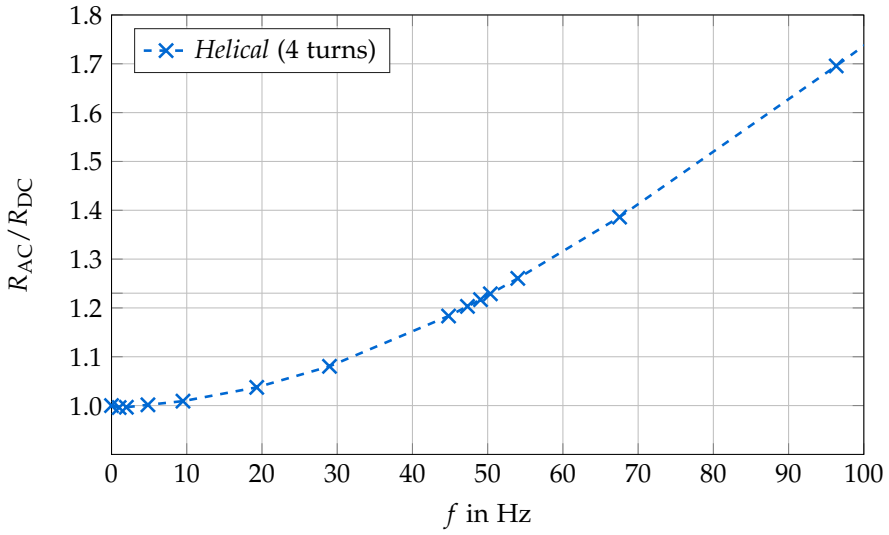

Figure 5.6: Resistance ratio curves of an enameled 2500 mm² copper *Milliken* conductor at 20 °C; the corresponding resistance ratio at 50 Hz is marked on the vertical axis as well

5.2 COMPARISON TO IEC STANDARD AND DISCUSSION OF RESULTS

All measurement results are plotted again in Figure 5.7 and compared to the IEC recommendation. It was already apparent in every section that the presented results differ from the IEC standard.

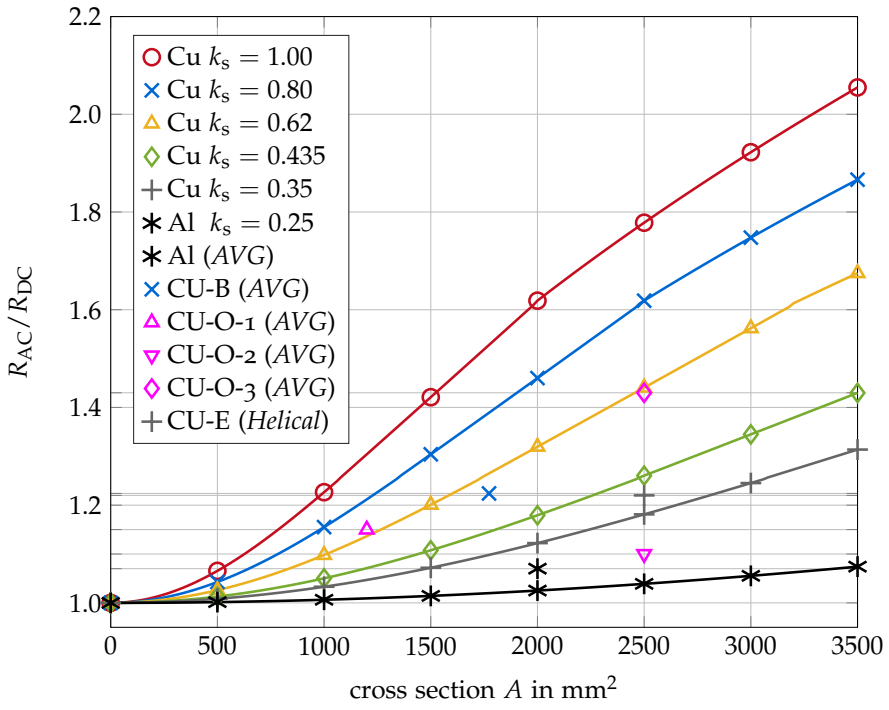

Figure 5.7: Resistance ratios at 50 Hz plotted over conductor cross section for different k_s factors at 20 °C according to IEC standard 60287-1-1:2006/AMD1:2014 including the results of the k_s factor measurements; the colors and styles of the markers show their belonging to the k_s factor; there is no recommendation for oxidized samples from the IEC

The following things can be concluded from the measurement results compared to the IEC standard recommendation:

- the aluminum conductor (AL) performed worse than expected;
- the blank copper conductor (CU-B), which experienced 88 heat cycles, performed better;
- the oxidized conductor CU-O-1 performed similar to the IEC recommendation for a copper *Milliken* conductor with unidirectional pitch;
- the oxidized conductor CU-O-2 performed even better than the recommendation for an enameled design;
- the oxidized conductor CU-O-3 also performed similar to the IEC recommendation for a copper *Milliken* conductor with unidirectional pitch;
- the enameled conductor (CU-E) performed slightly worse, where the measurement length was only 3 m however and may have influenced the outcome.

Again, these results should not be used to rate different *Milliken* conductor designs. The performance of each design strongly depends on the manufacturing process and quality and can vary for every other sample and maybe even along the sample length. Moreover, many other design choices influence the results. The consequence of these results is that an AC resistance measurement should be performed in any case, as the results can differ significantly from the recommendation by the IEC standard.

Figure 5.8 shows all measurement results up to a frequency of 300 Hz.

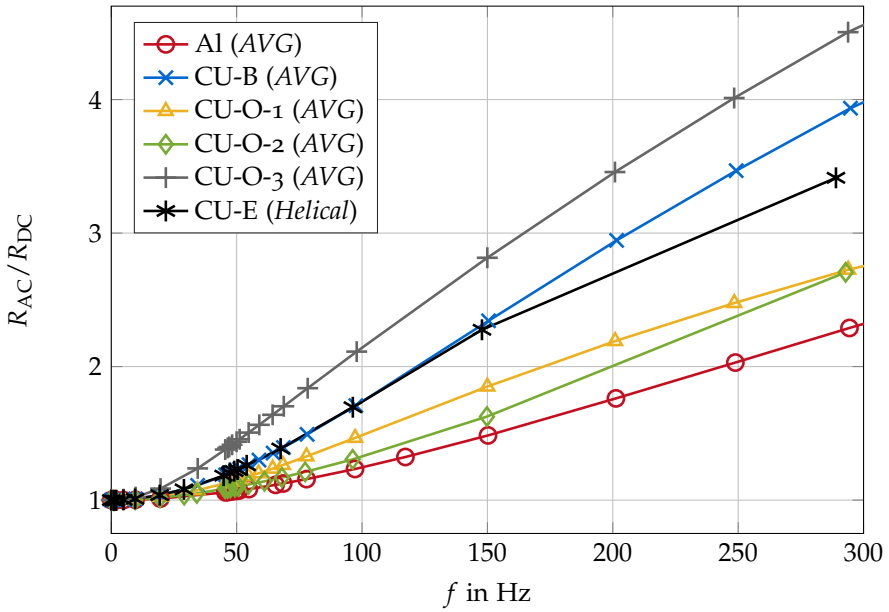

Figure 5.8: Resistance ratio of all measurements up to 300 Hz at 20 °C

Extended investigations on different *Milliken* conductor designs showed large deviations from the Bessel function, used for a cylindrical isolated conductor, at frequencies between 300 Hz and 1000 Hz. This is expected as multiple insulated conductors interacting with each other will introduce

higher order Bessel functions [Dwi23a]. The curves look similar to the ones shown for litz wires in [Alb17, Abb. 4.28] but already far below 1000 Hz.

What could also be observed in measurements is that in all cases, where the *sheath return method* was used, outer magnetic fields existed. Larger loops still affected the results, more specifically the reactance and resistance. In turn this means that the setup was not perfectly concentric, either geometrically or from the current distribution point of view. Only this condition could suppress outer fields as discussed earlier. But, due to allowed asymmetries in the sheath design, this was also expected from the previous findings.

Helical voltage loops with many turns showed good agreement to *AVG*. In all cases the deviation of the *helical* configuration to the *AVG* setup was smaller than the maximum differences between the separate pick-up loops (*top*, *left*, *bottom*, *right*) at 50 Hz.

6 CONCLUSION

I think and think for months and years.
Ninety-nine times, the conclusion is false.
The hundredth time I am right.
Albert Einstein

This chapter summarizes the outcomes of this thesis. First the main results of each chapter are concluded. Some of them are then further discussed. At the end, the limits of this thesis are shown and a recommendation for further research is given in the outlook.

6.1 SUMMARY

The main purpose of this work was to research, if and how an accurate AC loss measurement can be performed on power cables with large cross sections using the electrical measurement method.

Chapter 1 introduces the underlying problematic and defines the target value of this thesis, the isolated *Joule* losses of the inner conductor of a power cable. Then, the recent standards for power cable ratings are presented, which recommend the measurement of the AC resistance, but also provide empirical formulas for the AC resistance calculation. Afterwards, available measurement methods are presented, namely the calorimetric method and different electrical measurement methods. The latter is used in this work as it offers logistical advantages over the calorimetric approach. At the end of Chapter 1, the need for accurate AC resistance measurements is outlined again, by showing how AC losses can vary due to manufacturing quality. The measurement is of great importance, as the AC resistance of a cable is a critical parameter for the design of a cable system.

Chapter 2 describes the used measurement system in detail after listing some definitions and important terms at the beginning. It could be shown that the accuracy of the used system is high enough to distinguish different relevant effects in the measurement. It is then demonstrated how measurement values are interpolated and also how they are corrected to a desired temperature for evaluation. This is followed by reviewing the used simulation technique: the FEM in *Comsol Multiphysics*. Chapter 2 is concluded with a short overview and comparison of the available methods for the determination of *Joule* losses of a conductor. It is best to combine analytical formulas, simulations—such as the FEM—and measurements to obtain research results that come as close as possible to the *true* losses of a conductor.

Chapter 3 first presents some milestones of the research on AC losses and reasons that the MQS approximation can be used for the subsequent investigations. After a description of *skin effect* and *proximity effect*, some further concepts of AC loss mechanisms are introduced. A revised collection of analytical formulas is presented in detail and followed by some approximate formulas and a comparison of current distribution and AC resistances

of different cross sectional shapes. At the end, Chapter 3 displays the development and structure of power cable conductors, specifically stranded and *Milliken* conductors. Using copper as the conductor material, the latter can be subdivided into three different designs: blank, oxidized or enameled strands and is able to reduce AC losses significantly.

Chapter 4 points out what is actually being measured using an ADC AC voltmeter. At AC, it is the total electric field intensity over the internal measurement resistance, which is composed of the line integral of the electric field between both voltage tap-offs on the CUT and an inductive part caused by the alternating magnetic field present in the pick-up loop. In case of complex cross sectional conductor shapes or if other conductive parts are nearby, this magnetic field can become complex and influence the *measured* resistive voltage drop. The resistance measurement then depends on the location and geometric dimension of the pick-up loop. It was shown that all complex magnetic fields originating from the CUT have to be included in the voltage pick-up loop to account for the *true* losses of the CUT. Most important, even for insulated conductors the electrical measurement method is able to obtain the overall *true* losses of a conductor section, through the information stored in the complex magnetic field in the pick-up loop. For stranded and segmental conductors, whose current density distribution is expected of being nearly rotationally symmetric, the necessary radial extension of the pick-up loop—to capture sufficient complex magnetic field—is expected to be achieved at a distance identical to the diameter of the CUT. For typical measurement setups it was then shown that it is easy to avoid an influence of the return conductor on the *true* losses of the CUT, by increasing the spacing between both. For these setups, *measured* losses were compared to the *true* losses of the CUT for different positions of the pick-up loops. It could be shown that taking the average of 4 pick-up loops homogeneously arranged around the circumference of a CUT, delivers results of sufficient accuracy in every setup even for small loop sizes. Current homogenization and the placement of the voltage tap-offs are closely related. From the investigations performed, it was inferred that for the measurement, the terminals of a power cable with insulated strands should be blank. This has the advantage of enabling quick current homogenization along the conductor axis—which is a necessary requirement for representative results—on one hand and at the same time provide a defined position for the voltage tap-offs. With this, one avoids having to connect the voltage tap-offs to the exact same strand at both terminals. In practice however, it is often sufficient to check, if the method used for current injection and the position of the voltage tap-offs deliver the expected DC resistance. If this is the case, the chosen method is adequate for the AC resistance measurement as well. At the end of Chapter 4 a recommendation for preparation of the CUT, setup and procedure for the AC loss measurement is given. Using two symmetrical return conductors with a spacing larger than 0.5 m in combination with averaging the results obtained by 4 pick-up loops located at the surface of the cable, leads to results, which are sufficiently close to the *true* resistance of a *Milliken* conductor.

Chapter 5 shows measurement results of some *Milliken* conductor designs, which were obtained by applying the recommended techniques. It was shown that the measured values often did not coincide with the values

recommended by the recent IEC standard. This supports the demand for performing AC resistance measurements on power cable conductors to ensure that the expected or required AC resistance is met.

6.2 DISCUSSION AND OUTLOOK

COMMENTS ON METHODOLOGY AND PERFORMED INVESTIGATIONS

For the simulations performed in this thesis the well-established FEM technique was used. Comparisons with different analytical solutions showed the excellent agreement between both. For simple conductor shapes—such as a circular cross section—both results could also be verified by measurement. At the moment, a measurement is the only reliable approach to determine the AC resistance of a *Milliken* conductor, if performed properly. It is hence reasonable to benchmark the measurement by analytical calculations and FEM simulations prior to measurements of *Milliken* conductors. In practice, analytical solutions and the FEM are no suitable methods for the AC resistance determination of a *Milliken* conductor. True 3D FEM simulations of segmental conductors are not feasible at the moment due to restrictions in hardware resources and the lacking knowledge of some manufacturing influences on the design. The simulations of different measurement setups in this thesis therefore used a solid circular copper conductor as the CUT. It was shown that in general stranded conductor designs have lower *proximity effect* losses compared to solid conductors. Even though stranded and *Milliken* conductors still show *proximity effect* [Joa99], the results displayed in this thesis therefore possibly show stronger impacts on the measurement than present in a real measurement. On the other hand, asymmetries in the geometry of the setup and unknown factors from real setups, such as the exact geometry and electrical properties of laboratory floors or walls having rebars for example, could only be included in the simulations exemplarily. A previous example showed that a metallic fence placed 2 m from the CUT still significantly influenced the measurement of a rectangular conductor. Also deviations from the symmetric placement of the pick-up loops relative to the setup were not part of the investigations either. In addition to that, some possible geometric variations caused by the manufacturing process like ovality of the cable or the displacement of segments were not researched as well.

To differentiate between different effects in the measurement, possible geometric variations have mostly been analyzed separately. In reality, multiple effects could act upon the measurement at once, having stronger or different influences on the pick-up loops than indicated by the simulations. Nevertheless, using at least 4 pick-up loops to average the results showed to be a quite robust method against geometric asymmetries. It is also evident that in reality not every pick-up loop configuration shown in the simulation results can be realized in practice. For example when measuring a cable, one cannot simply place the voltage lead wires beneath the sheath. Also in case of *Setup III—symmetric return method*—the voltage pick-up loops on the sides of the closely spaced return conductors can of course not be routed through the return conductors. In Appendix A.2 it is shown that this does not present a limitation for the *AVG* setup. To resolve this issue, all pick-up loops or the return conductor can be rotated relative to the center of the CUT still delivering accurate results.

One additional remark about the *AVG* setup concerns the positioning of them on cables. The radial distance of the voltage loops d_{VL} is defined from the surface of the CUT. When analyzing *apparent* losses for the evaluation of the average value, the results at the same distances were used. But, the exact position of the CUT in a cross section of a cable is not known exactly due to eccentricity. Hence, the pick-up loops attached to the surface of the complete cable may have different distances d_{VL} to the surface of the CUT. Hence in reality, the *AVG* is maybe comprised of $top(d_{\mathrm{VL}})$, $bottom(d_{\mathrm{VL}})$, $right(d_{\mathrm{VL}} + 2\,\mathrm{mm})$ and $left(d_{\mathrm{VL}} - 2\,\mathrm{mm})$. When looking at the change in every setup for distances of 2 mm—which is the allowed maximum eccentricity—one can see that the error introduced by that is negligible.

When the *measured* resistance has to be evaluated at a different temperature than it was measured at, the resistance has to be adjusted. A way of doing that was shown in Section 2.4.2. It is based on the observation that different temperatures also change the conductivity of the sample. The conductivity in turn influences its AC losses. Hence, the ratio of AC to DC resistance changes with temperature. If geometric parameters of the conductor remain unchanged, this method can accurately correct the resistance from measurement temperature to the desired evaluation temperature. But, in case of conductors with insulated wires it is not clear at the moment if the interwire contact resistances also vary at higher temperatures. If so, this could equal a change in geometry. Assuming that the interwire resistances decrease with temperature, would turn a conductor with insulated wires into a solid conductor, which increases AC losses in return.

In publications authors should describe their setup in every detail, to increase reproducibility and classification of the presented results of *Milliken* conductor measurements. Especially the influence of the position of the voltage pick-up loop should be discussed more deeply.

COMMENTS ON THE MEASUREMENT RESULTS It was not possible to follow every recommendation in all measurements shown in Chapter 5. Some measurements were already performed parallel to open investigations. Nevertheless, additional FEM simulations for these specific setups and comparisons of possible influences to measurements performed according to the recommendation, helped increasing the trust in the results shown. For every measurement it was described in detail how the setup was build to increase transparency. Moreover, even though the results are of high accuracy, their only purpose is to give examples of the performance of different designs, as they only present a small empirical sample for this design type (blank, oxidized, ...). Samples of different manufacturers having the same design, can differ significantly in performance as argued previously.

Concerning the positioning of the voltage tap-offs it was often sufficient in the measurement to place the voltage tap-offs 0.5 m to 2 m away from the current injection on the blank surface of the segments. The calculated DC resistance was met even in enameled designs, where the current was only injected into one strand at the terminals. This means that many interwire contact resistances were present to guarantee the homogenization over all strands. Methods like this can therefore be used to check the functionality of the design itself. Nevertheless, the exact DC resistance of a *Milliken*

conductor can also not be calculated in advance as the exact helical paths of the strands and possible contacts between them are unknown.

Moreover, it was stated by some manufacturers that the cable geometry and performance of the CUT can vary along the whole cable and can be unique for every section. Assuming these variations are significant, this would mean that multiple short samples of a production length have to measured to obtain a result of statistical relevance. This however does not seem to be realizable in practice. This issue is similar to the topic of *Minimum Necessary Measurement Length* and presents a general challenge for every measurement method. Both issues can only be resolved when the complete production length is measured. This observation seems to increase the demand for a measurement on a cable drum, which does not seem feasible at the moment due to the inclusion of *proximity effect* and magnetic stray fields on the drum, which is often metallic because of mechanical constraints. In addition to that, it is also not clear how drumming and bending of the cable affects the performance, more specifically the insulation of the single strands of *Milliken* conductors. A measurement of the complete manufacturing length when buried on site would deliver the most accurate result. Despite considerations on how to realize such a measurement setup, this is also not a desired solution. If the measurement would deliver an AC resistance, which does not meet the demanded requirements, this would have to result in an exchange of the already buried cable.

A better solution would be to come as close as possible to the *true* resistance by measuring short samples in the laboratory, after performing additional investigations on *Milliken* conductors, which clarify the influence of the effects discussed above.

OUTLOOK This section is based on the discussion and presents ideas on further research, which is necessary—in the eyes of the author—to increase trust and accuracy of AC resistance measurements.

This includes the following:

- A comparison of electrical measurement methods and the calorimetric measurement method. Even though both techniques are used in practice, a direct comparison on a *Milliken* conductor at different temperatures is desired. This includes an estimate on the accuracy of both methods. Compliance of the measurement results would boost the trust in both methods and help the user to focus on the advantages of the approaches only, when selecting an appropriate method.
- For the same reason, a comparison of the typically used electrical measurement methods should be performed: using lock-in amplifiers on one hand and using AC ADC voltmeters on the other hand.
- The enunciated temperature correction method should be checked for applicability on *Milliken* conductors by performing measurement at different temperatures. This would answer the question of whether the insulation of the single wires is affected by temperature changes. This question needs to be answered for different conductor materials and designs.

- The remaining parameters influencing the *measured* resistance should be checked for their influence. This can be done by FEM simulations and includes:
  - The ovality of a cable and of the inner conductor.
  - The displacement of segments in *Milliken* conductors.
  - The losses induced in the pick-up loops by armored cable sheaths.
- Different lengths of conductor samples should be measured to check for the influence of the length upon the AC resistance.
- Also, the effect of drumming the cable should be investigated empirically by measuring a conductor before and after it has been on a drum. This should also be done with different designs, as the mechanical stress can possible influence enameled wires differently compared to oxidized strands for example.
- Further investigations regarding the AC resistance measurement on a drum are required to check if measuring a whole production length may be possible under certain conditions or using special precautions.
- Further theoretical considerations, FEM simulations and measurements could justify or reject the idea of using only one helically wound voltage loop instead of 4 voltage loops, whose results are averaged. This could save time and increase efficiency of the electrical method further. The idea of using the cable sheath as the rear voltage lead wire should also be investigated further together with the possibility of short-circuiting all 4 loops of the *AVG* setup on both sides.
- Long-term behavior of conductors with insulated strands should also be investigated, as thermal induced mechanical stress can possibly reduce interwire resistances and increase losses over the lifetime of a cable. Nevertheless, for blank conductors oxidization of the strands could also appear and increase the performance in long-terms.

A ADDITIONAL CONTENT

No man has the right to be an amateur in the matter of physical training. It is a shame for a man to grow old without seeing the beauty and strength of which his body is capable.

Socrates

A.1 PUBLISHED RESULTS OF MILLIKEN CONDUCTOR MEASUREMENTS

Regarding Table A.1: the k_s factor could not be calculated in most cases because often the DC resistance or lengths was not available. Moreover, if no frequency was given, the typical power frequency of the country, where the investigation was performed was assumed. If no temperature was given in the reference, then 20 °C was used and the "operating temperature" in [BM68] was assumed to be 90 °C. "Dis" in the reference stands for discussion, "4s" stands for 4 segments and so forth, "hp" stands for high pressure, "lp" for low pressure, "contra." stands for contradirectional and "uni." for unidirectional stranding of the different layers.

Table A.1: Collection of published R_{AC}/R_{DC} ratios for *Milliken* conductors (no *proximity effect* regarded)

A in mm^2	material	design/ insulation	f in Hz	T in °C	R_{AC}/R_{DC}	reference
1015	Al	blank	60	23	1.02	[Kat+78]
1015	Cu	blank	60	23	1.13	[Kat+78]
1015	Cu	blank	60	23	1.16	[Kat+78]
1015	Cu	blank	60	23	1.06	[Kat+78]
1015	Cu	blank	60	23	1.08	[Kat+78]
1015	Cu	blank	60	23	1.09	[Kat+78]
1015	Cu	enameled	60	23	1.05	[Kat+78]
1015	Cu	lead alloy	60	23	1.07	[Kat+78]
1015	Cu	lead alloy	60	23	1.09	[Kat+78]
1015	Cu	lead alloy	60	23	1.08	[Kat+78]
1015	Cu	tin	60	23	1.06	[Kat+78]
1200	Cu	blank	50	20	1.15	[Cig05, p. 14]
1269	Cu	blank	60	20	1.113	[Wis48]
1269	Cu	blank	60	23	1.2	[Kat+78]
1269	Cu	blank	60	23	1.1	[Kat+78]
1269	Cu	blank	60	23	1.08	[Kat+78]
1269	Cu	blank	60	23	1.07	[Kat+78]
1269	Cu	blank	60	80	1.07	[Wis48]
1400	Al	blank	50	90	1.05	[BM68]
1400	Cu	blank	50	20	1.18	[Cig05, p. 14]

1400	Cu	blank, contra.	50	90	1.18	[BM68]
1400	Cu	blank, uni.	50	90	1.13	[BM68]
1400	Cu	enameled	50	90	1.07	[BM68]
1400	Cu	sulphurated	50	90	1.15	[BM68]
1600	Cu	blank	50	20	1.23	[Cig05, p. 14]
1600	Cu	blank	50	20	1.04	[CMR77, Dis]
1600	Cu	blank	50	90	1.25	[DM07]
1600	Cu	blank (4s)	50	18	1.34	[BSF99]
1600	Cu	blank (5s)	50	27	1.11	[BSF99]
1600	Cu	blank (6s)	50	33	1.25	[BSF99]
1600	Cu	enameled	50	20	1.03	[Cig05, p. 14]
1600	Cu	enameled	50	90	1.04	[DM07]
1600	Cu	enameled (6s)	50	26	1.02	[BSF99]
1600	Cu	oxidized	50	20	1.07	[Cig05, p. 14]
1776	Cu	tin	60	23	1.17	[Kat+78]
1920	Cu	blank	50	20	1.33	[Cig05, p. 14]
2000	Al	blank, contra.	50	80	1.025	[CMR77]
2000	Al	blank, contra.	50	80	1.026	[CMR77]
2000	Cu	blank	50	20	1.34	[Cig05, p. 14]
2000	Cu	blank	50	20	1.27	[Cig05, p. 14]
2000	Cu	blank	50	20	1.24	[Cig05, p. 14]
2000	Cu	blank	50	20	1.378	[RSS11a]
2000	Cu	blank	50	20	1.328	[RSS11a]
2000	Cu	blank	50	20	1.495	[RSS11a]
2000	Cu	blank	50	20	1.448	[RSS11a]
2000	Cu	blank	50	80	1.16	[Joa98, p. 55]
2000	Cu	blank	50	80	1.23	[Joa98, p. 55]
2000	Cu	blank	50	80	1.232	[Joa98, p. 55]
2000	Cu	blank	50	85	1.359	[RSS11a]
2000	Cu	blank	50	90	1.35	[DM07]
2000	Cu	blank	50	90	1.352	[RSS11a]
2000	Cu	blank, contrad.	50	80	1.25	[CMR77]
2000	Cu	Cr-plated, contra.	50	80	1.15	[CMR77]
2000	Cu	enameled	50	20	1.04	[Cig05, p. 14]
2000	Cu	enameled	50	90	1.04	[DM07]
2000	Cu	enameled, contra.	50	80	1.1	[CMR77]
2000	Cu	enameled, contra.	50	80	1.05	[CMR77]
2000	Cu	oxidized (hp)	50	80	1.137	[Joa98, p. 55]
2000	Cu	oxidized (lp)	50	80	1.086	[Joa98, p. 55]
2072	Cu	blank	50	20	1.568	[RSS11a]
2385	Al	blank	60	23	1.05	[Kat+78]
2500	Cu	blank	50	20	1.36	[Cig05, p. 14]
2500	Cu	blank	50	80	1.2	[Joa98, p. 57]
2500	Cu	blank	50	90	1.45	[DM07]
2500	Cu	blank, contra.	50	80	1.232	[Joa98, p. 57]

2500	Cu	enameled	50	20	1.02	[Cig05, p. 14]
2500	Cu	enameled	50	90	1.065	[DM07]
2500	Cu	oil impregnated	50	80	1.14	[Joa98, p. 57]
2500	Cu	oil impregnated	50	80	1.151	[Joa98, p. 57]
2500	Cu	oxidized	50	20	1.08	[Cig05, p. 14]
2500	Cu	oxidized (hp)	50	80	1.23	[Joa98, p. 57]
2500	Cu	oxidized (lp)	50	80	1.152	[Joa98, p. 57]
2600	Cu	blank	50	20	1.1	[CMR77, Dis]

A.2 EXTENDED DISCUSSION ON AC LOSS MEASUREMENTS

Figure A.1 presents results of the *virtual* measurement on an hypothetical conductors with 4 insulated strands and two solid terminals. The current flows in z-direction and is homogeneously injected at both terminals.

Both models shown, consist of two solid terminals with an overall radius $r \approx 2.8\,\text{cm}$ and 4 strands in between them, which are insulated from one another by air. The current is injected into the face of one terminal, whereas the other terminal's cross section is grounded. In Model 1, all strands are electrically connected to both terminals. Therefore, the current flows from one terminal to the other over all strands. In Model 2, there is a small gap between the strand at the bottom side and the rearward terminal. Therefore, the measurement current will not flow through this strand from one terminal to the other. Nevertheless, *eddy currents* will build up in this strand due to the alternating electromagnetic fields from the other strands.

The *measured* resistance will eventually converge against the *true* resistance of the measured section in both cases. For Model 2 this means that the losses due to *eddy currents* in the bottom strand are also included. One can see that due to the large asymmetry of the models, $d_{\text{VL,min}}$, which is the distance to reach a deviation smaller than 1 % to the *true* resistance, is much larger than $3 \times r \approx 8.4\,\text{cm}$ in this case.

Another interesting case is that of two closely spaced conductors:

- If the conductors are connected in a *return circuit*, the *measured* resistance will converge against the *true* resistance of only this conductor, to which the voltage tap-offs are attached to (the CUT). Losses from the return conductors will not be included at very large d_{VL} anymore.
- If the conductors are in a *go circuit*—connected in parallel—the *measured* resistance converges against the *true* resistance of the measured section with increasing d_{VL}, which includes the losses of both conductors. This is consistent and also observed in the example of the 4 strand bundle above. For 2 unequal conductors, the separation of losses is a complex task (see Section 4.4.3).

In both cases, taking the average of the 4 pick-up loops $left$, $right$, top and $bottom$ will converge against the *true* resistance much quicker, than any of the above configurations separately. As long as the 4 pick-up loops are distributed homogeneously around the CUT's circumference (every 90° resulting in $left$, $right$, top and $bottom$), independent of the relative position of

the return conductor, by using the *AVG* setup the result quickly converges against the *true* losses of the CUT only.

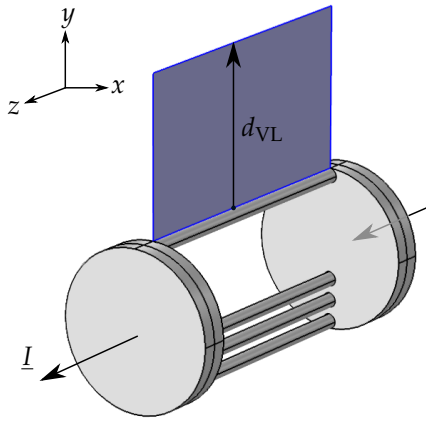

(a) Model 1: all 4 strands are connected through, pick-up loop in blue

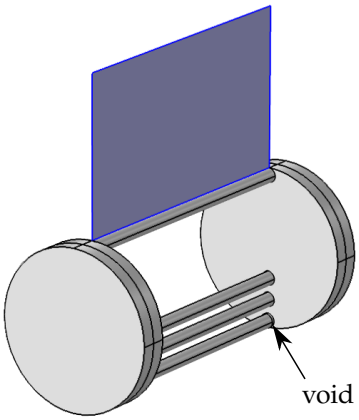

(b) Model 2: the bottom strand is not connected through, pick-up loop in blue

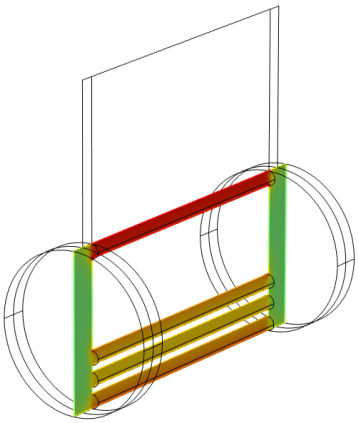

(c) Model 1 - $||\boldsymbol{J}||$ in the center plane

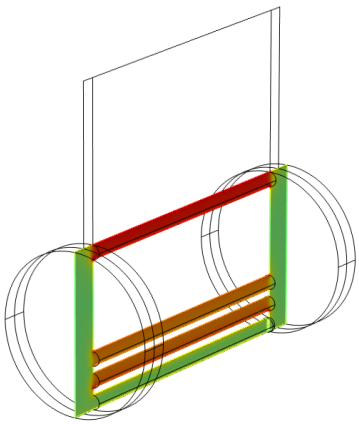

(d) Model 2 - $||\boldsymbol{J}||$ in the center plane

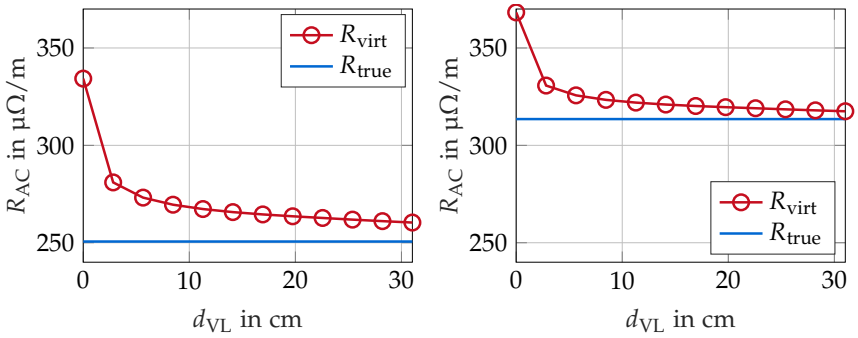

(e) *left:* convergence of *virtual* resistance in model 1; *right:* convergence of *virtual* resistance in model 2

Figure A.1: Results of additional investigations on stranded conductors; R_{true} are the overall losses in all small strands only (middle section); the simulation was performed at 500 Hz, the terminals for current injection have a cross section of 2500 mm^2; the small strands have a radius of 2.5 mm; the coordinate system in Figure A.1a is valid for all other figures as well

B

MATLAB CODE FOR ANALYTICAL FORMULAS

> Greatness is not a measure of how great you are
> but how great others came to be because of you.
> *Cus D'Amato*

The results obtained with the following *Matlab* codes have been tested and verified by comparison with FEM simulations in *Comsol Multiphysics*.

B.1 INFINITIVELY WIDE STRIP

Listing B.1: *Matlab* code for the resistance caluclation of an infinitively wide strip

```
%     Script to calculate the current density,
%     resistancea and reactance ratio of an
%     Infinitively Wide Strip
%     Date: 2016-10-20 - 12:40  / Author: Rene Suchantke

% Constants
mu_0            = 4*pi*1E-7         ;       % vacuum permability
% Input Parameters
f               = 0:1:300           ;       % frequency / Hz
sigma           = 58E6              ;       % conductivity / S/m
t               = 0.02              ;       % thickness of strip / m
mu_r            = 1                 ;       % permeability
% Calculation of Variables
y               = -t/2:t/100:t/2    ;       % generation of y-coordinate
omega           = 2*pi.*f           ;       % angular frequency / Hz
% Conversion to cgs units for use in orignal formulas
sigma           = sigma/(1E11)      ;       % [S/m]-->[abmhos/cm]=[GS/cm]
t               = t*100             ;       % [m]-->[cm]
y               = y*100             ;       % [m]-->[cm]
% Calculation of alpha
alpha           = sqrt(2*pi*sigma.*omega*mu_r)...
                  +(1i*sqrt(2*pi*sigma.*omega*mu_r));
% Current Density at 50 Hz normalized to the surface current density
J_ratio         = cosh(alpha(51).*y)/cosh(alpha(51)*(t/2));
% Resistance Ratio
R_ratio         = real((alpha*t)./...
                  (2*tanh((alpha*t)/2)));
R_ratio(1)      = 1;
% Reactance Ratio
X_ratio         = imag((alpha*t)./...
                  (2*tanh((alpha*t)/2)));
```

B.2 SOLID CYLINDRICAL CONDUCTOR

Listing B.2: *Matlab* code for the resistance caluclation of a solid cylindrical conductor

```
%     Script to calculate the current density,
%     resistancea and reactance ratio of a
%     Solid Cylindrical Conductor
%     Date: 2016-10-01 - 13:56  / Author: Rene Suchantke

% Constants
mu_0            = 4*pi*1E-7         ;       % vacuum permability
% Input Parameters
f               = 0:1:1000          ;       % frequency / Hz
sigma           = 58E6              ;       % conductivity / S/m
r_c             = 0.02              ;       % conductor radius / m
mu_r            = 1                 ;       % permeability
I               = 1                 ;       % conductor current / A
% Calculation of Variables
r               = -r_c:r_c/100:r_c  ;       % generation of r-coordinate
omega           = 2*pi.*f           ;       % angular frequency / Hz
R_DC            = 1/(sigma*pi*r_c^2);       % DC resistance / Ohm/m
L_DC            = mu_0*mu_r/(8*pi)  ;       % DC inductance / H/m
% Calculation of Function Argument m
m               = sqrt(-1i*omega*mu_0*mu_r*sigma);
% Current Density at 50 Hz Normalized to the DC Current Density
% by using the Bessel Function of the First Kind
J_AC            = (m(51)*I/(2*pi*r_c))*(besselj(0,m(51)*r)./...
                                        besselj(1,m(51)*r_c));
J_DC            = I/(pi*r_c^2);             % DC current density / A/m^2
J_ratio         = real(J_AC)/J_DC;          % current density ratio(50Hz)
% Resistance Ratio Calculated with Bessel Function of the First Kind
R_ratio   = real(((m*r_c/2).*besselj(0,m*r_c)./besselj(1,m*r_c)));
R_ratio(1)= 1;
% Inductance Ratio Calculated with Bessel Function of the First Kind
L_ratio         = (R_DC*8*pi./(omega.*mu_r*mu_0)).*...
           imag(((m*r_c/2).*besselj(0,m*r_c)./besselj(1,m*r_c)));
L_ratio(1)      = 1;
%% Additional Verification with Kelvin Function Formulas
k         = real(m)*sqrt(2);            % argument of Kelvin functions
% Generating the Kelvin Functions and Their Derivatives
v         = 0;                          % Order of Kelvin functions
ber_v     = real(besselj(v,k*r_c*exp(1i*3*pi/4))); % Generating Ber
bei_v     = imag(besselj(v,k*r_c*exp(1i*3*pi/4))); % Generating Bei
berD_v    = (real(besselj(v+1,k*r_c*1i*sqrt(1i)))+...
             imag(besselj(v+1,k*r_c*1i*sqrt(1i))))/sqrt(2)+...
             (v./k).*real(besselj(v,k*r_c*1i*sqrt(1i)));% Generating Ber'
beiD_v    = (imag(besselj(v+1,k*r_c*1i*sqrt(1i)))-...
             real(besselj(v+1,k*r_c*1i*sqrt(1i))))/sqrt(2)+...
             (v./k).*imag(besselj(v,k*r_c*1i*sqrt(1i)));% Generating Bei'
% Resistance Ratio Calculated with Bessel Function of the First Kind
R_ratio_V    = k*r_c/2.*...
           ((ber_v.*beiD_v)-(bei_v.*berD_v))./(berD_v.^2+beiD_v.^2);
R_ratio_V(1) = 1;
% Reactance Ratio Calculated with Bessel Function of the First Kind
L_ratio_V    = (R_DC*8*pi./(omega.*mu_r*mu_0)).*...
      k*r_c/2.*((ber_v.*berD_v)+(bei_v.*beiD_v))./(berD_v.^2+beiD_v.^2);
L_ratio_V(1) = 1;
% Principle of Similitude Parameter
```

```
p            = sqrt(f/R_DC).*1e-3;


R_AC_50 = R_ratio(51)*R_DC
X_AC_50 = L_ratio(51)*L_DC*2*pi*f(51)
```

B.3 TUBULAR CONDUCTOR

Listing B.3: *Matlab* code for the resistance caluclation of a tubular conductor

```
%     Script to calculate the current density,
%     resistancea and reactance ratio of a
%     Tubular Conductor
%     Date: 2017-01-10 - 17:56  / Author: Rene Suchantke

% Constants
mu_0            = 4*pi*1E-7         ;       % vacuum permability
% Input Parameters
f               = 0:1:1000          ;       % frequency / Hz
sigma           = 58E6              ;       % conductivity / S/m
r2              = 0.025;                    % outer conductor radius / m
r1              = 0.0125;                   % inner conductor radius / m
A               = pi*(r2^2-r1^2);           % cross section / m^2
mu_r            = 1                 ;       % permeability
% Calculation of Variables
omega           = 2*pi.*f           ;       % angular frequency / Hz
R_DC            = 1/(A*sigma)       ;       % DC resistance / Ohm/m
% Definition of variables according to AC calculation formula
k               = sqrt(2*pi*f*mu_r*mu_0.*sigma);
% Creation of Kelvin function arguments
kr_1            = k*r1;
kr_2            = k*r2;
% Current Density: Import of Comsol Results
r               = -r2:2*r2/192:r2  ;       % generation of r-coordinate
fileID =fopen('Tube50Hz.txt','r');
formatSpec = '%f %f';
B = fscanf(fileID,formatSpec);
n = 1;
for i=1:2:length(B)-1
    J_ratio(n)=B(i+1);
    rn(n)      =B(i);
    n = n+1;
end
% creating the kelvin functions with argument mr_1:
v               = 0;        % Order of the functions
ber_mr1         = real(besselj(v,kr_1*exp(3*pi*1i/4)));
bei_mr1         = imag(besselj(v,kr_1*exp(3*pi*1i/4)));
ker_mr1         = real(exp(-v*pi*1i/2)*besselk(v,kr_1*exp(pi*1i/4)));
kei_mr1         = imag(exp(-v*pi*1i/2)*besselk(v,kr_1*exp(pi*1i/4)));
% creating their derivatives - taken from:
v               = 1;        % Order of the functions
ber_mr1_diff1   = (real(besselj(v,kr_1*1i*sqrt(1i)))+...
                    imag(besselj(v,kr_1*1i*sqrt(1i))))/sqrt(2);
bei_mr1_diff1   = (imag(besselj(v,kr_1*1i*sqrt(1i)))-...
                    real(besselj(v,kr_1*1i*sqrt(1i))))/sqrt(2);
ker_mr1_diff1   = ( real(exp(-v*pi*1i/2)*besselk(v,kr_1*exp(pi*1i/4)))
    +...
```

```
                imag(exp(-v*pi*1i/2)*besselk(v,kr_1*exp(pi*1i/4))))/sqrt
                    (2);
kei_mr1_diff1   = (-real(exp(-v*pi*1i/2)*besselk(v,kr_1*exp(pi*1i/4)))
    +...
                imag(exp(-v*pi*1i/2)*besselk(v,kr_1*exp(pi*1i/4))))/sqrt
                    (2);
% creating the constant variable
C               = (ber_mr1_diff1 + 1i.*bei_mr1_diff1)./...
                  (ker_mr1_diff1 + 1i.*kei_mr1_diff1);
% creating the kelvin functions with argument mr_2:
v               = 0;        % Order of the functions
ber_mr2         = real(besselj(v,kr_2*exp(3*pi*1i/4)));
bei_mr2         = imag(besselj(v,kr_2*exp(3*pi*1i/4)));
ker_mr2         = real(exp(-v*pi*1i/2)*besselk(v,kr_2*exp(pi*1i/4)));
kei_mr2         = imag(exp(-v*pi*1i/2)*besselk(v,kr_2*exp(pi*1i/4)));
% creating their derivatives
v               = 1;        % Order of the functions
ber_mr2_diff1   = (real(besselj(v,kr_2*1i*sqrt(1i)))+...
                    imag(besselj(v,kr_2*1i*sqrt(1i))))/sqrt(2);
bei_mr2_diff1   = (imag(besselj(v,kr_2*1i*sqrt(1i)))-...
                    real(besselj(v,kr_2*1i*sqrt(1i))))/sqrt(2);
ker_mr2_diff1   = ( real(exp(-v*pi*1i/2)*besselk(v,kr_2*exp(pi*1i/4)))
    +...
                imag(exp(-v*pi*1i/2)*besselk(v,kr_2*exp(pi*1i/4))))/sqrt
                    (2);
kei_mr2_diff1   = (-real(exp(-v*pi*1i/2)*besselk(v,kr_2*exp(pi*1i/4)))
    +...
                imag(exp(-v*pi*1i/2)*besselk(v,kr_2*exp(pi*1i/4))))/sqrt
                    (2);
% put togehter the single parts of the equation
numerator       = ber_mr2 + 1i.*bei_mr2 - C.*(ker_mr2 + 1i.*kei_mr2);
denumerator     = ber_mr2_diff1 + 1i.*bei_mr2_diff1 - C.*(ker_mr2_diff1
    +...
                    1i.*kei_mr2_diff1);
part1           = (1i.*k*(r2^2-r1^2))/(2*r2);
part2           = numerator./denumerator;
% put together final equation
R_ratio         = real(part1.*part2);
R_ratio(1)      = 1;
L_DC            = mu_0*mu_r/(2*pi)*(r1^4/(r2^2-r1^2)^2*log(r2/r1)...
                    -((3*r1^2-r2^2)/(4*(r2^2-r1^2))));
L_ratio         = (R_DC./(2*pi.*f*L_DC)).*imag(part1.*part2);
L_ratio(1)      = 1;
% Principle of Similitude Parameter
p               = sqrt(f/R_DC).*1e-3;
```

C

DEFINITION OF USED FUNCTIONS AND OPERATORS

I have not failed.
I´ve just found 10,000 ways that won´t work.
Thomas A. Edison

In every definition, ν denotes the order of the function.

C.1 BESSEL FUNCTIONS

Bessel function of the first kind J_ν, taken from [Lam13]:

$$J_\nu(x) = \sum_{k=0}^{\infty} \frac{(-1)^k}{k!\Gamma(\nu+k+1)} \left(\frac{x}{2}\right)^{2k+\nu} \quad . \tag{C.1}$$

Bessel function of the second kind Y_ν, taken from [Lam13]:

$$Y_\nu(x) = \frac{\cos\nu\pi J_\nu(x) - J_{-\nu}(x)}{\sin\nu\pi} \quad . \tag{C.2}$$

Bessel function of the third kind H_ν (also called Hankel function), taken from [Liu16]:

$$H_\nu(x) = J_\nu(x) + \mathrm{j}Y_\nu(x) = \frac{J_{-\nu}(x) - \mathrm{e}^{-\nu\pi\mathrm{j}}J_\nu(x)}{\mathrm{j}\,\sin(\nu\pi)} \quad . \tag{C.3}$$

Modified Bessel function of the first kind I_ν, taken from [Kre]:

$$I_\nu(x) = \left(\frac{x}{2}\right)^\nu \sum_{k=0}^{\infty} \frac{1}{\Gamma(k+1)\Gamma(\nu+k+1)} \left(\frac{x}{2}\right)^{2k} \quad . \tag{C.4}$$

Modified Bessel function of the second kind K_ν, taken from [Kre]:

$$K_\nu(x) = \frac{\pi}{2}\frac{I_{-\nu}(x) - I_\nu(x)}{\sin(\nu\pi)} \quad . \tag{C.5}$$

C.2 KELVIN FUNCTIONS

The Kelvin functions, taken from [Wei] are defined as

$$ber_\nu(x) + i\,bei_\nu(x) = J_\nu(xe^{3\pi i/4}) \quad , \tag{C.6}$$

$$ker_\nu(x) + i\,kei_\nu(x) = e^{-\nu\pi i/2}K_\nu(xe^{\pi i/4}) \quad . \tag{C.7}$$

According to [Cas16a] and [Cas16b] their derivatives are

$$\mathrm{ber}'_\nu(x) = \frac{\mathrm{ber}_{\nu+1}(x) + \mathrm{bei}_{\nu+1}(x)}{\sqrt{2}} + \frac{\nu}{x}\mathrm{ber}_\nu(x) \quad , \tag{C.8}$$

$$\mathrm{bei}'_\nu(x) = \frac{\mathrm{bei}_{\nu+1}(x) - \mathrm{ber}_{\nu+1}(x)}{\sqrt{2}} + \frac{\nu}{x}\mathrm{bei}_\nu(x) \quad , \tag{C.9}$$

$$\mathrm{ker}'_\nu(x) = \frac{\mathrm{ker}_{\nu+1}(x) + \mathrm{kei}_{\nu+1}(x)}{\sqrt{2}} + \frac{\nu}{x}\mathrm{ker}_\nu(x) \quad , \tag{C.10}$$

$$\mathrm{kei}_\nu^{'}(x) = \frac{\mathrm{kei}_{\nu+1}(x) - \mathrm{ker}_{\nu+1}(x)}{\sqrt{2}} + \frac{\nu}{x}\mathrm{kei}_\nu(x) \ . \tag{C.11}$$

C.3 BASIC OPERATORS

The nabla operator is a vector and defined as follows in a Cartesian coordinate system:

$$\nabla = \vec{\nabla} = \left(\frac{\partial}{\partial x}, \frac{\partial}{\partial y}, \frac{\partial}{\partial z}\right)^\top \ . \tag{C.12}$$

Operators rot, div and grad are defined as follows

$$\vec{a} = \mathrm{rot}\ \vec{x} = \nabla \times \vec{x} \ , \tag{C.13}$$
$$a = \mathrm{div}\ \vec{x} = \nabla \cdot \vec{x} \ , \tag{C.14}$$
$$\vec{a} = \mathrm{grad}\ b = \nabla b \ . \tag{C.15}$$

C.4 DEFINITION OF ADDITIONAL BESSEL FUNCTION ARGUMENTS AND PREFACTORS

Formulas over multiple lines, terminated by a semicolon.

$$\begin{aligned}\Xi_1 = \frac{r_c}{r_1} G_1(kr_2) \cdot \\ \frac{1}{\left(G_1(kr_1)G_3(kr_2) - G_1(kr_2)G_2(kr_1)\right)^2 - \left(G_1(kr_2)G_2(kr_1) - G_1(kr_1)G_2(kr_2)\right)^2} \cdot \\ \Big[\left(G_1(kr_1)G_3(kr_2) - G_1(kr_2)G_2(kr_1)\right)\left(\mathrm{ber}_0'(kr_c)\mathrm{bei}_0'(kr_1) - \mathrm{bei}_0'(kr_c)\mathrm{ber}_0'(kr_1)\right) - \\ \left(G_1(kr_2)G_2(kr_1) - G_1(kr_1)G_2(kr_2)\right)\left(\mathrm{ber}_0'(kr_c)\mathrm{ber}_0'(kr_1) - \mathrm{bei}_0'(kr_c)\mathrm{bei}_0'(kr_1)\right)\Big] ;\end{aligned} \tag{C.16}$$

$$\begin{aligned}\Xi_2 = \frac{r_c}{r_1} G_1(kr_2)\Big[- \frac{\mathrm{ber}_0'(kr_c)\mathrm{ber}_0'(kr_1) - \mathrm{bei}_0'(kr_c)\mathrm{bei}_0'(kr_1)}{G_1(kr_1)G_3(kr_2) - G_1(kr_2)G_2(kr_1)} - \\ \frac{\left(G_1(kr_2)G_2(kr_1) - G_1(kr_1)G_2(kr_2)\right)\left(\mathrm{ber}_0'(kr_c)\mathrm{bei}_0'(kr_1) - \mathrm{bei}_0'(kr_c)\mathrm{ber}_0'(kr_1)\right)}{\left(G_1(kr_1)G_3(kr_2) - G_1(kr_2)G_2(kr_1)\right)^2 + \left(G_1(kr_2)G_2(kr_1) - G_1(kr_1)G_2(kr_2)\right)^2} + \\ \frac{\left(G_1(kr_2)G_2(kr_1) - G_1(kr_1)G_2(kr_2)\right)\left(\mathrm{ber}_0'(kr_c)\mathrm{ber}_0'(kr_1) - \mathrm{bei}_0'(kr_c)\mathrm{bei}_0'(kr_1)\right)}{\left(G_1(kr_1)G_3(kr_2) - G_1(kr_2)G_2(kr_1)\right)^2}\Big] ;\end{aligned} \tag{C.17}$$

$$\Xi_3 = \frac{-\Xi_1 G_2(kr_2) + \Xi_2 G_3(kr_2)}{G_1(kr_2)} \ ; \tag{C.18}$$

$$\Xi_4 = \frac{-\Xi_1 G_3(kr_2) - \Xi_2 G_2(kr_2)}{G_1(kr_2)} \ ; \tag{C.19}$$

where

$$G_1(x) = \mathrm{ber}_0'^2(x) + \mathrm{bei}_0'^2(x) \ , \tag{C.20}$$
$$G_2(x) = \mathrm{ber}_0'(x)\mathrm{ker}_0'(x) + \mathrm{bei}_0'(x)\mathrm{kei}_0'(x) \ , \tag{C.21}$$
$$G_3(x) = \mathrm{bei}_0'(x)\mathrm{ker}_0'(x) + \mathrm{ber}_0'(x)\mathrm{kei}_0'(x) \ . \tag{C.22}$$

D

ADDITIONAL PHOTOGRAPHS

I do not think you can name many great inventions
that have been made by married men.

Nikola Tesla

D.1 MEASUREMENT SYSTEM AND LABORATORY

Figure D.1 shows the recent version of the measurement system used. It requires the following connections for a measurement: a 230 V power supply, connection of the voltage loop, connection of the current path and a LAN cable for connection to the software on a computer.

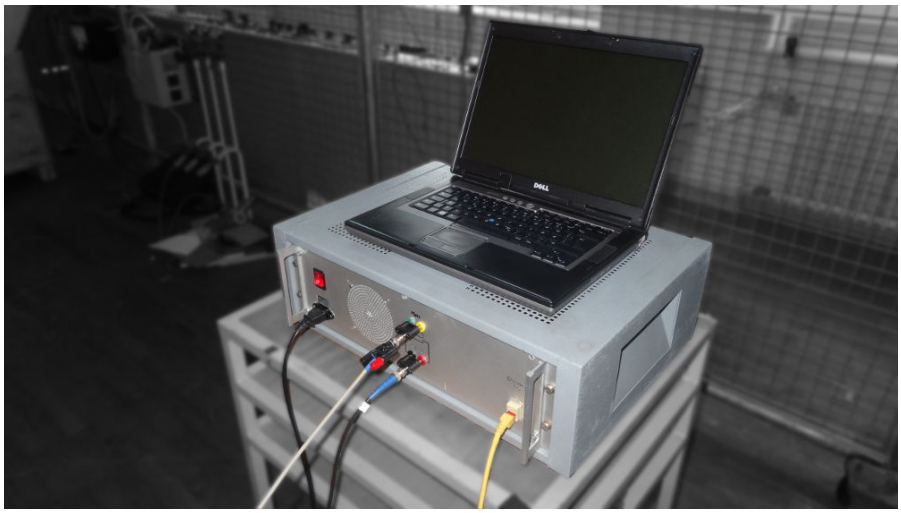

Figure D.1: Used measurement system including a laptop for the measurement software

Figure D.2: Photograph of the metallic fence in the laboratory

D.2 MILLIKEN CONDUCTOR MEASUREMENTS

D.2.1 *Aluminum Milliken Conductor — AL*

The following photographs are related to the investigations presented in Section 5.1.1.

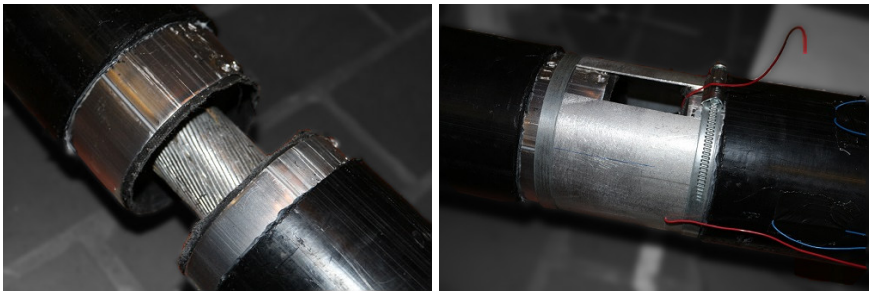

(a) Window for voltage tap-offs 2 m behind the current injection

(b) Setting up a coaxial *current transition* with 2 aluminum half shells

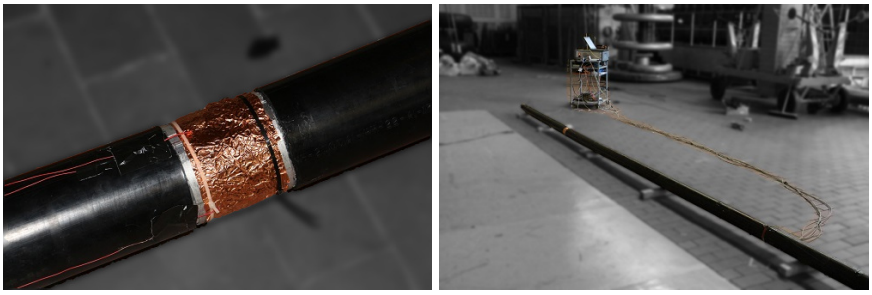

(c) Setting up a coaxial *current transition* with copper foil enveloping the half shells

(d) Short sample in the laboratory with the measurement system in the background

Figure D.3: Measurement setup of aluminum *Milliken* conductor with a cross section of 2000 mm^2 and the setup of coaxial *current transition;* voltage leads in blue and red

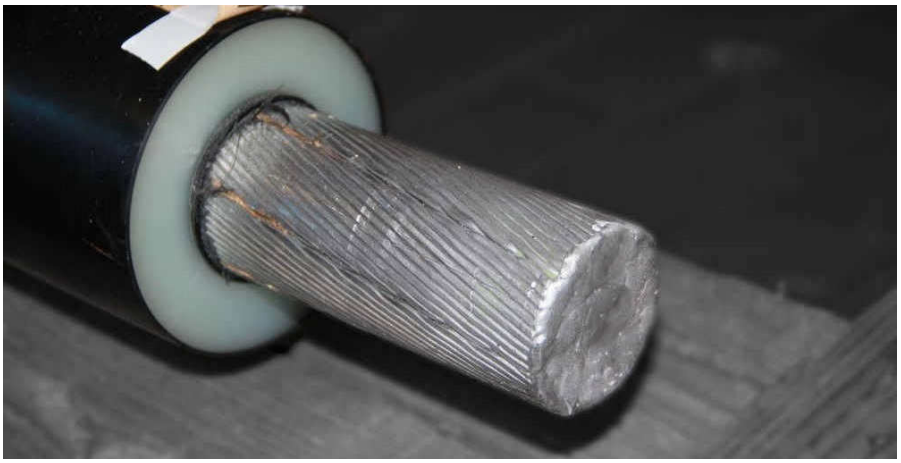

Figure D.4: Welded terminal of the aluminum *Milliken* conductor

D.2.2 *Copper Milliken Conductor — CU-B*

The following photographs are related to the investigations presented in Section 5.1.2.1.

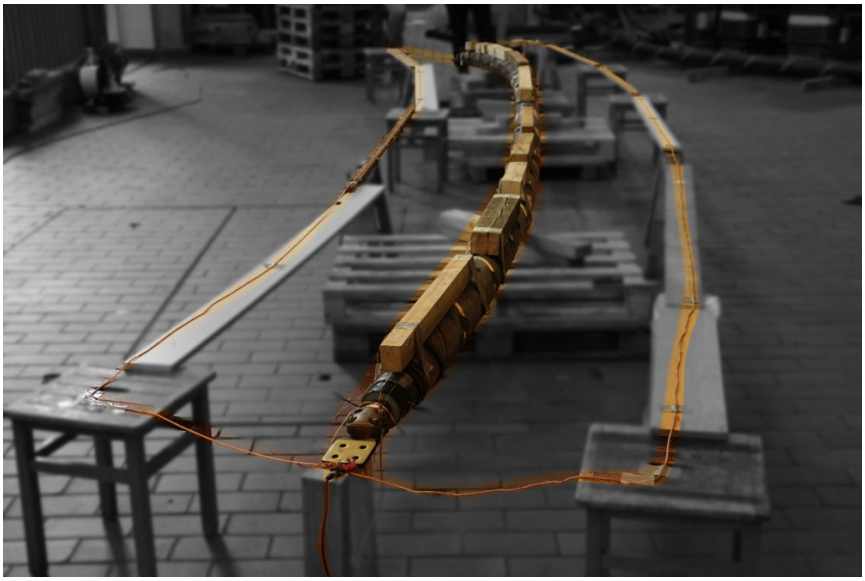

(a) *Symmetric sheath return method*, both return conductors are small copper litz wires spaced 70 cm from the CUT in the center

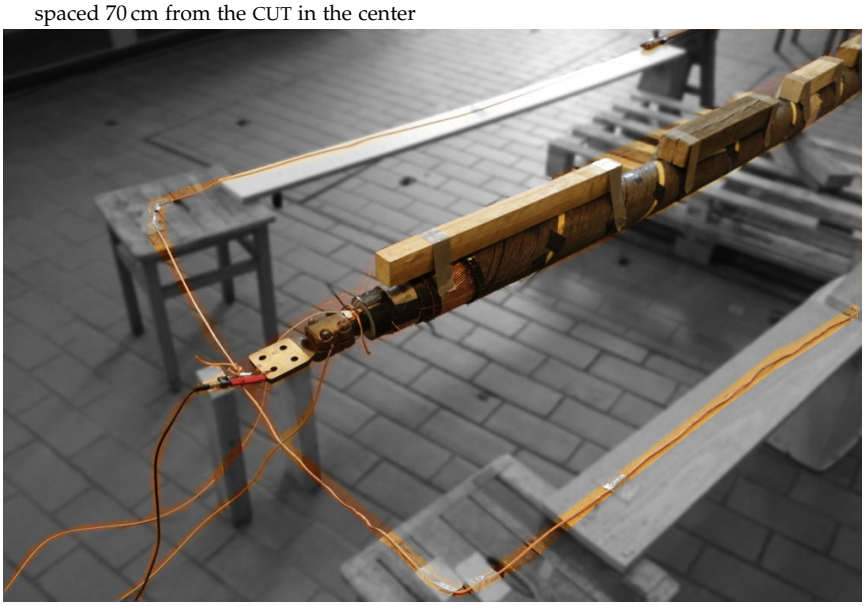

(b) Lower black corner shows the coaxial current feed line in black, the twisted pair voltage lead cable and the connection to the temperature sensor in white

Figure D.5: Setup for the *NSW* cable sample; the pieces of wood are used as spacers for a second *top* configuration with increased d_{VL} (comparing Figure 4.36 with Figure 4.37)

[50H+17] 50Hertz Transmission GmbH, TenneT TSO GmbH, Amprion GmbH, and TransnetBW GmbH. *Netzentwicklungsplan 2030 - 2.Entwurf: Teil I - Stand: 2. Mai 2017*. 2017. URL: https://www.netzentwicklungsplan.de/sites/default/files/paragraphs-files/NEP_2030_2_Entwurf_Teil1.pdf (visited on 11/23/2017).

[Alb11] Manfred Albach. *Grundlagen der Elektrotechnik: Band 1*. 3., aktualisierte Aufl. München: Pearson Studium, 2011. ISBN: 978-3868940794. URL: http://lib.myilibrary.com/detail.asp?id=404884 (visited on 09/20/2017).

[Alb17] Manfred Albach. *Induktivitäten in der Leistungselektronik: Spulen, Trafos und ihre parasitären Eigenschaften*. 2017. ISBN: 3-658-15080-7.

[AH82] Manfred Albach and Ludwig Hannakam. "Stromverteilung und Verluste in mehreren zylindrischen Massivleitern rechteckförmigen Querschnittes." In: *Archiv für Elektrotechnik* 64.5 (1982), pp. 285–288. DOI: 10.1007/BF01574759.

[And97] George J. Anders. *Rating of electric cables: Ampacity computations for transmission, distribution, and industrial applications*. IEEE Press power engineering series. New York: IEEE Press, 1997. ISBN: 9780780311770.

[And05] George J. Anders. *Rating of electric power cables in unfavorable thermal environment*. IEEE Press series on power engineering. Hoboken, N.J.: Wiley, 2005. ISBN: 0471718742.

[ADS99] P. Argaut, J. Y. Daurelle, and Sagem Sa. "Calculation method of power cables AC resistance with individually insulated strands." In: *Jicable 1999 - 5th International Conference on Insulated Power Cables*. Vol. 2. 1999, pp. 582–591.

[Arn41a] A.H.M. Arnold. "Proximity effect in solid and hollow round conductors." In: *Journal of the Institution of Electrical Engineers - Part I: General* 88.9 (1941), pp. 343–344. DOI: 10.1049/ji-1.1941.0077.

[Arn35] Alun Hugh Madoc Arnold. "The alternating-current resistance of parallel conductors of circular cross-section." In: *Journal of the Institution of Electrical Engineers* 77.463 (1935), pp. 49–58. DOI: 10.1049/jiee-1.1935.0121.

[Arn38] Alun Hugh Madoc Arnold. "The alternating-current resistance of hollow, square conductors." In: *Journal of the Institution of Electrical Engineers* 82.497 (1938), pp. 537–545. DOI: 10.1049/jiee-1.1938.0079.

[Arn41b] Alun Hugh Madoc Arnold. "Eddy-current losses in multicore paper-insulated lead-covered cables, armoured and unarmoured, carrying balanced 3-phase current." In: *Journal of the Institution of Electrical Engineers - Part II: Power Engineering* 88.1 (1941), pp. 52–63. DOI: 10.1049/ji-2.1941.0008.

[Arn46] Alun Hugh Madoc Arnold. *The alternating current resistance of non-magnetic conductors*. London, 1946.

[Ast55] N. F. Astbury. "Residual effects in the Campbell bridge method for the absolute measurement of resistance, and a note on a new bridge." In: *Proceedings of the IEE Part C: Monographs* 102.2 (1955), p. 279. DOI: 10.1049/pi-c.1955.0033.

[BM68] Edmund Ball and Gabriele Maschio. "The AC Resistance of Segmental Conductors as Used in Power Cables." In: *IEEE Transactions on Power Apparatus and Systems* PAS-87.4 (1968), pp. 1143–1148. DOI: 10.1109/TPAS.1968.292093.

[Bar06] Ramón Bargallo. *Finite Elements For Electrical Engineering*. 2006. URL: http://www.aedie.org/eeej/webrevista/articulos/librosONLINE/EFRBP2006FULL.pdf (visited on 11/15/2017).

[BM86] E. Baum and Gerd Mrozynski. "Stromverteilung in Druckkontakten auf zylindrischen Leitern." In: *Archiv für Elektrotechnik* 69.3 (1986), pp. 193–201. DOI: 10.1007/BF01574624.

[Ben07] Roberto Benato. "Multiconductor Cell Analysis Of Power Cable Steady State." In: *Jicable 2007 - 7th International Conference on Insulated Power Cables*. 2007.

[Ben09] Roberto Benato. "Multiconductor analysis of underground power transmission systems: EHV AC cables." In: *Electric Power Systems Research* 79.1 (2009), pp. 27–38. DOI: 10.1016/j.epsr.2008.05.016.

[BP10] Roberto Benato and Antonio Paolucci. *EHV AC undergrounding electrical power: Performance and planning*. Power systems. London: Springer, 2010. ISBN: 978-1-4471-2553-2.

[Bey86] M. Beyer. *Hochspannungstechnik: Theoretische und praktische Grundlagen*. Berlin, Heidelberg: Springer Berlin Heidelberg, 1986. ISBN: 364261633X.

[BD99] Jose Bezille and Pascal Deguines. "Conducteur multicouche a effet de peau red u it." Patent: EP 0 949636 A1. Michelle et. al. Bufflère and COMPAGNIE FINANCIERE ALCATEL. 1999.

[Bos08] Alain Bossavit. "What do voltmeters measure?" In: *COMPEL - The international journal for computation and mathematics in electrical and electronic engineering* 27.1 (2008), pp. 9–16. DOI: 10.1108/03321640810836582.

[BSF99] X. Bourgeat, J. Santana, and Abel Fustier. "A new methode for the measurement of power cables AC resistance." In: *Jicable 1999 - 5th International Conference on Insulated Power Cables*. Vol. 2. 1999, pp. 561–565.

[BB07] John R. Bowler and Nicola Bowler. "Theory of four-point alternating current potential drop measurements on conductive plates." In: *Proceedings of the Royal Society A: Mathematical, Physical and Engineering Sciences* 463.2079 (2007), pp. 817–836. DOI: 10.1098/rspa.2006.1791.

[Bra90] Heinrich Brakelmann. "Elektrischer Leiter vom Millikentyp mit verringerten Wirbelstromverlusten." Patent: DE4036169A1 (Germany). Felten & Guilleaume Energietechnik AG. 1990.

[Bra96] Heinrich Brakelmann. *Belastbarkeiten der Energiekabel. Berechnungsmethoden und Parameteranalysen*. VDE-Verlag GmbH, 1996. ISBN: 978-3800714063.

[Bri+16] Ana Isabel Brito, V. Maló Machado, M. E. Almeida, and M. Guerreiro das Neves. "Skin and proximity effects in the series-impedance of three-phase underground cables." In: *Electric Power Systems Research* 130 (2016), pp. 132–138. DOI: 10.1016/j.epsr.2015.08.027.

[BM11] Patrick de Bruyne and Gaël Mauron. *Effects of Contact Resistances in Multi-strand Cables on Linear Resistance Measurements*. Ed. by AESA Cortaillod. 2011. URL: https://www.aesa-cortaillod.com/fileadmin/documents/product/testing-equipment/Article_Contact_resistance_E_110525.pdf (visited on 05/08/2018).

[BA69] P. Burke and Robert H. Alden. "Current Density Probes." In: *IEEE Transactions on Power Apparatus and Systems* PAS-88.2 (1969), pp. 181–185. DOI: 10.1109/TPAS.1969.292420.

[Bür95] Jens Bürkner. "Grundlagenuntersuchungen zur Diagnose an Verbindungen der Elektroenergietechnik." PhD thesis. Dresden: Technische Universität Dresden, 1995.

[bur15] burster gmbh & co kg burster. *Precision High Capacity Resistors - Model 1282: Datasheet*. 2015. URL: https://www.burster.de/fileadmin/user_upload/redaktion/Documents/Products/Data-Sheets/Section_1/1282_EN.pdf (visited on 02/19/2018).

[Cal13] Luca Callegaro. *Electrical impedance: Principles, measurement, and applications*. Series in sensors. Boca Raton: CRC Press, 2013. ISBN: 9781439849101. URL: http://site.ebrary.com/lib/alltitles/docDetail.action?docID=10636366 (visited on 09/20/2017).

[Cam95] A. M. Campbell. "AC losses in high T/sub c/ superconductors." In: *IEEE Transactions on Applied Superconductivity* 5.2 (1995), pp. 682–687. DOI: 10.1109/77.402640.

[Car21] John R. Carson. "LIV. Wave propagation over parallel wires: The proximity effect." In: *Philosophical Magazine Series 6* 41.244 (1921), pp. 607–633. DOI: 10.1080/14786442108636251.

[Cas16a] LTD. Casio Computer CO. *Derivative Kelvin function of the 1st kind (chart) Calculator*. 2016. URL: http://keisan.casio.com/exec/system/1222655652 (visited on 10/17/2016).

[Cas16b] LTD. Casio Computer CO. *Derivative Kelvin function of the 2nd kind (chart) Calculator*. 2016. URL: http://keisan.casio.com/exec/system/1222656522 (visited on 10/17/2016).

[CMR77] F. Castelli, L. Maciotta-Rolandin, and P. Riner. "A new method for measuring the A. C. resistance of large cable conductors." In: *IEEE Transactions on Power Apparatus and Systems* 96.2 (1977), pp. 414–422. DOI: 10.1109/T-PAS.1977.32351.

[Cig05] Cigré, ed. *Large cross-sections and composite screens design: Working Group B1.03*. 272. CIGRE, 2005. URL: https://books.google.de/books/about/Large_Cross_sections_and_Composite_Scree.html?id=tUDDoQEACAAJ&redir_esc=y (visited on 05/16/2017).

[Cig18] Cigré, ed. *Basic principles and practical methods to measure the AC and DC resistance of conductors of power cables and overhead lines (still in draft at the date of submission)*. D1.54. CIGRE, 2018.

[Cle70] John R. Clem. "Theory of Flux-Flow Noise Voltage in Superconductors." In: *Physical Review B* 1.5 (1970), pp. 2140–2155. DOI: 10.1103/PhysRevB.1.2140.

[Coc29] J. D. Cockcroft. "Skin Effect in Rectangular Conductors at High Frequencies." In: *Proceedings of the Royal Society of London. Series A, Containing Papers of a Mathematical and Physical Character* 1929.Vol. 122, No. 790 (1929), pp. 533–542. URL: https://www.jstor.org/stable/95158?seq=1#fndtn-page_thumbnails_tab_contents (visited on 11/17/2016).

[Com13] Comsol. *AC/DC Module User's Guide*. 2013. URL: http://hpc.mtech.edu/comsol/pdf/ACDC_Module/ACDCModuleUsersGuide.pdf (visited on 05/30/2016).

[Com14] Comsol. *Essentials of Postprocessing and Visualization in COMSOL Multiphysics*. 2014. URL: http://lsun.people.ysu.edu/ECEN%203742/COMSOL%20RF%20Module/COMSOL_HANDBOOK_SERIES_Essentials_of_Postprocessing_and_Visualization.pdf (visited on 01/05/2017).

[Com15a] Comsol, ed. *COMSOL Multiphysics Reference Manual*. 2015.

[Com15b] Comsol. *Singularities in Finite Element Models: Dealing with Red Spots*. 2015. URL: https://www.comsol.com/blogs/singularities-in-finite-element-models-dealing-with-red-spots/ (visited on 12/08/2017).

[Com16a] Comsol. *Finite Element Mesh Refinement*. 2016. URL: https://www.comsol.de/multiphysics/mesh-refinement (visited on 05/24/2016).

[Com16b] Comsol. *The Finite Element Method (FEM)*. 2016. URL: https://www.comsol.de/multiphysics/finite-element-method (visited on 05/24/2016).

[Cos36] J. C. Costello. "Discussion on "The alternating-current resistance of tubular conductors"." In: *Journal of the Institution of Electrical Engineers* 79.479 (1936), pp. 595–596. DOI: 10.1049/jiee-1.1936.0199.

[Cur20] Harvey L. Curtis. "An integration method of deriving the alternating current resistance and inductance of conductors." In: *Journal of the Franklin Institute* 189.5 (1920), p. 655. DOI: 10.1016/S0016-0032(20)90381-2. URL: http://nvlpubs.nist.gov/nistpubs/ScientificPapers/nbsscientificpaper374vol16p93_A2b.pdf (visited on 08/11/2016).

[DZW14] Dong Dai, Xiaohui Zhang, and Juanjuan Wang. "Calculation of AC Resistance for Stranded Single-Core Power Cable Conductors." In: *IEEE Transactions on Magnetics* 50.11 (2014), pp. 1–4. DOI: 10.1109/TMAG.2014.2326040.

[Dal37] John L. Daley. *Distribution of alternating current in a rectangular conductor: Thesis (Ph.D.) - Yale University, 1937*. 1937. URL: http://search.library.yale.edu/catalog/3848242 (visited on 04/11/2017).

[Dal39] John L. Daley. "Current distribution in a rectangular conductor." In: *Electrical Engineering* 58.11 (1939), pp. 687–690. DOI: 10.1109/EE.1939.6431620.

[DR30] C. Dannatt and S. W. Redfearn. "The Efficient Utilization of Conductor Material in Busbar Sections: Loss Measurements in Bus Bars." In: *World Power* 1930.14 (1930), pp. 397–400, 492–496.

[Däu+00] M. Däumling, S. Krüger Olsen, C. Traeholt, Dag Willén, and A. Kühle. "Ac loss in superconducting power cables." In: *Studies of High Temperature Superconductors*. Vol. 33. 2000, p. 73.

[Del+15a] Timothe Delaforge, Herve Chazal, Jean-Luc Schanen, and Robert J. Pasterczyk. "Copper losses evaluation in multi-strands conductors formal solution based on the magnetic potential." In: *2015 IEEE Energy Conversion Congress and Exposition (ECCE)*. IEEE, 2015, pp. 3057–3063. ISBN: 978-1-4673-7151-3.

[Del+15b] Timothe Delaforge, Herve Chazal, Jean-Luc Schanen, and Robert J. Pasterczyk. "Increasing windings efficiency at high frequencies: Hollow conductors and clad metal conductors Formal solution based on the magnetic potential." In: *2015 IEEE Energy Conversion Congress and Exposition (ECCE)*. IEEE, 2015, pp. 5689–5695. ISBN: 978-1-4673-7151-3.

[Deu10] Deutsche Energie-Agentur GmbH. *dena-Netzstudie II: Integration erneuerbarer Energien in die deutsche Stromversorgung im Zeitraum 2015 – 2020 mit Ausblick 2025*. Berlin, 2010. URL: http://www.dena.de/fileadmin/user_upload/Publikationen/Erneuerbare/Dokumente/Endbericht_dena-Netzstudie_II.PDF (visited on 06/13/2016).

[Deu17] Deutsches Kupferinstitut - Copper Alliance. *Conductor Materials: Metals: familiar and versatile materials*. 2017. URL: https://www.kupferinstitut.de/en/materials/application/e-energie/conductor-materials.html (visited on 08/17/2017).

[Dol+98] P. Dolez, M. Aubin, W. Zhu, and J. Cave. "A comparison between ac losses obtained by the null calorimetric and a standard electrical method." In: *Superconductor Science and Technology* 11.12 (1998), pp. 1386–1390. DOI: 10.1088/0953-2048/11/12/006.

[DM07] David Dubois and Pierre Mirebeau. "The use of insulated wires Milliken conductors in high voltage power transmission underground AC lines." In: *Jicable 2007 - 7th International Conference on Insulated Power Cables*. 2007. URL: https://www.tib.eu/en/search/id/BLCP%3ACN072084613/The-use-of-insulated-wires-Milliken-conductors/?tx_tibsearch_search%5Bsearchspace%5D=tn (visited on 01/02/2017).

[Duc83] A. Ducluzaux. "Extra losses caused in high current conductors by skin and proximity effects." In: *Schneider Electric Cahier Techniques* no. 83 (1983). URL: https://www.ops-ecat.schneider-electric.com/cut.CatalogueRetrieverServlet/CatalogueRetrieverServlet?fct=get_element&env=publish&scp_id=Z000&el_typ=rendition&cat_id=DesignerV4&maj_v=2&min_v=14&nod_id=0000000008&doc_id=H383536&frm=pdf&usg=&dwnl=true (visited on 09/20/2017).

[Dwi18] Herbert Bristol Dwight. "Skin effect in tubular and flat conductors." In: *Proceedings of the American Institute of Electrical Engineers* 37.8 (1918), pp. 977–998. DOI: 10.1109/PAIEE.1918.6590850.

[Dwi23a] Herbert Bristol Dwight. "A precise method of calculation of skin effect in isolated tubes." In: *Journal of the American Institute of Electrical Engineers* 42.8 (1923), pp. 827–831. DOI: 10.1109/JoAIEE.1923.6593471.

[Dwi23b] Herbert Bristol Dwight. "Proximity effect in wires and thin tubes." In: *Journal of the American Institute of Electrical Engineers* 42.9 (1923), pp. 961–970. DOI: 10.1109/JoAIEE.1923.6593373.

[Dwi45] Herbert Bristol Dwight. *Electrical coils and conductors, their electrical characteristics and theory*. 1. New York: McGraw-Hill, 1945. ISBN: ASIN: B0007IT6Z0.

[Dwi47] Herbert Bristol Dwight. "Effective Resistance of Isolated Nonmagnetic Rectangular Conductors." In: *Transactions of the American Institute of Electrical Engineers* 66.1 (1947), pp. 549–552. DOI: 10.1109/T-AIEE.1947.5059478.

[DW24] Herbert Bristol Dwight and L. F. Woodruff. "Discussion: A precise method of calculation of skin effect in isolated tubes." In: *Journal of the A.I.E.E.* 43.8 (1924), pp. 760–761. DOI: 10.1109/JAIEE.1924.6534324.

[Edw11] Hiram Wheeler Edwards. "The Distribution of Current and the Variation of Resistance in Linear Conductors of Square and Rectangular Cross-section when carrying Alternating Currents of High Frequency." In: *Physical Review (Series I)* 33.3 (1911), pp. 184–202. DOI: 10.1103/PhysRevSeriesI.33.184.

[ES01] J. Edwards and T. K. Saha. "Diffusion of current into conductors." In: *Proceedings of the Australasian Universities* 2001 (2001), pp. 401–406.

[ES03] J. Edwards and T. K. Saha. "Establishment of current in conductors." In: *Proceedings of the Australasian Universities Power Engineering Conference*. 2003, pp. 1–12. URL: http://espace.library.uq.edu.au/view/UQ:9820 (visited on 12/07/2016).

[Ehr79] Matthias Ehrich. "Transiente und Quasistationäre Stromverdrängung ebener Leiteranordnungen." PhD thesis. Berlin: TU Berlin, 1979.

[Eri68a] T. J. Ericson. "The concepts of potential difference, voltage and E.M.F. I." In: *Physics Education* 3.5 (1968), pp. 238–241. DOI: 10.1088/0031-9120/3/5/001. (Visited on 09/27/2017).

[Eri68b] T. J. Ericson. "The concepts of potential difference, voltage and e.m.f. II." In: *Physics Education* 3.6 (1968), p. 294. URL: http://stacks.iop.org/0031-9120/3/i=6/a=001 (visited on 09/27/2017).

[Ern17] Daniel Erni. *Elektromagnetische Felddiffusion*. 2017. URL: http://www.ate.uni-due.de/data/tet/TET2_3_Felddiffusion.pdf (visited on 09/20/2017).

[EUR13] EUREL - Convention of National Associations of Electrical Engineers of Europe. "Electrical Power Vision 2040 for Europe." In: (2013). URL: http://www.eurel.org/home/TaskForces/Documents/EUREL-PV2040-Short_Version_Web.pdf (visited on 11/23/2017).

[Fer92] J. A. Ferreira. "Analytical computation of AC resistance of round and rectangular litz wire windings." In: *Electric Power Applications, IEE Proceedings B* 139.1 (1992), pp. 21–25.

[Fic07] Lars Ole Fichte. "Berechnung der Stromverteilung in einem System rechteckiger Massivleiter bei Wechselstrom durch Kombination der Separations- mit der Randintegralgleichungsmethode." PhD thesis. Hamburg: Helmut-Schmidt-Universität, 2007. URL: http://edoc.sub.uni-hamburg.de/hsu/volltexte/2007/910/ (visited on 05/12/2017).

[FEK04] Lars Ole Fichte, Matthias Ehrich, and Stefan Kurz. "An analytical solution to the eddy current problem of a conducting bar." In: *2004 International Symposium on Electromagnetic Compatibility*. Vol. EMC'04/Sendai. 2004, pp. 825–828. URL: http://www.ieice.org/proceedings/EMC04/PDF/4C2-2.pdf (visited on 06/11/2016).

[FG33] H. C. Forbes and L. J. Gorman. "Skin effect in rectangular conductors." In: *Electrical Engineering* 52.1 (1933), p. 49. DOI: 10.1109/EE.1933.6430584.

[Fre16] Walter Frei. *Comsol Blog - Keeping Track of Element Order in Multiphysics Models*. Ed. by Comsol. 2016. URL: https://www.comsol.com/blogs/keeping-track-of-element-order-in-multiphysics-models/ (visited on 09/20/2017).

[Fro05] Udo Fromm. "Optimized conductors for XLPE cables with a large cross-section." In: *European Transactions on Electrical Power* 15.2 (2005), pp. 109–121. DOI: 10.1002/etep.39.

[GG05] Igal Galili and Elisabetta Goihbarg. "Energy transfer in electrical circuits: A qualitative account." In: *American Journal of Physics* 73.2 (2005), pp. 141–144. DOI: 10.1119/1.1819932.

[Gan16] Sushil Kumar Ganguli. *Power Cable Technology*. s.l.: CRC Press, 2016. ISBN: 9781498709095. URL: http://gbv.eblib.com/patron/FullRecord.aspx?p=4514299.

[GP04] Omar Mohamed O. Gatous and José Pissolato. "Frequency-dependent skin-effect formulation for resistance and internal inductance of a solid cylindrical conductor." In: *IEE Proceedings - Microwaves, Antennas and Propagation* 151.3 (2004), p. 212. DOI: 10.1049/ip-map:20040469.

[Gat+14a] Omar Mohamed O. Gatous, José Pissolato, José Humberto A. Monteiro, Eduardo Coelho M. Costa, André Jinno G. Pinto, and Sérgio Kurokawa. "Simplified skin-effect formulation for power transmission lines." In: *IET Science, Measurement & Technology* 8.2 (2014), pp. 47–53. DOI: 10.1049/iet-smt.2013.0072.

[Gat+16] Michael Gatzsche, Nils Lücke, Steffen Großmann, Tom Kufner, and George Freudiger. "Evaluation of Electric-Thermal Performance of High-Power Contact Systems With the Voltage-Temperature Relation." In: *IEEE Transactions on Components, Packaging and Manufacturing Technology* (2016), pp. 1–12. DOI: 10.1109/TCPMT.2016.2587360.

[Gat+14b] Michael Gatzsche, Nils Lücke, Steffen Großmann, Tom Ledermann, and George Freudiger. *Impact of the Temperature-Induced Reduction of Joint Force on the Long-Term Behavior of Contact Elements with Material-Allocated Electrical and Mechanical Function: pp. 351-356*. Berlin: VDE-Verl., 2014. ISBN: 9783800736249.

[GHM] GHM Messtechnik GmbH. *GMH 3710 - PT100 High-Precision Thermometer: Datasheet*. URL: https://www.greisinger.de/files/upload/de/produkte/kat/k17_010_DE_oP.pdf (visited on 02/19/2018).

[GSR05] K. F. Goddard, J. K. Sykulski, and A. A. Roy. "Inductance and resistance calculations for isolated conductors." In: *IEE Proceedings - Science, Measurement and Technology* 152.1 (2005), pp. 7–14. DOI: 10.1049/ip-smt:20051057.

[GFŠ05] Fedor Gömöry, L. Frolek, and J. Šouc. "Non-uniform current distribution as the cause of false voltage signals in the ac loss measurement on a superconducting cable." In: *Superconductor Science and Technology* 18.5 (2005), pp. 780–790. DOI: 10.1088/0953-2048/18/5/035.

[Gra79] Peter Graneau. *Underground power transmission: The science, technology, and economics of high voltage cables*. A Wiley-Interscience publication. New York NY u.a.: Wiley, 1979. ISBN: 0-471-05757-6.

[Gro40] Hans-Georg Groß. "Die Berechnung der Stromverteilung in zylindrischen Leitern mit rechteckigem und elliptischem Querschnitt." In: *Archiv für Elektrotechnik*. Vol. XXXIV. Band, Heft 5. 1940, pp. 241–268. URL: https://link.springer.com/article/10.1007/BF01660161 (visited on 09/20/2017).

[GSG] GSG Geologie-Service GmbH. *GOF 115-PT: Datasheet*. URL: http://www.gsg-e-shop.de/media/files_public/rcrbmigiug/gof112-115-120_datasheet.pdf (visited on 02/19/2018).

[Hae37] S. J. Haefner. "Alternating-Current Resistance of Rectangular Conductors." In: *Proceedings of the IRE* 25.4 (1937), pp. 434–447. DOI: 10.1109/JRPROC.1937.229047.

[HA80] Ludwig Hannakam and Manfred Albach. "Leitende Zylinder im Felde senkrecht zu den Stirnseiten verlaufender erregender Leiter." In: *Archiv für Elektrotechnik* 62.6 (1980), pp. 335–342. DOI: 10.1007/BF01579003.

[HM76] Ludwig Hannakam and Gerd Mrozynski. "Skineffekt im endlich langen Zylinder bei Stromeinspeisung an den Stirnflächen." In: *Springer-Verlag - Archiv für Elektrotechnik* 58 (1976).

[HM89] Hermann A. Haus and James R. Melcher. *Electromagnetic fields and energy*. Englewood Cliffs N.J.: Prentice Hall, 1989. ISBN: 013249020X. URL: http://ocw.mit.edu/resources/res-6-001-electromagnetic-fields-and-energy-spring-2008/chapter-11/11.pdf (visited on 09/27/2017).

[Hea84] Oliver Heaviside. "Transmission of Energy into a Conducting Core." In: *The Electrician* (1884), p. 133.

[Hea85] Oliver Heaviside. "On the transmission of energy through wires by the electric current." In: *The Electrician* (1885), p. 178.

[Hea86a] Oliver Heaviside. "Electromagnetic induction and its propagation: 27. The variable period in a round wire with a concentric tube at any distance from the return current." In: *The Electrician* 17 (1886), p. 88.

[Hea86b] Oliver Heaviside. "Impedance Formulae For Short Lines. Resistance of Tubes." In: *The Electrician* (1886), p. 252.

[Hea86c] Oliver Heaviside. "Notes on the Self-Induction of Wires: Note 1." In: *The Electrician* (1886), p. 471.

[Hea92] Oliver Heaviside. "Electrical Papers - Vol. 1." In: (1892). URL: https://archive.org/details/electricalpapers01heavuoft (visited on 09/20/2017).

[Hea93] Oliver Heaviside. *Electromagnetic Theory - Vol. 1*. Vol. Vol. 1. London: The Electrician, 1893. URL: https://ia802205.us.archive.org/32/items/electromagnetict01heavrich/electromagnetict01heavrich.pdf (visited on 09/20/2017).

[Hea94] Oliver Heaviside. "Electrical Papers - Vol. 2." In: (1894). URL: https://archive.org/details/electricalpapers02heavrich (visited on 09/20/2017).

[Hen07] Heino Henke. *Elektromagnetische Felder: Theorie und Anwendung*. 3., erweiterte Auflage. Springer-Lehrbuch. Berlin, Heidelberg: Springer-Verlag Berlin Heidelberg, 2007. ISBN: 9783540710042. URL: http://site.ebrary.com/lib/alltitles/docDetail.action?docID=10171230 (visited on 09/20/2017).

[HDS10] Klaus Heuck, Klaus-Dieter Dettmann, and Detlef Schulz. *Elektrische Energieversorgung: Erzeugung, Übertragung und Verteilung elektrischer Energie für Studium und Praxis*. 8., überarbeitete und aktualisierte Auflage. Wiesbaden: Vieweg+Teubner Verlag / Springer Fachmedien Wiesbaden GmbH Wiesbaden, 2010. ISBN: 978-3-8348-9761-9. URL: http://dx.doi.org/10.1007/978-3-8348-9761-9.

[HIL17] HILO-TEST GmbH. *Current-Viewing Resistors Type ISM: Datasheet*. 2017. URL: http://www.hilo-test.de/media/pdf/datasheets/en/ISMETAB.pdf (visited on 02/16/2018).

[Hof12] Lutz Hofman. *Technologien zur Stromübertragung: Einführung*. 2012. URL: http://data.netzausbau.de/2012/Vortrag_Hofmann.pdf (visited on 06/13/2016).

[HR15] Marcus Högas and Karl-Erik Rydler. "Influence on measured conductor AC resistance of high voltage cables when the screen is used as return conductor." In: *Jicable 2015 - 9th International Conference on Insulated Power Cables*. 2015. URL: http://www.jicable.org/TOUT_JICABLE_FIRST_PAGE/2015/2015-F2-17_page1.pdf (visited on 09/20/2017).

[Hol58] Ragnar Holm. *Elektrische Kontakte / Electric Contacts Handbook*. 3rd ed. Berlin, Heidelberg and s.l.: Springer Berlin Heidelberg, 1958. ISBN: 978-3-662-25893-4. URL: http://dx.doi.org/10.1007/978-3-662-25893-4.

[HB81] S. J. Hudak and R. J. Bucci. *Fatigue Crack Growth Measurement and Data Analysis*. Vol. STP738. 1981. ISBN: 978-0-8031-0717-5. URL: https://books.google.de/books?id=FPaBZcnp8cYC&pg=PA117&lpg=PA117&dq=skin+effect+potential+measurement&source=bl&ots=OACPSWLeRQ&sig=uf0Ken3uL9c_xPhy2NWvN4I4hzg&hl=de&sa=X&ved=0ahUKEwjszar-mInMAhUBLhQKHas7CBsQ6AEIFTAC#v=onepage&q=skin%20effect%20potential%20measurement&f=false (visited on 09/20/2017).

[Hug86] D. E. Hughes. "Researches upon the Self-Induction of an Electric Current." In: *Proceedings of the Royal Society of London, Philosophical Transactions of the Royal Society* (1886). URL: https://archive.org/details/philtrans03111115 (visited on 09/20/2017).

[IEA17] IEA - International Energy Agency. "WEO 2017 - Executive Summary - German version: World Energy Outlook." In: (2017). (Visited on 11/23/2017).

[IEC06a] IEC - International Electrotechnical Commission. "Efficient Electrical Energy Transmission and Distribution." In: *International Regulatory Co-operation*. OECD Publishing, 2006, pp. 138–139. ISBN: 9789264266254. (Visited on 11/23/2017).

[IEC06b] IEC - International Electrotechnical Commission. *Electric cables - Calculation of the current rating - Part 1-1: Current rating equations (100 % load factor) and calculation of losses - IEC 60287-1-1:2006*. 2006.

[IEC14] IEC - International Electrotechnical Commission. *Electric cables - Calculation of the current rating - Part 1-1: Current rating equations (100 % load factor) and calculation of losses - IEC 60287-1-1:2006/AMD1:2014*. 2014.

[IP94] Institute of Electrical and Electronics Engineers and Power Engineering Society. *IEEE standard power cable ampacity tables*. New York, NY, 1994.

[Jac96] J. D. Jackson. "Surface charges on circuit wires and resistors play three roles." In: *American Journal of Physics* 64.7 (1996), pp. 855–870. DOI: 10.1119/1.18112.

[Jac70] R. L. Jackson. "Measurement of skin and proximity effects in circular conductors." In: *Proceedings of the Institution of Electrical Engineers* 117.7 (1970), p. 1435. DOI: 10.1049/piee.1970.0274.

[Jac34] W. Jackson. "Skin effect in rectangular conductors at high frequencies." In: *The London, Edinburgh, and Dublin Philosophical Magazine and Journal of Science* 18.119 (1934), pp. 433–441. DOI: 10.1080/14786443409462514.

[Joa98] Dominik F. P. Joachim. "Stromverdrängungseffekte bei Millikenleitern." PhD thesis. Duisburg: Universität Duisburg, 1998.

[Joa99] Dominik F. P. Joachim. "Einflussgrößen für Skin- und Proximityeffekt bei Millikenleitern mit großem Querschnitt." In: *e & i Elektrotechnik und Informationstechnik* 116.10 (1999), pp. 584–587. DOI: 10.1007/BF03158927.

[Jor82] D. W. Jordan. "D. E. Hughes Self-induction and the Skin-Effect." In: *Centaurus* 26 (1982). DOI: 10.1111/j.1600-0498.1982.tb00658.x.

[JB68] Edward C. Jordan and Keith G. Balmain. *Electromagnetic waves and radiating systems*. 2. ed. Prentice-Hall electrical engineering series. Englewood Cliffs, NJ: Prentice-Hall, 1968. ISBN: 978-0-13-249995-8.

[Juu+11] Jeppe Sogaard Juul, Esben Tore Molgaard, Jens Jensen, Niels Hessel Andersen, Asger Bech Abrahamsen, Dag Willén, Chresten Traholt, Carsten Thidemann, and Heidi Lentge. "AC Losses in Bi2Sr2Ca2Cu3O10+x Tapes and a 3.15-m-Long Single-Phase Cable." In: *IEEE Transactions on Applied Superconductivity* 21.6 (2011), pp. 3599–3603. DOI: 10.1109/TASC.2011.2166153.

[Kam11] Catrin Kammer. *Aluminium Taschenbuch: Band 3: Weiterverarbeitung und Anwendung*. 16., Aufl. Berlin: Beuth, 2011. ISBN: 3410220224.

[KAA95] Mamadou Kane, A. Ahmad, and Philippe Auriol. "Multiwire shielded cable parameter computation." In: *IEEE Transactions on Magnetics* 31.3 (1995), pp. 1646–1649. DOI: 10.1109/20.376350.

[KA94] Mamadou Kane and Philippe Auriol. "Analytical modelling of frequency parameters of lines." In: *Second International Conference on Computation in Electromagnetics*. 1994, pp. 239–242.

[Kat71] Carlos Katz. "Conductor for underground transmission of electric power." Patent: 3,598,899. 1971.

[Kat+78] Carlos Katz, G. S. Eager, G. W. Seman, F. G. Garcia, W. G. Smith, and J. W. McCourt. "Progress in the Determination of AC/DC Resistance Ratios of Pipe-Type Cable Systems." In: *IEEE Transactions on Power Apparatus and Systems* PAS-97.6 (1978), pp. 2262–2271. DOI: 10.1109/TPAS.1978.354730.

[KA16] A. E. Kennelly and H. A. Affel. "Skin-Effect Resistance Measurements of Conductors, at Radio-Frequencies up to 100,000 Cycles per Second." In: *Proceedings of the IRE* 4.6 (1916), pp. 523–574. DOI: 10.1109/JRPROC.1916.217281.

[KLP15] A. E. Kennelly, F. A. Laws, and P. H. Pierce. "Experimental Researches on Skin Effect in Conductors." In: *Transactions of the American Institute of Electrical Engineers* XXXIV.2 (1915), pp. 1953–2021. DOI: 10.1109/T-AIEE.1915.4765283.

[KAF04] Manfred Kirschvink, Karl Audenaerde, and Stefan Fassbinder. *Safety cables and circuit integrity*. 2004. URL: http://www.leonardo-energy.com/sites/leonardo-energy/files/root/Documents/2009/SafetyCables.pdf (visited on 08/17/2017).

[Kle81] W. Klein. "Experimental "paradox" in electrodynamics." In: *American Journal of Physics* 49.6 (1981), pp. 603–604. DOI: 10.1119/1.12471.

[Kni16] David W. Knight. "Practical continuous functions for the internal impedance of solid cylindrical conductors." In: *ResearchGate* (2016). DOI: 10.13140/RG.2.1.3865.1284. URL: http://g3ynh.info/zdocs/comps/Zint.pdf (visited on 11/16/2017).

[Kre] Martin Kreh. *Bessel Functions: Project for the Penn State - Göttingen Summer School on Number Theory*. Ed. by Pennsylvania State University - Department of Mathematics. URL: http://www.math.psu.edu/papikian/Kreh.pdf (visited on 11/02/2017).

[Lam13] Jim Lambers. *Bessel Functions of the Second Kind: MAT 415/515: Lecture 16 Notes*. Ed. by University of California, Berkeley - UCB Mathematics. 2013. URL: https://math.berkeley.edu/~linlin/121B/LambersBessel.pdf (visited on 10/13/2016).

[LŠT66] Jiří Lammeraner, Miloš Štafl, and G. A. Toombs. *Eddy currents*. London: Iliffe Books, 1966.

[LZ95] E. Lanzara and R. Zangara. "Potential difference measurements in the presence of a varying magnetic field." In: *Physics Education* 30.2 (1995), p. 85. URL: http://stacks.iop.org/0031-9120/30/i=2/a=006 (visited on 09/20/2017).

[LR61] Rhea P. Lapsley and N. J. Ridgewood. "Dynamically Balanced, Alternating-Current Electric Conductors." Patent: 2,972,658. 1961.

[LSW04] O. B. Laug, T. M. Soudders, and B. C. Waltrip. *A Four-Terminal Current Shunt with Calculable AC Response: NIST Technical Note 1462*. Ed. by Electronics and Electrical Engineering Laboratory. 2004. URL: http://www.nist.gov/customcf/get_pdf.cfm?pub_id=31690 (visited on 05/25/2016).

[Leh10] Günther Lehner. *Elektromagnetische Feldtheorie für Ingenieure und Physiker*. 7. bearb. Aufl. Berlin: Springer, 2010. ISBN: 9783642130427.

[Leu05] Pascal Leuchtmann. *Einführung in die elektromagnetische Feldtheorie*. Elektrotechnik : theoretische Elektrotechnik. München u.a.: Pearson Studium, 2005. ISBN: 3-8273-7144-9.

[Lew02] Walter Lewin. *Complete Breakdown of Intuition*. 2002. URL: https://www.youtube.com/watch?v=eqjl-qRy71w (visited on 09/15/2017).

[Liu16] Cory James Liu. "Skin effect in large bi-media power conductors." PhD thesis. Charlotte, USA: University of North Carolina, 2016. URL: http://gradworks.umi.com/10/11/10111917.html (visited on 05/12/2017).

[LCK15] Cory James Liu, Valentina Cecchi, and Sherif Kamel. "Analysis of AC resistance in non-ferrous bimetallic solid conductors." In: *2015 North American Power Symposium (NAPS)*. 2015, pp. 1–6.

[LBV11] Dino Lovric, Vedran Boras, and Slavko Vujević. "Accuracy of approximate formulas for internal impedance of tubular cylindrical conductors for large parameters." In: *Progress In Electromagnetics Research M* 16 (2011), pp. 171–184. DOI: 10.2528/PIERM10121503.

[MBD15] Paolo Maioli, Massimo Bechis, and Gaia Dell'Anna. "AC Resistance of submarine cables." In: *Jicable 2015 - 9th International Conference on Insulated Power Cables*. 2015.

[Man+08] I. Manke, N. Kardjilov, M. Strobl, A. Hilger, and J. Banhart. "Investigation of the skin effect in the bulk of electrical conductors with spin-polarized neutron radiography." In: *Journal of Applied Physics* 104.7 (2008), p. 076109. DOI: 10.1063/1.2992516.

[Man22] Charles Manneback. "An integral equation for skin effect in parallel conductors." In: *Journal of Math and Physics Vol. I 1922*. 1922, pp. 123–146. URL: https://babel.hathitrust.org/cgi/pt?id=inu.30000021044759;view=1up;seq=156;size=75 (visited on 09/20/2017).

[Mat10] Matelect. *PRACTICAL ASPECTS OF THE ACPD TECHNIQUE: For use with Matelect ACPD products: User manual*. 2010. URL: http://www.matelect.com/files/Download/ACPDTechnique%20v3.3b.pdf (visited on 05/30/2017).

[MBH51] L. W. Matsch, N. C. Basu, and G. R. Horcher. "Three-Phase Measurements of Resistance." In: *Transactions of the American Institute of Electrical Engineers* 70.1 (1951), pp. 350–354. DOI: 10.1109/T-AIEE.1951.5060414.

[Mat+83] Kenji Matsuura, Tokio Kihara, Hiromichi Yokoyama, Yoshihiro Moriyama, Toshihiro Miyazaki, and Tetsuji Itoh. "Development of calculation method for ac resistance of power cable conductors with individually insulated strands." In: *Electrical Engineering in Japan* 103.5 (1983), pp. 47–56. DOI: 10.1002/eej.4391030507.

[Max73a] James Clerk Maxwell. *A treatise on electricity and magnetism - Vol. 1: 1st edition*. 1873. URL: https://archive.org/stream/electricandmagne01maxwrich (visited on 04/22/2016).

[Max73b] James Clerk Maxwell. *A treatise on electricity and magnetism - Vol. 2: 1st edition*. 1873. URL: https://archive.org/stream/electricandmagne02maxwrich#page/n7/mode/2up (visited on 04/22/2016).

[Max92] James Clerk Maxwell. *A treatise on electricity and magnetism - Vol. 2*. 3rd ed. edited by J. J. Thomson, 1892. URL: https://archive.org/details/atreatiseonelec00thomgoog (visited on 10/11/2016).

[McL55] N. W. McLachlan. *Bessel Functions for Engineers*. 2nd. London: Oxford at the Clarendon Press, 1955. ISBN: 978-1124148625.

[Mea25] Sallie Pero Mead. "Wave Propagation Over Parallel Tubular Conductors: The Alternating Current Resistance." In: *Bell System Technical Journal* 4.2 (1925), pp. 327–338. DOI: 10.1002/j.1538-7305.1925.tb00951.x.

[Meu12] Dietmar Meurer. *Lecture: Power Cable Engineering: Part 8: High Power Systems WS 2012-2013 RWTH Aachen: Presentation*. 2012.

[ME49] Louis Meyerhoff and G. S. Eager. "A-C Resistance of Segmental Cables in Steel Pipe." In: *Transactions of the American Institute of Electrical Engineers* 68.2 (1949), pp. 816–834. DOI: 10.1109/T-AIEE.1949.5060018.

[Mie00] Gustav Mie. "Elektrische Wellen an zwei parallelen Drähten." In: *Annalen der Physik* 307.6 (1900), pp. 201–249. DOI: 10.1002/andp.19003070602. URL: http://onlinelibrary.wiley.com/doi/10.1002/andp.19003070602/pdf (visited on 09/20/2017).

[Mil33] Humphreys Milliken. "Electrical Cable." Patent: 1,904,162 (USA). 1933.

[Mil40] Humphreys Milliken. "Electrical Power Cable." Patent: 2,187,213 (USA). 1940.

[MY04] W. Mingli and F. Yu. "Numerical calculations of internal impedance of solid and tubular cylindrical conductors under large parameters." In: *IEE Proceedings - Generation, Transmission and Distribution* 151.1 (2004), p. 67. DOI: 10.1049/ip-gtd:20030981.

[Moo69] D. R. Moorcroft. "Faraday's Law—Demonstration of a Teaser." In: *American Journal of Physics* 37.2 (1969), p. 221. DOI: 10.1119/1.1975460.

[Moo70] D. R. Moorcroft. "Faraday's Law, Potential and Voltage—Discussion of a Teaser." In: *American Journal of Physics* 38.3 (1970), pp. 376–377. DOI: 10.1119/1.1976329.

[Mor13] Vincent T. Morgan. "The Current Distribution, Resistance and Internal Inductance of Linear Power System Conductors—A Review of Explicit Equations." In: *IEEE Transactions on Power Delivery* 28.3 (2013), pp. 1252–1262. DOI: 10.1109/TPWRD.2012.2213617.

[Mro03] Gerd Mrozynski. *Elektromagnetische Feldtheorie: Eine Aufgabensammlung*. 1. Aufl. Stuttgart u.a: Teubner, 2003. ISBN: 3519004399.

[MS13] Gerd Mrozynski and Matthias Stallein. *Electromagnetic field theory: A collection of problems*. Wiesbaden: Springer Vieweg, 2013. ISBN: 3-8348-1711-2.

[MG07] Günter Müller and Clemens Groth. *FEM für Praktiker*. 8., neu bearb. Aufl. Vol. 23. Edition expertsoft. Renningen: Expert-Verl., 2007. ISBN: 9783816926856. URL: http://deposit.d-nb.de/cgi-bin/dokserv?id=2856735&prov=M&dok_var=1&dok_ext=htm (visited on 09/20/2017).

[Mur89] P. N. Murgatroyd. "Calculation of proximity losses in multi-stranded conductor bunches." In: *IEE Proceedings A (Physical Science, Measurement and Instrumentation, Management and Education)* 136.3 (1989), pp. 115–120. DOI: 10.1049/ip-a-2.1989.0021.

[Nah02] Paul J. Nahin. *Oliver Heaviside: The life, work, and times of an electrical genius of the Victorian age*. Baltimore, Md. and London: Johns Hopkins University Press, 2002. ISBN: 0801869099.

[Nex11] Nexans. *60-500 kV High Voltage Underground Power Cables: XLPE insulated cables*. 2011. URL: http://www.nexans.com/Corporate/2013/60-500_kV_High_Voltage_full_BD2.pdf (visited on 09/20/2017).

[Nic05] Howard W. Nicholson. "What does the voltmeter read?" In: *American Journal of Physics* 73.12 (2005), pp. 1194–1196. DOI: 10.1119/1.1997171.

[Ols+99] S. Krüger Olsen, A. Kühle, C. Traeholt, O. Tonnesen, M. Däumling, C. N. Rasmussen, and Dag Willén. "Alternating current losses of a 10 metre long low loss superconducting cable conductor determined from phase sensitive measurements." In: *Superconductor Science and Technology* 12.6 (1999), p. 360. DOI: 10.1088/0953-2048/12/6/306. URL: http://iopscience.iop.org/article/10.1088/0953-2048/12/6/306/pdf (visited on 09/20/2017).

[Pag77] Chester H. Page. "Electromotive force, potential difference, and voltage." In: *American Journal of Physics* 45.10 (1977), pp. 978–980. DOI: 10.1119/1.10862.

[Pay16] Alan Payne. *The AC resistance of rectangular conductors*. 2016. URL: http://g3rbj.co.uk/wp-content/uploads/2016/06/The-ac-Resistance-of-Rectangular-Conductors-Cockcroft2.pdf (visited on 05/12/2017).

[PO99] Egon F. Peschke and Rainer von Olshausen. *Cable systems for high and extra high voltage: Development, manufacture, testing, installation and operation of cables and their accessories*. Erlangen: Publicis-MCD-Verl., 1999. ISBN: 3895781185.

[Pet84] P. C. Peters. "The role of induced emf's in simple circuits." In: *American Journal of Physics* 52.3 (1984), pp. 208–211. DOI: 10.1119/1.13692.

[Poy84] John Henry Poynting. "On the Transfer of Energy in the Electromagnetic Field." In: *Philosophical Transactions of the Royal Society of London* 175 (1884), pp. 343–361. DOI: 10.1098/rstl.1884.0016.

[Pre16] A. Press. "Resistance and Reactance of Massed Rectangular Conductors." In: *Physical Review* 8.4 (1916), pp. 417–422. DOI: 10.1103/PhysRev.8.417.

[RWv94] Simon Ramo, John R. Whinnery, and Theodore van Duzer. *Fields and waves in communication electronics*. 3. ed. Hoboken NJ: Wiley & Sons, 1994. ISBN: 0-471-58551-3.

[Rei82] F. Reif. "Generalized Ohm's law, potential difference, and voltage measurements." In: *American Journal of Physics* 50.11 (1982), pp. 1048–1049. DOI: 10.1119/1.12944.

[Roe15] Ludwig Roebel. "Electrical Conductor." Patent: 1,144,252. Ludwig Roebel from AG Brown Boveri and CIE of Baden, Switzerland. 1915.

[RSF93] Horst Rohlfing, Harry Schmidt, and Wilhelm Friedrich. *Tabellenbuch Elektrotechnik, Elektronik*. 527. - 552. Aufl. Friedrichs Fach- und Tabellenbücher. Bonn: Dümmler, 1993. ISBN: 3427530248.

[Rom82] Robert H. Romer. "What do "voltmeters" measure? Faraday's law in a multiply connected region." In: *American Journal of Physics* 50.12 (1982), pp. 1089–1093. DOI: 10.1119/1.12923.

[Ros18] Andreas Rosskopf. "Calculation of frequency dependent power losses in inductive systems with litz wire conductors by a coupled numeric approach." PhD thesis. Friedrich-Alexander-Universität Erlangen-Nürnberg (FAU), 2018.

[Ros+11] Hans Rossmanith, Marc Doebroenti, Manfred Albach, and Dietmar Exner. "Measurement and Characterization of High Frequency Losses in Nonideal Litz Wires." In: *IEEE Transactions on Power Electronics* 26.11 (2011), pp. 3386–3394. DOI: 10.1109/TPEL.2011.2143729.

[RC18] Edward J. Rothwell and Michael J. Cloud. *Electromagnetics*. Third edition. Boca Raton: CRC Press Taylor & Francis Group, 2018. ISBN: 9781498796569.

[Row06] David Michael Rowe, ed. *Thermoelectrics handbook: Macro to nano*. Boca Raton, Fla.: CRC/Taylor & Francis, 2006. ISBN: 0-8493-2264-2. URL: http://www.loc.gov/catdir/enhancements/fy0646/2005048533-d.html.

[Rus09] Alexander Russell. "The effective resistance and inductance of a concentric main, and methods of computing the ber and bei and allied functions." In: *Philosophical Magazine Series 6* 17.100 (1909), pp. 524–552. DOI: 10.1080/14786440408636628.

[RSS11a] Karl-Erik Rydler, Mats Sjöberg, and Jörgen Svahn. "A measuring system of conductor AC and DC resistance." In: *Jicable 2011 - 8th International Conference on Insulated Power Cables*. 2011.

[RSS11b] Karl-Erik Rydler, Mats Sjöberg, and Jörgen Svahn. "Presentation of: A measuring system of conductor AC and DC resistance." In: *Jicable 2011 - 8th International Conference on Insulated Power Cables*. 2011.

[Ryu+13] Kyung-woo Ryu, Z. Y. Li, Y. H. Ma, and S. D. Hwang. "Influence of Various Voltage Leads on AC Loss Measurement in a Double Layer BSCCO Conductor." In: *IEEE Transactions on Applied Superconductivity* 23.3 (2013), p. 8200304. DOI: 10.1109/TASC.2012.2232957.

[RL16] Kyung-woo Ryu and Zhuyong Li. "AC Loss Measurement of an HTS Cable Model With a Shield Through Virtual and Contactless Voltage Leads." In: *IEEE Transactions on Applied Superconductivity* 26.6 (2016), pp. 1–7. DOI: 10.1109/TASC.2016.2582801.

[Sal48] E. H. Salter. "Problems in the Measurement of A-C Resistance and Reactance of Large Conductors." In: *Transactions of the American Institute of Electrical Engineers* 67.2 (1948), pp. 1390–1397. DOI: 10.1109/T-AIEE.1948.5059833.

[Sal49] E. H. Salter. "Measuring conductor resistance and reactance." In: *Electrical Engineering* 68.2 (1949), p. 144. DOI: 10.1109/EE.1949.6444608.

[SSW35] E. H. Salter, G. B. Shanklin, and R. J. Wiseman. "Resistance and reactance of 3-conductor cables." In: *Electrical Engineering* 54.3 (1935), pp. 324–326. DOI: 10.1109/EE.1935.6539676.

[Sch10] Klaus Schon. *Stoßspannungs- und Stoßstrommesstechnik: Grundlagen - Messgeräte - Messverfahren*. Berlin Heidelberg: Springer-Verlag Berlin Heidelberg, 2010. ISBN: 978-3-642-13117-2. URL: http://dx.doi.org/10.1007/978-3-642-13117-2 (visited on 09/20/2017).

[Sch+15a] Gero Schröder, Dominik Häring, Andreas Weinlein, Axel Bossmann, Ronald Plath, Markus Valtin, and Maitham Majid. "AC resistance measurements on skin-effect reduced large conductor power cables with standard equipment." In: *Jicable 2015 - 9th International Conference on Insulated Power Cables*. 2015.

[SKP11a] Gero Schröder, Johannes Kaumanns, and Ronald Plath. "Advanced measurement of AC resistance on skin-effect reduced large conductor power cables." In: *Jicable 2011 - 8th International Conference on Insulated Power Cables*. 2011.

[SKP11b] Gero Schröder, Johannes Kaumanns, and Ronald Plath. "Large Conductor Power Cables – AC Resistance Measurement With Variable Frequency." In: *ISH 2011*. Ed. by Ernst Gockenbach and Christian Eichler. Berlin: VDE-Verl., 2011. ISBN: 3800733641.

[Sch+12] Gero Schröder, Johannes Kaumanns, K. Vaterrodt, and Ronald Plath. "Die Messung des frequenzabhängigen AC-Verlustwiderstandes von Hochspannungskabeln mit großen Leiterquerschnitten zur Bewertung der Skin-Effekt bedingten Zusatzverluste." In: *Diagnostik elektrischer Betriebsmittel 2012*. Ed. by S. Tenbohlen. ETG-Fachbericht. Berlin: VDE-Verl., 2012. ISBN: 978-3-8007-3465-8.

[Sch+14] Gero Schröder, René Suchantke, Hendrik Just, Rolf Schuhmann, and Ronald Plath. "Maßnahmen zur Reduzierung des Skin-Effekts bei Energiekabeln durch optimierte Leiterkonstruktionen und deren messtechnische Bewertung." In: *Diagnostik elektrischer Betriebsmittel 2014*. ETG-Fachbericht. Berlin u.a.: VDE-Verl., 2014. ISBN: 978-3-8007-3648-5.

[Sch+15b] Gero Schröder, Volker Waschk, Ronald Plath, Rolf Schuhmann, and René Suchantke. "Measures to reduce skin-effect losses in power cables with optimized conductor design and their evaluation by measurement." In: *Jicable 2015 - 9th International Conference on Insulated Power Cables*. 2015.

[Sch13] Rolf Schuhmann. "Skriptum zu den Vorlesungen Feldtheorie und Theoretische Elektrotechnik." 2013. URL: http://www.tet.tu-berlin.de/fileadmin/fg277/Lehrmaterialien/TET/skript%7B%5C_%7DTET.pdf (visited on 11/05/2017).

[Sie14] Siemens AG. *Fact Sheet: High-voltage direct current transmission (HVDC)*. 2014. URL: http://www.siemens.com/press/pool/de/feature/2013/energy/2013-08-x-win/factsheet-hvdc-e.pdf (visited on 06/08/2016).

[Sil30] F. B. Silsbee. "Notes on the design of 4-terminal resistance standards for alternating currents." In: *Bureau of Standards Journal of Research* 4.1 (1930), p. 73. DOI: 10.6028/jres.004.005. URL: http://nvlpubs.nist.gov/nistpubs/jres/4/jresv4n1p73_A2b.pdf (visited on 09/20/2017).

[Sil67] P. Silvester. "AC Resistance and Reactance of Isolated Rectangular Conductors." In: *IEEE Transactions on Power Apparatus and Systems* PAS-86.6 (1967), pp. 770–774. DOI: 10.1109/TPAS.1967.291888.

[Sjö13] Mats Sjöberg. *A measuring system of AC and DC conductor resistance: ABB Sweden & Technical Research Institute of Sweden (Presentation)*. 2013.

[Ski48] Hugh Hildreth Skilling. *Fundamentals of Electric Waves*. Vol. second edition, third printing. New York and London: John Wiley & Sons, Inc and Chapman & Hall, Ltd., 1948.

[Smi14] Glenn S. Smith. "A simple derivation for the skin effect in a round wire." In: *European Journal of Physics* 35.2 (2014), p. 025002. DOI: 10.1088/0143-0807/35/2/025002. URL: http://iopscience.iop.org/article/10.1088/0143-0807/35/2/025002/pdf (visited on 09/23/2016).

[Sno25] C. Snow. "Alternating current distribution in cylindrical conductors." In: *Bureau of Standards* Volume 20 (1925), pp. 277–338. URL: http://nvlpubs.nist.gov/nistpubs/ScientificPapers/nbsscientificpaper509vol20p277_A2b.pdf (visited on 08/10/2016).

[Som99] Arnold Sommerfeld. "Über das Problem der elektrodynamischen Drahtwellen." In: *Wied. Ann.* Vol. 67. 1899, 233ff. URL: http://www.worldcat.org/title/uber-das-problem-der-elektrodynamischen-drahtwellen/oclc/946386928?ap=citavi (visited on 09/20/2017).

[Sta+13] Marilena Stanculescu, Mihai Maricaru, V. Stefan-Minculete, and I. F. Hantila. "Analytical solution for Eddy current problem, using space eigenfunctions expansion." In: *Introduction to Tribology*. Ed. by Bharat Bhushan. PO19 8SQ, UK: John Wiley & Sons, Ltd, 2013, pp. 1–8. ISBN: 9781118403259.

[Sta95] Inc. Standford Research Systems. *About Lock-In Amplifiers: Application Note #3*. 1995. URL: http://www.thinksrs.com/downloads/PDFs/ApplicationNotes/AboutLIAs.pdf (visited on 05/18/2017).

[Str91] John William (Baron Rayleigh) Strutt, ed. *Scientific Papers*. Vol. II. London: C.J. Clay And Sons, 1891. URL: https://ia801409.us.archive.org/20/items/cu31924005544139/cu31924005544139.pdf (visited on 09/20/2017).

[Suc14] René Suchantke. *Investigations on AC losses of power cables with large cross sections and advanced conductor design: Master Thesis - TU Berlin*. Berlin, 2014.

[SPS16] René Suchantke, Ronald Plath, and Rolf Schuhmann. "Besonderheiten bei der Messung von Wechselstromwiderständen von kurzen Leitern und kurzen Kabelstücken mit großen Querschnitten: Difficulties with AC resistance measurements of short conductor- and cable samples with large cross-sections." In: *VDE-Hochspannungstechnik 2016*. ETG-Fachbericht. Berlin: VDE-Verlag, 2016. ISBN: 978-3-8007-4310-0.

[SPW15] René Suchantke, Ronald Plath, and Volker Waschk. "A numerical approach to optimize HVAC conductor designs based on parameter sweeps of influenceable construction steps." In: *ISH 2015 - The 19th International Symposium on High Voltage Engineering*. Vol. The 19th International Symposium on High Voltage Engineering. 2015.

[Sug81] Kouichi Sugiyama. "Development of inter-layer insulated segmental conductor with low skin effect for power cables." In: *Electrical Engineering in Japan* 101.6 (1981), pp. 98–108. DOI: 10.1002/eej.4391010613.

[SZ14] Charles R. Sullivan and Richard Y. Zhang. "Analytical model for effects of twisting on litz-wire losses." In: *2014 IEEE 15th Workshop on Control and Modeling for Power Electronics (COMPEL)*. 2014, pp. 1–10.

[SK08] Hiroshi Suzuki and Mamoru Kanaoka. "Theoretical investigation on skin effect factor of conductor in power cables." In: *Electrical Engineering in Japan* 165.1 (2008), pp. 18–34. DOI: 10.1002/eej.20576.

[Tag15] Tagesschau. *Koalition einig bei Kohle und Netzausbau*. 2015. URL: http://www.tagesschau.de/inland/kanzleramt-energie-kohle-trassen-103.html (visited on 06/13/2016).

[Tak88] Michio Takaoka. "Conductor for an electrical power cable and a method for manufacturing the same." Patent: 5,094,703 (USA). Takaoka et al. 1988.

[Tay70] J. E. Taylor. "Discussion on: Measurement of skin and proximity effects in circular conductors." In: *Proceedings of the Institution of Electrical Engineers* 117.11 (1970), p. 2202. DOI: 10.1049/piee.1970.0403.

[Tek16] Tektronix. *Low Level Measurements Handbook: Precision DC Current, Voltage, and Resistance Measurements*. 7th Edition. 2016. URL: http://www.tek.com/sites/tek.com/files/media/document/resources/LowLevelHandbook_7Ed.pdf (visited on 06/28/2016).

[Ter43] Frederick Emmons Terman. *Radio Engineers' Handbook*. 1st edition. McGraw-Hill Book Company, inc, 1943. ISBN: ASIN: B0007DOWRW. URL: http://www.itermoionici.it/letteratura_files/Radio-Engineers-Handbook.pdf (visited on 09/20/2017).

[TM93] Joseph John Thomson and James Clerk Maxwell. *Notes on recent researches in electricity and magnetism: Intended as a sequel to Professor Clerk-Maxwell's Treatise on electricity and magnetism*. Clarendon press series. Oxford: Clarendon Press, 1893. URL: http://www.worldcat.org/title/notes-on-recent-researches-in-electricity-and-magnetism-intended-as-a-sequel-to-professor-clerk-maxwells-treatise-on-electricity-and-magnetism/oclc/17546597?ap=citavi (visited on 09/20/2017).

[Tho89] William (Lord Kelvin) Thomson. "Inaugural address of the new President: Ether, electricity, and ponderable matter." In: *Journal of the Institution of Electrical Engineers* 18.77 (1889), pp. 4–36. DOI: 10.1049/jiee-1.1889.0001.

[TLJ90] William (Lord Kelvin) Thomson, Joseph Larmor, and James Prescott Joule. "Mathematical and Physical Papers: Elasticity, Heat, Electro-Magnetism." In: Vol. III (1890). URL: https://archive.org/details/mathematicaland03kelvgoog (visited on 09/21/2016).

[Too13] Toolcraft. *LDM 50 U: Datasheet*. 2013. URL: http://files.smdv.de/800000-824999/822736-an-01-ml-LASER_ENTFERNUNGSM_LDM_50_U_de_en_fr_nl.pdf (visited on 02/19/2018).

[Tsu+05] O. Tsukamoto, Y. Yamato, S. Nakamura, and J. Ogawa. "Measurements of AC Transport Current Losses in HTS Tapes in an Assembled Conductor." In: *IEEE Transactions on Applied Superconductivity* 15.2 (2005), pp. 2895–2898. DOI: 10.1109/TASC.2005.848257.

[TT14] J. Turowski and Marek Turowski. *Engineering electrodynamics: Electric machine, transformer, and power equipment design*. Boca Raton, FL: Taylor & Francis/CRC Press, 2014. ISBN: 1466589329.

[van07] Ursula van Rienen. *Vorlesungsskript Theoretische Elektrotechnik*. 2007. URL: https://www.ief.uni-rostock.de/index.php?eID=tx_nawsecuredl&u=0&g=0&t=1466097567&hash=ae24d8ac983a0078ae9a59755cd8ba20a8c4cf94&file=fileadmin/iaet/content/thet_Skript.pdf (visited on 06/16/2016).

[Vin16] Eduard Vinaricky, ed. *Elektrische Kontakte, Werkstoffe und Anwendungen: Grundlagen, Technologien, Prüfverfahren*. 3rd ed. Berlin and Heidelberg: Springer Vieweg, 2016. ISBN: 9783642454264.

[VBS09] Slavko Vujević, Vedran Boras, and Petar Sarajčev. "A novel algorithm for internal impedance computation of solid and tubular cylindrical conductors." In: *International Review of electrical engineering (IREE)*. Vol. 4; 6-Part B. 2009, pp. 1418–1425. URL: https://scholar.google.de/citations?view_op=view_citation&hl=de&user=x0tCkogAAAAJ&citation_for_view=x0tCkogAAAAJ:9yKSN-GCB0IC (visited on 09/20/2017).

[VML11] Slavko Vujević, Tonci Modric, and Dino Lovric. "The difference between voltage and potential difference." In: *Joint 3rd Int'l Workshop on Nonlinear Dynamics and Synchronization (INDS) & 16th Int'l Symposium on Theoretical Electrical Engineering (ISTET), 2011*. Ed. by Kyandoghere Kyamakaya. IEEE, 2011, pp. 1–7. ISBN: 978-1-4577-0759-9.

[WW10] Volker Waschk and Dag Willén. "Elektrisches Sektorleiterkabel vom Millikentyp." Patent: EP2141709A2. nkt cables GmbH. 2010.

[Wee81] W. L. Weeks. *Transmission and distribution of electrical energy*. New York: Harper & Row, 1981. ISBN: 9780060469825.

[Wei] Eric W. Weisstein. *Bei - From MathWorld–A Wolfram Web Resource*. URL: http://mathworld.wolfram.com/Bei.html (visited on 10/12/2016).

[Wil05] Markus Wilke. *Zur numerischen Berechnung quasistationärer elektromagnetischer Felder im Zeitbereich*. 1st ed. Göttingen: Cuvillier Verlag, 2005. ISBN: 3865373267.

[WS70] F. J. Wilkins and M. J. Swan. "Precision a.c./d.c. resistance standards." In: *Proceedings of the Institution of Electrical Engineers* 117.4 (1970), p. 841. DOI: 10.1049/piee.1970.0168.

[Wis48] R. J. Wiseman. "A-C Resistance of Large Size Conductors in Steel Pipe or Conduit." In: *Transactions of the American Institute of Electrical Engineers* 67.2 (1948), pp. 1745–1758. DOI: 10.1109/T-AIEE.1948.5059887.

[Yav11] Ido Yavetz. *From obscurity to enigma: The work of Oliver Heaviside, 1872-1889*. Reprint of the 1995 ed. Modern Birkhäuser Classics. Basel: Birkhäuser, 2011. ISBN: 9783034801775.

[YD63] F. J. Young and S. J. Dudzinsky. "An A-C bridge method to measure core loss." In: *Transactions of the American Institute of Electrical Engineers, Part I: Communication and Electronics* 82.5 (1963), pp. 630–634. DOI: 10.1109/TCE.1963.6373275.

[Zab53] J. Zaborszky. "Skin and Spiraling Effect in Stranded Conductors [includes discussion]." In: *Transactions of the American Institute of Electrical Engineers. Part III: Power Apparatus and Systems* 72.2 (1953). DOI: 10.1109/AIEEPAS.1953.4498672.

[ZGS13] Victor M. R. Zermeno, Francesco Grilli, and Frederic Sirois. "A full 3D time-dependent electromagnetic model for Roebel cables." In: *Superconductor Science and Technology* 26.5 (2013), p. 052001. DOI: 10.1088/0953-2048/26/5/052001.

[ZL13] Peng Zhang and Y. Y. Lau. "Constriction Resistance and Current Crowding in Vertical Thin Film Contact." In: *IEEE Journal of the Electron Devices Society* 1.3 (2013), pp. 83–90. DOI: 10.1109/JEDS.2013.2261435.

[Zha+14] Richard Y. Zhang, Jacob K. White, John G. Kassakian, and Charles R. Sullivan. "Realistic litz wire characterization using fast numerical simulations." In: *Twenty-Ninth Annual IEEE Applied Power Electronics Conference and Exposition (APEC), 2014*. Ed. by Haidong Yu. IEEE, 2014, pp. 738–745. ISBN: 978-1-4799-2325-0.